Groundwater – Surface Water Interactions
in the
Discrete Fracture Networks of Bedrock Rivers

by

Celia Sylvia Cassis Kennedy

A Thesis
presented to the
University of Guelph

In partial fulfillment of requirements
for the degree of
Doctor of Philosophy
in
Environmental Sciences

Guelph, Ontario, Canada

Abstract

Groundwater – Surface Water Interactions in the Discrete Fracture Networks of Bedrock Rivers

Celia Sylvia Cassis Kennedy
University of Guelph, 2017

Advisors:
Professor Beth Parker
Professor Gary Parkin
Professor Emmanuelle Arnaud

Bedrock rivers exist where surface water flows along an exposed riverbed aquifer, but little is known about their physical and chemical properties. Groundwater and surface water are linked at the streambed interface, leading to shared sustainability issues. The sharing of common pathways into and out of the streambed fracture networks provides opportunity for the exchange of thermal, chemical and biological constituents, affecting water quality and ecosystem health. Alluvial rivers exhibit granular beds and their flow patterns are well understood. Much of our water-resource management decisions are based on alluvial river conceptual models using an equivalent porous media (EPM) approach. Since bedrock rivers are more challenging to instrument, their complex flow patterns have not been addressed in the discrete fracture network (DFN) context, thus, there is a gap in the literature.

This is the first study of a bedrock river yielding a field-based conceptual model of the spatio-temporal variability of groundwater fluxes and head differentials between groundwater and surface water in the upper 0.30 m of an intact dolostone streambed. A field site along the Eramosa River, in Guelph, ON, Canada, was developed, where the longitudinally-stepped profile of a bedrock riffle-pool sequence exists within a channel meander. The new field site was heavily instrumented with an innovative monitoring system designed for use along vertical and bedding plane riverbed fractures. Thus, a three-fold contribution has been made, to advance our understanding of bedrock river flow systems, including: the design of tools for measuring hydraulic parameters, the development of a field site to test them, and the spatio-temporal conceptualization of groundwater – surface water exchanges along an intact bedrock river channel and glaciofluvial plain.

Groundwater flow (Q) measurements ranged from -0.4 – 55 mL/min, with uncertainties of 13 – 40%. Fluxes (q) of 0.12 – 0.99 m/day and average linear groundwater velocities ($\bar{v}$) of 7 – 985 m/day were estimated from flow. Relative head differentials (Δh_{rel}), measured under suction between groundwater and surface water, ranged from 0.001 – 0.023 m ± 0.001, and vertical hydraulic gradients ($\Delta h_{rel}/\Delta L$) ranged from 0.02 – 0.46. Groundwater velocities in a bedrock river were observed to be influenced by: (1) proximity to a vertical fracture, (2) topographic relief or elevation, (3) channel geometry and (4) regional boundary conditions.

Acknowledgments

Sincere thanks to advisory committee members, Dr. Beth Parker, Dr. Gary Parkin and Dr. Emmanuelle Arnaud for your time, editing efforts, scientific inputs and continued support. Special thanks to Dr. Parker for your efforts as principal investigator of the broader field research program, which made my work possible, and for numerous discussions, insights and access to resources during my pursuit of a field site, a research topic and with tool design/construction. Special thanks to Dr. John Cherry for your insights and encouragement during field site and portable drill selection, with tool design and for sitting on my examination committee. Thanks to both Dr. Parker and Dr. Cherry for your guidance and feedback on my many presentations and progress updates that were required during the course of this research. Sincere thanks to Dr. William Woessner for serving as external examiner.

The author gratefully acknowledges the funding support of: (1) Dr. Parker, NSERC Industrial Research Chair, (2) Dr. Cherry's NSERC Discovery Grant, (3) MEDI Ontario Research Excellence Fund Round 3 Project, (4) Grand River Conservation Authority Holmes Scholarship, and (5) University Consortium for Field-focused Groundwater Contamination Research.

I would like to recognize key support from: (1) Scouts Canada, for continued access to the Barber Scout Camp, Guelph, (2) Robert Ingleton, University of Waterloo, for your technical expertise, creativity and sense of humour in working through one design problem at a time with me, (3) Dr. Brewster Conant Jr., University of Waterloo, for collecting the infrared data and teaching me how to process it, (4) Art Timmerman and the Ministry of Natural Resources for your support and approval of the riverbed installations, (5) Grand River Conservation Authority, for access to streamflow data from the Water Survey of Canada Gauging Station at Watson Road, Guelph, (6) Dr. Patryk Quinn for many discussions regarding hydraulic test analysis methods and your edit inputs in Chapter 2, (7) Dr. Colby Steelman for your collaboration with parallel studies and your edit inputs in Chapter 3, (8) Dr. Peeter Pehme for your assistance with geophysical equipment and WellCAD software, (9) Jonathan Munn and Carlos Maldaner, Ph.D Candidates, for sharing your insights and your time to trouble-shooting field and software

challenges, (10) Dr. Jessica Meyer and Dr. Ben Swanson for your insights and assistance with ArcGIS software and preparing for my qualifying exam, (10) Steven Chapman, MSc., for discussions and insights regarding hydraulic test analysis methods, (11) Dr. Jon Warland, University of Guelph, for access to rainfall data from the Environment Canada Automated Climate Station at Guelph Turf Institute, (12) Dr. Andrea Bradford, University of Guelph, for the loan of your flow meter, (13) Aardvark Drilling for your expert collaboration with implementation of our new portable drill studies, (14) Van Harten Surveying for collecting many many GPS point measurements in the river with me, (15) Tom Koby, Koby Environmental, for working through the J-Plug™ modifications with me, (16) Emile Dijkstra at Schlumberger Water Services, for help with transducer programming, (17) Carl Keller and Ian Sharp, Flexible Liner Underground Technologies, for your help with FLUTe™ profiling and customized liners for small-diameter coreholes, (18) Dr. Thomas Doe, Golder Associates, for use of FracMan software v.7.5, and (19) Joshua Kennedy, EIT, Lakehead University, for the original BSM technical drawing.

Sincere thanks to my second family, the G360 Groundwater Gang. This diverse project brought out the best in people during some pretty adverse conditions in the field. It has truly been a pleasure to work with such a kind and dedicated group of individuals – something the world needs more of. Special mention of the field crew: Donovan Capes, Andrey Fomenko, Jon Munn, Carlos Maldaner, Colby Steelman, Tom Coleman, Dan Elliot, Tammy Zidar, Joanna Olesiuk, Carla Rose, Tara Harvey, Amanda Malenica, Paul Trudell, Paulo Casado, Keelin Scully, Rachael Harman-Denhoed, Ben Kennedy, Helene Thuret, Doug Miller, Jessica Power, Jeff Martin and Chris Morgan.

Heartfelt thanks to my sons, Joshua and Benjamin, for their love, support and helping hands at home, in the lab and in the field over the years. And to my husband (the most patient man in the world), who convinced me to leave the legal field and go back to school seventeen years ago. Bryan, you promised we wouldn't end up living in the streets and you have stood by me through it all; I cannot find the words.

Declaration of Work Performed

I declare that, with the exception of the items listed below, all work presented in this thesis was performed by me.

Dr. Beth Parker and Dr. John Cherry drew the first BSM on the back of an envelope during the University Consortium Fall Focus Meeting in Denver, Colorado, in 2012.

Robert Ingleton, Senior Field Technician, University of Waterloo, performed the physical construction of the BSMs, the drag probe, the piezometer casings, and the river stage gauges, and worked through practical design and installation challenges with me. He also performed the physical drilling of all river piezometers and stage gauges, and twelve of the BSMs.

Andrey Fomenko, MASc, G360 Institute for Groundwater Research, University of Guelph, collected downhole geophysical logs in the floodplain wells. He also performed the physical drilling of twelve of the BSMs.

Donovan Capes, BSc, G360 Institute for Groundwater Research, University of Guelph, performed the physical construction of the customized potentiomanometer and assisted with riverbed drilling.

Dr. Brewster Conant Jr., University of Waterloo, collected the aerial infrared and video images of the 12-km reach of the Eramosa River.

Jon Munn, PhD Candidate, G360 Institute for Groundwater Research, University of Guelph, provided insights as to the location of the floodplain wells from his thesis work on inclined coreholes and the regional fracture orientation.

Dr. Colby Steelman, PDF, G360 Institute for Groundwater Research, University of Guelph, provided insights as to the location of the floodplain wells from his surface geophysical surveys of the study site (i.e., ground-penetrating radar and surface electrical resistivity).

Aardvark Drilling, Guelph, Ontario, completed the drilling of all floodplain wells with the assistance of Robert Ingleton and Dan Elliot, Field Technicians, using drilling equipment owned by the G360 Institute for Groundwater Research.

Table of Contents

List of Tables

List of Figures

Chapter 1: Introduction

1.1 Relevance of Hydrogeologic Studies in Bedrock Rivers

Groundwater and surface water are linked at the streambed interface, leading to shared sustainability issues. The sharing of common pathways into and out of the riverbed interface provides opportunity for the exchange of thermal, chemical and biological constituents, affecting water quality and ecosystem health. Hydraulic pressures and flow regimes of these linked systems are dynamic, impacted by natural-world erosional changes to channel geomorphology and varying seasonal inputs of precipitation, together with anthropogenic activities such as groundwater and/or surface water pumping related to urban development, agriculture and industrial processes.

The term "alluvial river" describes sand or gravel riverbeds, which have been studied in the context of flow patterns as they relate to the physical properties of the fluvial sediment, streambed topography and channel geometry (Legleiter *et al.*, 2011; Conant 2004; Dumouchelle 2001; Woessner 1998; Winter *et al.*, 1998; Cey *et al.*, 1998; Harvey *et al.*, 1997: Harvey and Bencala 1993; Hendricks and White 1991; deVriend and Geldof 1983; Lee and Hynes 1978; Vaux 1968; Leopold and Wolman 1960). The term "bedrock river" refers to surface water flowing along an exposed sedimentary bedrock riverbed. This may include intact rock, weathered cobbles, and sharp angular bedrock fragments. Bedrock rivers are a common class of channel observed across four continents (Figure 1.1), but little is known about their physical and chemical properties (Tinkler and Wohl 1998). This gap in our understanding is a consequence of the small number and focus of published bedrock river studies, generally limited to fluvial and geomorphological processes (Hodge 2011; Bishop and Goldrick 2010; Whipple 2004; Wohl and Merritts 2001; Stock and Montgomery 1999; Jarrett 1984). Commonly formed by glacial meltwater, these rivers are often found at the lowest elevation in the watershed, stripped of their protective overburden and lacking in fine granular sediments.

The nature of groundwater – surface water exchanges in river systems is dynamic, impacted by changing geomorphologies and differential pressures or head. Consequently, the nature of groundwater – surface water interactions in rivers flowing on a bedrock riverbed aquifer is distinctly different from that of a sand or gravel streambed. The reason for these differences in flow patterns and exchanges between groundwater and surface water is their disparate erosional processes and resultant geomorphologies. An alluvial river generally exhibits a granular or unconsolidated bed with the sediment transport capacity to aggrade and degrade over a very short timescale (i.e., seasons or flood events) so that its channel geomorphology remains relatively constant (Leopold and Wolman 1960). Effective porosity of a sand-gravel bed is large, ranging from 25 – 50% (Freeze and Cherry 1979), while diffuse flux through its alluvial matrix is slow (i.e., centimeters per day) (Shaw and Prepas 1990; Lee and Hynes 1978; Lee 1977) and groundwater – surface water exchanges with the underlying aquifer are influenced by the size, shape and orientation of its sediment (Woessner 1998; Winter *et al.*, 1998). A sedimentary bedrock riverbed, on the other hand, is dominated by planar or irregular exposed rock, typically horizontally-bedded, and exhibiting longitudinally-stepped or terraced profiles weathered along joint sets knickpoints and fragmented bedding planes due to unidirectional denudation over a geologic timescale (i.e., centuries or longer) (Tinkler and Wohl 1998; Miller and Cluer 1998). Effective fracture porosity of sedimentary bedrock is small, ranging from 1 – 0.001% or 10^{-2} to 10^{-5} (Freeze and Cherry 1979; Parker 2007; Lipson *et al.*, 2005; Muldoon and Bradbury 2005), hence, advective flux through its discrete fracture networks is fast (i.e., tens of meters per day) and groundwater – surface water exchanges are influenced by the connectivity between the river and the channel aquifer, which is a function of fracture aperture, length and orientation. In the case of both bedrock and alluvial riverbeds, erosional forces carve out pools and deposit sediment in riffles, and channel water moves into and out of the streambed due to downstream differential pressures. Streamflow losses at riffles and gains at pools have been observed in alluvial rivers (Dumouchelle 2001; Woessner 1998; Harvey and Bencala 1993; Hendricks and White 1991; Vaux 1968). Conceptual models of gaining, losing, flow-through and parallel-flow conditions in alluvial streams

introduced by Woessner (1998) are well-known. However, given their inherent differences, knowledge gained from alluvial systems is not necessarily transferable to fractured rock systems.

Without the attenuative properties of sediment cover, connectivity of a bedrock river to underlying groundwater reserves can be direct and unbuffered, thus, the potential for groundwater and surface water to influence one another makes them particularly vulnerable (Allen and Lucas 2013, AquaResource Inc., 2010, Hayashi and van der Kamp 2009). Rivers gain water and solutes from groundwater systems or serve as sources of groundwater recharge. Groundwater pumping can deplete streams just as water-taking from streams can diminish groundwater reserves, and pollution of groundwater can degrade surface water while contaminants in surface water can be transferred to groundwater (Winter *et al.,* 1998). Groundwater interacting with surface water, therefore, has implications to drinking water supplies and riverine ecosystem health. In a short review paper, Hayashi and van der Kamp (2009) recognize the importance of mapping groundwater flux through riverbeds, given its high degree of variability, as well as the need to integrate and advance our understanding of subsurface hydrology as it relates to surface hydrology, soil science, plant physiology and atmospheric science. The importance of groundwater inputs to the hyporheic zone in the ecological context of alluvial systems is well-documented (Woessner 2000; Meyer 1997; Palmer 1993; Hakencamp *et al.,* 1993; Vallett *et al.,* 1990; Hynes 1983; Stanford and Gaufin 1974; Ward 1989), and the occurrence of spawning habitats for trout and salmon in bedrock rivers has also been studied (Fales and Rasmussen 2014; Rawson 2011; Mossop and Bradford 2006; Alexander and Caisse 2003; Armstrong *et al.,* 2003; Payne and Lapointe 1997; Bisson *et al.,* 1988). Hence, it is well understood and accepted that any investigation of these rivers, hydrological or ecological, requires strong consideration given to minimally-invasive tools and techniques.

Since the rigid channels of bedrock rivers are more challenging to instrument, our hydrogeologic understanding of groundwater – surface water exchanges is biased toward alluvial river conceptual models, assuming flow through granular media. Much of our water-resource management decisions are

based on flow and contaminant-transport models, constructed from either hypothetical numerical modelling studies, or from field data collected in alluvial river studies, using an equivalent porous media (EPM) approach (Bear 1972). This approach is inappropriate for predictive flow models in bedrock river environments, given that the fundamental differences between bedrock and alluvial systems are not accounted for. The discrete fracture network (DFN) approach is a more viable alternative to modelling groundwater flow in bedrock rivers because it recognizes that at every scale, groundwater flow in fractured rock is dominated by discrete pathways, observing the characteristics of fracture size, geometry and connectivity (Parker *et al.*, 2012). There is a gap in the literature with respect to our knowledge of bedrock rivers and a need for a new conceptual model that recognizes the distinct characteristics of discrete fracture networks and the resultant heterogeneity and anisotropy contributing to complex flow patterns in riverbed aquifers.

A field-based conceptual model of groundwater – surface water exchanges in a bedrock river would first require an appropriate field site, with a riverbed exhibiting intact bedrock reaches where vertical and bedding plane fractures terminating at surface can be measured, along with the topographic diversity of a riffle-pool sequence. The study reach would have to be heavily instrumented to provide the high-resolution data sets needed to inform the conceptual model. Recent advances with portable drills, multi-level monitoring and the data-logging capacity of wireless micro-transducers have improved the collection of high-resolution geologic, hydraulic and thermal information with reduced impacts to surrounding ecosystems (Steelman *et al.*, 2015; Hatch *et al.*, 2006; Conant *et al.*, 2004). Further, the DFN approach continues to be developed by the G360 Institute for Groundwater Research at the University of Guelph (Steeleman *et al.*, 2015; Fomenko Thesis 2015; Malenica Thesis 2015; Meyer *et al.*, 2014; Parker *et al.*, 2012; Munn Thesis 2012; Coleman Thesis 2012; Quinn *et al.*, 2011; Pehme *et al.*, 2010; Parker 2007), where innovative methods are applied to measure the rate and distribution of groundwater flow and contaminant transport through fractured rock. Methods developed to date were applied to the terrestrial installations in this study (i.e., core and geophysical logging, FLUTe™ profiling, floodplain

fracture mapping, surface geophysics); however, techniques for in-stream application needed to be established, expanding the DFN approach to include hyporheic flow in bedrock riverbed aquifers. DFN field-based flow and transport models do exist, and these require information pertaining to the 3-D geometry, hydraulic attributes and connectivity of fracture networks together with properties of the rock matrix (Parker *et al.,* 2012; Therrien and Sudicky 1996; Sudicky and McLaren 1992; Smith and Schwartz 1984). Until now, this information has not been collected in bedrock river environments.

This is the first study of a bedrock river yielding a field-based conceptual model of the spatio-temporal variability of groundwater discharge and vertical hydraulic gradients across an intact dolostone channel. The Eramosa River, in Guelph, ON, Canada, was selected for this purpose.

The study of groundwater – surface water exchanges in alluvial systems was advanced by the development of the seepage meter to measure groundwater discharge and recharge (Lee and Cherry 1978); a method which has endured for almost four decades (Russoniello and Michael 2015; Toran *et al.,* 2015; Rosenberry *et al.,* 2013; Fritz *et al.,* 2009; Rosenberry *et al.,* 2008; Rosenberry and Morin 2004; Cey *et al.,* 1998; Woessner and Sullivan 1984; Lee and Hynes 1978). Based on Darcy's Law [1856], the seepage meter is constructed from the 30-cm-long end-cut of a 208-L steel drum and covers a surface area of 0.25 m^2. Its thin metal skirt is forced into the streambed sediments to form a seal, so that groundwater can be captured into its raised profile. Since Lee and Cherry's (1978) design relies on the collapsing, self-sealing properties of a granular medium, attempts made to deploy seepage meters in bedrock rivers have been limited to only sediment-covered reaches (Alexander and Caisse 2003; Oxtobee and Novakowski 2002). Some success was achieved with a marine deployment by sealing the meter with hydraulic cement (Shinn *et al.,* 2002). Adaptations of this simple design that incorporate continuous recording with wired data-loggers and electronic flow meters has been reported (Fritz *et al.,* 2009; Rosenberry and Morin 2004; Paulsen, *et al.,* 2001; Krupa *et al.,* 1998; Taniguchi and Fukuo 1993), but these modifications are elaborate and expensive and their use is limited to alluvial environments that can accommodate on-shore computer installations. Direct measurement of hydraulic head in terrestrial fractured rock is currently

accomplished using drilled wells, often in clusters (Meyer *et al.,* 2014; Meyer *et al.,* 2008; Cherry *et al.,* 2007; Novakowski *et al.,* 2006; Taylor *et al.,* 2003; Oxtobee and Novakowski 2002; Novakowski and Lapcevic 1988), where groundwater flow rates are quantified from pumping tests (Cook 2003; Meier *et al.,* 1998; Paillet et al., 1987; Raven, K.G. 1986), and Thiem [1906] or Hvorslev [1951] methods, derived from Darcy's Law, are used to estimate bulk hydraulic conductivity of the discretely fractured formation.

The principal challenge at the root of this project was to design a tool that would effectively measure anticipated spatially and temporally variable groundwater flow and head differentials between groundwater and surface water in a fractured rock riverbed without disrupting riverbed ecological functioning [detailed in Chapter 2]. Initially conceived as an adaptation to Lee and Cherry's (1978) seepage meter for use in alluvial rivers, the "bedrock seepage meter" or BSM is a hybrid seepage meter – short interval well device, designed to measure hydraulic parameters at the reach scale in the shallow subsurface of an intact bedrock riverbed needed to inform a 3-D conceptual model.

1.2 Eramosa River – Basin Scale Background

Bedrock rivers trend along a regional Silurian dolostone escarpment (dipping 25^{o} SW) from the Genesee River at Rochester, NY, up through the Niagara Region and around the Michigan Basin (Figure 1.2). Just north of the Niagara Region, the 27-km channel of the Eramosa River, in Ontario, flows in a southwesterly direction from its headwaters above the Town of Everton, at an elevation of 400 m above sea level (masl), to a confluence with the Speed River at 300 masl, within the City of Guelph. The Eramosa River contains a 12-km reach of mostly exposed bedrock channel, along which, surface water flows between Wellington County Road 44 and Victoria Road (Figure 1.3). Supporting a population of 122,000 (2011 census), the City of Guelph has 19 municipal wells, supplemented by a surface water intake on the Eramosa River to recharge an overburden aquifer at Arkell Springs (Figures 1.3, 1.6). The Speed and Eramosa Rivers have subwatersheds within the Grand River System, which flows into Lake Erie at 175 masl at the Town of Dunnville (Figure 1.4). Local topography of the fluvial plain along the

Eramosa River exhibits a small slope, falling 2.8 m per km of channel and dipping to the southwest (Karrow 1968). Cut by glacial meltwaters, it flows through the Guelph Drumlin Field, receiving water largely from the Paris-Galt Moraine (Sadura *et al.,* 2006; GRCA 2005). Its streambed exhibits the Silurian-aged fractured dolostones of the Eramosa Formation, underlain by the Goat Island aquitard and the highly transmissive Gasport aquifer (Brunton 2009; Karrow 1968). These dolomitic formations often exhibit karstic features (i.e., dissolution-enhanced fractures or matrix pores observed in core and coreholes) (Steelman *et al.,* 2015; Fomenko 2015; Cole *et al.,* 2009; Kunert *et al.,* 1998). Gartner Lee Limited (2004) completed a wellhead protection study of the regional geology and recharge rates of 19 Guelph Area municipal wells and more than 4400 residential wells. Based on potentiometric surfaces identified in these wells, findings were that groundwater recharges along the Eramosa Riverbed (i.e., bed elevation is higher than nearby potentiometric surfaces) occurred between the Everton headwaters and Arkell Springs, and that groundwater discharge along the channel (i.e., bed elevation is less than nearby potentiometric surfaces) occurred from Arkell Springs in a downstream direction. Figure 1.5 is the resultant regional flow model for the Eramosa River from the Gartner Lee (2004) study. The potential for groundwater and surface water to influence one another within and around the Eramosa River has prompted a number of vulnerability studies and public health inquiries, particularly since the *Clean Water Act* was enacted in 2006 (AquaResource Inc., 2010; LERSP 2010; GRCA 1998).

1.3 Climate Change in the Eramosa River Basin

The impact of climate change and variability on the nature of groundwater – surface water exchanges is not well understood. Hayashi and van der Kamp (2009), discuss the complexity of water balance within the hydrologic cycle and the focus of research efforts directed towards prediction of groundwater responses to short- and long-term changes in climate (i.e., temperature and precipitation) and anthropogenic stresses (i.e., groundwater pumping and land use). Environment Canada (EC 2004) describes climate variability as the natural, high-frequency variation in climate, while climate change refers to long-term (i.e., several decades or more) trends that may be either natural or human-induced.

Canadian studies of the potential impacts of climate change on the hydrologic cycle are focused on numerical models and the link between streamflow and glacier runoff, with little research on the sensitivity of aquifers to key climate change variables, such as temperature and precipitation (EC 2004). The Intergovernmental Panel on Climate Change (IPCC) published its 1st Assessment Report in 1990, and by the 4th (IPCC 2007) and 5th (IPCC 2013) Assessment Reports, it concluded that possible impacts of climate change were: increased snow melt and sea level due to increased temperatures, changes in precipitation and evaporation patterns, and increased frequency and magnitude of hydrologic extremes (i.e., droughts and floods). In a collaboration under the umbrella of the *Climate Change Action Fund,* the National Water Research Institute, Meteorological Service of Canada, Geological Survey of Canada, and the Ontario Ministries of Environment and Natural Resources, compiled streamflow data from a network of 174 watersheds located across southwestern Ontario, separated into surface runoff and groundwater discharge components and analyzed to estimate the portion of excess precipitation that recharges groundwater for use in predictive models running climate change scenarios (EC 2004). The study predicted increased flows during the winter due to reduced snow accumulation and decreased flows during spring-summer due to the corresponding reduced snow melt (EC 2004). Thus, potential for impacts on both groundwater and surface water were demonstrated.

More recently, review papers have compiled findings from studies over the past decade (Zhang 2015; Taylor *et al.*, 2012). In a global context, Taylor *et al.*, (2012) reported that: (1) changes in precipitation and temperature extremes are projected to increase; and (2) links between climate and groundwater are complicated by land use changes. For example, long-term drought conditions influence groundwater recharge and discharge; however, in the case of agricultural land use, an increase in the irrigation-water-demand also occurs. On the other hand, groundwater influences climate through contributions to soil moisture, where irrigation during a growing season can increase local evapotranspiration from crops and downwind precipitation. Zhang (2015) reported on water resource management using predictive models and the uncertainties associated with them at various scales and cautioned that: (1) non-climatic factors such as land use changes and water use/demands affect

sustainability of water resources; and (2) predictive models assessing climate change impacts tend to assume that these non-climatic factors remain unchanged.

The impact of the climate change variables, temperature and precipitation, on the nature of groundwater – surface water exchanges in the Eramosa River has not been studied. A 50-year search was conducted to ascertain City of Guelph census years where streamflow (from the Watson Road Gauge Station), rainfall and temperature data were available for the month of August, when river stage is typically at its lowest point and no longer influenced by snowmelt. Table 1.1 reflects that the average August streamflow rises and falls, the total August rainfall varies with little-to-no change in mean temperature and the urban population has grown by 300%. Population growth in a city that relies on groundwater for its drinking water supply translates to a significant increase in the municipal-water-demand.

The scientific driver behind this dissertation is the advancement of our understanding of groundwater – surface water interactions in a discretely-fractured bedrock river environment. In practicality, a field research site had to be located and developed and an innovative monitoring system for data collection designed and deployed.

1.4 Hypothesis and Objectives

The overall intention of this research was to study the hydrologic setting of a fractured rock riverbed by quantifying the spatio-temporal variability of groundwater fluxes and head differentials between groundwater and surface water, with emphasis on design of effective field methods and research site procurement and development. The hypotheses being addressed are stated below:

> *Groundwater flux into sedimentary bedrock rivers occurs through hydraulically-connected vertical joints and bedding plane fractures, creating a 3-D fracture network with variable hydraulic connectivity in the riverbed interface.*
>
> *At the reach scale, spatio-temporal variability of groundwater discharging to surface water is a function of hydraulic connectivity and differential pressures within the discrete fracture networks*

of an intact bedrock riverbed, where point measurements are impacted by: (1) proximity to a vertical fracture, (2) topographic elevation, (3) channel geometry, (4) seasonal fluctuations in precipitation, and (5) the regional flow system.

A fundamental requirement to any field-based research is an appropriate field site; therefore, these hypotheses were addressed through a series of objectives:

1. Identify and develop a field research site.
2. Instrument the site with groundwater and surface water infrastructure to monitor ambient flow rates, hydraulic head and conduct hydraulic tests to quantify Darcy fluxes.
3. Understand and characterize the variability of the hydrologic regimes observed through spatial and temporal analysis of field data collected.

1.5 Field Site Identification

The selection of the Eramosa River site was based on the following site selection criteria:

1. The streambed exhibits exposed intact bedrock so that vertical fractures, as preferential pathways for groundwater discharge, can be measured.
2. The presence of sediments is minimal, since fine sediment is known to clog fractures, and large sediment, in the form of sharp angular bedrock fragments, constrains instrumentation of the area.
3. Groundwater discharge is evident through physical indicators such as seeps, temperature differentials, topography or regional flow patterns.
4. Height of river stage is sufficiently low (i.e., < 1 m) to permit fracture mapping and installation of monitoring devices.
5. Accessibility in the form of physical access (i.e., close proximity to the University of Guelph for transport of equipment and people), as well as agreeable land owners and regulatory agencies.

Based on these criteria, the Eramosa River, with its exposed bedrock reaches and close proximity to the University of Guelph G360 Bedrock Aquifer Field Facility, was selected for reconnaissance. The specific site used in this research was then identified through a series of field surveys conducted in 2012. An aerial infrared temperature (IRT) survey was conducted along a 12-km reach (Figure 1.4), detailed in Appendix A, to detect potential study sites where groundwater is discharging to surface water. A stream survey was conducted by kayak along the same 12-km reach to: (a) ground-truth IRT findings using a drag probe (i.e., temperature and electrical conductivity sensor), (b) map streambed transitions between bedrock and sediment-cover, and (c) conduct bathymetric and hydrometric surveys to identify dimensions and surface water flow conditions to assess the feasibility of monitoring device installations and fracture mapping, detailed in Appendix A. The Barber Scout Camp, a 2600 m^2 site along the Eramosa River, was identified as the best fit to the criteria.

1.6 Study Site – Reach Scale Background

Figure 1.6 provides a brief overview of the Scout Camp Site investigated in this thesis, including: install elevations at the site and proximity to various land uses, municipal wells, Arkell Springs and the surface water gauge at Watson Road. Elevations of the screened intervals of municipal wells within a 3-km radius of the study site were compared to the total vertical depth of the Scout Camp installations, including: 8 lined floodplain wells, 6 cased river piezometers and 24 seepage meters sealed into the bedrock channel. Consistent with Karrow's 1968 description of the Eramosa River, the topographic relief within a 3-km radius of the Scout Camp is low. Figure 1.7 represents a sub-basin-scale contour map, showing a consistent elevation of 310 – 315 masl along the channel. Topographic highs of 340 – 360 masl are identified north and south of the channel. A series of cross-sections were applied somewhat orthogonal to surface water flow to illustrate these elevation changes in a 3D context in relation to the channel and are shown in Figure 1.8. Land surface elevations along the south side of the channel continue to gradually increase for up to 2 km before reaching their topographic high. The slope along the north side of the river is more intense, reaching its topographic high less than 1 km from the channel centre. Figure

1.9 shows the sub-basin-scale contour map inset into the basin-scale geologic and contour maps constructed by Gartner Lee (2004). In basin-scale context, the uppermost geologic formation commonly observed in the Guelph Area, the Guelph Formation (Fm), is absent along the Eramosa River. In fact, the Guelph Fm is absent north and south of the channel from its headwaters at Everton, in a downstream direction to the Scout Camp, leaving only the persistent Eramosa Fm exposed at surface. Since Gartner Lee's basin maps pre-date the Silurian stratigraphy revisions completed by Brunton (2009), the surficial geology where the Guelph Fm is absent is referred to simply as the Amabel Fm. A bedrock paleo-valley in the vicinity of the Carter Wells and the margin between the Guelph and Amabel Fms was reported by Opazo *et al.*, (2016) and by Cole *et al.*, (2009), which may influence groundwater flow. Cole *et al.*, (2009) found that high-yield wells were inversely correlated with distance to bedrock paleo-valleys, as they may be associated with highly-fractured zones. Figure 1.10 provides a conceptual glimpse of the geologic profile along cross-section A – A' (Figure 1.7) using core information obtained from the Reformatory Quarry (Brunton 2009), the Carter Wells (Opazo *et al.*, 2016) and this thesis research (well SCA2).

1.7 Field Site Logistics and Legalities

Since this study entailed streambed and floodplain investigations, steps were undertaken to ensure the successful development of a research field site. The terms of an access agreement were negotiated with Scouts Canada (Ottawa, ON) and a 5-year contract was executed by the University of Guelph and the land owner. Given the nature of land use (i.e., youth camp), stipulations included that University of Guelph staff and students receive police clearances and provide youth outreach workshops from time-to-time. The terms of an access agreement were negotiated with the Ministry of Natural Resources and Forestry (Guelph, ON), including an exemption from the regulation pertaining to *no in-water work* during trout spawning season (i.e., March 14 – July 30) and a stipulation that all streambed installations be approved by the Ministry and comply with the *Navigable Waters Protection Act 1985.* A 1-year contract was executed by the University of Guelph and the Ministry, which has been extended on two occasions,

following progress updates. Attempts to secure floodplain access to the North side of the channel with a different land owner proved unsuccessful, which meant that all studies would have to be confined to the channel, itself, and the fluvial plain on the south side of the channel within the Scout Camp property.

Water Survey of Canada operates one gauging station on the Eramosa River at Watson Road, which is monitored by the local conservation authority. The terms of a data licensing agreement were negotiated and a contract signed with the Grand River Conservation Authority (Cambridge, ON) in order to receive continuous streamflow data from the Watson Road Gauging Station, 900 m upstream of the study site. Eight years of precipitation data collected by Environment Canada at the Guelph Turf Institute, 1.8 km downstream of the study site, was obtained; however, the station ceased functioning in 2012. The meteorological station was rebranded the Environment Canada Automated Climate Station, where rainfall data has since been collected from a tipping bucket maintained by the University of Guelph. The closest snowfall data collection option was located at the Waterloo Airport, 24 km southwest of the site. No reliable barometric pressure data could be found in the vicinity of the study site. Consequently, two SWS Baro-Divers™ (Schlumberger Water Services, Delft, The Netherlands) were installed in trees along the floodplain at the study site.

1.8 Bedrock River Field Site Baseline Data Collection and Equipment Testing

In March – April, 2013, a surface geophysical study was conducted over a 2600 m^2 area, where fractured sedimentary bedrock is exposed along the streambed and floodplain. Ground-penetrating radar (GPR) reflection profiles and common-midpoint (CMP) soundings were applied to detect changes in subsurface density to infer the depth and dominant orientation of fractures to a depth of 6 m below ground surface (bgs). For consistent referencing of data from all studies conducted at the research site, the streambed and floodplain were divided into transects orthogonal to channel boundaries and surface water flow, at 10-m intervals, and surveyed by Van Harten Surveying Inc., (Guelph, ON), using a Leica Diva GPS, where 15 readings per measurement were taken and averaged to produce 1-cm accuracy, using

permanent reference stations corrected to orthometric elevations with Geoid Model HTv2.0 supplied by Natural Resources Canada.

Conducting a hydrogeological study in fractured rock requires drilling. Typical truck-mounted drilling rigs have limitations, such as size, weight, water and fuel consumption where remote, ecologically-sensitive river environments are concerned. Four portable drills were researched and field-tested with diamond coring bits for this project, as described in Appendix B. The Prospector (Hydracore Drills, Delta, BC, Canada) for installing floodplain wells up to 60 m deep [diameter 7.5 cm (NQ or 3 in)], the Winkie Drill (Minex, Virginia, MN, USA) for installing floodplain piezometers up to 10 m deep [diameter 6 cm (BQ or 2.4 in)], the Shaw Backpack Drill (Shaw Tool Ltd., Yamhill, OR, USA) for installing riverbed piezometers up to 3 m deep [diameter 5 cm (2 in)], and the DR520 Concrete Drill (Norton Construction Products, Stephenville, TX, USA) for installing bedrock seepage meters [diameter 10 cm (4 in)] and setting the casings for the floodplain wells. The services of Aardvark Drilling Inc. (Guelph, ON) were contracted to oversee drilling operations in accordance with the *Ontario Water Resources Act, R.R.O. 1990, Regulation 903.* A drilling strategy and health and safety plan (HASP) were prepared to comply with drilling regulations, insurance requirements and to preserve the ecological integrity of the site.

In April – May 2013, The Prospector (Hydracore Drills, Delta, BC, Canada) was used to create three corehole pairs drilled in the bedrock floodplain to a depth of 30 meters below ground surface (mbgs) and continuously cored, with each pair consisting of one inclined and one vertical hole. The purpose of the inclined holes, plunging at 60° with azimuths 50°, 195° and 340° was to inform the 3-D fracture network geometry beneath and adjacent to the channel (Appendix C). Azimuths were selected on the basis of surface geophysical surveys. The depth of the coreholes was chosen to collect representative continuous cores from the three formations in this shallow dolostone aquifer, with the inclined holes intended to reduce bias by intersecting more vertical fractures, better inform the 3-D fracture intensity and network condition (Munn 2012), and to accommodate future hydraulic testing. Following development,

FLUTe™ liners (Alcade, NM, USA) were installed in all six coreholes to minimize disruption to the natural flow system and prevent hydraulic cross-connection. All core extracted was photographed, logged (i.e., fractures and lithology) and boxed for future reference. Floodplain wells were cased to a depth of 0.6 m (2 ft) below ground surface and 0.6 m (2 ft) above ground surface, in accordance with the *Ontario Water Resources Act, R.R.O. 1990, Regulation 903*. Surface casings were customized with removable couplings to easily accommodate geophysical probes and hydraulic test equipment. Well covers were customized: (a) in aluminum to allow for easy removal and installation; and (b) in size and position to accommodate instrumentation and minimize the need for cover removal; a common inconvenience when working with monitoring wells. Two vertical shallow coreholes were drilled to a depth of 10 mbgs and lined in December 2013 to complement shallow subsurface hydraulic monitoring. Fracture position, length and orientation was logged along the length of the floodplain coreholes, in the Z-dimension (detailed in Appendix C) and across the riverbed, in the X-Y dimension (detailed in Appendix D) to inform the 3-D conceptual model.

1.9 Thesis Organization

The research presented in this thesis is the first study of a bedrock river yielding a field-based conceptual model of the spatio-temporal variability of groundwater discharge in an intact sedimentary bedrock riverbed. To develop the methods and fulfill the objectives of the study, a new research site was developed, where researchers continue to advance our knowledge of bedrock river hydraulics. Chapters 2 and 3 have been prepared as stand-alone manuscripts for submission to peer-reviewed journals and are meant to be self-contained, thus, some unavoidable redundancy has resulted. This chapter, Chapter 1, introduces the general topic of bedrock rivers and relevance of this thesis, summarizes the research objectives, describes the multi-faceted research approach and outlines the organization of the thesis. Chapter 2 describes a new tool developed for use in fractured rock riverbeds to quantify groundwater flux and head differentials between groundwater and surface water at an appropriate field-scale and analysis methods to evaluate groundwater – surface water exchanges. Chapter 3 reports on the first field study of a

bedrock river, where hyporheic flow was measured and groundwater - surface water exchanges characterized. Chapter 4 highlights principal findings, summarizes the original contributions and makes recommendations for future research. Appendices A-D provide additional details related to the selection and creation of the bedrock river field site that are relied upon for the data interpretation in the thesis and provide support to future research projects. Some of the baseline datasets collected in collaboration with C. Steelman have already been published (Steelman *et al.*, 2017).

1.10 Tables and Figures

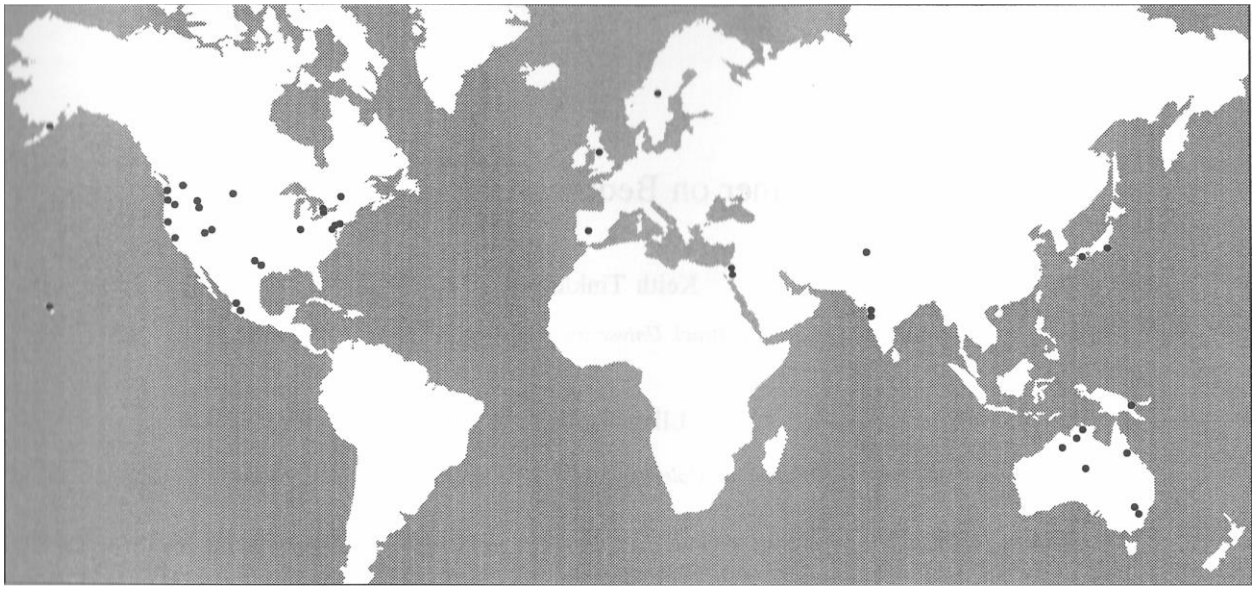

Figure 1.1. Map of world distribution of bedrock river studies (Tinkler and Wohl 1998), which largely focus on stream discharge rates, flooding, fluvial erosion/incision and geomorphological processes.

Figure 1.2. Pattern of persistent Silurian dolostone escarpment, indicated in red, extending from the Genesee River at Rochester, NY, up through Niagara Region and around the Michigan Basin. City of Guelph is shown along the Grand River System indicated by ★ [map by C.J. Moss].

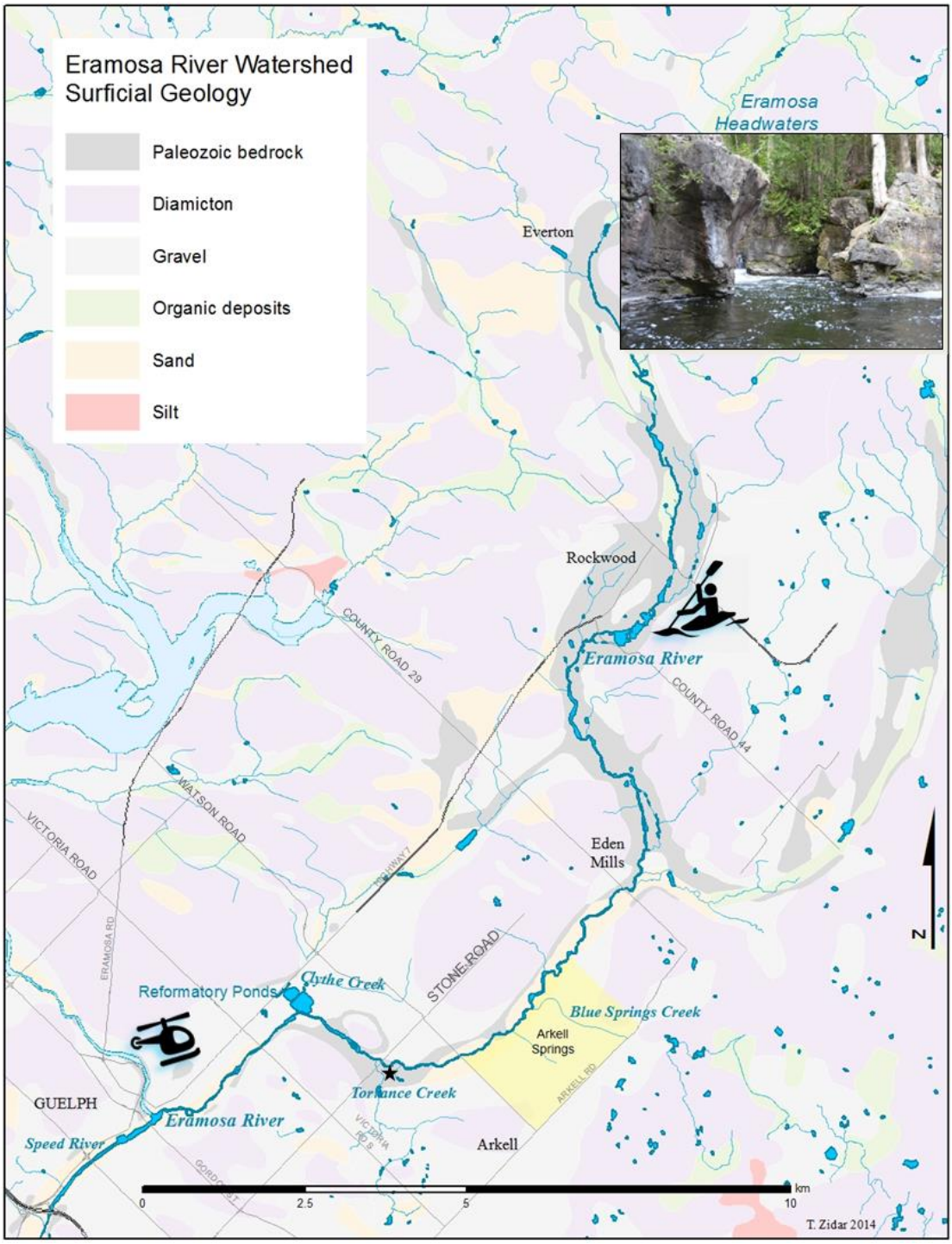

Figure 1.3. The Eramosa River flows along exposed Silurian dolostone (i.e., deposited 430 mya during the Paleozoic Era), for 27 km, from the incised channel of its headwaters near Everton (365 masl) to where its confluence with the Speed River (310 masl) in Guelph, where topographic relief is low. The ends of the 12-km reach surveyed by air and by kayak are indicated, along with the location of the selected study site ★ [map drafted by T. Zidar, using ArcGIS and surficial geology from the Ontario Geological Survey 2010].

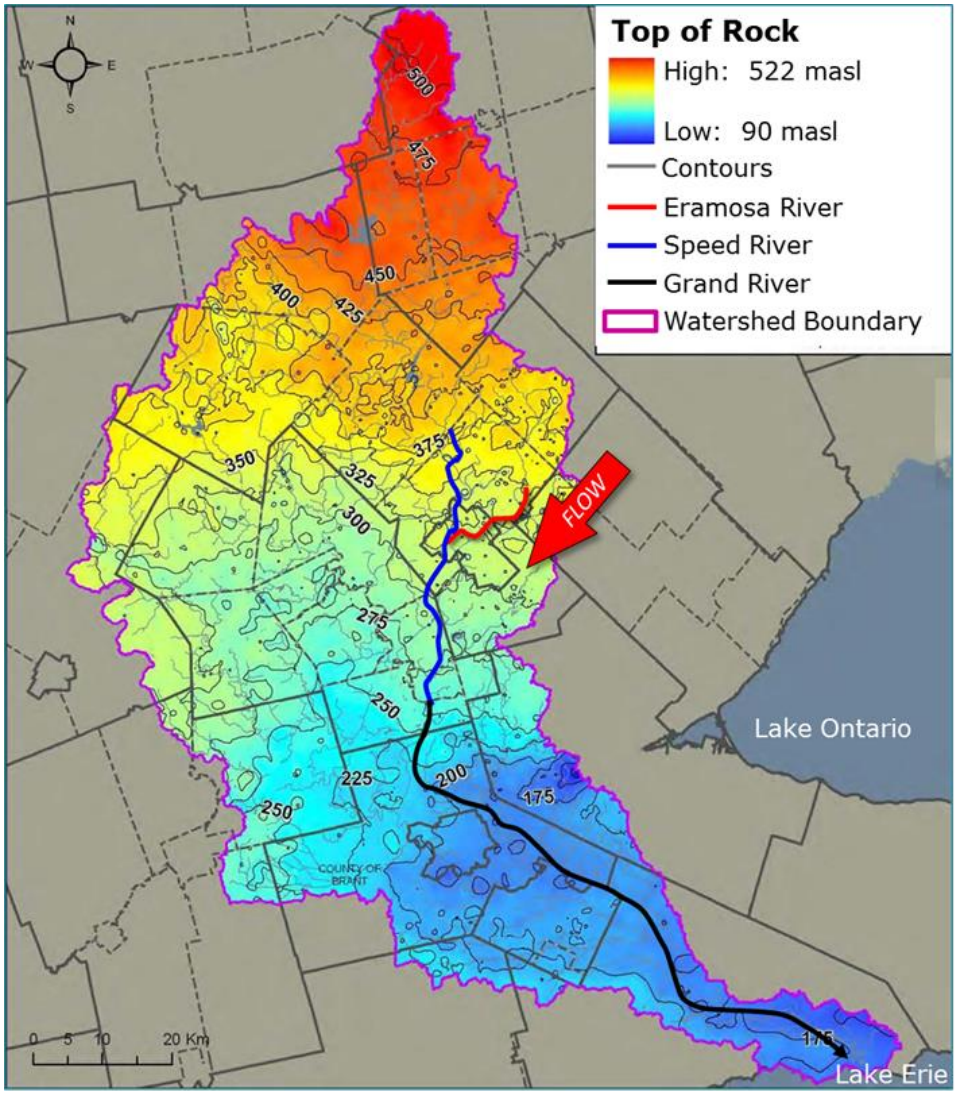

Figure 1.4. Bedrock topography map of the Grand River Watershed, spanning an area of 6800 km^2, encompassing the tributaries of the Speed and Eramosa Rivers and flowing into Lake Erie at an elevation of 175 masl. Colour ramp refers to the bedrock surface elevation. Adapted from Lake Erie SWP (November 2010).

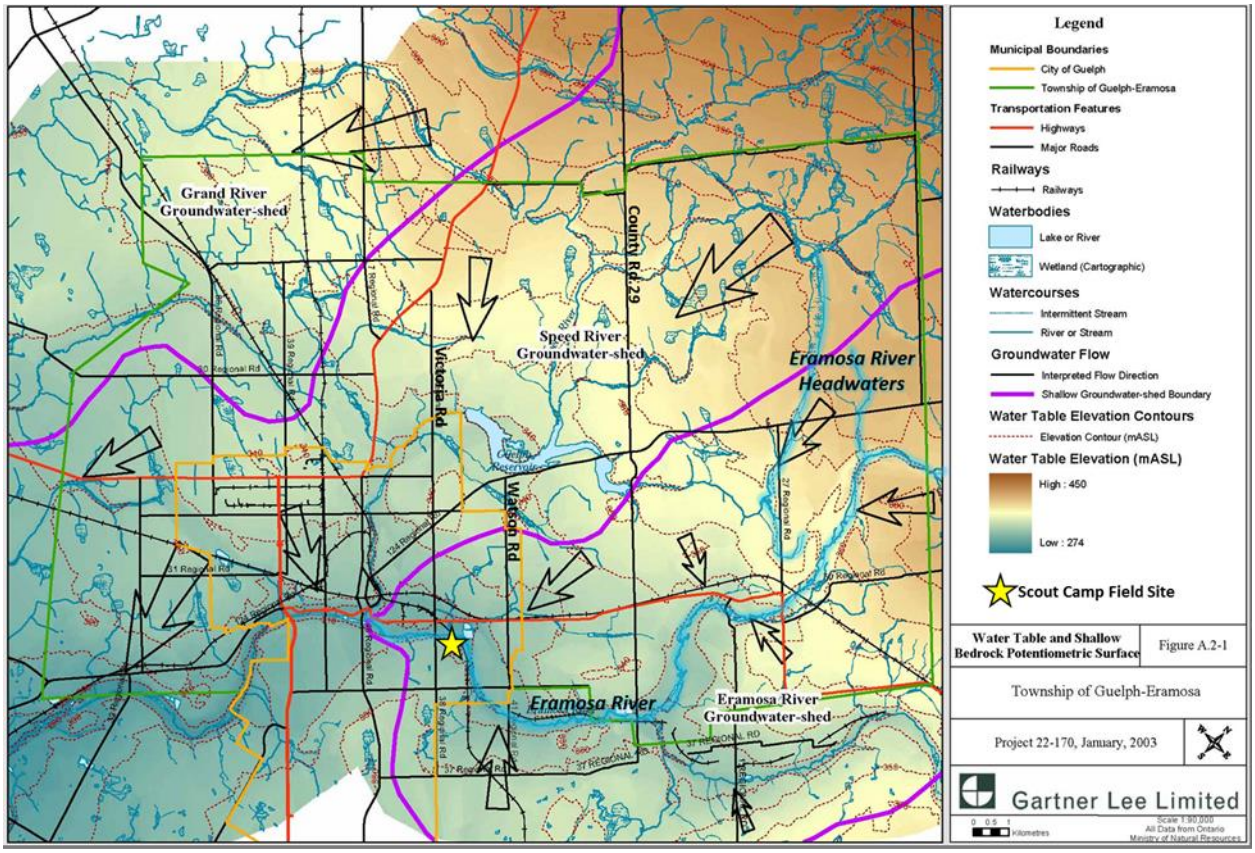

Figure 1.5. Regional flow model for the shallow water table within the Eramosa River Watershed, based on a wellhead protection study (Gartner Lee 2004). Arrows outlined in black indicate direction of groundwater flow. Location of Scout Camp study site is indicated.

Table 1.1. Historical record of mean August streamflow measurements collected at the Watson Road Gauging Station, Guelph, ON (Water Survey of Canada), total August rainfall and mean August atmospheric temperatures in the Guelph region (Environment Canada), and population (City of Guelph Archives). Record is constrained by years when census, streamflow, rainfall and temperature data was available.

Year	Streamflow [m^3/s]	Rainfall [mm]	Temperature Air [^oC]	Population City of Guelph
1964	1.4	151	16	40 000
1968	2.9	155	19	51 400
1986	3.2	129	17	78 235
1994	0.5	65	18	88 000
1999	0.3	64	18	96 000
2004	1.3	45	17	115 000
2014	**1.7**	**101**	**17**	**122 000**

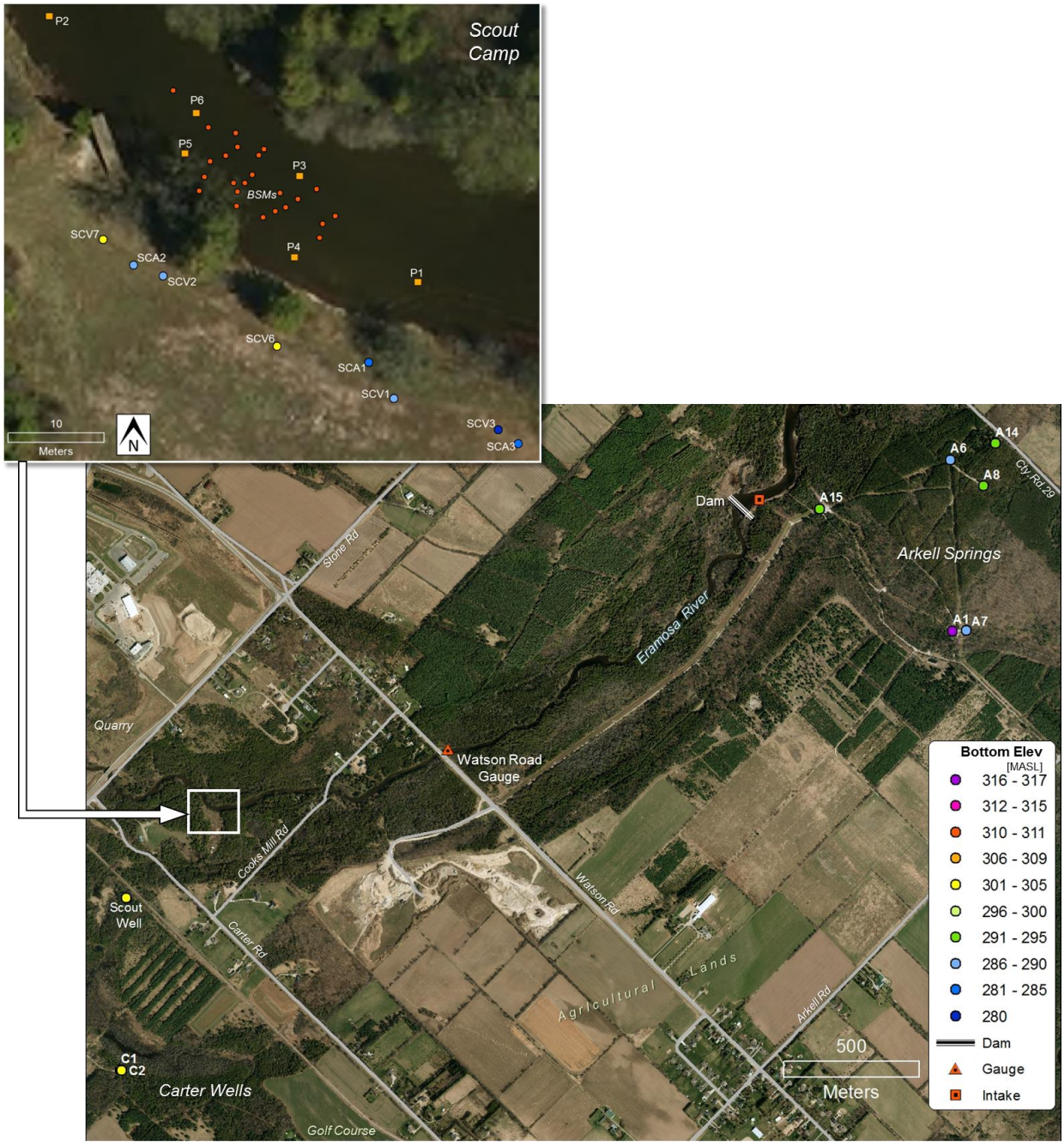

Figure 1.6. Location of Scout Camp study site (inset) in relation to municipal (Arkell and Carter) production wells. Colour ramp refers to elevation of open interval or bottom-of-well. Installations at Scout Camp include: lined floodplain wells ●, riverbed piezometers ■ and bedrock seepage meters or BSMs ●. Land uses within a 3-km radius of the study site are indicated. [NAD 1983 UTM Zone 17N Geographic Coordinate System; MNR SWOOP 2010; City of Guelph 2014; ESRI ArcMap v.10.2.1].

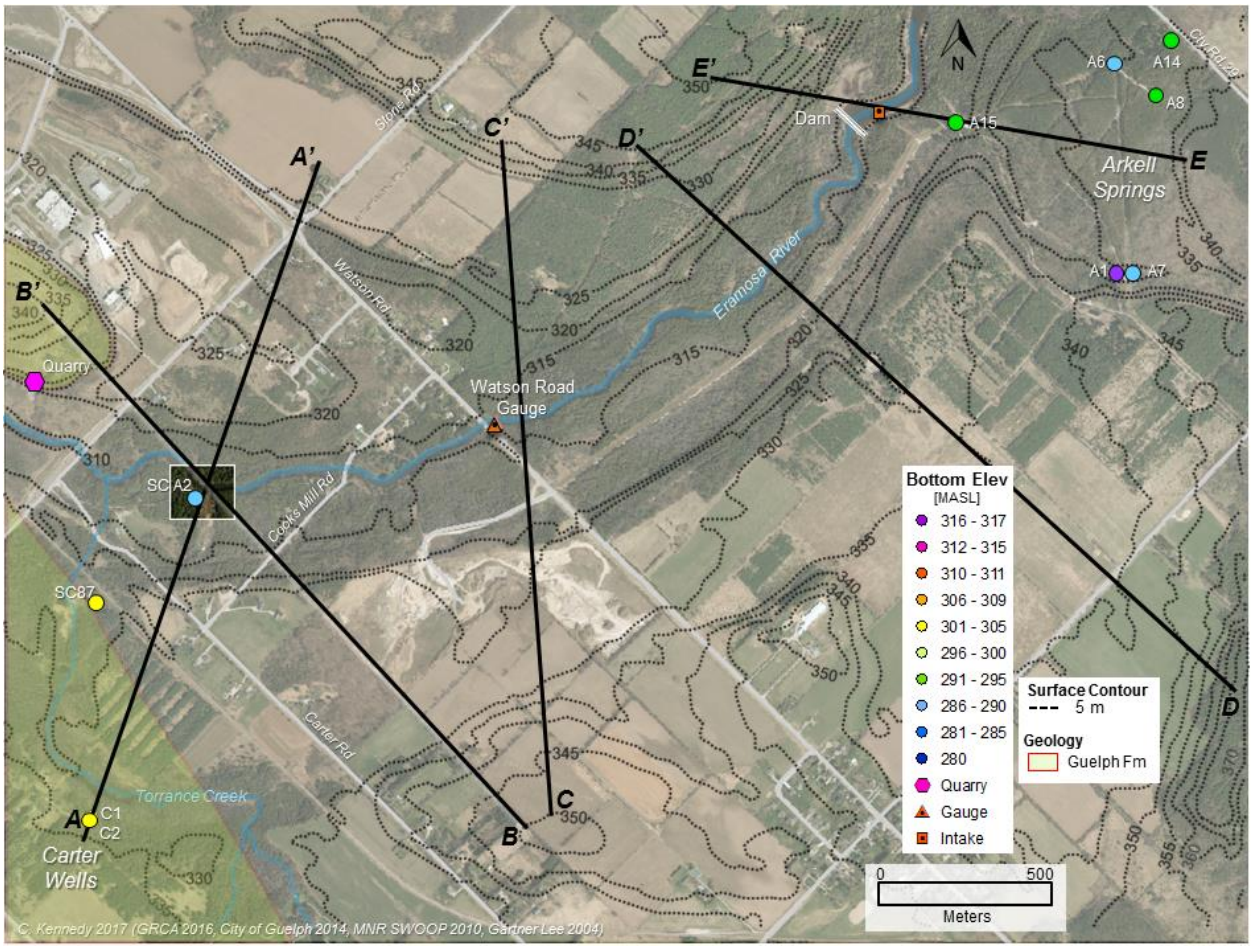

Figure 1.7. Sub-basin-scale contour map within a 3-km radius of the Scout Camp, comparing topographic surface elevations to screened or open intervals of municipal pumping wells and lined floodplain well SCA2 at the study site. Cross-sectional transects A – A' and B – B' were drawn across the riverbed at its lowest elevation, and at 1-km intervals (approximately) to evaluate elevation changes. Arkell wells, A6, A7, A8, A14 and A15, are screened in the Amabel Fm, while A1 is in the overburden. Carter wells, C1 and C2, are installed in the Guelph Fm. Scout Camp SCA2 is installed in the Gasport Fm (previously known as part of the Amabel Fm). [NAD 1983 UTM Zone 17N Geographic Coordinate System; MNR SWOOP 2010; City of Guelph 2014; GRCA 2015; ESRI ArcMap v.10.2.1].

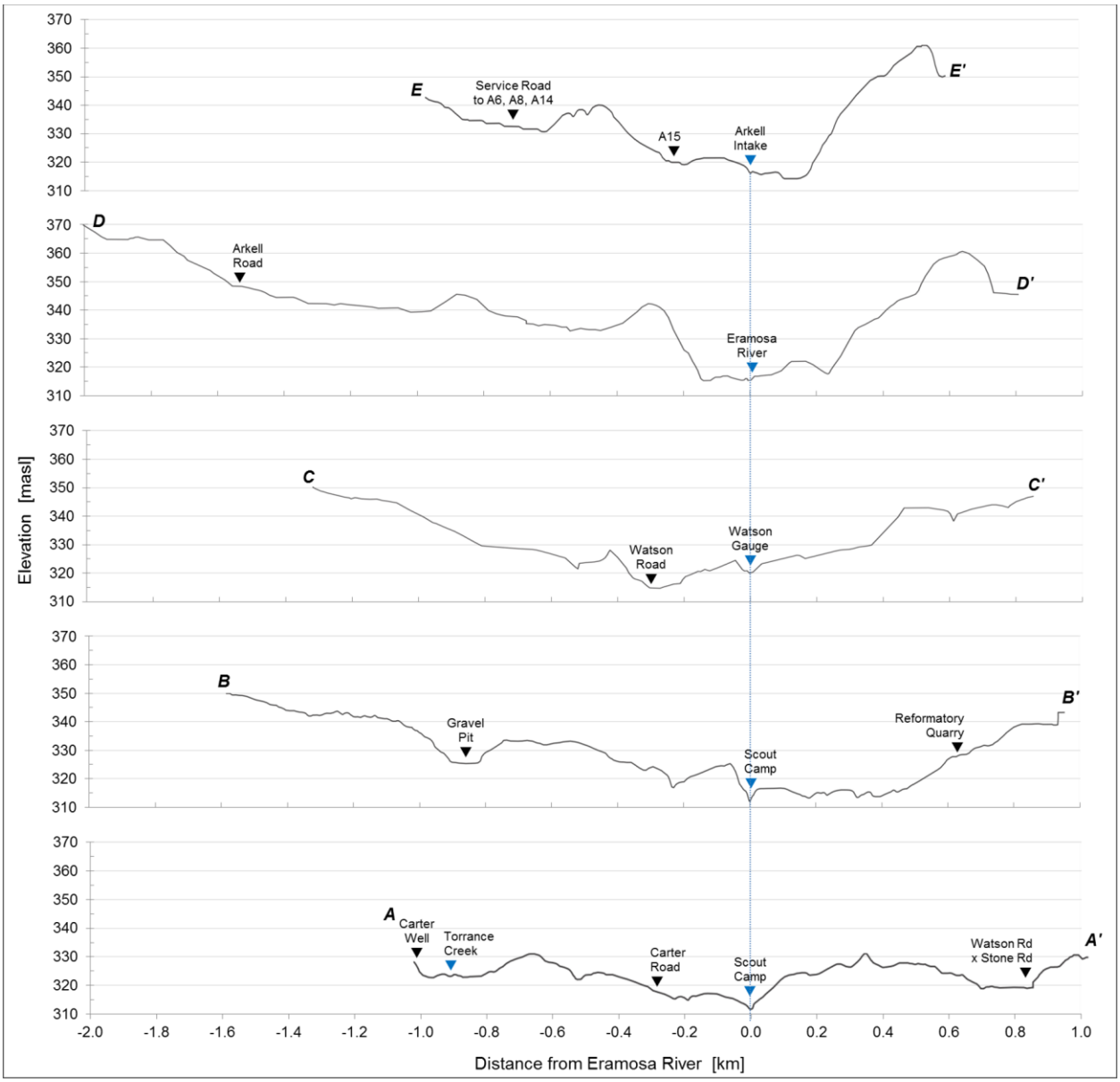

Figure 1.8. Topographic cross-sections of transects drawn somewhat perpendicular to surface water flow in Figure 1.7, comparing distances from the channel centre to the topographic high. All transects were drawn in a South – North direction. Transects A – A' and B – B' cross at the lowest elevation at the study site.

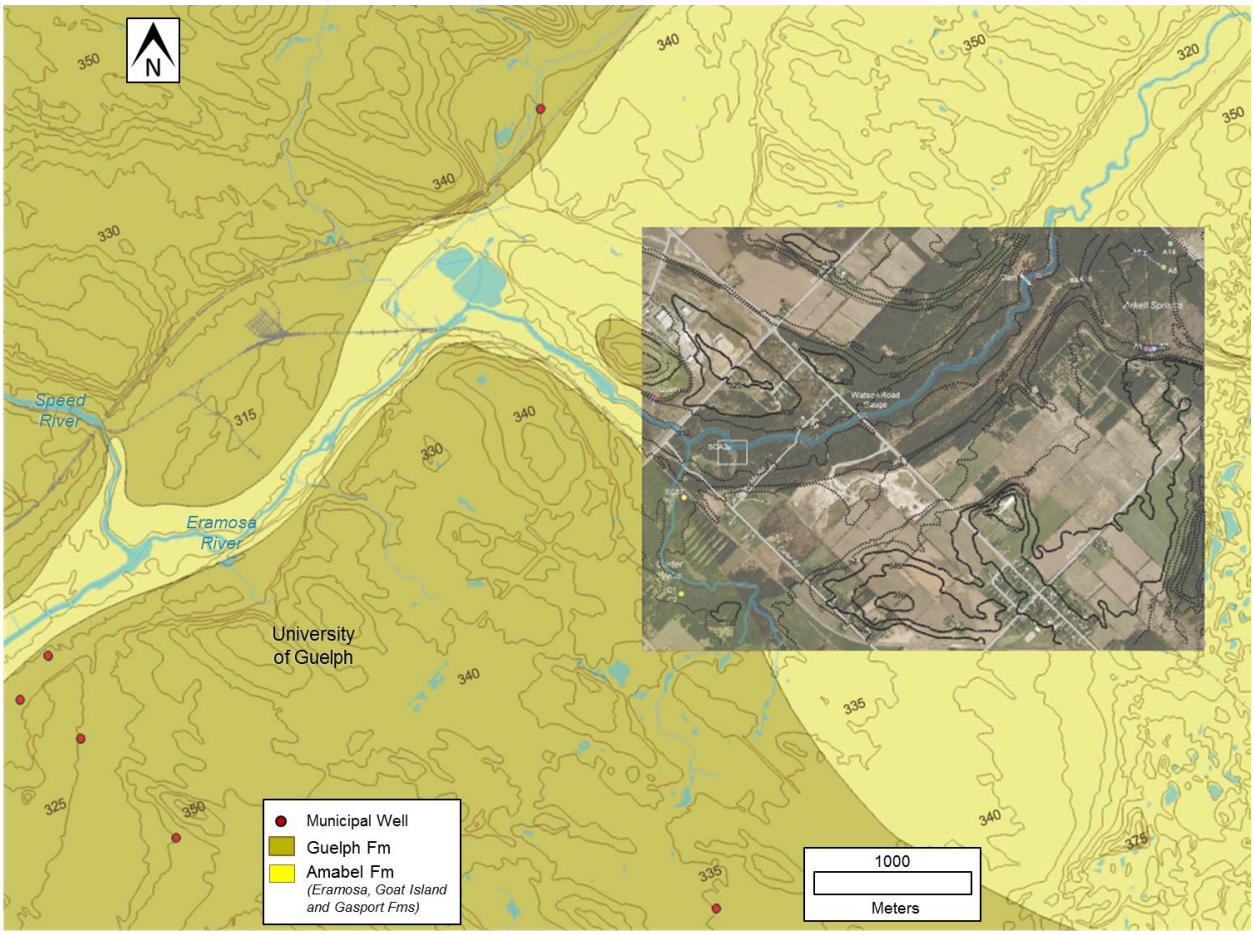

Figure 1.9. Basin-scale map of paleo geology and topographic surface contours (adapted from Gartner Lee 2004) with inset of Figure 1.7, putting sub-basin containing study site into regional context. [NAD 1983 UTM Zone 17N Geographic Coordinate System; GRCA 2015; ESRI ArcMap v.10.2.1].

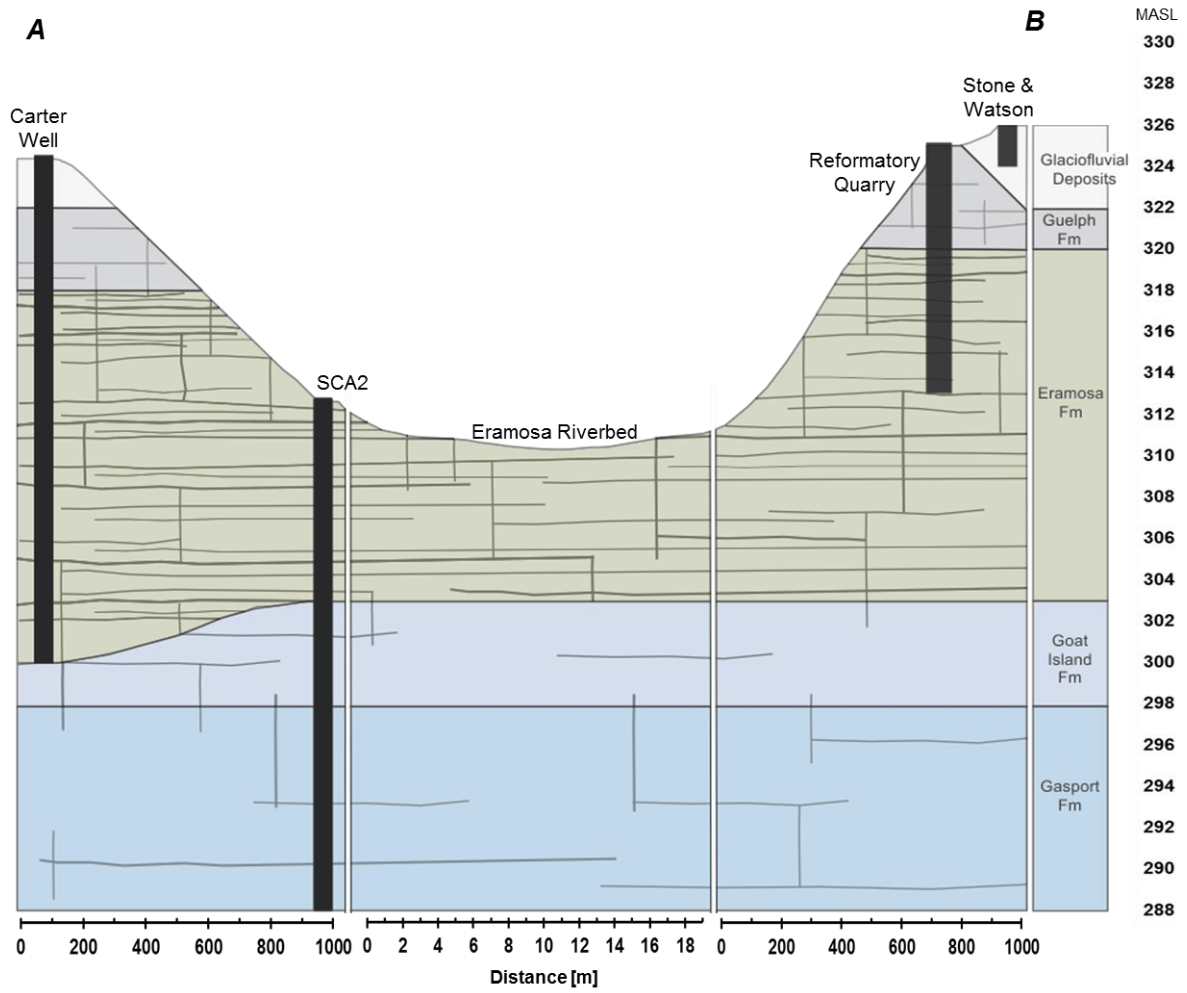

Figure 1.10. Generalized geologic cross-section of the study site, extended 1 km north and south of the channel shown as Transect A – A' in Figure 1.7, and including findings from the Carter Wells (Opazo *et al.,* 2016) and the Reformatory Quarry (Brunton 2009).

Chapter 2: A New Device for Quantifying Flux across the Groundwater - Surface Water Interface of an Intact Bedrock Riverbed

2.1 Introduction

Seepage meters have been used to measure groundwater discharge and recharge across the alluvial beds of lakes and rivers since the late 1970s (Lee 1977; Lee and Cherry 1978; Lee and Hynes 1978), but little work has been done in the measurement of similar parameters in surface water bodies bounded by bedrock. Based on Darcy's Law [1856], the seepage meter was initially designed to quantify nutrient inputs to surface water from groundwater discharge through an alluvial lake or river bed (Lee and Cherry 1978); a concept based on a device created by Israelsen and Reeve (1944) to measure seepage losses along irrigation canals. Constructed from the 30-cm-long end-cut of a 208-L steel drum and covering a surface area of 0.25 m^2, the thin metal skirt of the alluvial seepage meter is forced into the streambed sediments to form a seal, so that groundwater can be captured into its raised profile. Given the nature of Lee and Cherry's (1978) design, which relies on the collapsing, self-sealing properties of a granular medium, attempts made to deploy seepage meters in bedrock rivers were limited to only sediment-covered reaches (Alexander and Caisse 2003; Oxtobee and Novakowski 2002). This author knows of only one study where a seepage meter was deployed in an intact bedrock environment. Shinn et al., (2002) had limited success deploying a number of variations of the Lee design in a marine environment, using hydraulic cement to seal the device to the ocean floor, in the absence of granular sediment. In these studies, the substantial size of the seepage meter was retained from Lee and Cherry's (1978) design and the equivalent porous media (EPM) approach to quantifying flux was not modified to accommodate a fractured rock environment. Modifications to Lee and Cherry's (1978) seepage meter, incorporating continuous record capability with data-loggers and electronic flow meters, have been reported (Fritz et al., 2009; Rosenberry and Morin 2004; Krupa et al., 1998; Taniguchi and Fukuo 1993). These modifications, however, are elaborate and expensive and their use is limited to alluvial environments that can accommodate cables and on-shore computer installations for data-logging.

Since groundwater flow across a fractured sedimentary rockbed is dominated by its discrete fracture networks (Parker 2007; Parker *et al.*, 2012), a different approach using a smaller device recessed into the rock matrix where fractures are intersected, may be more appropriate for measuring groundwater discharge or flow (Q). It would also be beneficial to include in this device design, the wireless capacity to measure hydraulic head as a useful feature for quantifying head differentials between groundwater and surface water (Δh) and vertical hydraulic gradients (i) over space and time. With independent measurements of Q and Δh, average linear groundwater velocities ($\bar{v}$) and specific capacities ($Q/\Delta h$) can be derived to evaluate transmissivity and hydraulic connectivity of the intersected fractures and bedding planes within the streambed. Figure 2.1 summarizes the direct field measurements attainable with this multi-purpose tool and the indirect parameters that can be derived from those measurements.

This study was undertaken to develop a seepage meter – short interval well hybrid device to identify locations and periods of groundwater discharge along a segment of intact sedimentary bedrock riverbed, where vertical joints and bedding plane fractures are visible at surface. Coined the "bedrock seepage meter", or BSM, its compact design intercepts the channel fracture network to a depth of 0.30 m and is sealed from the river by a 0.05-m rubber packer. Head differentials between groundwater and surface water are measured in the unit with a potentiomanometer or by pressure transducer. The device is portable, simple to use, economical to build, minimally invasive to install and robust enough to withstand winter anchor ice. The BSM is partnered with a bedrock river stage gauge (instrumented with a transducer) and a sealed riverbed piezometer, installed to a depth of 3.0 m with a light-weight portable rock drill, to monitor groundwater beneath the channel.

The goal of this paper is to introduce a design for a bedrock seepage meter device that has multiple functions and present data from application of an advanced method at the bedrock river field research station to demonstrate its ability to measure groundwater flow into surface water, the direction and magnitude of head differentials between groundwater and surface water, as well as other hydraulic

and water quality parameters, in support of an evaluation of its performance for quantifying groundwater – surface water interactions in bedrock rivers.

2.2 Background

2.2.1 Differences between Bedrock Rivers and Alluvial Rivers.

The nature of groundwater – surface water interactions in a bedrock river is distinctly different from that of an alluvial channel, lined with sand and gravel. The term "bedrock river" refers to surface water flowing along an exposed bedrock riverbed. Commonly formed by glacial meltwater, these rivers are often found at the lowest elevation in the watershed, stripped of their protective overburden and lacking in fine granular sediments. Differences in flow patterns and exchanges between groundwater and surface water in these two classes of channel have been observed, largely due to their disparate erosional processes and resultant geomorphologies. Conceptual models of two gaining rivers are presented in Figure 2.2. Groundwater discharge through an alluvial streambed crosses equipotential lines and flows towards sediments beneath the channel, where hydraulic conductivities are higher (Figure 2.2A). An alluvial river generally exhibits a granular or unconsolidated bed with the sediment transport capacity to aggrade and degrade over a very short timescale (i.e., seasons or flood events) so that its channel geomorphology remains relatively constant (Leopold and Wolman 1960) (Figure 2.2A-B). Effective porosity of a sand-gravel bed is large, ranging from 25 – 50% (Freeze and Cherry 1979), while diffuse flow through its alluvial matrix is slow (i.e. centimeters per day) and groundwater – surface water exchanges with the underlying aquifer are influenced by the size, shape and orientation of its porous sediment (Woessner 2000; Winter *et al.*, 1998; Lee and Hynes 1978). A sedimentary bedrock riverbed is typically dominated by planar or irregular exposed rock, horizontally-bedded and exhibiting longitudinally-stepped or terraced profiles weathered along joint sets, knickpoints and fragmented bedding planes due to unidirectional denudation over a geologic timescale (i.e., centuries or longer) (Tinkler and Wohl 1998; Miller and Cluer 1998). Effective fracture porosity of sedimentary bedrock is small, ranging from 1 – 0.001% or 10^{-2} – 10^{-5} (Freeze and Cherry 1979; Parker 2007; Lipson *et al.*, 2005;

Muldoon and Bradbury 2005), while advective flow through its discrete fracture networks is fast (i.e., tens of meters per day) and groundwater – surface water exchanges are influenced by the connectivity between the river and the channel aquifer, which is a function of fracture aperture, length and orientation.

In the case of both bedrock and alluvial beds, erosional forces carve out pools and deposit sediment in riffles, and channel water moves into and out of mounds of streambed material, mixing with the groundwater along its path, due to downstream differential pressures. It circulates through the shallow streambed environment, often entering the subsurface at the heads of riffles and then reappearing at the heads of pools (Dumouchelle 2001; Woessner 2000; Woessner 1998; Harvey and Bencala 1993; Hendricks and White 1991). Since the rigid channels of bedrock rivers are more challenging to instrument, our hydrogeologic understanding of groundwater – surface water exchanges is biased toward alluvial river conceptual models, assuming flow through granular media. Given their inherent differences, however, knowledge gained from alluvial systems is not necessarily transferable to fractured rock systems.

2.2.2 Field Site Description

In this study, field tests of the BSM device were conducted along a 1110 m^2 segment of the Eramosa River, in Guelph, ON, Canada, where fractured sedimentary bedrock is exposed along its streambed and floodplain (Figure 2.3). The site was selected to field-test this new device because the riverbed aquifer is an expansive intact dolostone outcrop, exhibiting horizontal bedding partings with vertical joint sets that terminate at surface forming a 3-D fracture network. The study reach encompasses a riffle-pool-riffle sequence over a channel length of 70 m within a river bend. Channel width is 18 – 20 m and depth of the surface water column ranges from 0.1 m in summer to 0.8 m during spring freshet. Anchor ice is often observed in the study reach prior to the formation of surface ice cover in mid-January, which generally remains for about 3 months. Three bedrock seepage meters out of 24 installations, identified as BSMs 4, 10 and 15 *("the subset")*, and the data collected from them, were selected for this chapter to demonstrate the nature of the data obtainable from these devices, the range of

values and reproducibility of results, based on different installation types and locations in the channel (Figure 2.3).

2.2.3 Streamflow Conditions for Reporting

Since groundwater – surface water interactions can behave very differently in high and low river stage conditions (NHC 2010; Madsen and Skotner 2005; Oxtobee and Novakowski 2002; Dingman 2002; Palmer 1993; Hynes 1983), results are reported in a split format to minimize variability and permit the detection of differences in groundwater discharge influenced by a changing water table. Hourly streamflow, measured at Watson Road Gauging Station, and managed by the Grand River Conservation Authority (Cambridge, ON, Canada), was used to categorize river conditions. High river stage at the study site coincides with streamflow values >1.5 m^3/s at Watson Road, while low river stage corresponds to streamflow <1.5 m^3/s (Figure 3.3). This designated threshold of 1.5 m^3/s is an assignment of a streamflow value recorded by a nearby government gauging station that coincides with observed declines in river stage at the study site; thus, it is an independent benchmark upon which to define high and low river stage conditions for the purpose of data analysis and interpretation.

2.3 Device Design and Installation

The BSM, depicted in Figure 2.4A-C, is a low-profile design that fits into a 0.10-m diameter cavity drilled into the riverbed to a depth of 0.30 m with a DR520 portable concrete drill (Norton Construction Products, Stephenville, TX, USA) and a diamond coring bit, supported above the river stage with scaffolding. This cavity serves as the BSM interface to the groundwater beneath the river (i.e., groundwater flows into the cavity from flowing fractures that intersect the cavity). It intersects a horizontal area at the bottom of 0.008 m^2 and a vertical cylindrical area of 0.08 m^2. Figure 2.4D is a photo of the core retrieved during the installation of 12 BSMs at the field site with the top and bottom of different seepage cavity cores marked with a yellow line. This photo shows that: (1) the core is smooth where the rock is intact, (2) horizontal fractures are ubiquitous in all cavities, and (3) vertical fractures are

present in some of the cavities. The depth and diameter of the cavities easily accommodate physical inspection by running a hand over their walls. In this case, very little roughness or broken zones due to missing pieces of rock were detected upon inspection of the cavity walls. The core hole depth of 0.30 m was chosen for BSM installations to maximize recovery while minimizing the strain on portable drilling equipment and challenges with core retrieval that increase with depth. Further, this depth can accommodate a range of transducers.

The BSM consists of a modified 0.10-m diameter J-plug™ (Koby Environmental, Clarence, NY, USA), with a 0.05-m thick expandable rubber packer, which seals the drilled cavity from the channel (Figure 2.4A). A stainless steel centre bolt [1.9-cm (¾-inch)] replaces the plastic standard found in off-the-shelf J-plugs™, to control expansion of the packer. The riverbed dolostone in this study exhibited a high frequency of bedding plane fractures. Experience has shown that packer seal integrity is maximized by distancing the cavity at least 0.05 m from a vertical fracture terminating at the channel surface (Figures 2.4A*i,* 2.4B), and that drilling directly on a vertical fracture can compromise any existing plane of weakness in the rock strata, resulting in breakage when the packer is expanded (Figures 2.4A*ii,* 2.4C). This mechanical vulnerability was not observed in seepage cavities intersecting either vertical fractures that terminate beneath ground surface, or that pass through the cavity beneath the packer (Figure 2.4A*iii*).

A stainless steel tube [7.6 x 1.3-cm (3 x ½-inch)] is fed through a drilled hole in the plastic cap of the J-plug™ and connected to a brass ball valve [1.3-cm (½-inch)], with brass compression fittings [2.2-cm (7/8-inch)], the outlet of which connects to a polyvinyl tube (1.3-cm OD; 1-cm ID). The ball valve allows the BSM to be easily fit into cavities with low permeability by allowing water to escape from the cavity during installation. Seepage is collected in an expandable polyvinyl Hefty—Alligator™ 3.7-L storage bag (Reynolds Consumer Products, Lake Forest, IL,USA), *("the collection bag"),* affixed to the tube by a barbed brass connector and an elastic band (Figure 2.5). Field tests of an earlier prototype yielded two key observations resulting in design modifications to improve mechanical efficiency of the BSM: (1) integrity of the seal was compromised when packer thickness was too small, at 3 cm, which

was increased to 5 cm; and (2) volumetric flow was constrained by inadequate tube and valve diameter of 0.64 cm (¼ inch), which was increased to 1.3 cm (½-inch) (Russoniello and Michael 2015; Belanger and Montgomery 1992).

Canadian winters influence streamflow and its management through the ice-effect phenomenon, where the high rate of cold temperature-related equipment failures may be confused with valid data during episodes of re-arrangement of ice in the channel (EC 2003). During the winter 2014-15, no physical or data-collection equipment failures were observed among the 30 BSM, river piezometer and stage gauge devices installed at the study site.

2.4 Measurement Methods

2.4.1 Measuring Volumetric Flow (Q)

To measure flow (Q), the polyvinyl tube and collection bag, pre-wetted to reduce friction and collapsed to remove air resistance (per insights from Lee and Cherry 1978; Lee and Hynes 1978; Lee 1977), are attached to an in-situ BSM in a two-step process: (1) with the open end of the tube sealed with a thumb or finger, the tube is positioned vertically over the BSM outlet; and (2) the thumb seal is removed as the tube is pushed into the outlet, creating a closed system between the seepage cavity and the collection bag. The pressure differential between the cavity and the river pushes water up the tube towards the bag, moving any air present in the tube into the collection bag. Since groundwater discharges into the bag at the river elevation, it is assumed that the hydraulic gradient becomes fixed and constant and steady state flow will occur within several seconds (Figure 2.5A). When groundwater overcomes the negligible amount of frictional resistance imposed by the polyvinyl tube, evidence of an upward gradient is observed (Figure 2.5B).

Flow (Q) is reported as the volume of seepage collected (ΔV) and measured with a graduated cylinder (± 1%) during a known test time (t) of 10 or 20 min, using a model 228 stopwatch (± 0.01 s) (SportLine, Elmsford, NY, USA) [Equation 1], with two modifications. Since seepage is collected with a

bag and tube attachment that, upon removal, incorporates the volume of water that filled the tube during equilibration, ΔV was corrected for by the tube volume (i.e., 22 cm^3) (Figure 2.5A). Since the observed time to reach constant driving head conditions (i.e., a full seepage tube) was delayed by 30-60 s, t was corrected for by a midpoint value of 45 s ± 15 s,

$$Q = \frac{\Delta V - 22\ cm^3}{t - 45\ s}\ \ [cm^3 s^{-1}] \qquad [1].$$

A sensitivity study was conducted to evaluate the impact of test time (t) on measured steady-state flow (Q). A series of short tests (i.e., $t = 10$ min) and long tests (i.e., $t = 20$ min) were conducted over a 2-week period at high and low stage (n = 216). In 54% of the tests, Q was higher in the short tests; in 27% of the tests, Q was higher in the long tests, and in 19% of the tests, there was no difference in Q between the short and long tests (data not shown). Thus, a steady state condition during tests was assumed.

Designed as a short-interval, open-screened artesian well, certain assumptions are associated with the BSM installed in fractured rock, specifically: (1) flow out of the well occurs in an upward vertical direction, through an open valve and tube attached to a collection bag resting on the river surface; (2) steady state flow exists during each BSM flow test (i.e., head is constant with time); and (3) Darcy's Law [1856] is valid. It is further assumed that no Bernoulli effect occurred, given the low-profile design of the BSM, and that no occurrences of obstructed ΔV due to a collection bag twisting in surface water currents were observed (Shinn *et al.*, 2002; Libello and MacIntyre 1994). Uncertainties inherent with Q measurements, being the sum of ± 1% of ΔV and ± 2.7% (when t = 10 min) or 1.3% (when t = 20 min), were added to the standard error (SE) associated with sample size (n = 28 tests per BSM) when reporting mean results.

2.4.2 Darcy Flux (q) and Groundwater Velocity ($\overline{v}$) inferred from Q

Given the geometry of the fractured rock BSM installation, two approaches were considered in calculating Darcy flux (q). Similar to Lee and Cherry (1979), flux (q_1) was computed using the area of the bottom of the cavity (A_1), which is normal to the vertical gradient of interest [Equation 2],

$$q_1 = \frac{Q}{A_1} = \frac{Q}{\pi r^2} = \frac{Q}{\pi(5\ cm)^2} = \frac{Q}{81\ cm^2}\ \ [cm/s] \qquad [2].$$

This geometry is consistent with vertical flow along vertical fractures dominating the flux into the BSM.

Assuming radial flow, flux (q_2) was also computed using the vertical cylindrical surface area of the cavity (A_2) [Equation 3],

$$q_2 = \frac{Q}{A_2} = \frac{Q}{2\pi rL} = \frac{Q}{2\pi(5\ cm)(25\ cm)} = \frac{Q}{798\ cm^2}\ [cm/s] \qquad [3].$$

This approach is built off of the observation of bedding parallel partings intersecting the BSM cavity and dominating the flow into the cavity and upward through the valve.

The radial flow scenario [Equation 3] was chosen as a more accurate method of determining flux, since the streambed dolostone in this study exhibited a high frequency of bedding plane fractures compared to vertical fractures and a low-porosity matrix of 1.4% (data not shown). Thus, it was assumed that flow is dominated by the fractures and that the bottom of a seepage cavity had a higher probability of intersecting intact low-porosity matrix rather than a vertical fracture. Fluxes (q_2) in the subset shall herein be referred to simply as q. Uncertainties inherent with mean q values originate with their root Q measurements.

For densely-fractured aquifers, there are often questions as to whether the EPM or continuum approach is valid at the problem scale. The techniques described above for calculating q are EPM methods that assume a homogeneous, isotropic formation, where conductivity distribution requires good hydraulic connection of a fracture network to the BSM. In studies of contaminant migration in sand and gravel, average linear groundwater velocity ($\bar{v}$) is estimated from q divided by effective porosity of the media (ϕ_m), which is accepted as ranging from 25 – 50% or 0.2 – 0.5 (Freeze and Cherry 1979). While this concept is also applicable in fractured rock, $\bar{v}$ is equal to q divided by the bulk fracture porosity (ϕ_f) and for intact fractured rock, effective porosities are very small, with values in the order of 1 – 0.001% or 10^{-2} to 10^{-5} (Freeze and Cherry 1979; Parker 2007; Lipson *et al.*, 2005). For dolostone, Muldoon and

Bradbury (2005) reported ϕ_f values of 10^{-2}, while Munn (2012) and Belan (2010) reported ϕ_f values of 10^{-4}. Average linear groundwater velocities ($\bar{v}$) through the seepage cavities were, therefore, estimated using q divided by an estimated fracture porosity for weathered streambed dolostone of 0.1% or 10^{-3} [Equation 4]. An expected outcome, then, is that $\bar{v}$ is much faster in fractured rock than in porous media,

$$\bar{v} = \frac{Q}{A * \phi_f} = \frac{q}{\phi_f} = \frac{q}{10^{-3}} \quad [m/s] \qquad [4].$$

2.4.3 Measuring Head Differentials between Groundwater and Surface Water

The BSM accommodates a range of transducer types and head differentials between groundwater and surface water can be measured by way of two independent methods, giving differential head (Δh) and relative head difference (Δh_{rel}). Since the BSM functions like a small monitoring well (Figure 2.6A), it is assumed that: (1) the well fully penetrates the hydrogeologic unit of infinite extent, overlain by a constant head boundary (i.e., the river); (2) the hydrogeologic unit is partially-to-fully confined, being separated from the river by a 0.05-m layer of dolostone with low matrix permeability and a high frequency of vertical fractures terminating at surface; (3) diameter of the well is 0.10 m and thickness (b) of the hydrogeologic unit intersected is 0.25 m; and (4) flow into the well through the formation is radial, non-uniform and likely exhibits an oblong cone of depression when withdrawal exceeds aquifer recharge [Thiem 1906]. In this shallow interval, the hydrogeologic unit is a sequence of layers of bedding or strata.

Groundwater head or total hydraulic head in the seepage cavity (h_2) was calculated as:

$$h_2 = h_{p2} + h_{z2} \quad [m] \qquad [5],$$

where pressure head (h_{p2}) was measured using absolute (non-vented) wireless SWS Mini-Divers™ and Micro-Divers™ (Schlumberger Water Services, Delft, The Netherlands) with the transducer suspended in the BSM by a steel cable at a depth of 0.30 meters below ground surface (mbgs). Elevation head (h_{z2}) was measured using a Leica Viva GS08plus GPS (Leica Geosystems Inc., Norcross, GA, USA) at ground

surface ± 0.01 m (Figure 2.6A). Groundwater head in the subset, measured each morning prior to conducting seepage tests, ranged from 310.91 m above sea level (masl) ± 0.02 m at low stage, to 311.10 masl ± 0.02 m at high river stage conditions (Table 2.1). Velocity head (h_v) in the seepage cavities, estimated from flux values as 10^{-6} to 10^{-7} m/s, was assumed negligible and, therefore, not included in the h_2 calculation. A sensitivity test was conducted to evaluate constant head conditions and the time lag to reach equilibrium in the BSMs during seepage tests. Transducers programmed at 1-s intervals were deployed in five BSMs during two 24-hour tests (n = 10). Pressure head stabilized in all BSMs within 15 to 20 s, therefore, constant head during tests is assumed (data not shown).

Surface water head or total hydraulic head in the river (h_1) was calculated as:

$$h_1 = h_{p1} + h_{z1} + h_v \quad [m] \qquad [6],$$

where pressure head (h_{p1}), or river stage, was measured with centralized stage gauges (SG) at upstream and downstream locations (Figures 2.3.and 2.6B), as well as with a bathymetric tool, consisting of a tape measure enclosed in a Plexiglas™ stilling tube to dampen turbulence, to collect localized river depth measurements near each BSM ± 0.0005 m (Figure 2.6C). Findings revealed that the accuracy of centralized stage gauge measurements was adequate for transient monitoring; however, the precision of localized measurements was necessary for tests conducted under steady state conditions, since river stage can be sloped, particularly along channel meanders influenced by centrifugal force (Legleiter et al., 2011; Tinkler and Wohl 1998; Harvey and Bencala 1993). Elevation head (h_{z1}) was measured at ground surface as previously-described. Localized velocity head (h_v) in the river was estimated according to [Equation 7] (Hichin 2004; Freeze and Cherry 1979; Lambe and Whitman 1969),

$$h_v = \frac{v^2}{2g} \qquad [m] \qquad [7],$$

where:

h_v = velocity head [m]

v = laminar or streamflow velocity [m/s]

g = acceleration due to gravity [m/s^2]

Streamflow velocities (v) ± 2% were measured near each BSM at 60% of the channel depth using a Flo-Mate 2000 flow meter and a wading rod (Marsh-McBirney Inc., Frederick, MD, USA) and computed using the velocity-area method (ASTM D3858; Dingman 2002) (Figure 2.6D). Surface water head in the subset, measured each morning prior to conducting seepage tests, ranged from 310.81 masl ± 0.02 m at low stage, to 311.04 masl ± 0.02 m at high river stage conditions (Table 2.1). It is assumed that both the bathymetry tool and the wading rod were held perpendicular to a horizontal channel surface.

Differential head (Δh) was calculated using the independent measurements of groundwater head and surface water head [Equation 8]. Uncertainties inherent with head measurements, being the sum of accuracies of the transducers (± 0.005 – 0.01 m), the bathymetry tool (± 0.0005 m), the GPS (± 0.01 m), and the flow meter (± 2%), were added to the standard error (SE) associated with sample size (i.e., n = 5 high stage days and 7 low stage days) when reporting mean Δh results,

$$\Delta h = h_2 - h_1 \quad [m] \qquad [8].$$

Relative head difference (Δh_{rel}) between groundwater and surface water was measured directly with a potentiomanometer (Winter *et al.*, 1988) designed for use with the BSM (Figure 2.6E), that works on the principle that relative heads will not change when they are raised under common suction. A flexible Tygon® tube seals the BSM outlet and, with all valves open, seepage and surface water are drawn into the manometer under suction applied with a model 2500 vacuum pump (KAL Equipment Ltd., Vernon, BC, Canada) and preserved with a pinch clamp. Once the bubble level at the top of the unit and the oscillating water levels in the manometer tubes stabilize, groundwater and surface water heads under suction are recorded and relative differential head is quantified according to Equation 9, with very small uncertainties (ie ., ± 0.0005 m).

$$\Delta h_{rel} = h_2 - h_1 \quad [m] \qquad [9].$$

2.4.4 Vertical Gradients (i) from Head Differentials

Spatial distribution of potentiometric surfaces and vertical gradients along a streambed can be evaluated from differential heads measured at each BSM. Vertical gradients (i) across a 0.05-m layer of fractured dolostone (ΔL) due to the BSM packer thickness were estimated as:

$$i = \frac{\Delta h_{rel}}{\Delta L} \qquad [10].$$

2.4.5 Indirect Evaluation of Hydraulic Properties

Geometry of the BSM installation in the formation makes the Thiem equation, derived from Darcy's Law for steady-state radial flow to a well, appropriate for estimating hydraulic conductivity (K) or transmissivity (T) of the dolostone fracture network [integrated simplified version],

$$T = Kb = \frac{Q}{2\pi(h_2 - h_1)} Ln\left(\frac{r_2}{r_1}\right) \qquad [11],$$

where:

Q = flow through any cylindrical section of aquifer toward BSM

b = aquifer thickness, assumed to be 25 cm

h_1 = surface water head

h_2 = groundwater head

r_1 = radius of seepage cavity, being 5 cm

r_2 = estimated radius of influence.

Since effective radius of a well (r_2) is difficult to estimate accurately (Jacob and Lohman 1952), steady state specific capacity ($Q/\Delta h_{rel}$) was selected as an alternative parameter to evaluate the relative hydraulic property variability of the streambed aquifer with the direct measurements attainable from the BSM. Specific capacity refers to the transmissivity or productivity of a well, defined as the flow or pumping rate (Q) divided by the drawdown or change in hydraulic head (Δh_{rel}) in the aquifer at the well screen boundary (Theis *et al.,* 1963; Freeze and Cherry 1979) [Equation 12]. A linear relationship has been observed between specific capacity and transmissivity (T), (Razack and Huntley 1991; Thomasson *et al.*, 1960; Jacob and Lohman 1952).

$$\text{Specific Capacity} = \frac{Q}{\Delta h_{rel}} \quad \left[\frac{m^2}{s}\right] \qquad [12].$$

2.4.6 Geochemical Sampling with BSMs

The BSM design allows for geochemical sampling of groundwater in the shallow bedrock. Volumetric flow (Q) collected with the BSM was transferred to sample bottles for major ion analysis as a source of water quality data to answer any number of scientific questions. In this study, in order to evaluate groundwater – surface water interaction in the seepage cavities, concentrations of targeted major ions were measured in samples collected from the river and from piezometers, P3 and P5 (Figure 2.3).

These low-profile river piezometers were drilled 3.0 m into the streambed with the Shaw Backpack Drill™ (Shaw Tool, Yamhill, OR, USA) and a 5-cm-diameter diamond coring bit (Figure 2.7A). A 0.4-m-long screen was sealed at a depth of 2.6 mbgs with a stainless steel casing [2.54 cm (1-inch) ID] using the grout-in-place method (Pierce *et al.,* 2017). The casing accommodates an SWS Micro-Diver™ (Schlumberger Water Services, Delft, The Netherlands) for monitoring and is sealed at the streambed surface with a threaded brass collar and plug (Figure 2.7B). A threaded removable PVC standpipe is used to collect manual water levels and water samples (Figure 2.7C) with a Geopump peristaltic pump (Geotech Environmental Equipment, Inc., Denver, CO, USA). Until recently, there were no studies known to the author of anyone using the concept of a low-profile piezometer sealed at the streambed surface for long-term deployment. Noorduijn *et al.* (2015) reported successful use of non-vented pressure transducers in a sealed monitoring well field-tested in an alluvial stream. Head differentials between the surface water and the groundwater at 3.0 mbgs were used in conjunction with geochemistry to evaluate hydraulic gradients across the streambed.

Nitrate concentrations [NO^-_3] were measured in 100-mL filtered (0.45-µm) samples, using ion chromatography (EPA 300.0); analysis completed by ALS Global Laboratories (Waterloo, ON, Canada).

Mass fluxes of nitrate flowing through BSMs 4, 10 and 15 were also estimated [Equation 13] (Guilbeault *et al.*, 2005),

$$\left(Q\frac{m^3}{s}\right)\left([NO_3{}^-]\frac{mg}{L}\right)\left(1000\frac{L}{m^3}\right) = Mass\ Flux\ \frac{mg}{s} \qquad [13].$$

2.4.7 Transient Measurements of Temperature and Hydraulic Head

The BSM, river piezometer and stage gauge designs were field-tested over a 1-year period (May 2014 – May 2015), instrumented with a range of transducers to collect continuous records of pressure and temperature at 15-min intervals. In the BSM, a blended head condition (Lambe and Whitman 1969) exists in the 0.25-m open interval below the 0.05-m packer seal. Choice of transducer for monitoring pressure head in the BSMs installed in shallow river environments is critical to achieving accurate results. The 10-m SWS Divers™ (Schlumberger Water Services, Delft, The Netherlands) used in this study were economical and provided consistent results. Accuracy of the CTD- and Mini-Divers™ were marginally better (at ± 0.05%) than the Micro-Diver™ (at ± 0.1%); however, uncertainties could be improved by refining the manufacturer's programming for use in depths of < 3 m and deploying all the same model of transducer from the same batch (i.e., age) because transducers drift over time. Accuracy of pressure transducers is quantified by manufacturers as a percentage of their full scale or range. All transducers underwent calibration tests to verify their proximity to true measured depths (and whether or not that value is within the prescribed accuracy for that model) and resulting calibrated correction factors were applied to raw data collected. This procedure should be conducted before and after deployment and/or at regular intervals, since transducers drift over time.

2.5 Data Analysis and Performance Evaluation

In this section, data collected from the subset is presented to demonstrate the BSM's capacity to directly measure groundwater flow and head differentials between groundwater and surface water, and to evaluate its performance. Since interactions between groundwater and surface water are influenced by channel topography (Dumouchelle 2001; Woessner 1998; Harvey and Bencala 1993; Toth 1970; Hubbert

1940), it is important to identify the installation type and environment of the BSMs relative to one another when assessing results. The BSMs in the subset are installed at elevations between 310.43 – 310.49 masl; therefore, it is likely that they intersect at least some of the same stratigraphic layers. BSM 4 is installed on a vertical fracture terminating at surface (Figures 2.4Aii; 2.4C), in the downstream pool near the end of the longitudinally-stepped riverbed profile (Figure 2.2). BSM 10 is installed on a vertical fracture terminating beneath the packer (Figures 2.4Aiii; 2.4B), in the pool centre. BSM 15 intersects only bedding plane fractures (Figure 2.4Ai), in the upstream riffle – pool transition zone.

2.5.1 Groundwater Velocities in Streambed Fracture Networks

Flow (Q) observed in the BSM study subset increased in a downstream direction (i.e., BSM 15 < BSM 10 < BSM 4) in both high and low river stage conditions, ranging from 3 – 36 mL/min ± 16 – 24% (Table 2.2). Groundwater fluxes (q) in the subset ranged from 10^{-7} – 10^{-6} m/s, or 3 – 64 cm/day (Figure 2.8A; Table 2.2), which is reasonable, given that the overall magnitude of q variations in fractured rock is generally the same as for granular media (Parker 2007; Freeze and Cherry 1979). Using traditional seepage meters, Oxtobee and Novakowski (2002) reported fluxes in the sediment-covered segments of a bedrock river of $2x10^{-4}$ m/s and Alexander and Caisse (2003) reported fluxes in the sand-and-gravel-covered reaches of a bedrock river as $2x10^{-10}$ – $2x10^{-6}$ m/s. In alluvial environments, Lee (1977) reported fluxes ranging from $1x10^{-7}$ – $3x10^{-6}$ m/s in lakes and estuaries with thick sediments. Lee and Hynes (1978) reported fluxes in a sand-and-gravel riverbed of $1x10^{-9}$ – $9x10^{-6}$ m/s. Shaw and Prepas (1990) found q-values of $3x10^{-10}$ – $2x10^{-7}$ m/s in granular lakebeds. Toran *et al.*, (2015) measured downward fluxes of 0 to $-3x10^{-5}$ m/s in lakebed sediments.

Flux values appear to correlate to both position along the channel and exposure to vertical fractures. In the upstream pool head, BSM 15, intercepting only bedding plane fractures, yielded fluxes of 3 – 6 cm/day. In the pool, BSM 10, intercepting a vertical fracture below its packer, showed fluxes of 19 – 37 cm/day. BSM 4, located downstream in the pool and intercepting a vertical fracture terminating at surface, yielded fluxes of 63 – 64 cm/day.

Average linear groundwater velocities ($\bar{v}$) estimated from q-values and an estimated fracture porosity (ϕ_f) for weathered streambed dolostone of 0.1% or 10^{-3} ranged from 54 - 635 m/day (Table 2.2). In tracer tests, commonly used to measure groundwater velocities, Perrin *et al.,* (2011) reported values of 50 – 550 m/day for dolostone from unpublished consultant studies conducted in Cambridge, ON, Novakowski *et al.,* (1999) reported $\bar{v}$ of 30 m/d, and Muldoon and Bradbury (2005) reported 0.5 – 32 m/d. While the variability of q in fractured rock is similar to that of porous media, given their vast difference in porosities (i.e., $\phi_m >> \phi_f$), the range of $\bar{v}$ in fractured rock is orders-of-magnitude larger than that of granular media (Parker 2007). For example, very small groundwater velocities were reported for sand-silt-clay, as $5x10^{-5}$ – 1.0 m/d (Conant 2004) and for clay-till, as $4x10^{-6}$ – $7x10^{-6}$ m/d (Desaulnier *et al.,* 1981).

Groundwater velocities reported in this study are based on estimates of the bulk fracture porosity for dolostone and the uncertainties associated with it, since tests to estimate hydraulic apertures intersecting the BSMs were not conducted. Quinn *et al.,* (2011) estimated $\bar{v}$ in dolostone from fracture apertures, using constant head step tests and cubic law, ranging from 0.9 – 50.8 m/day where a single fracture is assumed, and from 0.3 – 11.7 m/day where the number of fractures identified in the core log is assumed; and further, refers to the challenges associated with identifying the number of hydraulically-active fractures. Similarly, Novakowski *et al.,* (2006) used tracer tests to estimate $\bar{v}$ for limestone as 1 – 33 m/d for a single fracture and 2 – 388 m/d for the bulk fracture network.

In sum, BSM test results yielded reasonable measurements for volumetric flow and approximated values for flux and average linear velocity of groundwater in fractured dolostone.

2.5.2 Hydraulic Head Differentials and Gradients in a Bedrock Riverbed

Head differentials (Δh) between groundwater and surface water using BSM transducers and bathymetric measurements ranged from 0.01 – 0.10 m ± 0.03, due to cumulative transducer uncertainties (Table 2.1). Groundwater – surface water relative head differences (Δh_{rel}) from potentiomanometer

measurements ranged from 0.001 – 0.023 m ± 0.001, based on the accuracy of the potentiomanometer (Table 2.1). Relative head difference (Δh_{rel}) declined in a downstream direction (i.e., BSM 15 > BSM 10 > BSM 4) at both high and low river stage, while differential head (Δh) showed almost no significant differences between the subset BSMs, with the exception of BSM 4 at high stage.

The most notable observation when comparing Δh with Δh_{rel} is the order-of-magnitude difference (i.e., $\Delta h >> \Delta h_{rel}$). The constant head boundary of the river and the low-permeability of the dolostone matrix are known variables, but the hydraulic conductivity (K) of the discretely-fractured dolostone is not known. Hydraulic potential measurements, according to Hubbert (1940), reflect flow from high head to low head, or in the direction of decreasing head, as indicated by a minus sign in Equation 14 [Darcy's Law 1856], and the distance between groundwater and surface water across a dolostone boundary is equivalent to the packer seal thickness (i.e., $dL = 0.05$ m),

$$q = \frac{Q}{A} = -K\frac{dh}{dL} \qquad [14],$$

where: q = groundwater seepage flux [$m^3\ m^{-2}\ s^{-1}$]
Q = groundwater flow rate [$m^3\ s^{-1}$]
A = area through which seepage occurs [m^2]
dh/dL = hydraulic gradient [differential head (m) / distance (m)]
K = hydraulic conductivity [$m\ s^{-1}$]

Since this is not a one-dimensional flow system in homogeneous isotropic porous medium, but rather, a strongly-anisotropic network of discrete fractures, each point measurement of differential head at a BSM location contributes to only one small component of the hydraulic gradient. It is to be expected, then, that head differentials between groundwater and surface water would be very small, as measured with the potentiomanometer. For example, in any anisotropic system, whether alluvial or fractured rock, hydraulic conductivity (K) varies with the direction of measurement at a point in the geologic formation. In alluvial systems, where flow through granular media is diffusive, vertical head losses occur as groundwater flows upward through layers of different grain size, orientation and K. In thinly-bedded dolostone, flow through

fractures is advective and the ratio of horizontal-to-vertical fractures is biased toward lateral groundwater flow. Hence, groundwater flowing along many highly transmissive bedding plane fractures relies on connectivity with few vertical fractures to discharge through the channel into the river. In other words, anisotropy favours groundwater discharge in a fractured rock riverbed because a small vertical K connected with a large horizontal K can make a substantial contribution to the vertical component of gradient driving groundwater movement up through the bedrock channel.

The use of potentiomanometers to measure Δh_{rel} in alluvial rivers is common (Ong and Zlotnik 2011; Rosenberry *et al.*, 2008; Winter *et al.*, 1988; Woessner and Sullivan 1984; Lee and Cherry 1978); however, this author is not aware of any studies where this tool was used in bedrock rivers, nor with any installation other than a mini-piezometer or a direct-push probe. None of the common limitations reported in alluvial river studies apply to the case of BSMs in bedrock rivers, such as: slow stabilization times in low-permeability sediments, probes clogged with fine sediments, poor seals in coarse sands and gravels and biogenic gas bubbles from sediments infiltrating the manometer tube. In this study, the potentiomanometer appeared to achieve a good seal at the BSM outlet with relative ease and water levels stabilized within 3-5 min. Lab tests were conducted to confirm that no Venturi effect was observed at the streambed inlet, where smooth intact bedrock likely imposes less resistance to surface water flow than a sand or gravel bed (data not shown).

The accuracy of pressure transducers used in this study and the uncertainties associated with them, particularly where absolute measurements in shallow water are concerned, has already been discussed (in section 2.4.3). While further investigation of the BSM-potentiomanometer efficiency may be useful, the Δh_{rel} data collected in this study appeared more consistent and meaningful than the Δh achieved with individual transducers due to associated measurement uncertainties.

Vertical components of hydraulic gradient between the groundwater and surface water across a thin bed of fractured dolostone, ranged from 0.02 – 0.46 m. Vertical gradients (i) declined in a

downstream direction, while groundwater flux (q) increased, demonstrating an inverse relationship in the subset (Figure 2.8) but typical relationship between observed gradients and permeability. These results may be a consequence of strong anisotropy in the discrete fracture networks of the channel, since a linear relationship between q and i has been observed in porous media (Freeze and Cherry 1979; Rogers and Klute 1971; Olsen and Swartzendruber 1968). It is also recognized that the component of gradient measured is a small contributor to the forces driving the fluxes measured in this complex flow system.

2.5.3 Relating Flow and Differential Head Measurements

Specific capacities ranged from 10^{-6} to 10^{-4} m^2/s, where BSM 4 > BSM 10 > BSM 15 (Figure 2.9). Plotting differential head (Δh_{rel}) versus mean flow (Q) demonstrates an increase in specific capacity, or transmissivity, in a downstream direction that also coincides with increased exposure to fractures (Figures 2.9; 2.4). In other words, BSMs installed on vertical fractures have higher specific capacities, and order-of-magnitude differences indicate variable transmissivities between point measurements in the fracture network.

2.5.4 Nitrate Geochemistry in BSMs

Water samples can be collected from BSMs for geochemical or microbial analysis, routinely sought after to answer questions regarding the origin and quality of groundwater and surface water to assess the extent of their interactions. Sample collection of a time-sensitive nature is easily accommodated by synchronizing collection bag deployment and retrieval. Nitrate concentrations are presented here to demonstrate the use of geochemical analyses to evaluate water quality in the BSMs compared to the river and deeper sources of groundwater in the context of groundwater – surface water interactions. Nitrate (NO^-_3) can be naturally occurring in the subsurface due to nitrogen cycling involving microbial activity in the biosphere, but concentrations can also be elevated due to sewage and fertilizer-derived nitrogen. Nitrate concentrations in BSM 4 and in the river were similar (i.e., 0.71 – 0.73 mg/L ± 0.05), indicating that the high fluxes measured at this location contained a substantial component of

surface water (Figure 2.10). In other words, BSM 4 is likely a recipient of recirculated surface water or strongly influenced by surface water chemistry, with little residence time in the rock or opportunity for nitrate reduction. Perrin *et al.*, (2011) found that large fracture apertures and high groundwater velocities in dolostone were unfavourable factors for nitrate reduction. No significant difference was observed in NO^-_3 concentrations in BSMs 10 and 15, which were 20 – 40% lower in concentration than the river, indicating a smaller component of surface water recirculating through these seepage cavities. It is noteworthy that BSMs 10 and 15 also yielded smaller groundwater fluxes (q). Mass fluxes of nitrate flowing through BSMs 4, 10 and 15 were estimated as 4.E-05, 2.E-05 and 2.E-06 mg/day, respectively. These results indicate that differences in chemical fluxes into the BSMs may be useful in estimating the component of surface water recirculating through the seepage cavities.

Samples of deeper groundwater (i.e., 3.0 mbgs) collected from river piezometers, P3 and P5, yielded non-detects for nitrate (i.e., < 0.10 mg/L). This may indicate an upward hydraulic gradient and upward flow preventing surface water quality influences at these depths or simply that reducing conditions exist at this depth (Carter 2011).

2.5.5 Transient Monitoring of Temperature and Head Differentials

The BSM design allows for deployment of transducers that can provide long-term monitoring of pressure, temperature and hydraulic conductivity (in conjunction with the piezometers and river stage gauges). In this field test, absolute pressure and temperature were the focus, and data are presented here to show the capacity of the BSM to provide insight into transient groundwater conditions within a bedrock riverbed. Two 60-day snapshots were extracted from the 2014-15 continuous records to evaluate differences during two key hydraulic conditions: (1) late summer – early fall, when river stage is very low (Figure 2.11A), and (2) high stage approaching winter freeze-up (Figure 2.11B).

The continuous temperature record of the groundwater in P3 is a smooth line, ranging from 13.7 – 14.7^{o}C in the summer – fall record (Figure 2.11A), which is consistent with the differential head (Δh) that

indicates an upward gradient reflected in the hydraulic record, but also indicates some influence at depth from the warmer overlying channel water, since groundwater in the Guelph Region is generally 10^{o}C (data not shown). Two distinct trends are observed in the summer-fall temperature records for the BSMs. BSM 4 and the river show high variability (i.e., ranging from 10.5 – 22.9^{o}C), fluctuating with atmospheric temperature changes (data not shown), which is consistent with the hydraulic record, where Δh of BSM 4 is close to zero. BSMs 10 and 15 exhibit relatively smaller temperature variations (i.e., ranging from 12.1 – 20.2^{o}C), indicating the moderating effect of groundwater discharging to surface water, which is consistent with the hydraulic record, showing a Δh ranging from 5 – 11 cm above that of the river (Figure 2.11A).

The continuous winter temperature record of the groundwater in P3 is a smooth declining line, ranging from 8.4 – 4.9^{o}C (Figure 2.11B), which is consistent with the upward gradient reflected in the hydraulic record. Since the groundwater temperature in P3 falls below the Guelph Area groundwater temperature of 10^{o}C, the seasonal land surface temperature fluctuations are not completely buffered at 3.0 mbgs, indicating that the temperature envelope or heterothermic zone extends beyond this depth (Anderson 20050; Constantz and Stonestrom 2003). The winter BSM temperature profiles separate so that BSMs 10 and 15 are consistently warmer than BSM 4 (consistent with stronger influence of SW at BSM 4 discussed earlier). In addition, hydraulic head in the BSMs fluctuates erratically as seasonal streambed anchor ice and surface ice form in the channel in mid-January (Figure 2.11B). Groundwater temperatures in BSM 4 declined from 4.3 – 0.4^{o}C, while surface water temperatures fell from 4.5 – 0.1^{o}C (with an uncertainty of ± 0.1^{o}C in all measurements), and a Δh of zero was maintained. Groundwater temperatures in BSMs 10 and 15 fell from 3.9^{o}C – 0.6 and 0.8^{o}C respectively, indicating an influence from warmer groundwater discharging into the seepage cavities, and supported by Δh values ranging from 7 – 11 cm above the river (Figure 2.11B).

2.5.6 Uncertainties

The relative importance of measurement uncertainties increases greatly in shallow and small spatial scale environments, where differences in target measurements are often small. Since pressure transducer accuracy declines with depth range, choice of instrumentation and independent accuracy verification is critical. Pressure transducers were field-tested inside the static water column of a FLUTe™ (Flexible Liner Underground Technologies, Alcalde, NM, USA) and calibrated using the straight-line and differences analysis methods. Temperature accuracies were verified by submerging transducers, programmed to collect data at 30-s intervals, in an Isotemp™ 110 controlled temperature water bath for 2 hours (Fisher Scientific, Toronto, ON, Canada). Temperature and pressure accuracies of the SWS MiniDivers™, MicroDivers™ and CTD Divers™ used in this study were within the manufacturer's specifications (Table 2.3; Schlumberger Water Services, Delft, The Netherlands). Accuracies of the bathymetric tool and potentiomanometer designed in this study were assigned using one-half of the smallest metric scale unit shown on their manufactured rulers (Table 2.3; Taylor 1997). The uncertainties associated with all parameter estimates from BSM measurements in this study are summarized in Table 2.3.

2.6 Conclusions

The bedrock seepage meter (BSM) is an innovative tool design that is extremely versatile in its capacity to advance our understanding of groundwater – surface water interactions in bedrock rivers (Figure 2.1). Initially conceived as an adaptation to Lee and Cherry's (1978) seepage meter for use in alluvial rivers, it features a tube and collection bag for measuring volumetric flow, with ball valves to open and close the system. Drilled into an intact bedrock streambed in order to access groundwater beneath the riverbed, the BSM also serves as a well, intersecting fractures in the aquifer it penetrates to monitor hydraulic head and and in-situ parameters using probes. The BSM is durable, easy to use, cost effective and minimally-invasive to install; important attributes for investigating vulnerable streambed

aquifers. Canadian winters are known to influence streamflow and its management through the ice-effect phenomenon, where the high rate of cold temperature-related equipment failures may be confused with valid data during episodes of re-arrangement of ice in the channel (EC 2003). During the winter 2014-15, no physical or data-collection equipment failures were observed among the 30 BSM, river piezometer and stage gauge devices installed at the study site.

Core from the seepage cavities can be retrieved for fracture logs, physical properties testing (i.e., porosity and permeability) and geochemical analysis. The seepage cavity securely accommodates a range of transducers, for wireless monitoring of hydraulic head, temperature and electrical conductivity, and installation depth can be scaled to the monitoring depth required. The BSM can also be used to collect groundwater samples for hydro-chemical or other water quality analyses. The compact size and low profile is minimally invasive, accommodating long-term monitoring at multiple locations that does not disrupt streamflow (when the valve is closed and the seepage tube is removed) and removes the need for long equilibration times prior to conducting hydraulic tests.

The BSM was successfully field-tested in a shallow bedrock river (i.e., surface water column < 2 m) from 2013-15. Measured flows (Q) of 3 – 36 mL/min in fractured dolostone yielded flux (q) estimates of 10^{-7} – 10^{-6} m/s and fracture velocities ($\bar{v}$) of 54 – 635 m/day (Table 2.2). Measured head differentials (Δh), using transducers and manual depth measurements, of 0.01 – 0.09 m, were up to an order-of-magnitude higher than relative head differences (Δh_{rel}), measured with a customized potentiomanometer, of 0.001 – 0.023 m (Table 2.1). Hydraulic properties of the streambed aquifer were evaluated using parameters derived from direct measurements of Q, Δh, and Δh_{rel} including: vertical components of hydraulic gradient (i), ranging from 0.02 – 0.46, and well specific capacities ($Q/\Delta h_{rel}$), ranging from 7.6 x 10^{-6} to 6.5 x 10^{-4} m^2/s. Vertical components of gradient declined in a downstream direction, while q increased (i.e., BSM 4 > BSM 10 > BSM15) (Figure 2.8), along with transmissivity (indicated by specific capacity estimates) (Figure 2.9).

Hydro-chemical sampling to analyze for major ion concentrations, such as nitrate (NO^-_3), indicate: (1) that concentrations in samples collected from the river and from BSM 4 are similar, and also significantly different from groundwater samples collected at 3.0 mbgs (i.e., P3 and P5); and (2) that concentrations in samples collected from BSMs 10 and 15 are similar, and also significantly different from all of the samples described in (1) above. Nitrate results support hydraulic findings. Transient temperature and hydraulic records indicate: (1) that BSM 4 is connected to the river through similar seasonal temperatures and a negative differential head value; (2) that P3 exhibits an upward gradient, maintaining a positive differential head value and stable groundwater temperatures, minimally affected by the overlying surface water channel; and (3) that groundwater discharge is occurring in BSMs 10 and 15, exhibiting positive (upward) head differentials, moderate temperatures in summer and warmer temperatures in winter.

Direct measurements of flow and head differentials demonstrate a correlation to both position along the channel and exposure to vertical fractures. Specifically, BSM 15, installed in bedding plane fractures in the upstream riffle-pool transition zone yielded the smallest fluxes and largest head differentials and upward component of gradient. BSM 4, installed near the end of the longitudinal profile on a vertical fracture terminating at surface yielded the largest fluxes and the smallest head differentials. BSM 10, installed in the pool on a vertical fracture terminating below its packer, yielded fluxes and head differentials between those of BSMs 4 and 15. Estimates of flux based on steady-state radial flow are in good agreement with derived values for vertical gradient and specific capacity.

Choice of transducer specifications for monitoring absolute pressure head in the BSMs installed in shallow river-groundwater environments is critical to achieving the necessary precision and accuracy. The 10-m SWS Divers™, narrowest range transducers used in this study, were economical and provided consistent results. Accuracy could be improved by refining the manufacturer's programming for use in depths of < 3 m and deploying all the same model of transducer from the same batch (i.e., age) because transducers drift over time. Accuracy of pressure transducers is quantified by manufacturers as a

percentage of their full scale or range. It is recommended from this study that all transducers should undergo calibration tests to verify their individual performance, i.e. proximity to true measured depths (and whether or not that value is within the prescribed accuracy for that model) and resulting calibrated correction factors should be applied to raw data collected to improve the precision and accuracy of the results for such fine-scale studies (maybe need to work in some words on the value of this scale of study, too).

2.7 Future Work

This is the first field test of the BSM design in a bedrock river, where not all of its capabilities were exploited. It also has the potential to accommodate single well hydraulic tests, such as slug tests.

Use of the tube-and-bag attachment presented challenges related to the volume of seepage collected during a known test time, which could be addressed with modification to the test method; whereby, commencing the test with a known quantity of water in the seepage tube , no equilibration time need be accounted for in the flow (Q) calculation.

The accuracy of collection bags to quantify flow in traditional seepage meters has received a great deal of attention over past decades (Rosenberry et al., 2008; Schincariol and McNeil 2002; Fryar et al., 2000; Isiorho and Meyer 1999; Shinn et al., 2002; Cable et al., 1997; Libelo and MacIntyre 1994; Shaw and Prepas 1989; Lee and Hynes 1978; Lee 1977), which is linked to the amount of turbulence or waves in the surface water. Since this study was conducted in calm waters, a field test in deeper, more turbulent waters may be useful to further evaluate the low-profile design efficiency. This study was conducted at a clean site, but the BSM should be field-tested at a contaminated site to estimate gradients, measure flow and collect samples for contaminant parent and degradation chemical analysis. Only 3 field measurement events of the potentiomanometer were conducted during this study; further testing with the BSMs would be beneficial to further evaluate device performance.

2.8 Tables and Figures

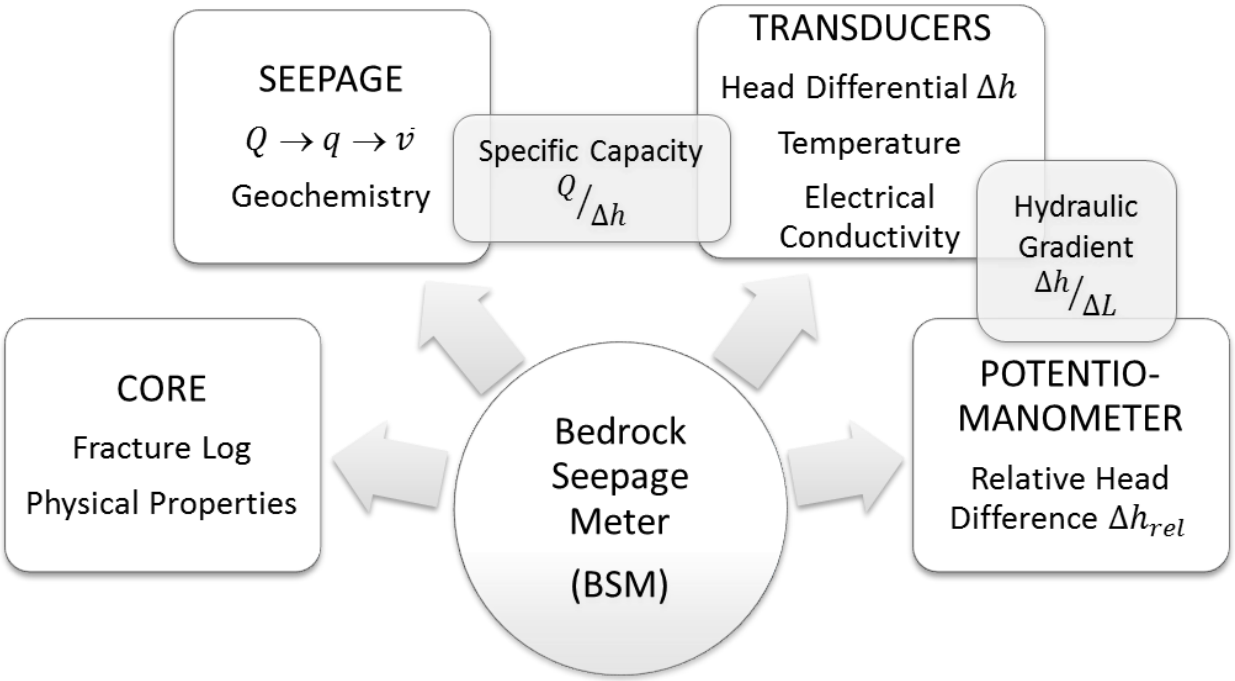

Figure 2.1. Flow chart illustrating multi-purpose range of the bedrock seepage meter to quantify hydraulic parameters in the context of groundwater – surface water interaction studies in bedrock rivers.

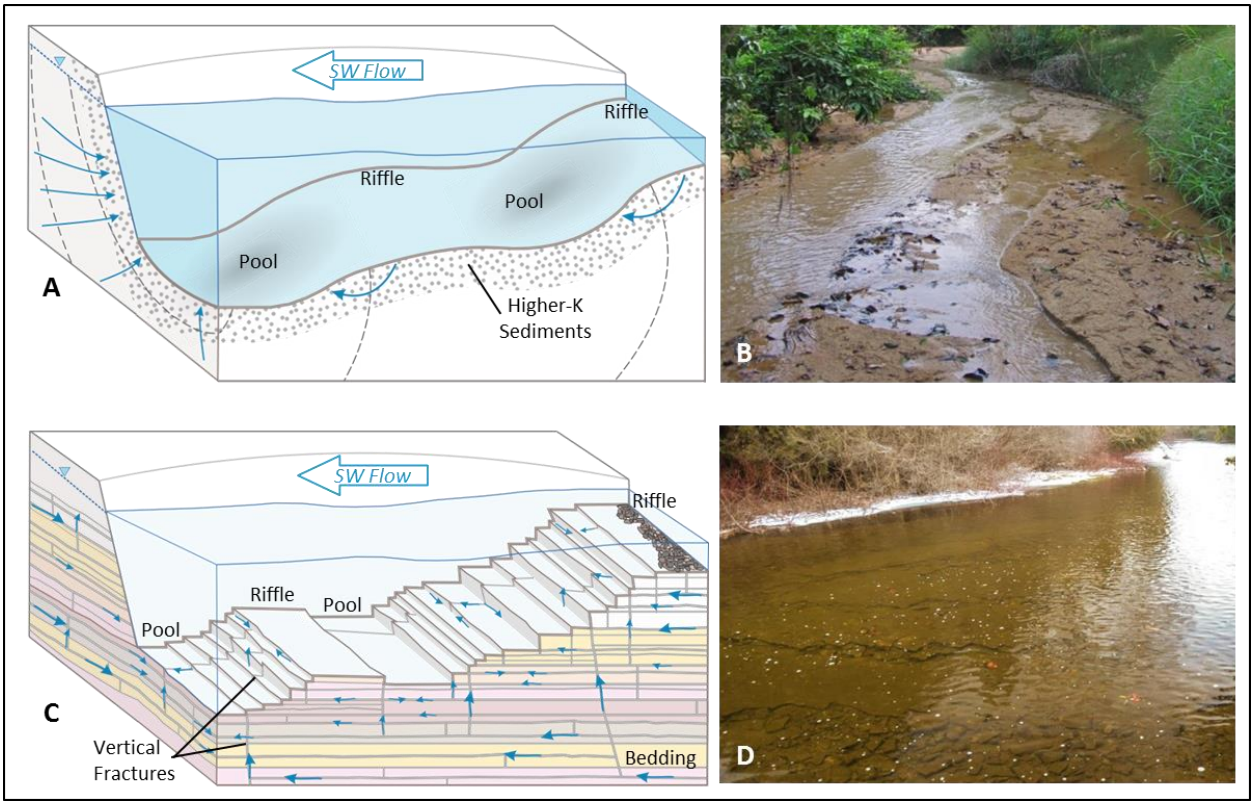

Figure 2.2. Examples of gaining rivers, where the river stage is lower than the water table of the adjacent floodplain, and where different flow patterns arise from different geomorphologies. **(A)** Conceptual model of an alluvial river lined with unconsolidated sediments of varying hydraulic conductivities (K) (adapted from Woessner 1998); and **(B)** photograph of an alluvial stream, exhibiting short-term erosion and deposition. **(C)** Conceptual model of an intact fractured bedrock streambed, where groundwater discharge is dominated by the network of vertical and bedding plane fractures; and **(D)** photograph of the Eramosa River dolostone bed, where very long-term erosion of the rock strata has formed bedding steps in a downstream direction.

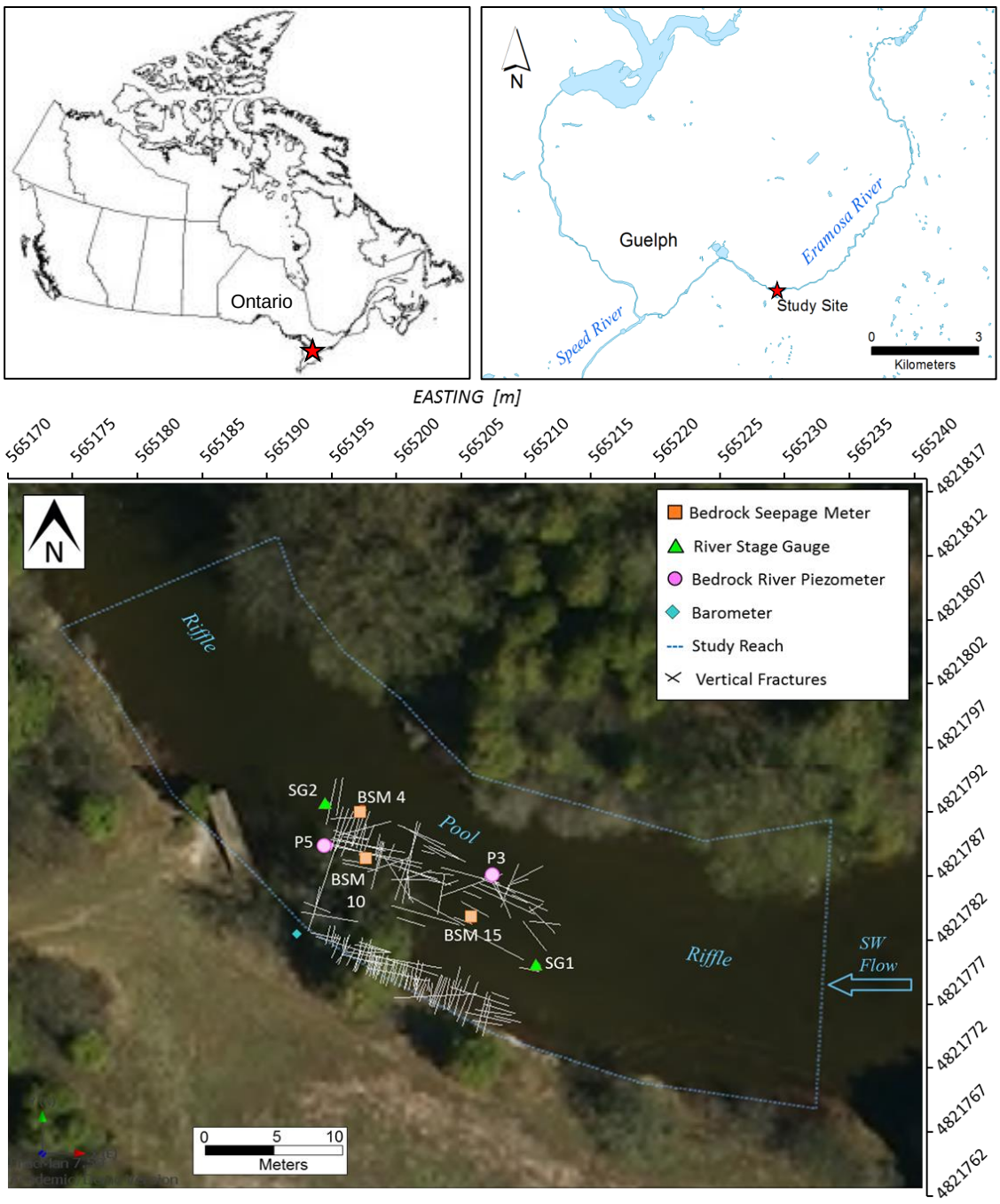

Figure 2.3. Location of study reach along the Eramosa River, in Guelph, ON, Canada, which flows in a southeasterly direction, and encompasses a riffle-pool sequence within a river bend. Dolostone outcrops exhibit horizontal bedding fractures and vertical fractures that terminate at surface, which were mapped with FracMan v.7.5 (Golder Associates Inc., Redmond, USA). Spatial distribution of *the subset*, BSMs 4, 10 and 15, along with river stage gauges (SG1 and SG2) and river piezometers (P3 and P5). [NAD 1983 UTM Zone 17N Geographic Coordinate System; MNR SWOOP 2010; ESRI ArcMap v.10.2.1; FracMan v.7.5]

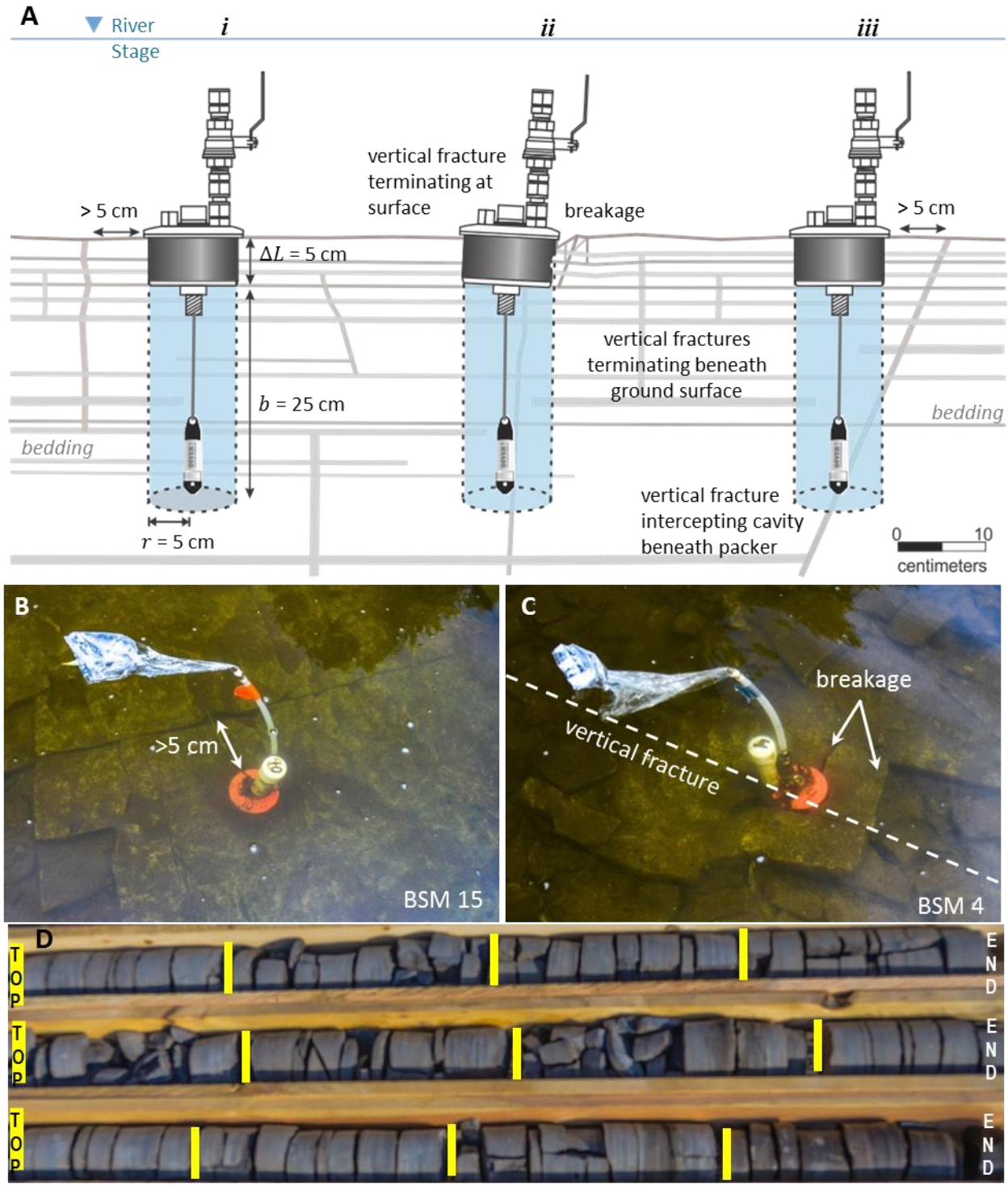

Figure 2.4. Conceptual diagram of BSM installation types. **(A*i*)** Secure install near vertical fractures terminating at and beneath ground surface. **(A*ii*)** Leaky install on a vertical fracture terminating at surface. **(A*iii*)** Secure install intercepting a high angle fracture beneath the packer seal. **(B)** BSM 10, installed near a vertical fracture. **(C)** BSM 4, installed on a vertical fracture. **(D)** Core retrieved from 12 seepage cavities showing frequency and distribution of bedding plane and vertical fractures intercepted.

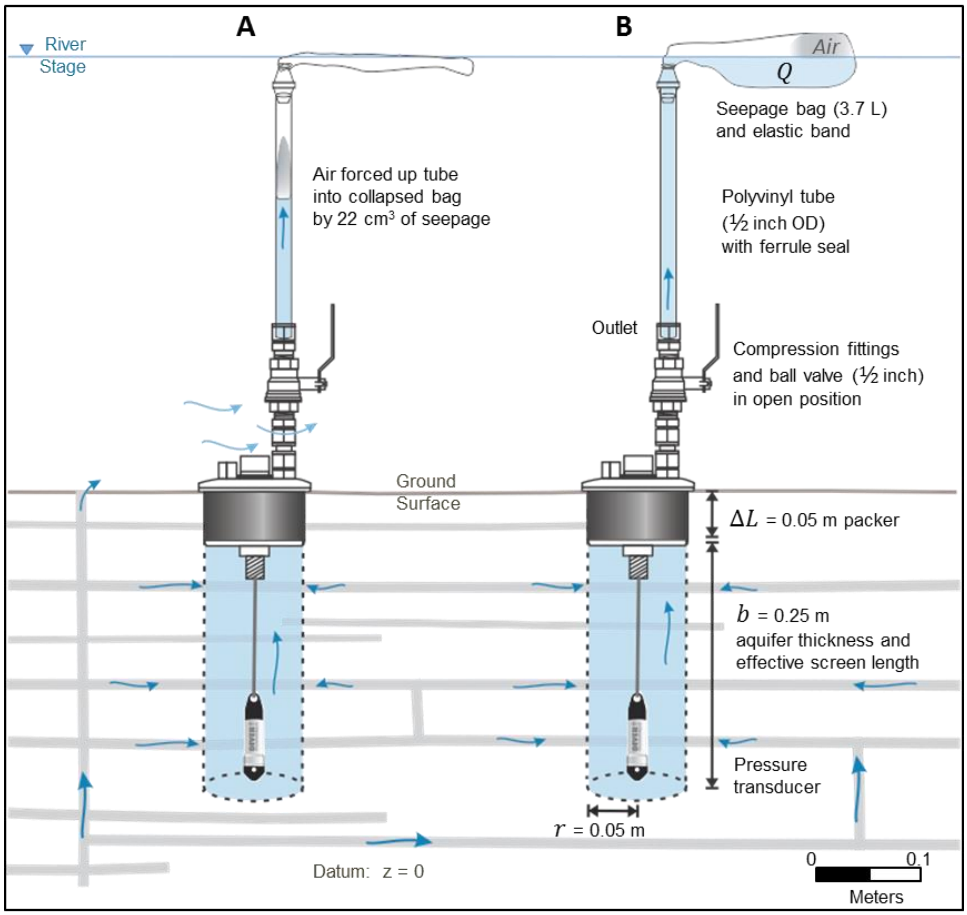

Figure 2.5. Conceptual diagram of BSM configuration to measure volumetric flow (Q), where **(A)** collapsed bag and tube are attached to outlet creating a closed system and groundwater overcomes the frictional resistance of the tube so that constant driving head conditions are reached, and **(B)** water spills over into the collection bag and evidence of an upward gradient is observed.

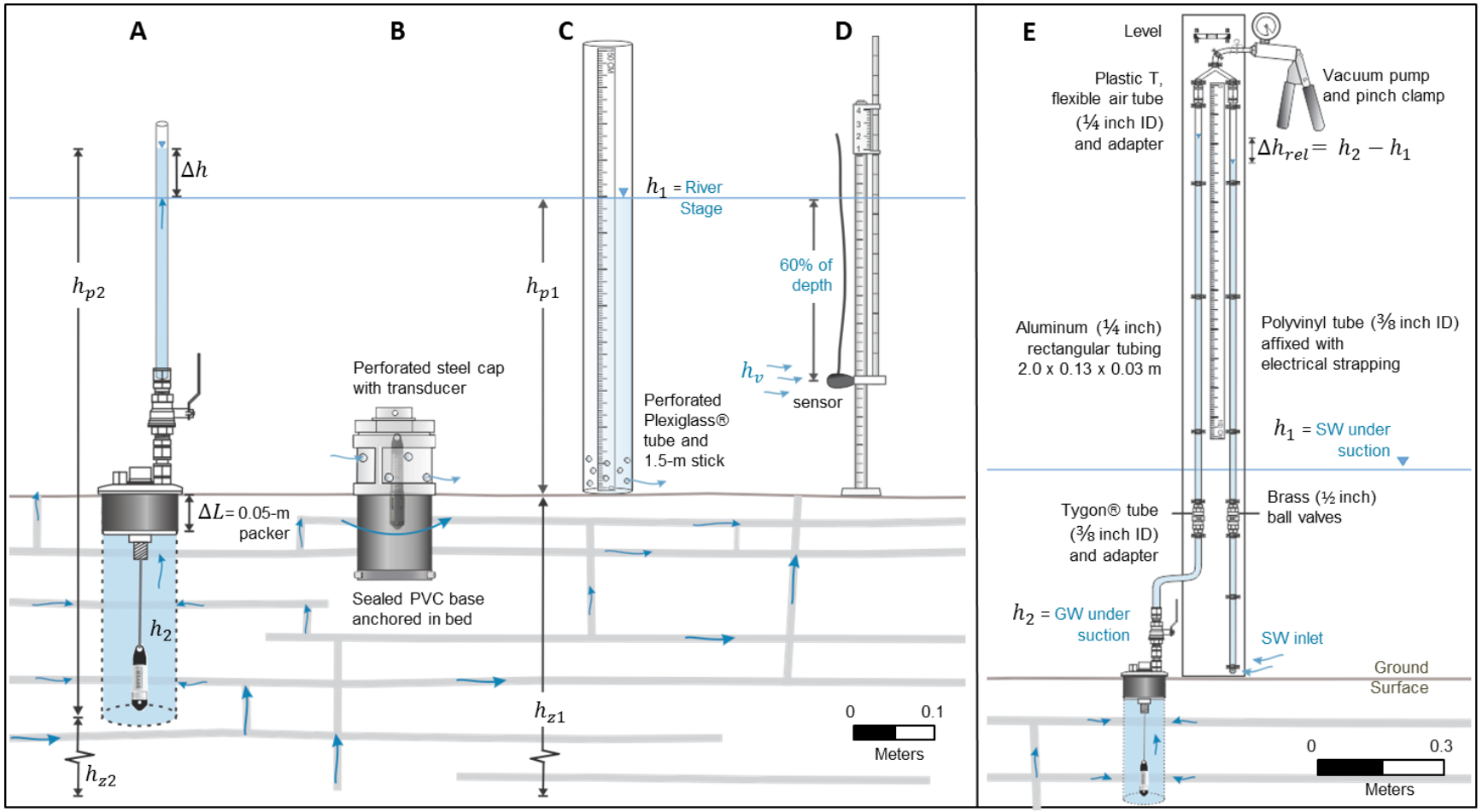

Figure 2.6. Conceptual diagram of bedrock river tool set to measure hydraulic head differentials (Δh and Δh_{rel}), including: **(A)** BSM to measure groundwater head from elevation head and pressure head in the seepage cavity ($h_2 = h_{p2} + h_{z2}$). Seepage tube demonstrates upward gradient and differential head ($\Delta h = h_2 - h_1$). **(B)** River stage gauge for centralized transient monitoring of surface water head (h_1). **(C)** Bathymetric tool to measure surface water head near each BSM ($h_1 = h_{p1} + h_{z1} + h_v$), where velocity head ($h_v$) is simultaneously measured using **(D)** a flow meter. **(E)** Potentiomanometer for direct measurement of relative head difference (Δh_{rel}) between the groundwater and surface water under suction.

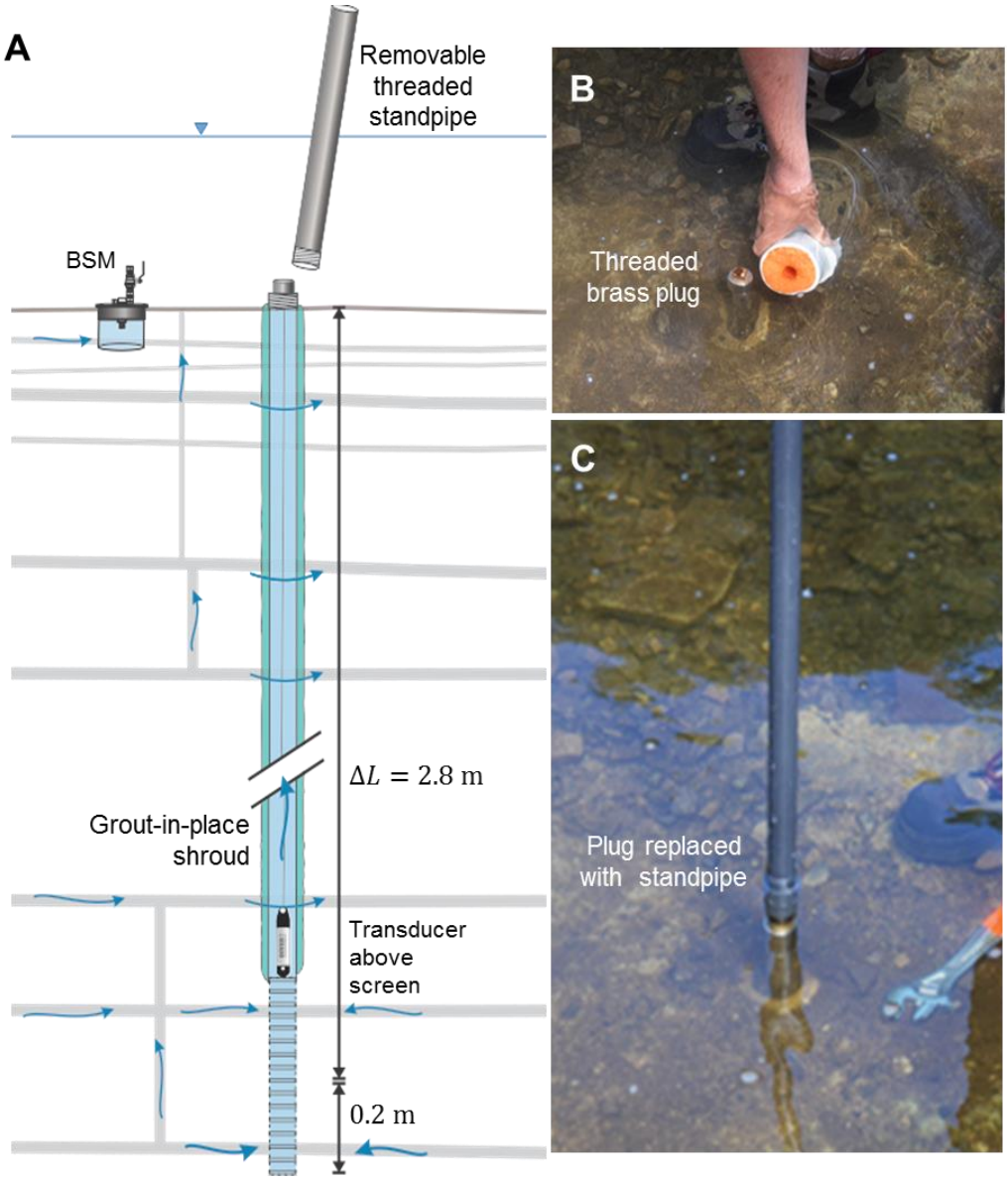

Figure 2.7. **(A)** Conceptual diagram of a bedrock river piezometer drilled 3.0 m into the streambed with a 5-cm diamond coring bit. The grout-in-place method (Pierce *et al.,* 2017) was adapted for use in riverbeds. The piezometer is instrumented with a transducer, is sealed with a removable threaded brass plug, and exhibits a low profile during monitoring. **(B)** A fitted protective cap was constructed from PVC . **(C)** The threaded brass plug can be exchanged for a threaded PVC standpipe to collect samples and manual water level measurements.

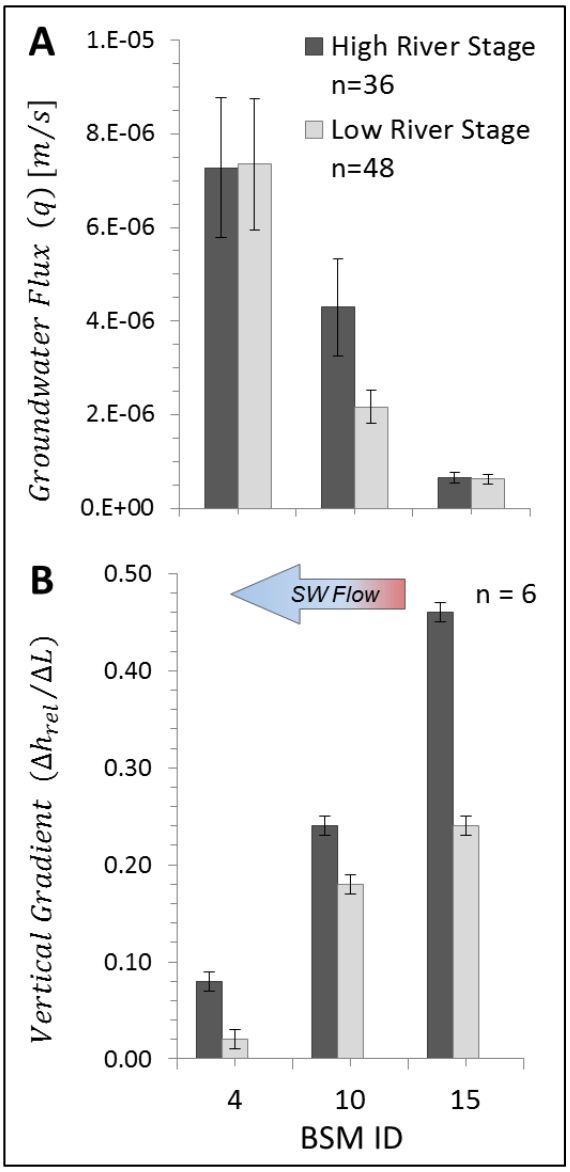

Figure 2.8. Comparison of **(A)** groundwater flux (q) estimated from flow (Q) measured during 12 high stage and 16 low stage constant head seepage tests in July-August 2014, and **(B)** vertical gradients ($\Delta h_{rel}/\Delta L$) across a 0.05-m layer of dolostone, derived from potentiomanometer measurements collected during 2 sampling events, one at high stage (July 11) and one at low river stage (August 13).

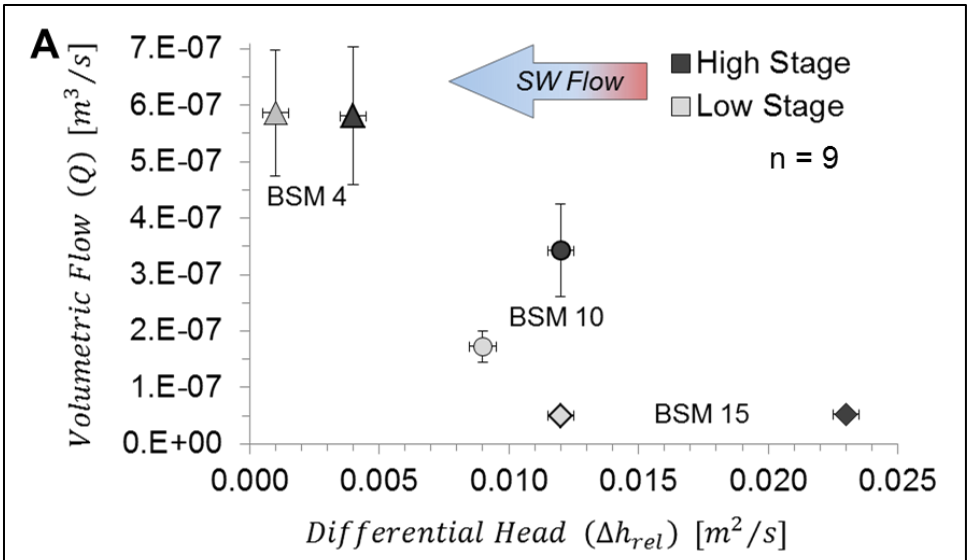

B

BSM ID #	Specific Capacity [m²/s]	
	High Stage 11-JUL-2014	Low Stage 13-AUG-2014
4	2.2E-04	6.5E-04
10	3.0E-05	1.9E-05
15	3.4E-06	7.6E-06

Figure 2.9. Specific capacity ($\boldsymbol{Q}/\Delta\boldsymbol{h_{rel}}$) of BSMs 4 (▲), 10 (●) and 15 (◆), estimated from measurements collected during a snapshot in time, when groundwater flow ($\boldsymbol{Q}$) and relative head difference ($\Delta\boldsymbol{h_{rel}}$) were measured at high stage and at low river stage, on July 11 and August 13, 2014, respectively.

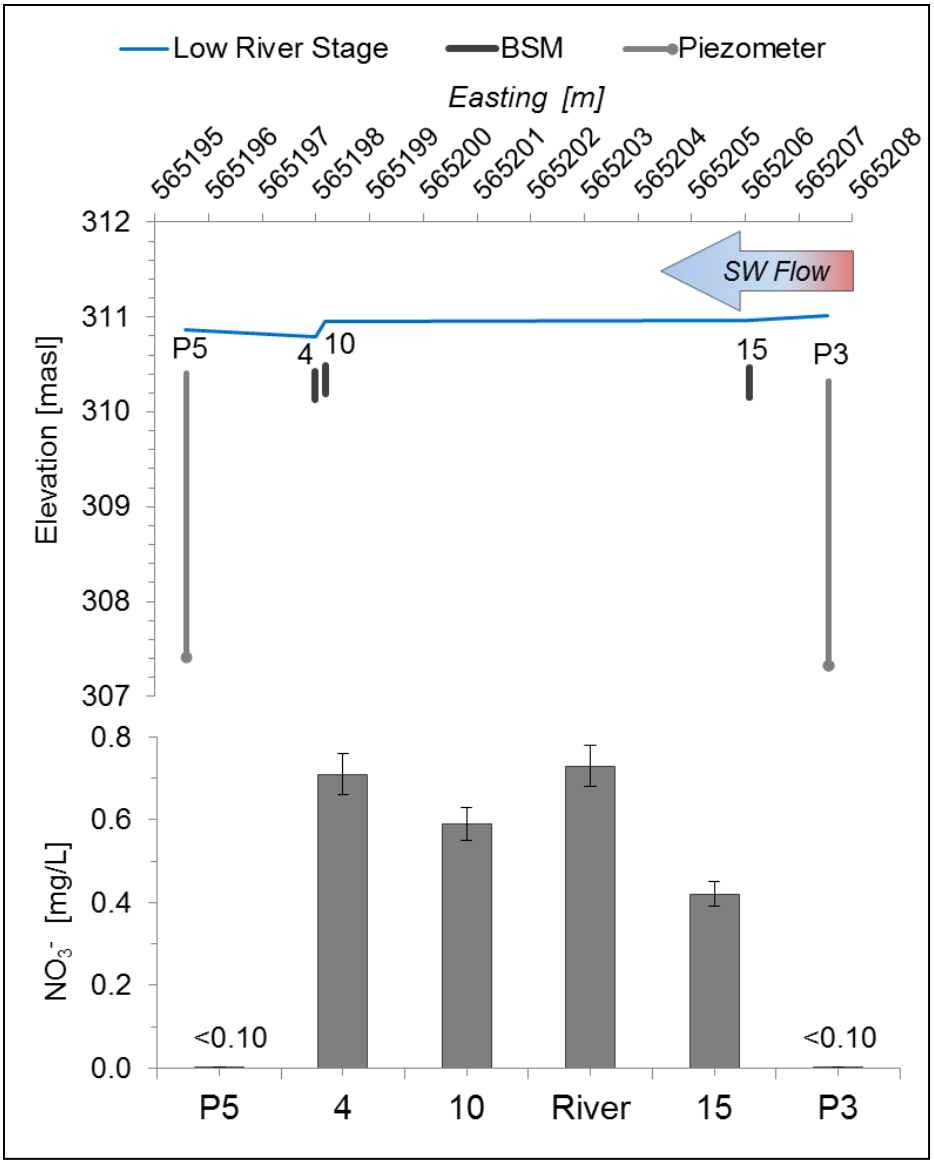

Figure 2.10. Spatial distribution of nitrate concentrations [NO_3^-], measured in units of mg/L, from one sampling event conducted at low river stage (14-AUG-2014).

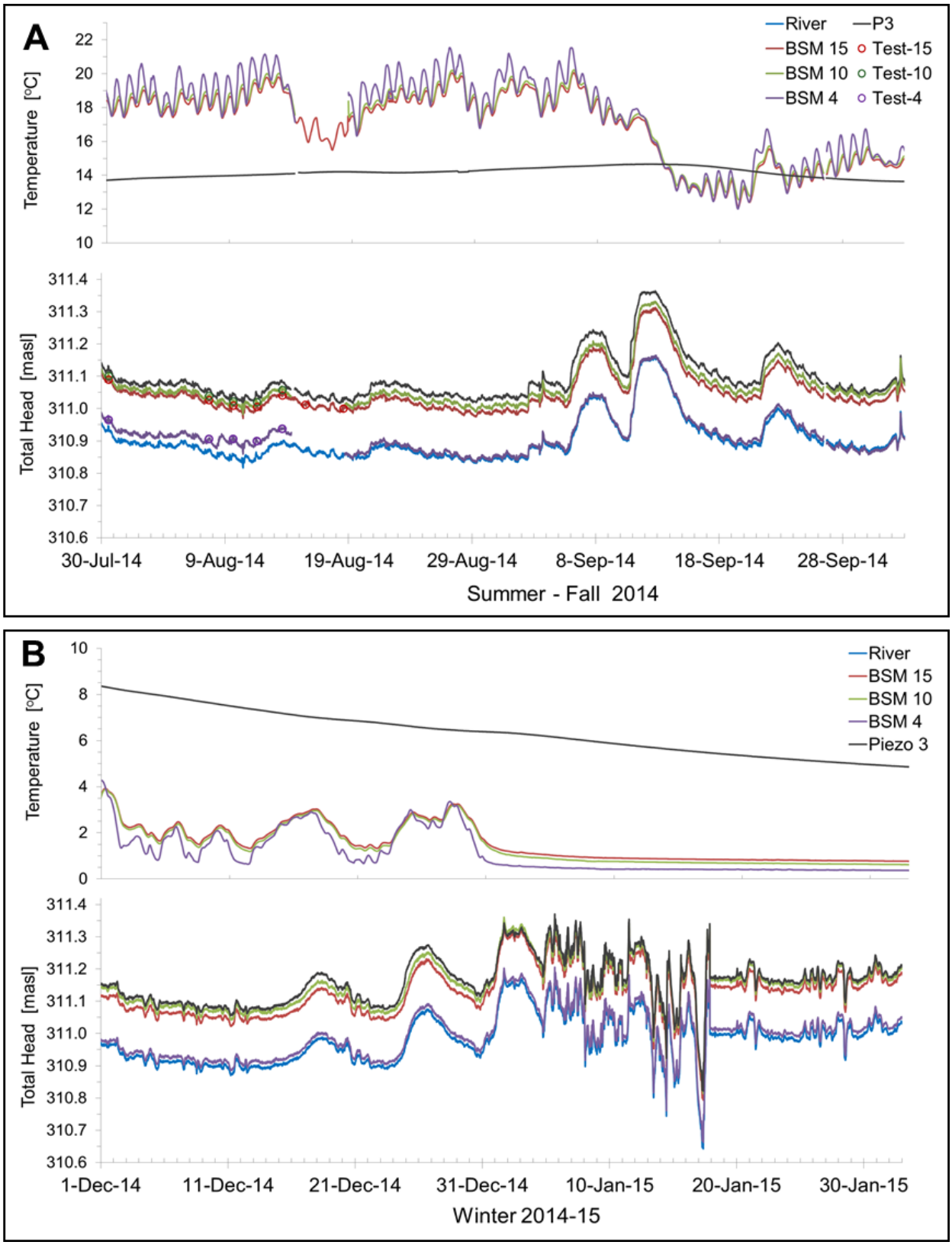

Figure 2.11. Continuous record of temperature and hydraulic head, collected at 15-min intervals in the subset BSMs, the river and piezometer P3 during: **(A)** Summer-Fall 2014; and **(B)** Winter 2014-15.

Table 2.1. Mean differential head (Δh) estimated using groundwater head (h_2), measured with BSM transducers for a 2-hr period (i.e., 6:00-8:00), collected at 1-min intervals, on the mornings of the 12 test days, in both (A) high stage and (B) low river stage conditions, and surface water head (h_1), measured later the same mornings near the BSMs with the bathymetry tool. Relative head difference (Δh_{rel}) was measured with the potentiomanometer in typical (A) high stage (July 11 2014) and (B) low river stage conditions (August 13 2014).

A. HIGH RIVER STAGE

BSM ID #	**Groundwater Head** [n = 1800] h_2 [masl]	**Surface Water Head** [n = 15] h_1 [masl]	**Diff. Head** [n = 15] Δh [m]	**Relative Head Diff.** [n = 6] Δh_{rel} [m]
15	311.101 ± *0.020*	311.041 ± *0.018*	0.06 ± *0.04*	0.023 ± *0.001*
10	311.100 ± *0.015*	311.018 ± *0.017*	0.08 ± *0.03*	0.012 ± *0.001*
4	310.956 ± *0.015*	310.948 ± *0.018*	0.01 ± *0.03*	0.004 ± *0.001*

B. LOW RIVER STAGE

BSM ID #	**Groundwater Head** [n = 2520] h_2 [masl]	**Surface Water Head** [n = 21] h_1 [masl]	**Diff. Head** [n = 21] Δh [m]	**Relative Head Diff.** [n = 6] Δh_{rel} [m]
15	311.012 ± *0.020*	310.980 ± *0.015*	0.03 ± *0.03*	0.012 ± *0.001*
10	311.034 ± *0.015*	310.961 ± *0.014*	0.07 ± *0.03*	0.009 ± *0.001*
4	310.910 ± *0.015*	310.807 ± *0.018*	0.10 ± *0.03*	0.001 ± *0.001*

Uncertainty of Δh = Σ SE of n + accuracy of groundwater h_p and h_z + accuracy of surface water h_p, h_z and h_v

Uncertainty of Δh_{rel} = Accuracy of potentiomanometer

Table 2.2. Mean groundwater flux (q) and average linear groundwater velocity ($\bar{v}$), listed in a downstream direction, and inferred from flow (Q) measured in 28 constant head seepage tests conducted on separate 12 days (i.e., July 10, 11, 24, 28, 29, 31, August 7, 9, 11, 13, 15, 18) during the summer of 2014, under (A) high stage, and (B) low river stage conditions.

A. HIGH RIVER STAGE

BSM ID #	**Flow** [n = 36] Q [m^3/s]	**Groundwater Flux** q [m/s]	**Fracture Velocity** $\bar{v}$ [m/s]
15	5.2E-08 ± *17%*	6.6E-07	6.6E-04
10	3.4E-07 ± *24%*	4.3E-06	4.3E-03
4	5.8E-07 ± *21%*	7.3E-06	7.3E-03

B. LOW RIVER STAGE

BSM ID #	**Flow** [n = 48] Q [m^3/s]	**Groundwater Flux** q [m/s]	**Fracture Velocity** $\bar{v}$ [m/s]
15	5.0E-08 ± *16%*	6.2E-07	6.2E-04
10	1.7E-07 ± *16%*	2.2E-06	2.2E-03
4	5.9E-07 ± *19%*	7.4E-06	7.4E-03

Uncertainty = Σ SE of n + accuracy of ΔV + accuracy of t

Table 2.3. Summary of component accuracy values yielding field measurement uncertainties.

Measurement	Units	Device		Manufacturer	Accuracy ±
Elevation Head h_z	m	Leica Viva GS08plus GPS		Leica Geosystems Inc. Norcross, GA, USA	0.01
Pressure Head h_p	m	BSMs 4, 10	MiniDiver	Schlumberger Water Services (SWS), Delft, The Netherlands	0.005
		BSM 15	MicroDiver		0.01
		Piezometers	MicroDiver		0.01
		Stage Gauges	CTD Diver		0.005
		10-m range SWS transducers			
Relative Head Difference Δh_{rel}	m	Potentiomanometer		G360 Institute for Groundwater Research, University of Guelph	0.0005
River Depth	m	Bathymetric Tool		G360	0.0005
Seepage Volume ΔV	mL	Graduated Cylinders		Pyrex® Vista™ Lowell, MA, USA	1%
Surface Water Velocity h_v	m/s	Flo-Mate 2000 Flow Meter		Marsh-McBirney Inc. Frederick, MA, USA	2%
Temperature	^{o}C	MicroDiver, MiniDiver, and CTD Diver		Van Essen Instruments	0.1
Test Time t	s	Equilibration Estimate			15
		Stopwatch Model 228		SportLine Elmsford, NY, USA	0.01
GEOCHEMISTRY: Major Ion	mg/L	Nitrate Analysis		ALS Global Laboratories Waterloo, ON, Canada	0.05

Chapter 3: Characterization of Groundwater – Surface Water Interactions in a Bedrock River Riffle-Pool Sequence

3.1 Introduction

Groundwater and surface water are linked at the streambed interface, leading to shared sustainability issues. The sharing of common pathways into and out of the riverbed interface provides opportunity for the exchange of thermal, chemical and biological constituents, affecting water quality and ecosystem health. Hydraulic pressures and flow regimes of these linked systems are dynamic, impacted by natural-world erosional changes to channel geomorphology and varying seasonal inputs of precipitation, together with anthropogenic activities such as groundwater and/or surface water pumping related to urban development, agricultural and industrial processes.

The term "bedrock river" refers to surface water flowing along an exposed sedimentary bedrock riverbed. Bedrock rivers are a common class of channel observed across four continents (Tinkler and Wohl 1998), but little is known about their physical and chemical characteristics or hydraulic properties. Commonly formed by glacial meltwater, these rivers are often found at the lowest elevation in the watershed, stripped of their protective overburden and lacking in fine granular sediments. Since the rigid channels of bedrock rivers are more challenging to instrument, hydrogeologic understanding and conceptual models of groundwater – surface water interactions are biased toward alluvial rivers.

An alluvial river generally exhibits a granular or unconsolidated bed with the sediment transport capacity to aggrade and degrade over a very short timescale (i.e., seasons or flood events) so that its channel geomorphology remains relatively constant (Leopold and Wolman 1960). Effective porosity of a sand-gravel channel is large, ranging from 25 – 50% (Freeze and Cherry 1979), while diffuse flow through its alluvial matrix is slow (i.e., centimeters per day) and groundwater – surface water exchanges with the underlying aquifer are influenced by the size, shape and orientation of its porous sediment (Woessner 1998; Winter *et al.*, 1998). A sedimentary bedrock riverbed, on the other hand, is dominated by planar or irregular exposed rock, typically horizontally-bedded, and exhibiting longitudinally-stepped

or terraced profiles weathered along joint sets, knickpoints and fragmented bedding planes due to unidirectional denudation over a geologic timescale (i.e., centuries or longer) (Tinkler and Wohl 1998; Miller and Cluer 1998). Effective (advective) porosity of a bedrock channel is controlled by its fractures and is extremely small, ranging from 1 – 0.001% or 10^{-2} – 10^{-5} (Freeze and Cherry 1979; Parker 2007; Lipson *et al.*, 2005; Muldoon and Bradbury 2005), while average linear groundwater velocities through its fracture network is fast (i.e., tens of meters per day) and groundwater – surface water exchanges are influenced by the connectivity between the river and the channel aquifer, which is a function of fracture aperture, length and orientation. It is hypothesized that, given their inherent differences, knowledge gained from alluvial systems is not necessarily transferable to fractured rock systems.

The purpose of this study was to measure the spatio-temporal distribution of groundwater discharge rates and head differentials between the surface water and the upper 0.30 m of a highly-instrumented bedrock riverbed along a 1110 m^2 riffle-pool sequence within a channel meander exhibiting intact dolostone. This chapter endeavours to present results and interpretations of findings that demonstrate some of the quantifiable differences in groundwater – surface water exchanges between highly-anisotropic fractured bedrock channels and alluvial channels.

3.1.1 Perspectives Surrounding Groundwater – Surface Water Interactions in Riverbeds

Exchanges between groundwater and surface water flow systems are subject to influences applied at various scales. At the basin-scale, the impact of groundwater flow systems on exchanges in rivers is a function of regional topography. Toth (1963) identified nested groundwater flow systems, with local, intermediate and regional components. Water in a local flow system migrates to a nearby discharge area, like a river, while water in a regional flow system travels greater distances, often discharging to major surface water bodies (Sophocleous 2002). An intermediate flow system exhibits one or more topographic highs and lows between its discharge and recharge areas (Sophocleous 2002). In an area where there is pronounced local relief, only local systems develop; where local relief is negligible, only regional systems develop (Toth 1963).

At the reach-scale, interactions between groundwater and surface water are influenced by channel topography. Hubbert (1940) conceptualized directional groundwater flow, driven by a water-table surface that is a "subdued replica" of the land surface topography. Toth (1970) described the hydrogeologic environment of groundwater flow systems as a function of topography, geology and climate. In the case of both bedrock and alluvial beds, erosional forces carve out pools and deposit sediment in riffles, and channel water moves into and out of the streambed (mixing with the groundwater along its path) due to downstream differential pressures. In alluvial rivers, streamflow losses at riffles and gains at pools have been observed. Vaux (1968) described stream water interchanges in a sandy streambed, with upwells observed where sediment thickness declined or the bed profile was concave (i.e., a pool), and downwells observed where sediment thickness increased or the bed profile was convex (i.e., a riffle). Streamflow losses at riffles and gains at pools have been described as the circulation of channel water through the shallow subsurface sediment, entering at riffles and reappearing at the heads of pools (Dumouchelle 2001; Woessner 1998; Harvey and Bencala 1993; Hendricks and White 1991).

Over the past 25 years, three authors have contributed key concepts and summations compiled from alluvial river studies to advance our understanding of groundwater – surface water exchanges. Palmer (1993) describes obstacles encountered by river ecologists impeding studies aimed at quantifying how populations of hyporheos or particular hyporheic processes are influenced by groundwater and surface water inputs to the hyporheic zone. The list includes: (1) delineation of hyporheic zone boundaries through hydrologic and geomorphic investigation, (2) quantifying and manipulating subsurface flows at a range of scales to evaluate the extent of their spatial variability, (3) minimizing the invasiveness of experimental methods, and (4) quantifying groundwater and surface water inputs. Palmer (1993) points out the lack of quantitative subsurface flow – stream functioning studies and recognizes the need for minimally-invasive tools for collecting depth-discrete measurements within streambeds. Further, that a shift in focus from: trying to force ecosystem studies to conform to some generic hyporheic model, to:

embracing individual system heterogeneity in order to understand why systems differ. These priorities are equally important in hydrological studies.

Winter *et al.,* (1998) speaks to how effective land use and water resources management requires an understanding of the linkages between groundwater and surface water. Specifically, Winter *et al.,* (1998) describes the potential for groundwater and surface water to influence one another, where rivers gain water and solutes from groundwater systems or serve as sources of groundwater recharge. Winter *et al.,* (1998) explains how groundwater pumping can deplete streams just as water-taking from streams can diminish groundwater reserves, and pollution of groundwater can degrade surface water while contaminants in surface water can be transferred to groundwater. In short, groundwater and surface water are a single resource and need to be managed as such.

Woessner (1998) presented conceptual models of groundwater and surface water flow into and out of an alluvial stream channel, categorized on the basis of relative differences between stream stage and the adjacent floodplain water table, thereby creating a gradient. Groundwater – surface water exchanges in segments of a stream may be characterized as: a gaining condition (where stream stage elevation is less than the water table elevation in the adjacent floodplain), a losing condition (where stream stage elevation, or head, is greater than that of the floodplain) or a flow-through condition (where the floodplain head elevation is greater than the stream stage on one side of the channel and the condition is reversed on the opposite side of the channel) (Woessner 1998). A parallel-flow condition also exists, where the elevations of the stream stage and water table are equal and zero-exchange occurs (Woessner 1998). The influence of channel geometry on these conditions was demonstrated by Woessner (1998 and 2000), specifically: gaining, losing and zero-exchange reaches likely occur when the stream channel is orientated parallel to the fluvial plain, and flow-through reaches are observed when a channel cuts perpendicular to groundwater flow in the fluvial plain (i.e., a meander). Woessner (2000) modelled the influence of hydraulic conductivity (K) of the streambed sediments on subsurface flow, where mixing of groundwater and surface water occurs in the high-K, near-channel sediments (i.e., the hyporheic zone) as deep as 1.7 mbgs. A riffle – pool sequence, representing changes in channel topographic relief, illustrates

how pressure head differences also influence flow; in that, surface water enters the streambed at the heads of riffles and exits at the riffle base in pools (Woessner 2000). With the introduction of these conceptual models, Woessner (1998 and 2000) emphasized two points: (1) that the collective intelligence of hydrogeologists and ecologists is needed to construct comprehensive conceptual models of groundwater – surface water interactions, at both the channel and fluvial plain scale, using quantifiable physical and geochemical parameters to evaluate stream health and water quality; and (2) that simplistic 2-D cross-sectional representations of groundwater flow to a stream have inadvertently stifled our conceptualization of the complexities of groundwater – surface water exchanges, since contrasts in hydraulic conductivity are not represented. The overviews of Palmer, Winter, Woessner and others collectively give perspective on the state of knowledge and conceptualization of groundwater interacting with surface water. While these concepts may be generally applicable in both alluvial and bedrock systems, no quantitative field studies in fractured rock channels have been documented to demonstrate this.

Tinkler and Wohl (1998) presented the first (and only) review of existing knowledge of bedrock rivers, limited to mainly streamflow and geomorphology studies. According to Tinkler and Wohl (1998), a bedrock riverbed is a resistant boundary that represents the catchment area or drainage basin bedrock. Consequently, base level changes (i.e., the lowest point at which erosion by running water can occur) caused by channel erosion impacts basin geomorphology (over a geologic timescale) and local stream velocities are permanently modified. In other words, rock removed from the channel bed lowers the local base level since, unlike alluvial riverbeds, bedrock channels are not self-repairing and do not conserve morphology. Streamflow is often faster in bedrock channels and variable, with the capacity to generate sub-critical to super-critical flow conditions within a cross-sectional transect (i.e., the ratio of surface water velocity to wave speed, quantified by the Froude number) (Tinkler and Wohl 1998). It is hypothesized that bedrock rivers are fundamentally different from alluvial systems due to their rigid boundaries and complex advective flow patterns dominated by a network of fractures that variably connect groundwater and surface water.

An essential component of any conceptual model of groundwater – surface water exchanges, hydraulic conductivity (along with head differentials) in the channel controls the rate of subsurface flow, regardless of the mechanism (i.e., granular sediments or bedrock fractures). If conceptual models are to be constructed on the basis of quantitative parameters that are both hydrologic and ecologic in nature, then expansion of the hyporheic definition is needed. The term *"hyporheos"* refers to the fauna residing in a layer of varying thickness and substrate in a streambed. Coined by Orghidan (1955), its origin is Greek, where *"hypo"* means "under" and *"-rheos"* means "flow". Consequently, ecologists adapted the term *"hyporheic zone"* to refer to this layered habitat below the surface water column and the biogeochemical processes occurring within it, which historically, have been limited to alluvial streambeds. Palmer (1993) describes the hyporheic zone as a 3-D habitat that is poorly understood because it is hydrologically complex, relatively inaccessible and difficult to manipulate in field studies. A statement which easily applies to both bedrock and alluvial riverbeds. There is a perspective among researchers that the nature of a hyporheic domain is limited to alluvial streambeds and that reaches of exposed bedrock are excluded from its delineation (Palmer 1993; Hynes 1983; Stanford and Gaufin 1974; Ward 1989). Perhaps this exclusion of bedrock reaches has persisted due to a lack of tools and methods to study them. Spawning habitats for trout and salmon in the cobble-covered reaches of bedrock rivers have been studied (Fales and Rasmussen 2014; Rawson 2011; Mossop and Bradford 2006; Alexander and Caisse 2003; Armstrong *et al.*, 2003; Payne and Lapointe 1997; Bisson *et al.*, 1988). It is reasonable to assume, therefore, that nutrient transport and hyporheic mixing occurs in riverbed fractures to support a range of hyporheos conditions associated with spawning populations.

3.1.2 Seepage Meter Applications in Rivers

The study of groundwater – surface water exchanges in alluvial systems was advanced by the development of the seepage meter to measure groundwater discharge and recharge (Lee and Cherry 1978); a method that has endured for almost four decades (Russoniello and Michael 2015; Toran *et al.*, 2015; Rosenberry *et al.*, 2013; Fritz *et al.*, 2009; Rosenberry *et al.*, 2008; Rosenberry and Morin 2004;

Cey *et al.,* 1998; Woessner and Sullivan 1984). The number of published bedrock river studies is very limited, with the majority focusing on fluvial and geomorphological processes (Hodge 2011; Whipple 2004; Jarrett 1984). Oxtobee and Novakowski (2002) conducted a field study of Twenty Mile Creek, a bedrock creek in Smithville, ON, Canada. They concluded that the groundwater – surface water interaction was limited, due to the absence of hydraulically-active vertical fractures. Alexander and Caisse (2003) conducted a field study of the Catamaran Brook, a bedrock river and salmon habitat in central New Brunswick, Canada. They concluded that groundwater discharge was very limited in the sand-and-gravel-covered reaches. In both studies, attempts were made to measure groundwater discharge with traditional seepage meters, thereby limiting their deployment to sediment-covered reaches of bedrock rivers (Alexander and Caisse 2003; Oxtobee and Novakowski 2002).

In order to conduct a field study of an intact bedrock riverbed, tools and methods were developed to quantify hydraulic parameters [detailed in Chapter 2]. Initially conceived as an adaptation to Lee and Cherry's (1978) seepage meter for use in alluvial rivers, the "bedrock seepage meter" or BSM, is a hybrid device, designed to measure seepage and quantify groundwater flux in the upper 0.30 m of an intact bedrock riverbed by intercepting fractures within this very short hyporheic interval. Recent advances with portable drills, multi-level monitoring and the data-logging capacity of wireless micro-transducers have improved the collection of high-resolution geologic, hydraulic and thermal information with reduced impacts to surrounding ecosystems (Steelman *et al.,* 2015; Hatch *et al.,* 2006; Conant *et al.,* 2004). The BSM is a minimally-invasive, portable device that is drilled into the bedrock streambed and sealed at the streambed interface with a 0.05-m rubber packer [see Chapter 2, Fig. 2.4, 2.5].

3.1.3 The Bedrock River Conceptual Model Problem

Much of our water-resource management decisions are based on flow and contaminant-transport models, constructed from either hypothetical numerical modelling studies, or from field data collected in alluvial river studies, using an equivalent porous media (EPM) approach (Bear 1972). This approach to predictive models of flow and transport in bedrock river environments is inappropriate since interactions

between groundwater and surface water in alluvial and bedrock channels may be similarly controlled by head differentials and hydraulic conductivities, but the mechanisms are different. The discrete fracture network (DFN) approach is a more viable alternative, as it recognizes that at every scale, groundwater flow in fractured rock is dominated by discrete pathways, observing the characteristics of fracture size, geometry and connectivity (Parker *et al.,* 2012). There is a need for a new conceptual model, which recognizes the distinct characteristics of discrete fracture networks and the resultant heterogeneity and anisotropy contributing to complex flow patterns in riverbed aquifers, as depicted in Figure 3.1.

This is the first study of a bedrock river yielding a field-based conceptual model of the spatio-temporal variability of groundwater discharge and vertical hydraulic gradients through the discrete fracture networks of an intact dolostone streambed. The Eramosa River, in Guelph, ON, Canada, was selected for this purpose.

3.1.4 Eramosa River – Background

The Eramosa River is a 27-km channel, with almost half of it exhibiting exposed bedrock, flowing in a southwesterly direction from its headwaters above the Town of Everton, at an elevation of 400 m above sea level (masl), to a confluence with the Speed River at 300 masl, within the City of Guelph (Figure 1.3). Supporting a population of 122,000 (2011 census), the City of Guelph, has 23 municipal production wells, supplemented by a surface water intake on the Eramosa River to recharge the overburden aquifer at Arkell Springs (Figure 3.2). Local topography of the fluvial plain along the Eramosa River exhibits a small slope, falling 2.8 m per km of channel and dipping to the southwest (Karrow 1968). Its streambed exhibits the fractured dolostone of the Eramosa Formation (Fm), underlain by the Goat Island aquitard and the highly transmissive Gasport aquifer (Brunton 2009; Karrow 1968). These underlying dolomitic formations often exhibit karstic features (i.e. dissolution-enhanced fractures or conduits) (Steelman *et al.,* 2015; Cole *et al.,* 2009; Kunert *et al.,* 1998). Gartner Lee Limited (2004) completed a well-head protection study of the regional geology and recharge rates of 19 Guelph Area municipal wells and more than 4400 residential wells. Based on potentiometric surfaces identified in

wells, they found that groundwater recharge along the Eramosa riverbed (i.e., bed elevation is higher than nearby potentiometric surfaces) occurred between the Everton headwaters and Arkell Springs, and that groundwater discharge along the channel (i.e., bed elevation is less than nearby potentiometric surfaces) occurred from Arkell Springs in a downstream direction, where more than half the length of the channel is identified as a groundwater discharge area (Figures 1.5; 3.2). The potential for groundwater and surface water to influence one another within and around the Eramosa River has prompted a number of vulnerability studies and public health inquiries, particularly since the *Clean Water Act* was enacted in 2006 (AquaResource Inc., 2010; LERSP 2010; GRCA 1998).

3.1.5 Field site location along the channel.

The study site is located at the Barber Scout Camp, a 2600 m^2 property along the south side of the Eramosa River, in Guelph, ON, Canada. The study reach exists in a river bend or meander, 900 m downstream of the Watson Road Gauging Station (Figure 3.2)., where the shoreline along the south side of the channel recedes and advances at high and low stage respectively. Since it is well known (or generally expected) that groundwater – surface water interactions can behave very differently in high and low river stage conditions (e.g., NHC 2010; Madsen and Skotner 2005; Oxtobee and Novakowski 2002; Dingman 2002; Palmer 1993; Hynes 1983), results are reported in a split format to minimize variability and permit the detection of differences in groundwater discharge influenced by a changing water table. Hourly streamflow, measured at the Watson Road Gauging Station, owned by the Water Survey of Canada and managed by the Grand River Conservation Authority (Cambridge, ON, Canada), was used to categorize river conditions. High river stage at the study site coincides with streamflow values >1.5 m^3/s at Watson Road, while low river stage corresponds to streamflow <1.5 m^3/s (Figure 3.3). This designated threshold of 1.5 m^3/s is an assignment of a streamflow value recorded by a nearby government gauging station that coincides with observed declines in river stage at the study site; thus, it is an independent benchmark upon which to define high and low river stage conditions for the purpose of data analysis and interpretation.

Channel geometry, studied mainly in alluvial rivers, is known to influence surface water and hyporheic flow; thus, the Scout Camp site provided an opportunity to investigate groundwater – surface water exchanges in the river bend of a bedrock river. River bends formed by glacial meltwater have been known to exhibit a relationship between meander length and channel width; Leopold and Wolman (1960) found the radius of curvature of such meanders to be 2-3 times the width of the channel. Since these meanders carry little or no sediment, their shapes are determined primarily by flow dynamics rather than by sediment load, as is the case in alluvial rivers. The study reach exhibits a channel width of about 20 m (in summer), and the radius of curvature is estimated at 50 m (Figure 3.2). Surface water velocity in a river bend is a function of the distribution of energy loss resulting from variability in resistance to flow along the surface of the channel. In a bedrock channel, this variability is heightened by diverse riverbed asperity, ranging from flat, intact carbonate rock pavement, intersected by hydraulically-active vertical and bedding plane fractures, to rubble cover in the form of sharp angular bedrock fragments. A small stream was observed crossing the neck of the meander at the study site on the north side of the channel (Figure 3.2). Peterson and Sickbert (2006), studied the hyporheic zone beneath a stream crossing the meander neck of an alluvial river in Illinois using head and temperature measurements, and found that the hyporheic flowpath followed the shortest route (i.e., across the neck of the meander beneath the stream). Differences in surface water and hyporheic flow patterns have also been identified at the entrance and exit of river bends in alluvial rivers (deVriend and Geldof 1983). The relationship between groundwater fluxes, hydraulic gradients and the amount of water in the hyporheic zone was studied in the Speed River by Howard *et al.,* (2006) and Storey *et al.,* (2003), which confluences with the Eramosa River and shares the same regional aquifer [Chapter 1, Fig.1.3, 1.4]. Field-based modelling of groundwater – surface water exchanges along a 13-m alluvial reach of the Speed River revealed that when groundwater flux into the river is small, the extent of the hyporheic zone is pronounced, and as hydraulic gradient in the aquifer increases, the hyporheic zone shrinks (Howard *et al.,* 2006; Storey *et al.,* 2003). The location of this study reach facilitated examination of these relationships in a bedrock river context.

3.1.6 Field site description.

The study reach covers an area of 1110 m^2 of fractured sedimentary bedrock, encompassing a riffle-pool-riffle sequence (Figure 3.4A). The adjacent floodplain exhibits low topographic relief, with a negative slope of 2-3% towards the channel. Extensive outcropping is observed on the south side of the channel, where vegetation is sparse. The north side of the channel exhibits a point bar and encroaching vegetation. The site was selected because its river channel is cut along an intact Silurian dolostone aquifer outcrop. Fracture logs from core, acoustic televiewer (ATV) and optical televiewer (OTV) images, obtained from six floodplain coreholes, drilled as part of another study at the site [detailed in Appendix D], revealed predominantly horizontal bedding fractures and a number of vertical fractures in the upper 3.0 m of the riverbed (Figure 3.4B). BSMs were installed along vertical fractures terminating at the streambed surface (Figure 3.4C), which were observed wherever large sediments in the form of sharp angular bedrock fragments (i.e., rubble zones) were absent (Figure 3.4D). Fracture-mapping [detailed in Appendix E] revealed two dominant fracture orientations in the channel. A north - south orientation, orthogonal to channel flow, particularly along the south shore (Figure 3.3D – 3.4E), and an east - west orientation parallel to channel flow (Figure 3.4D - 3.4F). The channel declines by up to 0.6 m from riffle to pool (Figure 3.5) and depth of the surface water column ranges from 0.1 m in summer to 0.8 m during spring freshet. A longitudinally-stepped declining profile is observed between transects 2 and 3, impacting the installation depths of the BSMs, as conceptualized in Figure 3.1. The Eramosa Fm at the site extends to an elevation of ~300.0 masl [Appendix C, Fig. C-1], and the deepest BSM reaches an elevation of 310.0 masl. While all BSMs are installed in the same geologic formation, they do not all intersect the same stratigraphic horizons or bedding features, identified by the many bedding planes intersected, as illustrated in Figure 3.1.

3.2 Methods

This study relies on novel data obtained from the new BSM and associated devices evaluated in Chapter 2, topographic, bathymetric and hydrometric surveys along the channel, and DFN logs collected

at the streambed surface and along the length of inclined floodplain coreholes plunging beneath the channel to inform the study reach conceptual model. The framework of the conceptual model is further informed by use of the site topography, the channel geometry and bathymetry and streambed fracture mapping. BSMs were deployed on and near vertical fractures observed at the riverbed surface [Chapter 2, Fig. 2.6A]. River stage gauges were installed at upstream and downstream locations near the channel centre to monitor surface water [Chapter 2, Fig. 2.6B]. River piezometers were deployed to monitor groundwater at the upstream and downstream boundaries of the study reach and along the north and south sides of the channel [Chapter 2, Fig. 2.7].

During the 2014 field season, hydrometric surveys were collected along streambed transects to quantify streamflow at 5- and 10-m intervals along the channel to evaluate gaining and losing conditions. Seepage was measured to evaluate the rate and distribution of groundwater discharging to surface water with the rise and fall of the water table. Head differentials between groundwater and surface water were measured to evaluate the flux – gradient relationship within gaining and losing segments. Continuous records were collected in the BSMs from May 2014 – May 2015 to evaluate seasonal changes in hydraulic head and temperature in the hyporheic zone compared to that of the river and the deeper groundwater in the piezometers.

3.2.1 Bathymetric and Hydrometric Surveys.

The study reach was divided into 10 transects orthogonal to surface water flow, at 5 and 10-m intervals. The height of river stage (H), or surface water depth, was measured at 1-m intervals along transects using a bathymetric tool [Chapter 2, Fig. 2.6C]. Data was collected during 10 sampling events at high and low stage from June – August, 2014. Bathymetric profiles and surveyed transects were used to generate a 3-D contoured conceptual model of the study reach (Figure 3.5). Surface water velocity (v) was measured, in conjunction with river stage, at 60% of the channel depth using a Flo-Mate 2000 flow meter and a wading rod (Marsh-McBirney Inc., Frederick, MD, USA). Laminar streamflow (Q^{sw}), or stream discharge, was estimated using the velocity-area method [Equation 2] (ASTM D3858; Dingman

2002). Since the area (A) at each point measurement is simply a product of the 1-m slice multiplied by H, these values are equal,

$$Q_i{}^{sw} = (v)(A) = (v)(H)$$

$$Q^{sw} = \sum Q_i{}^{sw} \quad [m^3 s^{-1}] \qquad [2]$$

where:

$Q_i{}^{sw}$ = streamflow at each 1-m interval along transect [m^3 s^{-1}]

Q^{sw} = cumulative streamflow along entire transect [m^3 s^{-1}]

A = surface area at each point measurement [m^2]

H = height of river stage [m]

v = surface water velocity [m s^{-1}]

The stream depth – discharge relationship (ASTM 5541; USGS 2002) was plotted along each transect to evaluate surface water flow patterns within the riffle-pool sequence along the channel meander. Cumulative streamflow (Q^{sw}) was plotted at high and low stage to identify gaining and losing conditions. One of the challenges faced in estimating streamflow (Q^{sw}) in bedrock rivers is their tendency to exhibit trans-critical flow (i.e., a combination of sub-critical to super-critical flow conditions), both longitudinally and across transects, which is a mixed regime of sub-critical ($Fr < 1$), critical ($Fr = 1$), and super-critical ($Fr > 1$) flow (Tinkler and Wohl 1998). Streamflow variability was evaluated by estimating the Froud Number (Fr) along all transects [Equation 3],

$$Fr = \frac{v}{wave\ speed} = \frac{v}{\sqrt{gH}} \quad [unitless] \qquad [3],$$

where: v = surface water velocity [m s^{-1}]

g = force due to gravity [m s^{-2}]

H = height of river stage [m]

Surface water head or total hydraulic head in the river (h_1) was calculated as:

$$h_1 = h_{p1} + h_{z1} + h_v \quad [m] \qquad [4],$$

where pressure head (h_{p1}), or river stage, was measured with centralized stage gauges at upstream and downstream locations (Figure 3.4A), as well as with a bathymetric tool, to collect localized river depth measurements near each BSM [Chapter 2, Fig.2.6B-C]. Findings in Chapter 2 revealed that the accuracy of centralized stage gauge measurements was adequate for transient monitoring; however, the precision of localized measurements with the bathymetric tool was necessary for tests conducted under steady state conditions, since river stage can be sloped, particularly along channel meanders influenced by centrifugal force (Legleiter et al., 2011; Tinkler and Wohl 1998; Harvey and Bencala 1993). Elevation head (h_{z1}) was measured using a Leica Viva GS08plus GPS (Leica Geosystems Inc., Norcross, GA, USA). Velocity head (h_v) in the river was estimated according to [Equation 5] (Hichin 2004; Freeze and Cherry 1979; Lambe and Whitman 1969),

$$h_v = \frac{v^2}{2g} \qquad [m] \qquad [5],$$

where:

h_v = velocity head [m]

v = laminar or streamflow velocity [m/s]

g = acceleration due to gravity [m/s^2]

Streamflow velocities (v) were measured at 60% of the channel depth using a Flo-Mate 2000 flow meter and a wading rod (Marsh-McBirney Inc., Frederick, MD, USA) and the velocity-area method (ASTM D3858; Dingman 2002) [Chapter 2, Fig.2.6D].

3.2.2 Streambed Infrastructure to Monitor Groundwater and Surface Water

Using methods developed in Chapter 2, the study reach was instrumented with: two river stage gauges (SG1-SG2) to monitor surface water head (stage) (h_1) and temperature, two shallow bedrock river piezometers (P1-P2) to monitor groundwater head (h_2) at 0.7 mbgs, four river piezometers (P3-P6), equally distributed, to monitor groundwater head (h_2) at 3.0 mbgs, and 24 bedrock seepage meters (BSMs 1-24) to monitor groundwater head (h_2) and measure groundwater flow (Q) during constant head seepage tests. With the exception of BSMs 2, 4 and 5, installed directly on vertical fractures, devices were

predominantly installed near vertical fractures, distributed across the streambed where intact dolostone pavement was exposed and not encroached upon by large sediments or rubble (Figures 3.4A, 3.4C). BSMs top of rock installations range from 310.30 – 310.63 masl, with the bottom of the deepest hole at 310.00 masl; therefore, not all BSMs intersect the same litho-stratigraphic layer or bedding plane.

River stage gauges were instrumented with SWS CTD Divers™ (Schlumberger Water Services, Delft, The Netherlands). Piezometers were instrumented with smaller-diameter Micro-Divers™, and 12 out of 24 BSMs were instrumented with Mini- and Micro-Divers™. The relative importance of component uncertainties increases greatly in shallow environments, where differences are small. Since pressure transducer accuracy declines with depth range, choice of instrumentation and independent accuracy verification is critical . Pressure transducers were field-tested inside the static water column of a FLUTe™ (Flexible Liner Underground Technologies, Alcalde, NM, USA) and calibrated using the straight-line and differences analysis methods. Details of the range and uncertainty associated with all absolute (non-vented) transducers used in this study are summarized in Table 3.1.

3.2.3 BSM Measurements – Direct and Indirect

Chapter 2 established that the BSM works well in its capacity to measure groundwater discharge and hydraulic head differentials between groundwater and surface water and for hydro-chemical sampling. Methods summarized below are detailed in Chapter 2. Recall that surface water flow, or streamflow, is represented as Q^{sw}. Groundwater flow, represented as Q, was measured in seepage tests during a known test time (t) of 10 or 20 min and reported as:

$$Q = \frac{\Delta V - 22\ cm^3}{t - 45\ s}\ \ [cm^3 s^{-1}] \qquad [6],$$

where the volume of water collected (ΔV) was corrected by the device tube volume (ie, 22 cm^3) and t was corrected by the equilibration time (i.e., 45 s) [Chapter 2, Fig. 2.5].

Assuming radial flow and that Darcy's Law is valid, groundwater flux (q) was estimated according to Equation 7, where A represents the vertical cylindrical surface area of the seepage cavity.

$$q = \frac{Q}{A} = \frac{Q}{2\pi rL} = \frac{Q}{2\pi(5\ cm)(25\ cm)} = \frac{Q}{798\ cm^2}\ [m/s] \qquad [7].$$

The bulk fracture porosity (ϕ_f) for intact fractured rock is very small, with values in the order of 1 – 0.001% or 10^{-2} to 10^{-5} (Freeze and Cherry 1979; Parker 2007; Lipson *et al.*, 2005). For dolostone, Muldoon and Bradbury (2005) reported ϕ_f values of 10^{-2}, while Munn (2012) and Belan (2010) reported ϕ_f values of 10^{-4}. Average linear groundwater velocities ($\bar{v}$) through the seepage cavities were, therefore, estimated using q divided by an estimated fracture porosity for weathered streambed dolostone of 0.1% or 10^{-3} [Equation 8],

$$\bar{v} = \frac{Q}{A * \phi_f} = \frac{q}{\phi_f} = \frac{q}{10^{-3}}\ [m/s] \qquad [8]$$

Groundwater head or total hydraulic head in the seepage cavity (h_2) was calculated as:

$$h_2 = h_{p2} + h_{z2}\ \ [m] \qquad [9],$$

where pressure head (h_{p2}) was measured using absolute (non-vented) wireless SWS Mini-Divers™ and Micro-Divers™ (Schlumberger Water Services, Delft, The Netherlands). Elevation head (h_{z2}) was measured using a Leica Viva GS08plus GPS (Leica Geosystems Inc., Norcross, GA, USA).

Head differentials between groundwater and surface water (Δh) were quantified from independent measurements of groundwater head and surface water head [Chapter 2, Fig. 2.6A, 2.6C], as:

$$\Delta h = h_2 - h_1 \qquad [10].$$

Relative head differentials between groundwater and surface water (Δh_{rel}) were measured directly with a potentiomanometer designed for use with the BSMs [Chapter 2, Fig. 2.6E]. Findings in Chapter 2 revealed that Δh_{rel} was a more reliable measurement than the Δh achieved with transducers and a

bathymetric tool for the following reasons: (1) uncertainties inherent with two head measurements are large (i.e., the sum of accuracies of the transducers, the bathymetry tool, the GPS, the flow meter, and the standard error associated with sample size, as summarized in Table 3.1), (2) uncertainties with one direct potentiomanometer measurement are small, and (3) since this a strongly-anisotropic discrete fracture network and the head differentials measured contribute to only one small component of the hydraulic gradient, they are expected to be very small, as demonstrated with the potentiomanometer. Therefore, it was the preferred choice to estimate vertical hydraulic gradients (i) from point measurements across a 0.05-m layer of fractured dolostone (ΔL) as:

$$i = \frac{\Delta h_{rel}}{\Delta L} \qquad [11].$$

Specific capacity refers to the transmissivity or productivity of a well or seepage cavity, defined as the flow rate (Q) divided by the drawdown or change in hydraulic head (Δh_{rel}) in the aquifer at the well screen boundary [Equation 13] (Theis *et al.*, 1963; Freeze and Cherry 1979),

$$\text{Specific Capacity} = \frac{Q}{\Delta h_{rel}} \qquad [13].$$

3.3 Results and Discussion

3.3.1 Quantifying Groundwater Flux and Vertical Gradients from Streambed Measurements

Independent streambed measurements of flow from steady state tests, and head from temporal monitoring and point measurements were used to estimate groundwater velocities and hydraulic gradients, and to evaluate the transmissivity of the streambed at each BSM. Groundwater flow (Q) measurements ranged from 3 – 35 mL/min at high stage and from -0.4 – 55 mL/min at low stage ± 20% (Table 3.2). Assuming radial flow, these measurements yielded fluxes (q) of 0.05 – 0.63 m/day at high stage and 0.12 – 0.99 m/day at low stage (Table 3.2). Assuming a bulk fracture porosity (ϕ_f) of the

streambed dolostone of 0.1% or 10^{-3}, these measurements also yielded average linear groundwater velocities ($\bar{v}$) of 55 – 629 m/day at high stage and 7 – 985 m/day at low stage (Table 3.2).

The relative head difference between groundwater and surface water (Δh_{rel}), directly measured with a potentiomanometer, ranged from 0.001 – 0.023 m at high stage and from 0.001 – 0.012 m at low stage ± 0.001 (Table 3.3). Vertical hydraulic gradients across a 5-cm layer of streambed dolostone ($\Delta h_{rel}/\Delta L$) ranged from 0.02 – 0.46 (Table 3.4). Differential heads (Δh) from independent measurements of groundwater head (i.e., using transducers) and surface water head (i.e., using bathymetry) ranged from 0.01 – 0.15 m, with a range of uncertainties (estimates provided in Table 3.3). As previously discussed, Δh_{rel} is a direct measurement with a smaller uncertainty (of ± 0.001 m) and was, therefore, favoured as the more accurate representative of the differential head and hydraulic gradient.

The specific capacity calculation is a useful method to assess relative transmissivity of the bedrock streambed at each BSM location because: (1) it uses direct, independent measurements of flow and head differentials; and (2) unlike the hydraulic conductivity calculation, it does not require any radius of influence estimates and the uncertainties associated with assumptions with the analytical solution used to calculate them (Chapter 2). In general, high specific capacities indicate an aquifer with a higher transmissivity and low specific capacities coincide with lower transmissivities. In this case, BSM radius and depth are consistent across all installations and will not bias results as could otherwise be the case (Theis *et al.,* 1963). Specific capacities ($Q/\Delta h_{rel}$) ranged from 2 x 10^{-6} to 9 x 10^{-4} m^2/s (Table 3.4). Normalization of these results, shown in Table 3.4, reflects a range in transmissivity of 2-3 orders of magnitude, emphasizing the heterogeneous nature of the flow system.

3.3.2 Spatial Variability of Groundwater Discharge in a Bedrock Channel

Spatial analysis of point measurements collected with the BSMs was conducted with consideration given to: (1) high and low river stage (or water table) conditions, as described in section 3.1.5; (2) location of BSM relative to the fracture network; and (3) elevation of the BSM relative to the

channel topography. The BSM is a short-interval artesian well, each with a 0.30-m open interval that may be partially or fully penetrating a hydrogeologic unit not yet defined in this system, between 310.00 – 310.63 masl (i.e., in the Z-dimension). Twenty-four BSMs are spatially distributed across the study reach, both transversely and longitudinally (i.e., in the X-Y dimensions). Hence, the spatial variability of hydraulic results were assessed in a 3-D context. Figure 3.6 demonstrates this concept, where the spatial distribution of the BSMs, identified by number, is represented within a topographic model of the channel and an overlay of the streambed fracture map. Consideration was also given to site-specific complementary data, including: (1) dominant orientation and length of the fractures terminating at the streambed surface (Figure 3.4D); (2) the high ratio of bedding plane to vertical fractures (Figure 3.4B); and (3) location of rubble cover (Figure 3.4D) [further detailed in Appendices C and D].

Prior to constructing conceptual models, numeric assessment of hydraulic results were conducted by dividing the BSMs into elevation classifications of shallow (310.50 – 310.63 masl), mid-depth (310.40 – 310.49 masl) and deep (310.30 – 310.39 masl) installations (Figure 3.6). Results by elevation class are summarized in Figure 3.7, including fluxes (Figure 3.7A – 3.7C) and vertical hydraulic gradients (Figure 3.7D – 3.7F) at high and low river stage. A blended head condition (Lambe and Whitman 1969) exists in the 25-cm open interval below the 5-cm packer seal of the BSM, meaning that a head measurement from a BSM represents the entire interval and all of its intersecting fractures. There is a high ratio of horizontal-to-vertical fractures at this site (Figure 3.4B), thus, it is more likely that a drilled seepage cavity will intercept bedding plane fractures than vertical fractures.

Trends observed in BSMs 2, 4 and 5, installed on vertical fractures terminating at surface, include: large fluxes in BSMs 2 and 4 (i.e., 42 – 99 cm/day) and moderate fluxes in BSM 5 (i.e., 7 – 20 cm/day) (Table 3.2), with all three BSMs yielding hydraulic gradients that were small (≤ 0.08) at high stage and very small (≤ 0.04) at low river stage (Table 3.4; Figure 3.7). Trends observed in BSMs 1 and 10, with cavities intersecting vertical fractures beneath the packer seal, include: high fluxes (19 – 45 cm/day) and moderate gradients (0.12 – 0.24) (Figure 3.7). Fluxes in the upstream riffle – pool transition

zone (indicated in red on Figure 3.7) tend to be smaller (3 – 16 cm/day), with no observable trend in hydraulic gradient. In general, hydraulic gradients at high river stage are larger than at low stage, with three exceptions (Figure 3.7D-F). Hydraulic gradients in BSMs 9, 16 and 17 are higher at low stage. Flux in BSM 9 declines at high stage, while no difference in flux is observed in BSMs 16 and 17. The deep BSMs (i.e., 310.30 – 310.39 masl) installed in the pool (indicated in blue on Figure 3.7) tend to reflect lower hydraulic gradients (≤ 0.10) than at the shallow (≤ 0.24) and mid-depth (≤ 0.20) elevations, particularly at low stage (Figure 3.7D-F). BSM 3, located at the end of the longitudinal step sequence (Figure 3.6), yielded consistently high fluxes (27 – 30 cm/day) and small gradients (0.04 – 0.10) (Figure 3.7C, F).

Assessment of hydraulic results included a correlation analysis between independent measurements of flow (Q) and differential head (Δh_{rel}). This relationship was found to be weakly linear and inverse, with Pearson Coefficients ranging from R = -0.10 to -0.42 (Figure 3.8), with one exception. Correlation in the shallow BSMs, located mainly along the south side of the channel, is weakly linear and direct (i.e., R = 0.30) (Figure 3.8D). High Q and Δh_{rel} values in riffle BSMs tend to skew results. Flow was collected in deep BSMs 2, 6, 18 and 22 on the north side of the channel, when the differential head between groundwater and surface water was unresolvable (not detected) (Figure 3.8). It is difficult to resolve a relationship, linear or otherwise, between Q and Δh_{rel} given that: (1) anisotropy is strong in a three-dimensional flow system of discrete fracture networks; (2) hydraulic conductivities and boundary conditions are not known; and (3) the vertical head differentials measured provide only one small component of the hydraulic gradient. The glaciofluvial plain of the study site exhibits low topographic relief and, therefore, influence from the regional flow system, shown in Figure 1.5, is expected (Toth 1963).

Conceptual models give spatial context, from both a topographic and fracture network perspective, to quantified parameters of flux (Figures 3.9 – 3.10) and vertical gradient (Figures 3.11 – 3.12) in the study reach. At high stage, high fluxes (q) (i.e. above the median of 12 cm/day) are observed

longitudinally, along the north side of the channel, and transversely, along transects 2 and 3½, as delineated within the red outline on Figure 3.9. Lower fluxes (i.e., ≤ 12 cm/day) are observed between transects 2½ and 3. At low stage, the zone of higher fluxes (q) (i.e., above the median of 6 cm/day) recedes away from the south side of the channel and extends to BSMs 17 and 19 along the thalweg (Figure 3.10). Groundwater discharge in BSMs 16, 17, 19 and 21 is not impacted by a change in water table elevation and q–values do not change between high and low river stage. The high-q delineation shapes were applied to the conceptual models of hydraulic gradient at high (Figure 3.11) and low (Figure 3.12) stage. At high stage, small hydraulic gradients were observed in the high-q zone, with two exceptions (Figure 3.11); the upstream cluster of BSMs 1, 12 and 13 and BSM 10 near channel centre (Figure 3.11). BSMs 1 and 10 are installed on vertical fractures terminating beneath their packers (Figure 2.4A*iii*). At low stage, this trend continued, except BSMs 12 and 13 were now part of the low-q zone (Figure 3.12). At high and low stage, large gradients were observed in the low-q zone, except along the north (i.e., BSMs 18 and 22) and south (i.e., BSMs 9, 11, 23) perimeter of the zone (Figures 3.11 – 3.12).

BSMs installed on vertical fractures terminating either at surface (i.e., BSMs 2, 4 and 5) or beneath the packer (i.e., BSMs 1 and 10) yielded high fluxes, ranging from 7 – 99 cm/day, regardless of elevation or position along the channel. Vertical hydraulic gradients were small in BSMs 2, 4 and 5, at ≤ 0.08, and moderate in BSMs 1 and 10, at 0.12 – 0.24, indicating a difference in the flux – gradient relationship between the two installation types. Compared to BSMs on vertical fractures terminating at surface, results show that installations on vertical fractures that do not run the full length of the seepage cavity have larger gradients, but similar fluxes.

Groundwater discharging to surface water has been quantified as flux (q) (Figure 3.7) and conceptualized in a spatial context in Figures 3.9 – 3.10. Delineation of high- and low- q zones and their contributions to baseflow in the X-Y dimension can be linked to surface water in the channel using plots of cumulative streamflow (Q^{sw}) (Figure 3.13A), bathymetric profiles (Figure 3.13B-K), and discharge rating curves (Figure 3.14). Elevation of the south side of the channel is up to 0.30 m higher than the

north side, as reflected in the bathymetric transect profiles shown in Figure 3.13. At transect 2, the river stage exhibits a -0.5% slope from south to north, as the channel geometry bends (Figure 3.13D). A transverse topographic influence (i.e., in the Z-dimension) may, therefore, account for less groundwater discharge measured along the south side of the channel, particularly at low stage. Elevation of the channel centre also declines by up to 0.6 m from riffle to pool, as reflected in the thalweg profile shown in Figure 3.5, applying a longitudinal topographic influence, resulting in groundwater discharge observed in the pool (i.e., downstream of transect 3). Stream discharge (Q^{sw}) rating curves, constructed from hydrometric surveys (Figure 3.14), demonstrate a change in the depth-discharge relationship as the channel transitions from riffle (Figures 3.14A-B) to pool (Figures 3.14C-G) to riffle (Figures 3.14H-I). Specifically, the largest Q^{sw} occurs across the moderate-to-deep part of the pool, as opposed to only in the deepest part of a riffle segment. This trend is intensified at low stage. Beyond these topographic correlations, there are vertical fractures terminating at surface, representing the discrete fracture network within the streambed aquifer to consider. The largest fluxes, at both high and low stage, were measured in BSMs directly connected to vertical fractures, with two exceptions. BSM 7 is not installed on a vertical fracture, however, it is installed in a part of the pool where a high fracture density was measured and is likely indirectly linked to one via a hydraulically-active bedding plane fracture. BSM 3 is installed at the end of the longitudinal step sequence where numerous weathered bedding plane fractures terminate at surface, providing a preferential pathway for groundwater to discharge to surface water. Since groundwater discharge was measured in BSMs 672 times during this study, it may be inferred that flux is a function of the connectivity between hydraulically-active vertical fractures and bedding plane fractures terminating along the 3-D riverbed surface.

In the context of an alluvial riverbed, small q expands hyporheic extent, while large gradients shrink hyporheic extent, as observed in the Speed River (Howard *et al.*, 2006; Storey *et al.*, 2003). These findings may be interpreted as: more hyporheic water residing in a riverbed beneath low-q zones, and less hyporheic water residing in a riverbed where large vertical gradients are observed. In this study of a

bedrock river, low-q zones were observed at the riffle – pool transition and along the south side of the channel, where river stage elevation is likely higher than the water table in the adjacent glaciofluvial plain. Since the spatial distribution of large vertical gradients in the study reach was variable, but often coincided with low-q zones, this concept does not appear to be transferable to this bedrock river environment.

Differential head between deeper groundwater and surface water, measured in river piezometers reflect upward, vertical hydraulic gradients beneath the BSMs. Upward gradients were observed in 5 of 6 river piezometers. P1 and P2, installed at the upstream and downstream riffles of the study reach (Figure 3.4A) and screened at a depth of 0.7 mbgs (Table 3.5), yielded vertical hydraulic gradients at high stage of 1.10 and zero, respectively. P3 – P6, installed closer to the BSMs and screened at a depth of 3.0 mbgs (Table 3.5), yielded hydraulic gradients ranging from 0.90 to 1.60 at high stage, with the largest gradients occurring on the north side of the channel and in a downstream direction (Figure 3.11). At low stage, vertical gradients in all river piezometers were all about half that of their high-stage gradients, except for P2 which maintained a zero gradient (Figure 3.12). Upward gradients in the river piezometers is expected, since they are installed deeper in the system, and the regional flow model has identified groundwater discharging toward the channel in the area of the study site (Figure 1.5).

3.3.3 Streamflow Variability

Hydrometric surveys along transects revealed that cumulative streamflow or surface water discharge (Q^{sw}) at high stage was 40% higher in the riffle zone (i.e., along transects 0 – 2) and 33% higher in the pool compared to low stage (Figure 3.13A). Froud values ranged from 0.1 – 0.2 (data not shown), indicating that with the exception of possibly spring freshet, only subcritical flow was observed and streamflow variability across transects was not large. Reduced Q^{sw} is observed at the streambed transition from upstream riffle to downstream pool, with losses of 0.38 m^3/s at high stage and 0.15 m^3/s at low stage (Figures 3.13A – 3.13D). These results coincide with the low-q zone identified in Figures 3.9-3.10. Increased Q^{sw} of up to 0.15 m^3/s is observed in the pool that remains constant at high stage. At low

stage, a similar increase of 0.15 m^3/s is observed in the pool (Figure 3.13A, 3.13E-H), with the exception of transect 5 (Figures 3.13A, 3.13I), as the longitudinal profile of the rockbed starts to step up towards the next riffle at transect 7. These results coincide with the high-*q* zone identified in Figures 3.9-3.10. No BSMs were installed near transect 5, where the streambed was dominated by rubble; however, the presence of rubble may be an indicator of clogged fractures that impede groundwater discharge. Having said that, it is difficult to conclude gaining or losing conditions in a short reach-scale study where fluxes are small, gradients are variable, and channel geometry reflects a meander bending through the fluvial plain.

3.3.4 Hydraulic Connectivity Identified from Disturbances.

Two abrupt, short-term declines in surface water head were observed in the upstream river stage gauge SG1, while the downstream gauge, SG2 and the Watson Gauge, remained stable (Figure 3.3). The decline in head in the SG1 from June 5-13, 2014, coincided with a decline in upstream riverbed piezometer P1 and two field events. On June 5, 24 BSMs field-tested in 2013-14 were removed from the riverbed, leaving the seepage cavities open for ≤ 1 hour, before the new prototypes were deployed. Four days later, on June 9, FLUTe™ liners were removed from the three floodplain well pairs installed along the south side of the channel (i.e., SCA1-V1, SCA2-V2 and SCA3-V3) and re-deployed over a 3-hour period [refer to site map in Appendix D, Fig.D-1]. Head in the river and in P1 recovered 4 days later, on June 13. The decline in head in the SG1 from July 10-27, 2014, also coincided with a decline in P1 and three field events. On July 10, all BSMs were removed for inspection and maintenance. On July 14-15, riverbed piezometers P3-P6 were drilled and sealed with 40-cm screens at 3 mbgs. Over the next 8 days (i.e., July 15-23), packer testing was conducted in 6 of the 8 floodplain wells. Head in the river and in P1 recovered 4 days later, on July 27th. Only one seepage test was conducted (on July 24th) during the period of disruption. These results show evidence of a flowpath from inflection point 1 into the floodplain along the concave bend south of the channel (Figure 3.2). Groundwater flow along this path increased when the FLUTe™ liners in the floodplain wells were disturbed, resulting in an upstream decline in surface water

head, while surface water head downstream (i.e., at SG2) remained stable (Figure 3.3). Removal of the BSMs from their cavities initiated surface water head losses upstream, but not downstream, indicating increased flow of recirculated water escaping from the open cavities in the pool. The drilling of P3-P6 created potential for cross-connection along their 3-m lengths prior to being sealed that likely contributed to upstream head losses, since recovery of SG1 and P1 did not occur between July 10-15.

Cumulative knowledge of groundwater fluxes, streamflow gains and losses, and responses to controlled disturbances provide insights concerning hyporheic flow patterns in the X-Y-Z-dimension. Excluding BSMs 1 and 2 (installed on vertical fractures), mean fluxes in the upstream riffle – pool transition zone ranged from 3 – 16 cm/day, with hydraulic gradients ≥ 0.10, and hydrometric surveys revealed that a losing condition was occurring in this segment of the study reach. Location of the riffle coincides with the start of a river bend, where surface water flows along a small creek cutting across the neck of the meander on the north side of the channel and into the floodplain bank on the south side, contributing to streamflow losses. Short-term declines in surface water head, resulting from flow system disturbances, observed in the upstream stage gauge, SG1, show evidence of a hyporheic flowpath from the riffle zone into the floodplain along the concave bend on the south side of the channel. On two occasions, removal of FLUTe™ liners from floodplain wells disturbed the flow system by cross-connecting elevations, resulting in an upstream decline in surface water head that was not observed downstream at SG2

3.3.5 Temporal Variability in Hydraulic Head and Temperature

A spatio-temporal assessment of head and temperature across the study reach was conducted using continuous records collected over a one-year period, from May 2014 – May 2015, in 12 of the 24 BSMs installed in the study reach. Sixty-day snapshots of the temporal records were extracted to present the two key end-member conditions: low river stage in late summer (i.e., August – September 2014) (Figure 3.15A), and high river stage approaching and during winter freeze-up (i.e., December 2014 – January 2015) (Figure 3.15B). All continuous records from BSMs, river piezometers and stage gauges

were collected using calibrated, non-vented transducers with temperature accuracies of ± 0.1°C and pressure head uncertainties listed in Table 3.1 (refer to Chapter 2, section 2.5.6 re temperature calibration of transducers). The BSM elevation classification was applied to evaluate disparities between records against the topography of the channel and correspondingly different litho-stratigraphic intervals at depth (Figure 3.1). Groundwater head (h_2) in all BSMs was higher than the surface water head (h_1), except for BSM 4, where a zero differential was observed (Figure 3.15A-B). Summer trends were observed, depending on elevation, where the shallow BSMs reflected head differentials between groundwater and surface water of 0.16 – 0.19 m and the deep BSMs yielded head differentials of 0.10 – 0.15 m. Except for BSM 4, the head record for the mid-depth BSMs fell within the deep and shallow classes (Figure 3.15A).

It is possible that this layering of the head records is linked to the slope of the water table elevation identified from hydrometric surveys, since many of the shallow BSMs are on the south side of the channel, while the deep BSMs tend to occupy the north side. The air temperature record, measured with an on-site barometric pressure / temperature sensor, ranged from 0 – 39°C (data not shown). The temperature record for the river showed a high degree of variability, ranging from 10.5 – 22.9°C, due to atmospheric influences. BSM 4 reflected similar variability, indicating that surface water was circulating through the seepage cavity (Figure 3.15A). The other 11 BSMs yielded less variable temperature records, ranging from 12.1 – 19.9°C, due to the moderating effect of (cooler) groundwater discharging into the seepage cavities (Figure 3.15A). In winter, similar trends were observed, where the shallow class reflected a head differential between groundwater and surface water of 0.18 – 0.22 m and the deep BSMs yielded a head differential of 0.12 – 0.17 m. The head record for the mid-depth BSMs fell within the deep and shallow classes, except for BSM4, which was similar to the river (Figure 3.15B). A period of variability occurred during freeze-up in early January, but all continuous head records remained consistent relative to each other. The on-site air temperature record ranged from -20 to 10°C (data not shown). The temperature record for the river reflected some variability, ranging from 0.1 – 4.4°C, due to atmospheric influences. Compared to summer, cold winter temperature differentials between groundwater

and surface water were more discernable. The variability of the temperature record for BSM 4 was similar to the river until freeze-up, when a differential of 0.3^{o}C stabilized (Figure 3.15B). The other BSMs yielded less variable temperature records, ranging from 0.9 – 4.0^{o}C, due to the moderating effect of (warmer) groundwater discharge, until freeze-up, when a differential of 0.8^{o}C stabilized, with one exception (Figure 3.15B). BSM 2 exhibited a short-term decline of up to 1^{o}C in early December, indicating an influx of surface water into the seepage cavity, and some minor variability in late January (Figure 3.15B). BSMs 2 and 4 are installed on vertical fractures terminating at surface. In the case of BSM 2, there is no evidence in the head record of surface water entering the seepage cavity, even when short-term temperature changes indicate a surface water influence. The transient record for BSM 4, on the other hand, indicates constant connectivity to the river, with similar hydraulic head and variability in temperature, summer and winter. These results reflect a strong surface water influence in BSM 4, indicating a leaky installation where the volumetric flow collected was likely a mix of groundwater and surface water. BSM 2 yielded much higher fluxes at low stage compared to high stage and compared to BSM 4, and short-term variability in the winter temperature record was observed only at low stage, indicating that surface water enters the fractures intersecting the seepage cavity only when the water table declines.

3.3.6 Temporal Variability in Hydraulic Head and Temperature with Depth

Representative continuous records for each BSM class (i.e., shallow, mid-depth and deep) were plotted with the transient records for the river piezometers to compare the head and temperature of groundwater in the hyporheic zone with that of groundwater at greater depths (Figure 3.16). In summer, shallow piezometers P1 and P2, screened at 0.7 mbgs (Table 3.5), yielded temperature records that were up to 1^{o}C (± 0.1^{o}C) cooler than the BSMs, indicating a (cool) groundwater influence (Figure 3.16A). The deeper piezometers, P3 – P6, screened at 3.0 mbgs (Table 3.5), exhibited very consistent temperature records ranging from 13.8 – 14.8^{o}C (± 0.1^{o}C) and a differential that was up to 20^{o}C below that of the river. (Figure 3.16A). This trend continued until mid-September, when seasonal atmospheric and surface

water temperatures started to fall, resulting in a decline in the thermal records for P1, P2 and all BSMs to below that of the deeper groundwater in P3 – P6. The transient head record for P2, located in the downstream riffle, is similar to the river, while head in the other 5 river piezometers is similar to the BSMs. P4, on the south side of the channel, exhibited higher hydraulic peaks than the other piezometers (Figure 3.16A).

In winter, temperature differentials between groundwater and surface water reflected in the continuous records were smallest in the BSMs, at ≤ 1.3^{o}C, followed by the shallow piezometers, at ≤ 2.8^{o}C, and the deep piezometers, at ≤ 7.3^{o}C (Figure 3.16B). Thermal variability ranged from 1.6 – 4.5^{o}C in P1-P2, and from 4.8 – 8.3^{o}C in P3, P5 and P6. Compared to the other deep piezometers, variability in P4 was slightly higher, ranging from 5.1– 8.5^{o}C. Trends in the hydraulic records identified in summer were also observed in winter, where head in P2 was similar to that of the river, head in P1 and P3 – P6 was similar to the BSMs, and P4 exhibited higher hydraulic peaks than the other piezometers (Figure 3.16B). Compared to the BSMs, reduced variability in the temperature records for P1 and P2 indicates that groundwater has a stronger influence on hyporheic temperatures in winter at 0.7 mbgs than at 0.3 mbgs. The hydraulic record for P2 indicates a strong surface water influence, however, the temperature record reflects a groundwater presence similar to that of P1. Compared to the BSMs, the temperature records for P3 – P6 indicate that groundwater discharge is occurring, evidenced by similar consistency, with no evidence of a surface water influence in summer or winter. The hydraulic records for P1 and P3 – P6 indicate groundwater discharge at all locations during summer and winter. P4 exhibits higher hydraulic peaks than the other piezometers and a slightly larger thermal differential between groundwater and surface water in winter, indicating a stronger groundwater influence.

Temporal temperature records indicate that a hydraulically-active hyporheic fracture network has been intersected by the BSMs and by the shallow piezometers (i.e., between 0.30 – 0.70 mbgs or 309.95 – 310.58 masl), reflecting less variable temperatures that are cooler in summer and warmer in winter. Groundwater in the Guelph area maintains a temperature of ~10^{o}C and temperatures in the screened

intervals of the deep piezometers (i.e., 3.0 mbgs or 307.35 – 308.22 masl) reached temperatures that were about 5^{o}C colder in winter and 5^{o}C warmer in summer. Thus, hyporheic mixing of groundwater and surface water extends to a depth of at least 307.35 masl. The shallow piezometers, P1 and P2 reflect some interesting qualitative and quantitative results. P1 in installed in the upstream riffle at the entrance of the channel bend, where a losing condition is observed. P2 is installed in the downstream riffle at the exit of the channel bend, where a gaining condition is observed. Encroaching rubble at these two installations made the measurement of streambed fractures impossible, so their influence is unknown; however, the core log for SCA1 plunging beneath P1 reveals numerous vertical and high angle fractures. The head records for these shallow piezometers shows an upward gradient of 0.05 – 1.10 in P1 and a zero gradient in P2. However, P1 and P2 have similar temperature profiles, summer and winter, that are less variable than the BSMs but more variable than the deeper piezometers, P3 – P6. These results indicate a moderate groundwater influence in the zero gradient P2 likely due to a flow-through or parallel-flow condition.

3.4 Conclusions

The purpose of quantifying groundwater fluxes and vertical hydraulic gradients using four independent measurements (i.e., flow from seepage tests and head from temporal monitoring and manual point measurements using a potentiomanometer and a bathymetric tool), was to reduce bias from the data used to characterize groundwater – surface water interactions within the study reach. Interpretation of groundwater and surface water data sets in combination with topographic and geologic data sets is complex, involving numerous linkages and interdependencies. Consequently, four key considerations were used to evaluate spatial variability of point measurements, namely: (1) a split data format of high and low river stage to detect changes in response to a declining water table; (2) identification of fracture density, geometry and proximity to BSM installations; (3) elevation of the BSM relative to the channel topography and stratigraphy; and (4) position of the BSM relative to channel meander geometry.

On a regional scale, a strong influence of groundwater discharging to the river in accordance with the regional flow model was expected (Gartner Lee 2004), since the glaciofluvial plain of the study site exhibits low topographic relief (Toth 1963). On a reach scale, volumetric flow (Q) measurements ranged from 3 – 35 mL/min at high stage and from 0 – 55 mL/min at low stage, with uncertainties that ranged from 13 – 40% (n = 672). Assuming radial flow, these measurements yielded fluxes (q) of 0.05 – 0.63 m/day at high stage and 0.12 – 0.99 m/day at low stage. Assuming a bulk fracture porosity (ϕ_f) for the streambed dolostone of 0.1% or 10^{-3}, these measurements also yielded average linear groundwater velocities ($\bar{v}$) of 55 – 629 m/day at high stage and 7 – 985 m/day at low stage. Head differentials (Δh) between groundwater and surface water estimated from groundwater head (h_2) transducer measurements and surface water head (h_1) manual measurements, ranging from 0.01 – 0.15 m, had high uncertainties and showed poor agreement with potentiomanometer measurements. Relative head differentials (Δh_{rel}) between groundwater and surface water directly measured with a potentiomanometer reflected more consistent results and much smaller uncertainties, ranging from 0.001 – 0.023 m at high stage and from 0.001 – 0.012 m at low stage ± 0.001. Vertical hydraulic gradients across a 5-cm layer of streambed dolostone ($\Delta h_{rel}/\Delta L$) ranged from 0.02 – 0.46. Specific capacities from flow and relative head difference measurements ($Q/\Delta h_{rel}$) ranged from 2 x 10^{-6} to 9 x 10^{-4} m^2/s, indicating a wide range of transmissivities in the streambed fracture network.

This is the first study of a bedrock river conducted using the BSM to evaluate groundwater – surface water exchanges. BSMs installed on vertical fractures terminating either at surface or passing through the cavity beneath the packer yield the highest fluxes, indicating that groundwater is discharging to surface water through vertical fractures. BSMs installed in bedding plane fractures and near vertical fractures terminating at surface yield groundwater fluxes, indicating that bedding plane fractures provide preferential pathways for groundwater to move through the hyporheic zone until it finds an exit opportunity to the channel.

Installing BSMs directly on fractures terminating at surface is challenging, as discussed in Chapter 2. BSMs installed on vertical fractures terminating either at surface (i.e., BSMs 2, 4 and 5) or beneath the packer (i.e., BSMs 1 and 10) yielded high fluxes, ranging from 7 – 99 cm/day, regardless of elevation or position along the channel. Vertical hydraulic gradients were small in BSMs 2, 4 and 5, at ≤ 0.08, and moderate in BSMs 1 and 10, at 0.12 – 0.24, indicating that installations on vertical fractures that do not run the full length of the seepage cavity have larger gradients, but similar fluxes. Insights gained from measurements collected in upstream BSM 2 and downstream BSM 4 were very useful in assessing both the bedrock river environment and this new tool. The temporal hydraulic record for BSM 4 reflected a strong surface water influence, indicating a leaky installation where the volumetric flow collected was likely a mix of groundwater and surface water. BSM 2 yielded much higher fluxes at low stage compared to high stage and compared to BSM 4. Short-term variability was observed in the winter temperature record for BSM 2 at low stage, indicating that surface water enters the fractures intersecting BSM 2 when the water table declines.

In addition to the geologic influence of observable vertical fractures, spatial distribution of flux and vertical gradients is strongly linked to topographic elevation. Groundwater discharging to surface water is greatest along the north side of the channel and in the pool downstream of transect 3. Elevation of the north side of the channel is generally lower, indicating a topographic influence is observed in the transverse direction. Elevation of the pool is lower than the riffle, indicating a topographic influence in the longitudinal direction.

Excluding BSMs 1 and 2 (installed on vertical fractures), mean fluxes in the upstream riffle – pool transition zone were small and hydrometric surveys revealed that a losing condition was occurring in this segment of the study reach. Location of the riffle coincides with the start of a river bend, where surface water flows along a small creek cutting across the neck of the meander on the north side of the channel and into the floodplain bank on the south side, contributing to streamflow losses. Short-term declines in surface water head, resulting from controlled flow system disturbances, observed in the

upstream stage gauge, SG1, show evidence of a hyporheic flowpath from the riffle zone into the floodplain along the concave bend on the south side of the channel.

Temporal monitoring in 12 of 24 BSMs revealed that groundwater head in all BSMs was higher than the surface water head (i.e., an upward gradient), except for BSM 4, where a zero gradient was observed. The continuous hydraulic record for piezometers P3 – P6 also indicated upward gradients. The summer temperature record for the river and for BSM 4 showed similar variabilities due to atmospheric influences, indicating a strong surface water influence. The other 11 BSMs yielded less variable temperature records, due to the moderating effect of cooler groundwater discharge. The winter temperature record for BSM 4 was close to zero and similar to that of the river, while the other 11 BSMs reflected a warmer groundwater influence. Temporal temperature records indicate that a hydraulically-active hyporheic fracture network has been intersected by the BSMs and by the shallow piezometers (i.e., between 0.30 – 0.70 mbgs or 309.95 – 310.58 masl), reflecting less variable temperatures that are cooler in summer and warmer in winter. Since groundwater in the Guelph area maintains a temperature of ~10^{o}C and temperatures in the screened intervals of the deep piezometers (i.e., 3.0 mbgs or 307.35 – 308.22 masl) reached temperatures that were about 5^{o}C colder in winter and 5^{o}C warmer in summer, hyporheic mixing of groundwater and surface water extends to a depth of at least 3.0 m below the riverbed or elevation of 307.35 masl.

The shallow piezometer, P1, is installed in the upstream riffle at the entrance of the concave bend on the south side of the channel, and P2 is in the downstream riffle at the exit of the channel bend. The reconnaissance infrared temperature survey, detailed in Appendix A, revealed a thermal signature indicating potential groundwater discharge along the south side of the channel near P2 [Appendix A, Fig. A-9]. The continuous head records reflect an upward gradient of 0.05 – 1.10 in P1 and a zero gradient in P2. P1 and P2 have similar temperature profiles, summer and winter, that are less variable than the BSMs but more variable than the deeper piezometers, P3 – P6, indicating a groundwater influence. These results indicate that a parallel-flow condition exists near P2.

The extent of hyporheic flow in discrete fracture networks interpreted from this study is based on point measurements collected on or near vertical fractures terminating at surface where intact dolostone pavement is exposed and rubble is absent. It was observed during the 2013 – 2015 field seasons that when streamflow energies are high (i.e., during spring freshet), deposition does not occur in these regions of exposed pavement, and sediment particles as large as boulders are continually evacuated in a downstream direction beyond transect 4. Streamflow (Q^{sw}) measurements indicate a gaining condition begins near transect 3 and continues in a downstream direction, likely due to contributions to baseflow. Having said that, losing Q^{sw} values are only moderately smaller than gaining Q^{sw}, fluxes are small, gradients are variable, and channel geometry reflects a meander bending through the fluvial plain. These subtle changes, therefore, may also be indicative of flow-through segments within the study reach.

3.5 Tables and Figures

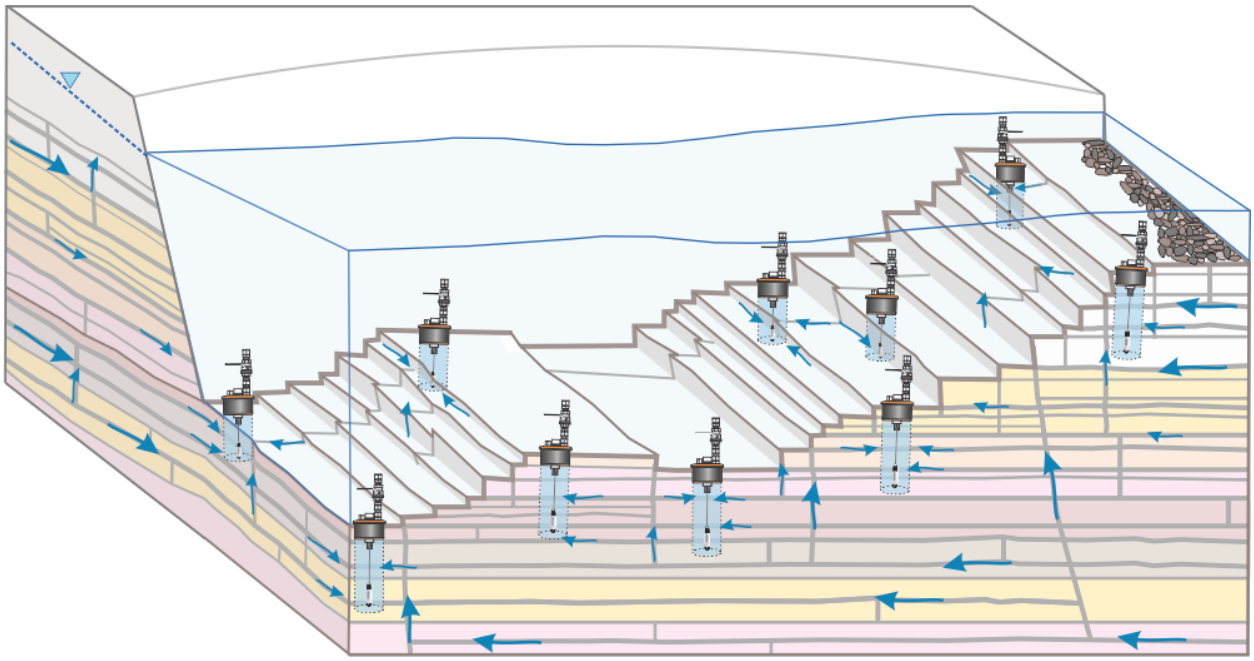

Figure 3.1. Conceptual model of a riffle-pool transition in a sedimentary bedrock streambed, illustrating how installation of BSMs along a typical longitudinally-stepped profile can result in partial-to-full penetration of different hydrogeologic units within a small area, thus, capturing the potentially-variable discrete fracture network of stratigraphic units at depth and along the profile.

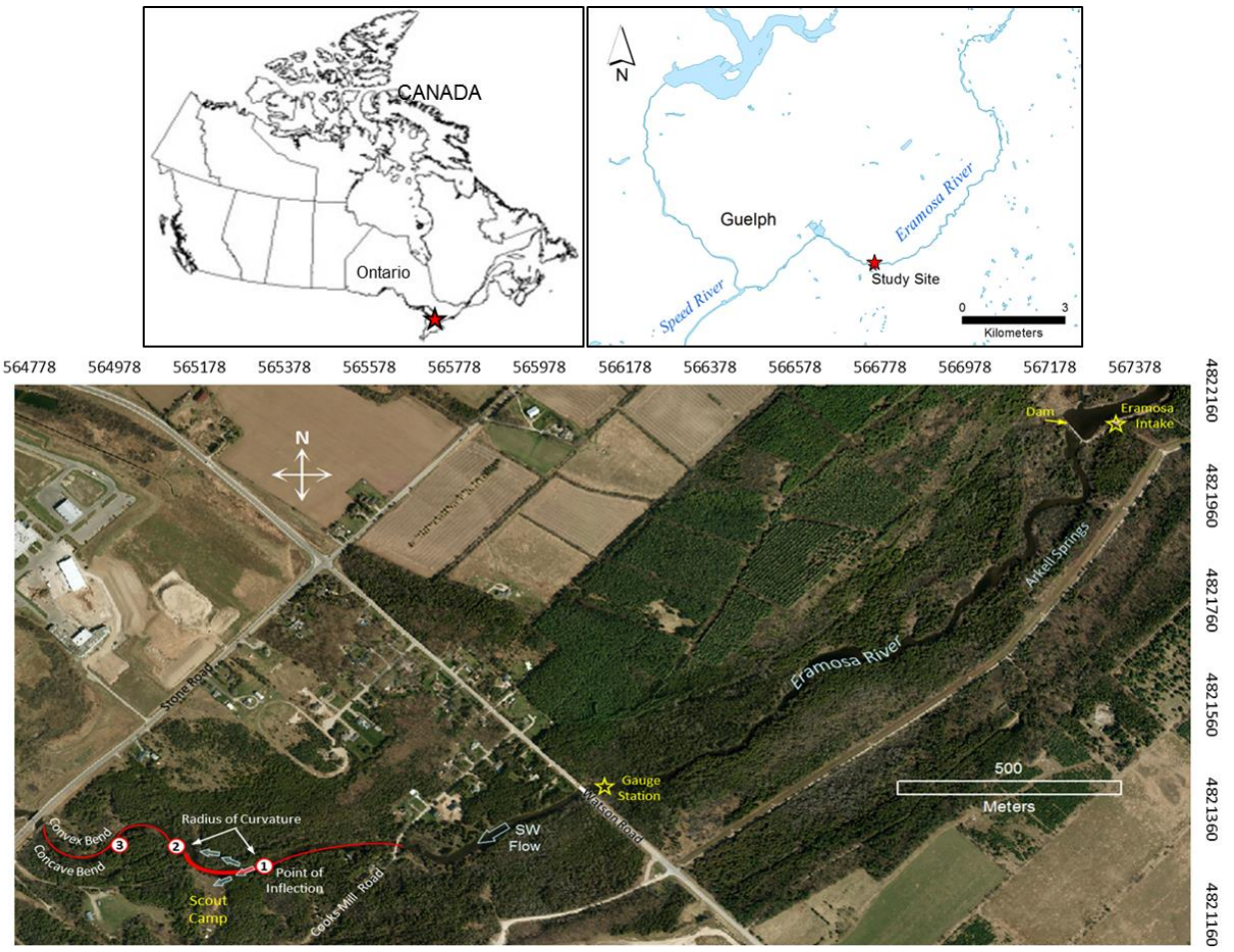

Figure 3.2. Aerial view of the Eramosa River which exhibits a relatively straight channel from the Watson Road Gauging Station to the study site, where a concave bend exists along the south shore between inflection points 1 and 2. The shore-to-shore width of the channel is about 20 m (in summer) and the radius of curvature between inflection points 1 and 2 is about 50 m. Surface water velocity slows by 50% as it passes the first inflection point. Surface water can be observed flowing toward the south bank and over the neck of the convex bend along the north bank. [NAD 1983 UTM Zone 17N Geographic Coordinate System; MNR SWOOP 2010; ESRI ArcMap v.10.2.1].

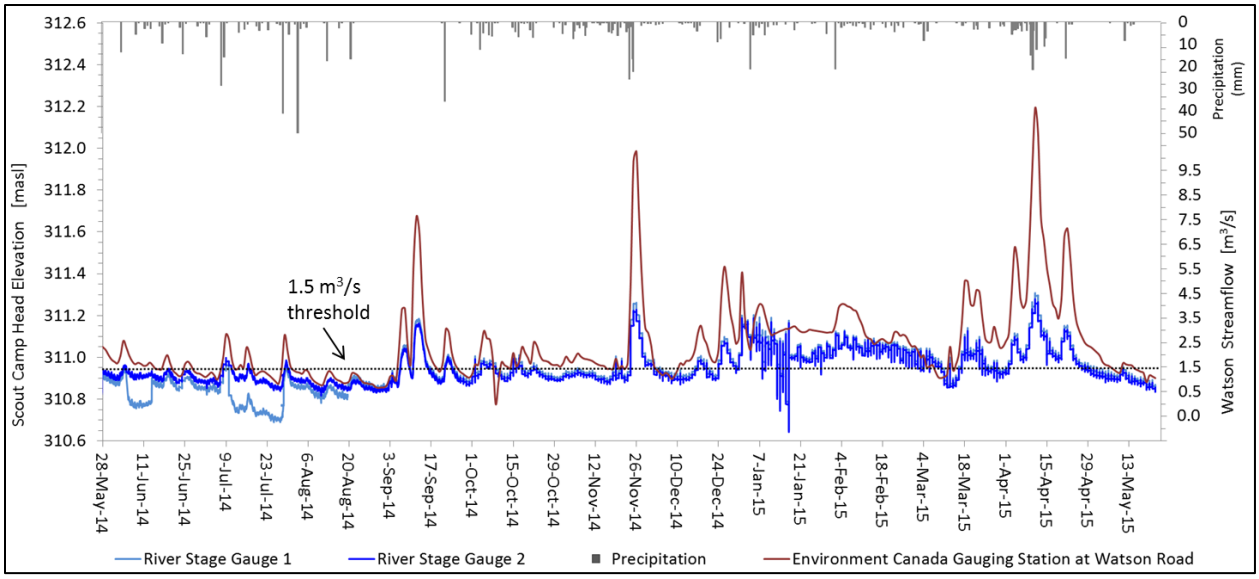

Figure 3.3. The 2014-15 continuous streamflow record obtained from the Watson Road Gauging Station, shown here by the red line, was designated as an independant benchmark upon which to define river stage conditions at the study site. High river stage observed at the Scout Camp coincided with streamflow values >1.5 m^3/s, while low stage coincided with streamflow <1.5 m^3/s at the Watson Road Gauge Station. The height of river stage, monitored at 15-min intervals by two river stage gauges installed at the study site, is represented by the blue lines. The precipitation record indicates that river peaks generally coincide with rainfall events. Upstream stage gauge SG1 responded to field activities that disturbed the flow system in June and July 2014, while the downstream SG2 was unaffected.

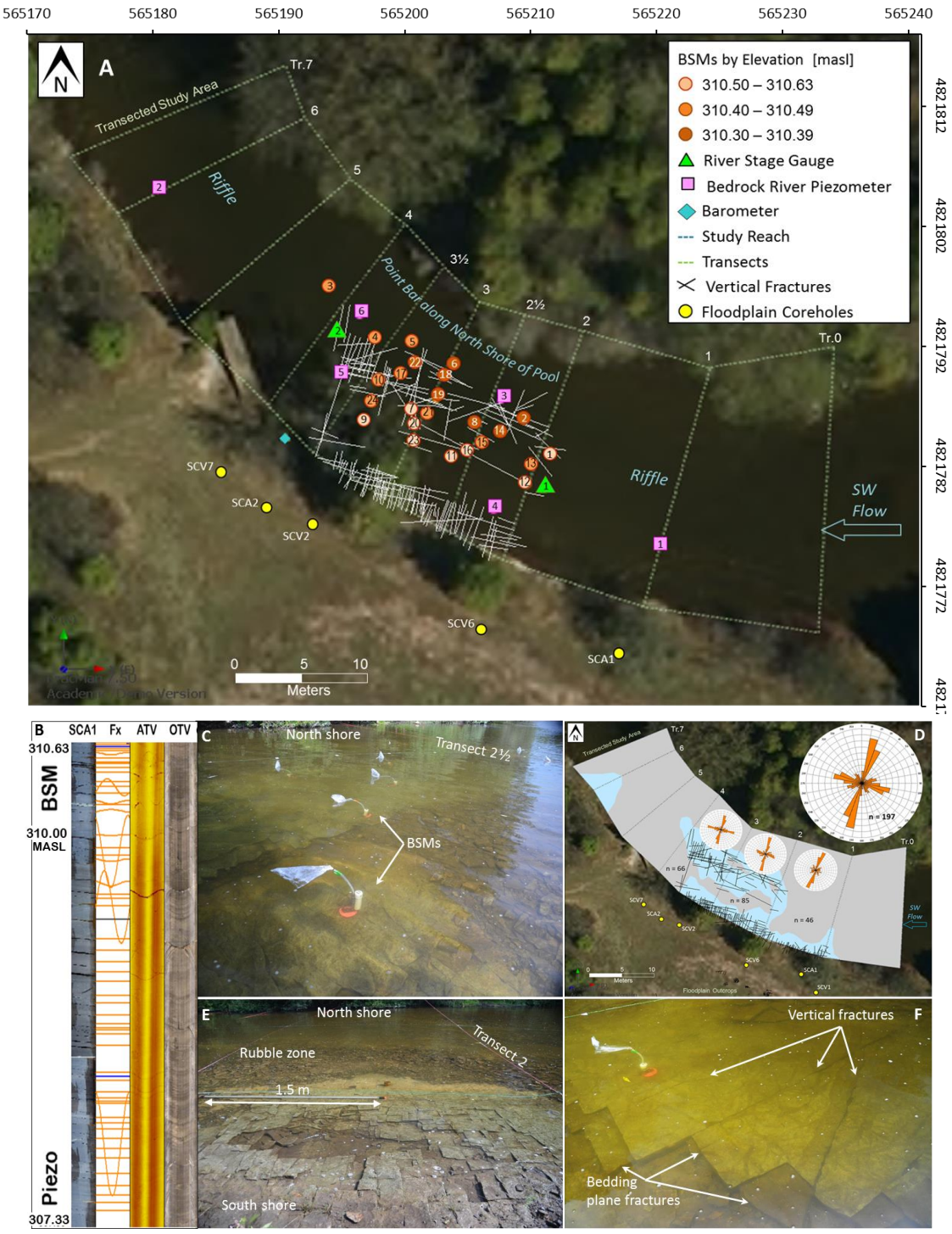

Figure 3.4. (A) Transected study reach of the Eramosa River [UTM Zone 17T] has a surface area of 1110 m^2, which is instrumented where intact bedrock is exposed. Fractures were measured at the bed surface and **(B)** at depth, through core extraction and geophysical logs. **(C)** BSMs are installed along vertical fractures terminating at surface and spatially distributed between transects 1-4. **(D)** Dominant fracture orientations are illustrated by Rose diagrams. Nearly 80% of the study reach is covered by rubble (gray fill). **(E)** Fracture density along the South shore is much higher than **(F)** along channel centre, where long vertical fractures were targeted. [NAD 1983 UTM Zone 17N Geographic Coordinate System; MNR SWOOP 2010; ESRI ArcMap v.10.2.1; WellCAD v.5.0; FracMan v.7.5]

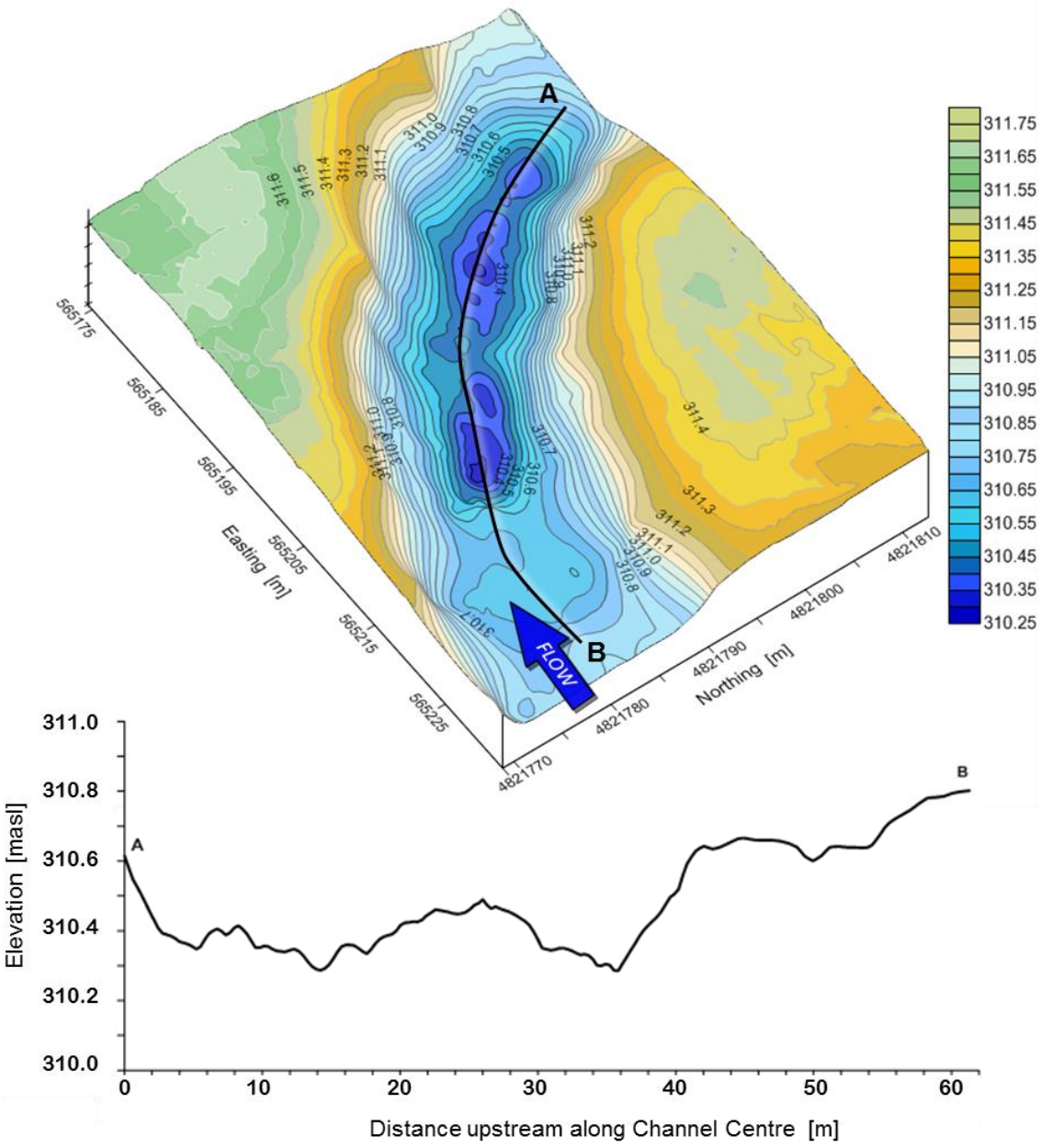

Figure 3.5. Elevation surface (3-D) of study reach topography, measured using GPS and bathymetric surveys, and modelled with Surfer (v.13.6 Golden Software, Golden CO, USA). A 0.6-m decline in elevation is observed from riffle to pool and the thalweg more-or-less follows the channel centre. Contour interval is 310.00 – 311.60 masl. NAD 1983 UTM Zone 17N Geographic Coordinate System.

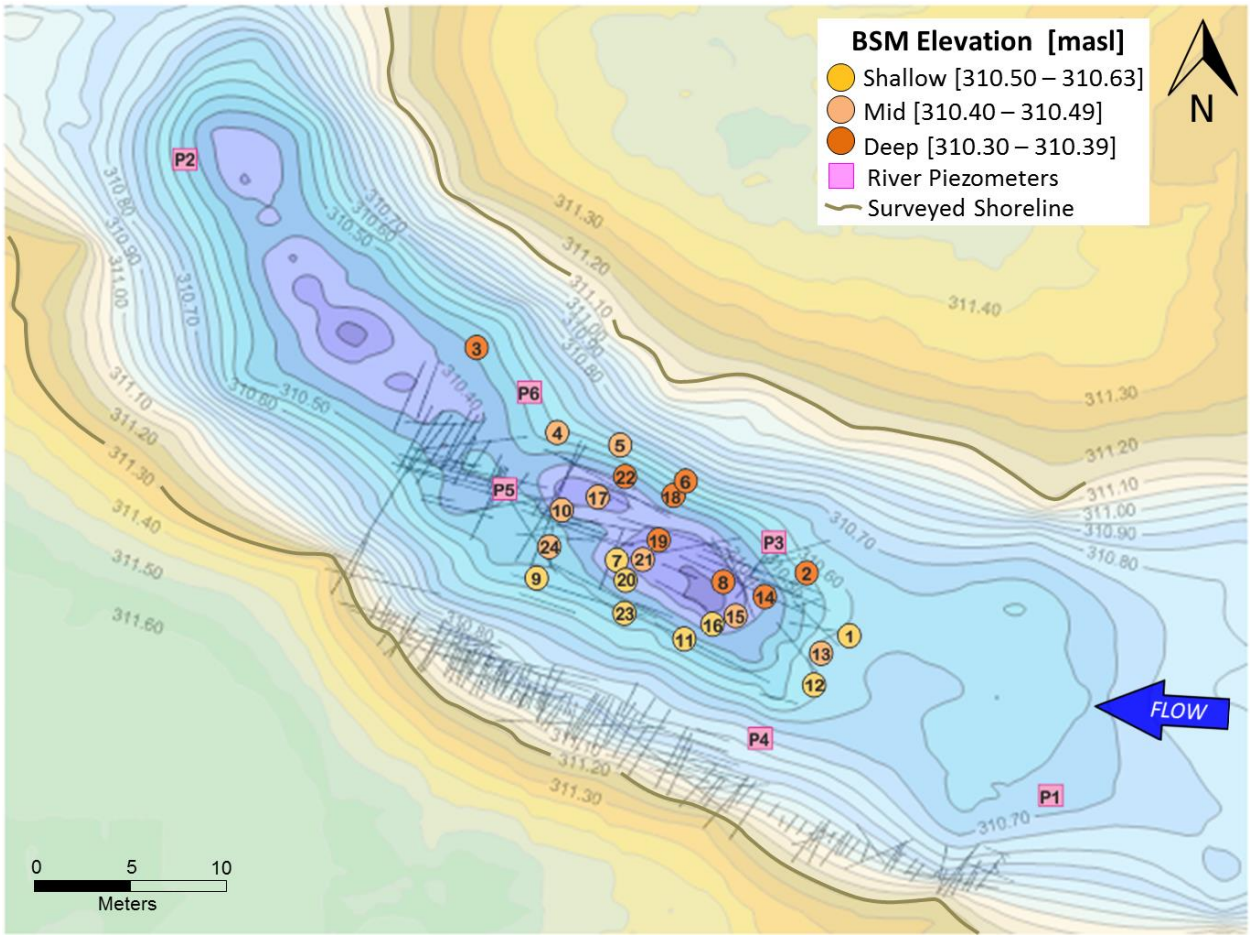

Figure 3.6. Modelled elevation surface (2-D) of study reach, where topographic layer was overlaid with vertical fracture distribution, measured at surface, and constructed with FracMan Software (v.7.5, Golder Associates Inc. – FracMan Technology Group, Redmond, WA, USA). 3-D spatial distribution of the BSMs, identified by number, is represented in this 2-D plane by elevation classifications of shallow (310.50 – 310.63 masl), mid-depth (310.40 – 310.49 masl) and deep (310.30 – 310.39 masl) installations. Contour interval is 310.00 – 311.60 masl. NAD 1983 UTM Zone 17N Geographic Coordinate System.

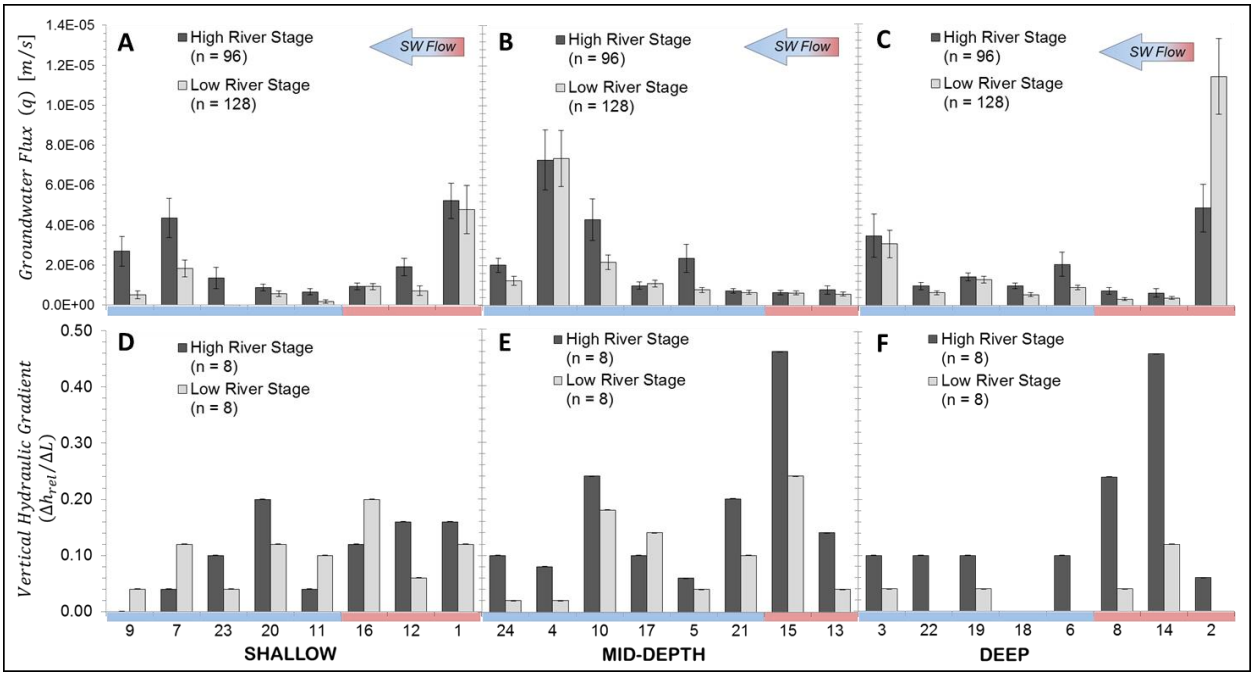

Figure 3.7. Numeric comparison of **(A-C)** groundwater fluxes and **(D-F)** vertical hydraulic gradients at high and low river stage, by elevation classes of: **(A,D)** shallow (310.50—310.63 masl), **(B,E)** mid-depth (310.40—310.49 masl) and **(C,F)** deep (310.30—310.39 masl) BSM installations. From left to right, each class of BSMs is show in an upstream direction, where coloured bars identify the downstream pool [■] and the upstream riffle-transition [■] zones. Fluxes (q) were estimated from flow (Q) measurements (± 20% uncertainty) during constant head seepage tests conducted at high (n = 288) and low (n = 384) river stage. Vertical gradients across a 5-cm layer of dolostone were estimated from potentiomanometer measurements (± 0.5 mm uncertainty) (n = 48).

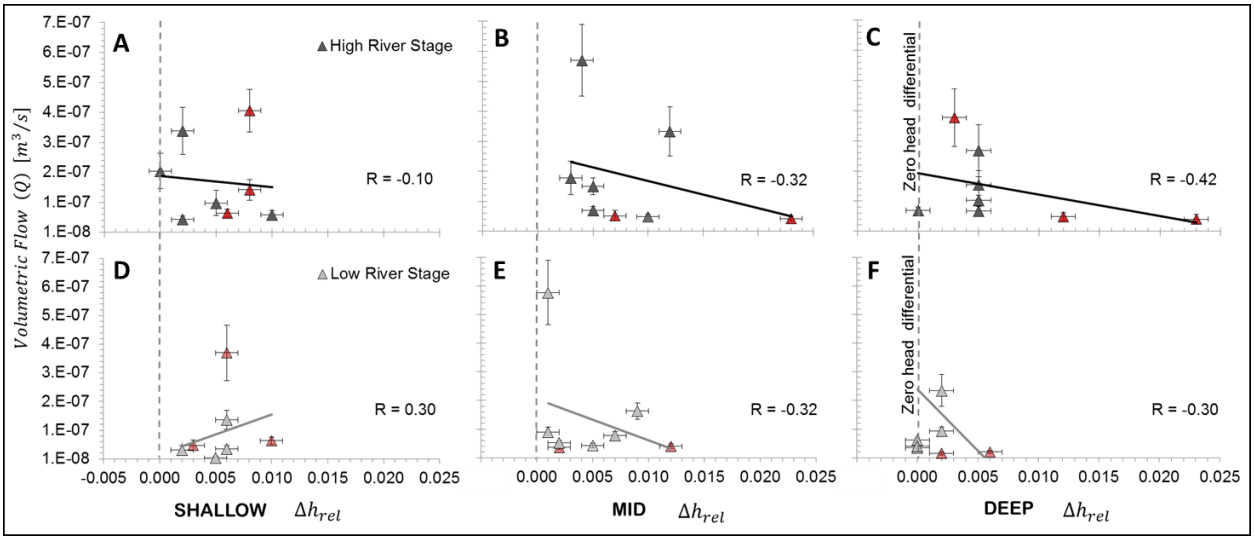

Figure 3.8. Pearson coefficients (R) show correlation of independent measurements of relative head differential between groundwater and surface water (n = 48) and flow (n = 672) at **(A-C)** high and **(D-F)** and low river stage, plotted by elevation class of **(A,D)** shallow (310.50—310.63 masl), **(B,E)** mid-depth (310.40—310.49 masl) and **(C,F)** deep (310.30—310.39 masl) BSM installations. BSMs installed in the riffle zone, indicated in red, tend to skew results.

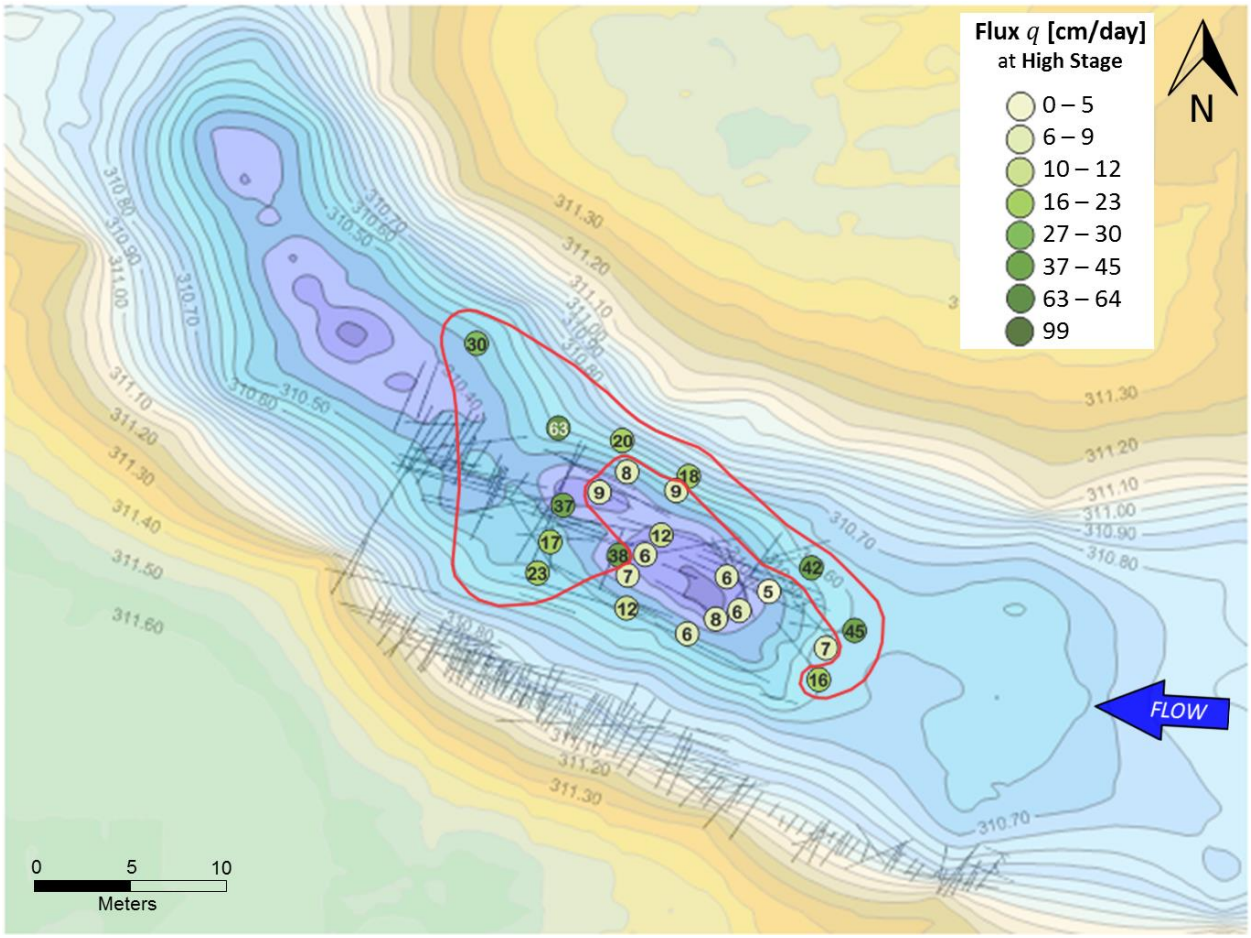

Figure 3.9. Spatial distribution of groundwater fluxes (q) estimated from flow (Q) measurements at high river stage (n = 288) within the contoured elevation model of the study site. Fluxes are indicated by value within the BSM symbol and by colour-ranking. The high-q zone is delineated by a red line using the median of 12 cm/day in high stage conditions. Refer to Figure 3.6 for BSM ID numbers. [NAD 1983 UTM Zone 17N Geographic Coordinate System; Surfer v.13.6; FracMan v.7.5].

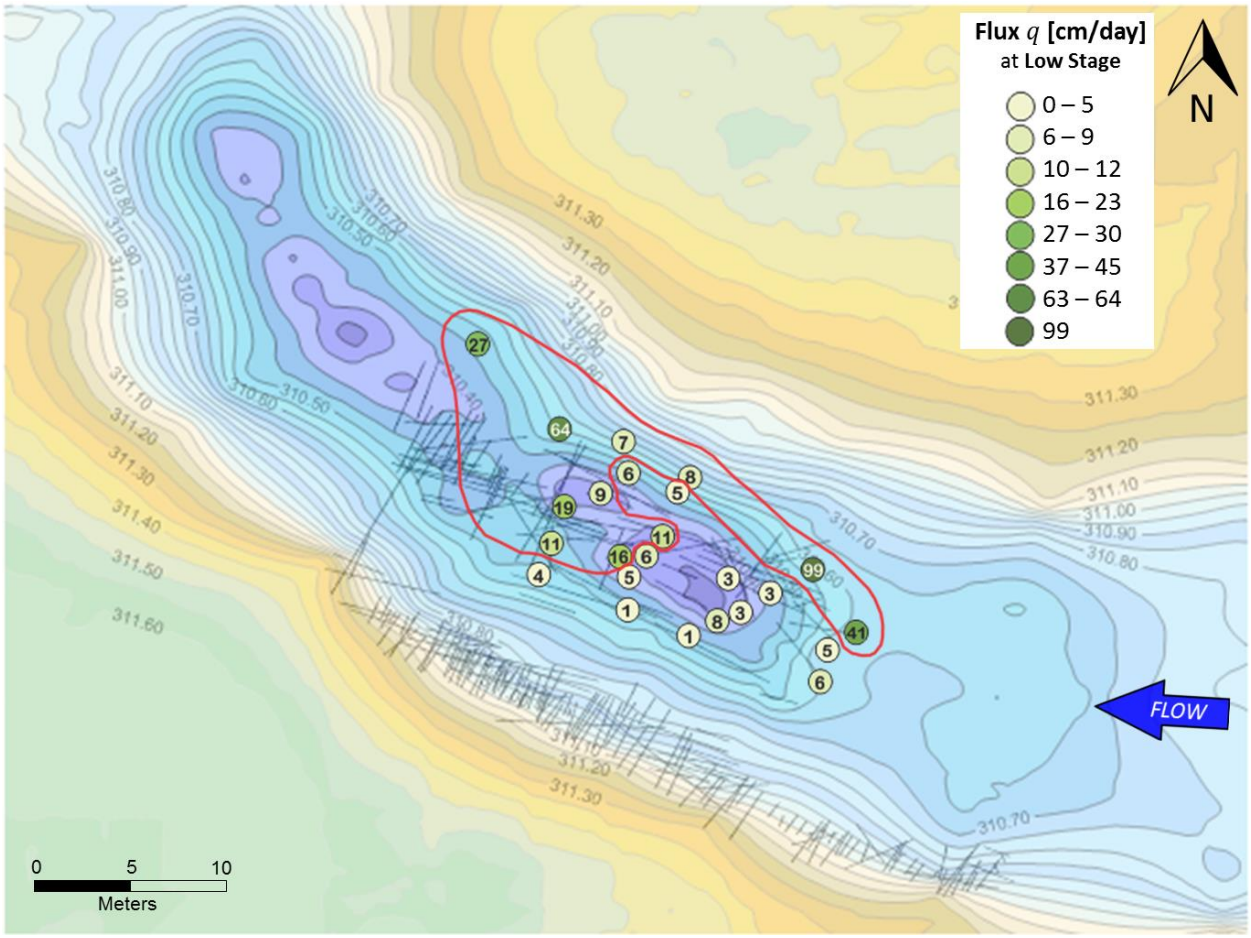

Figure 3.10. Spatial distribution of groundwater fluxes (q) estimated from flow (Q) measurements at low river stage (n = 384) within the contoured elevation model of the study site. Fluxes are indicated by value within the BSM symbol and by colour-ranking. The high-q zone is delineated by a receding red line using the median of 6 cm/day in low stage conditions. Refer to Figure 3.6 for BSM ID numbers. [NAD 1983 UTM Zone 17N Geographic Coordinate System; Surfer v.13.6; FracMan v.7.5].

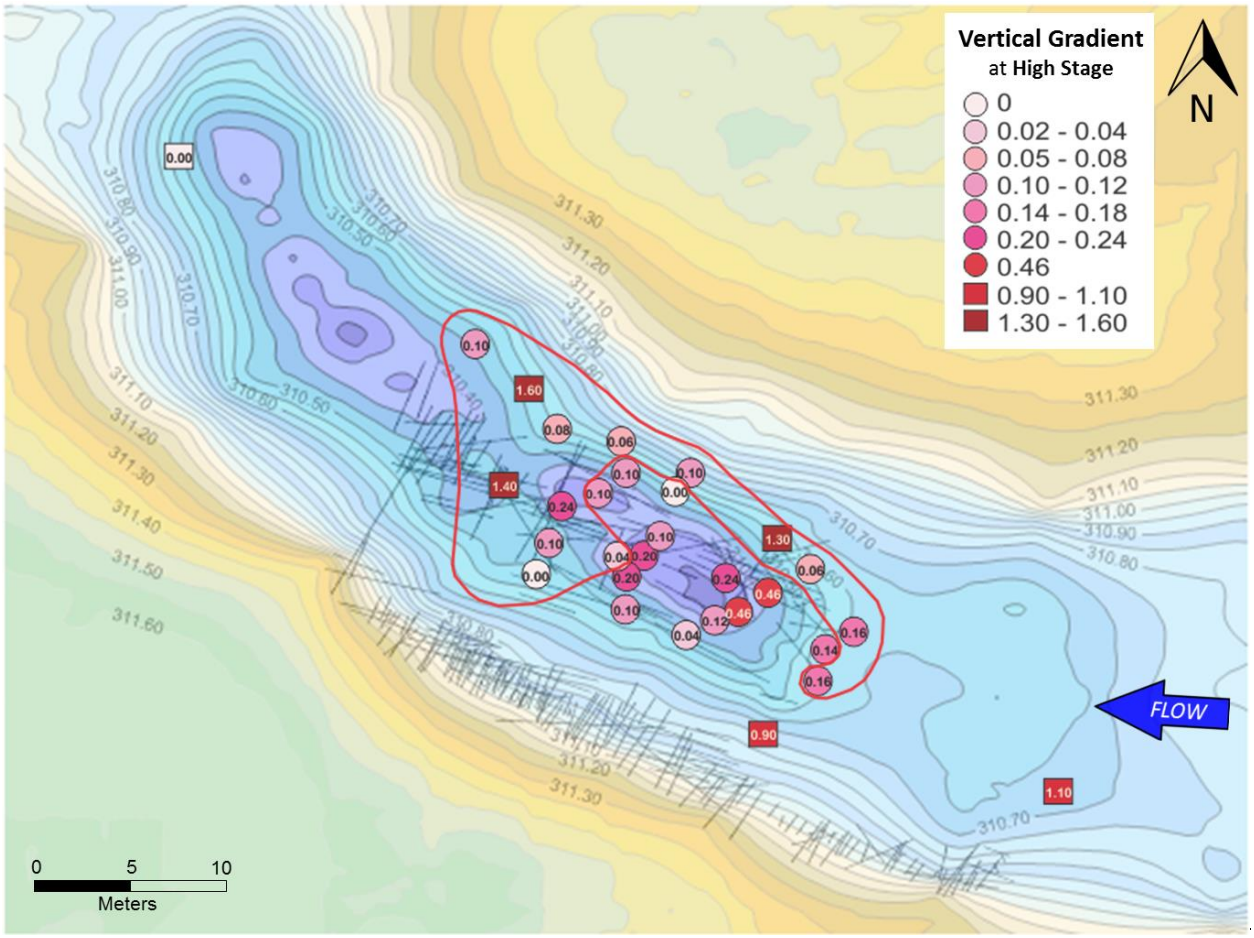

Figure 3.11. Spatial distribution of vertical hydraulic gradients ($\Delta h_{rel}/\Delta L$) at high river stage within the contoured elevation model of the study site. Monitoring devices are identified as BSMs (●) and river piezometers (■). Gradients are indicated by value within the device symbol and by colour-ranking. The high-q zone from Figure 3.9 is delineated by a red line. Refer to Figure 3.6 for BSM ID numbers. [NAD 1983 UTM Zone 17N Geographic Coordinate System; Surfer v.13.6; FracMan v.7.5].

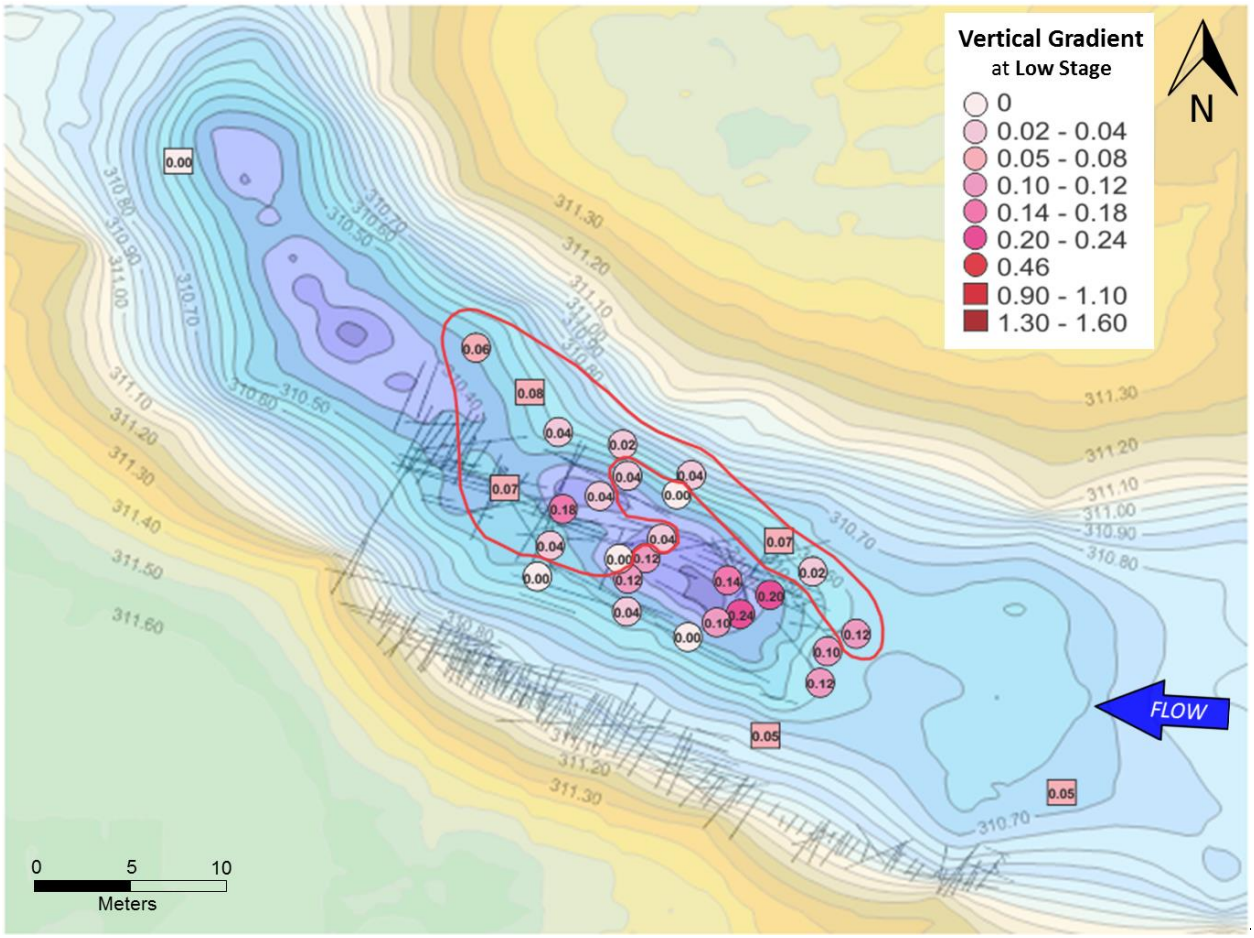

Figure 3.12. Spatial distribution of vertical hydraulic gradients ($\Delta h_{rel}/\Delta L$) at low river stage within the contoured elevation model of the study site. Monitoring devices are identified as BSMs (●) and river piezometers (■). Gradients are indicated by value within the device symbol and by colour-ranking. The high-q zone from Figure 3.10 is delineated by a red line. Refer to Figure 3.6 for BSM ID numbers. [NAD 1983 UTM Zone 17N Geographic Coordinate System; Surfer v.13.6; FracMan v.7.5].

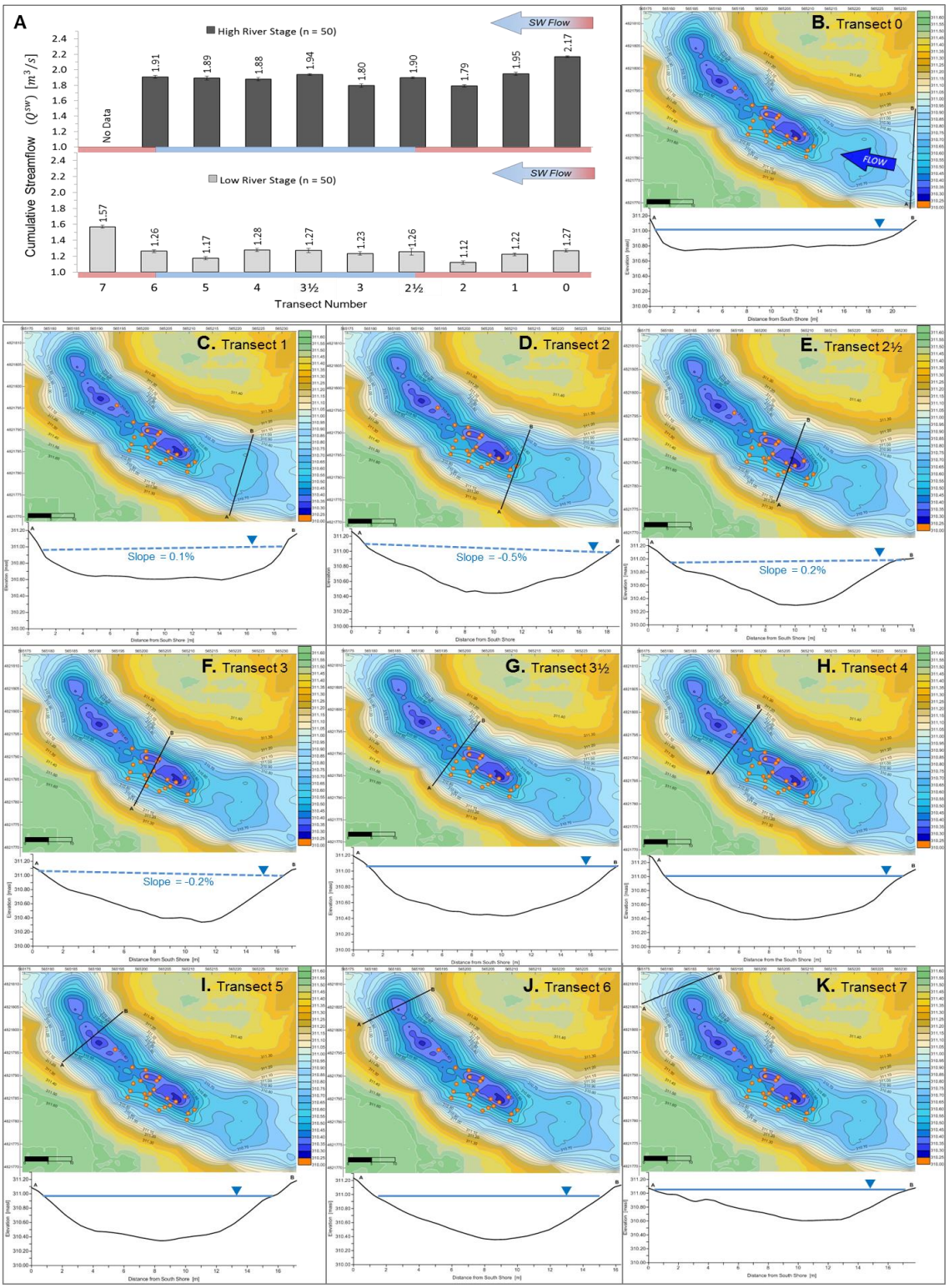

Figure 3.13. (A) Cumulative discharge (Q^{sw}) measured at 1-m intervals along **(B-K)** transects in July-August 2014 at high and low stage, revealed variable trends within the riffle [■] and pool [■] sequence. Error bars represent SD, ranging from ± 0.03 - 0.09 m^3/s. Uncertainties of ± 0.7 – 2.2% include the accuracies of the bathymetry tool (0.001 m) and flow meter (2%), and the SE associated with sample size (n = 538 point measurements x 10 sampling events). Spatial distribution of BSMs is indicated (●). River stage is represented by a blue line; dashed for sloped and solid for horizontal (i.e., slope of zero).

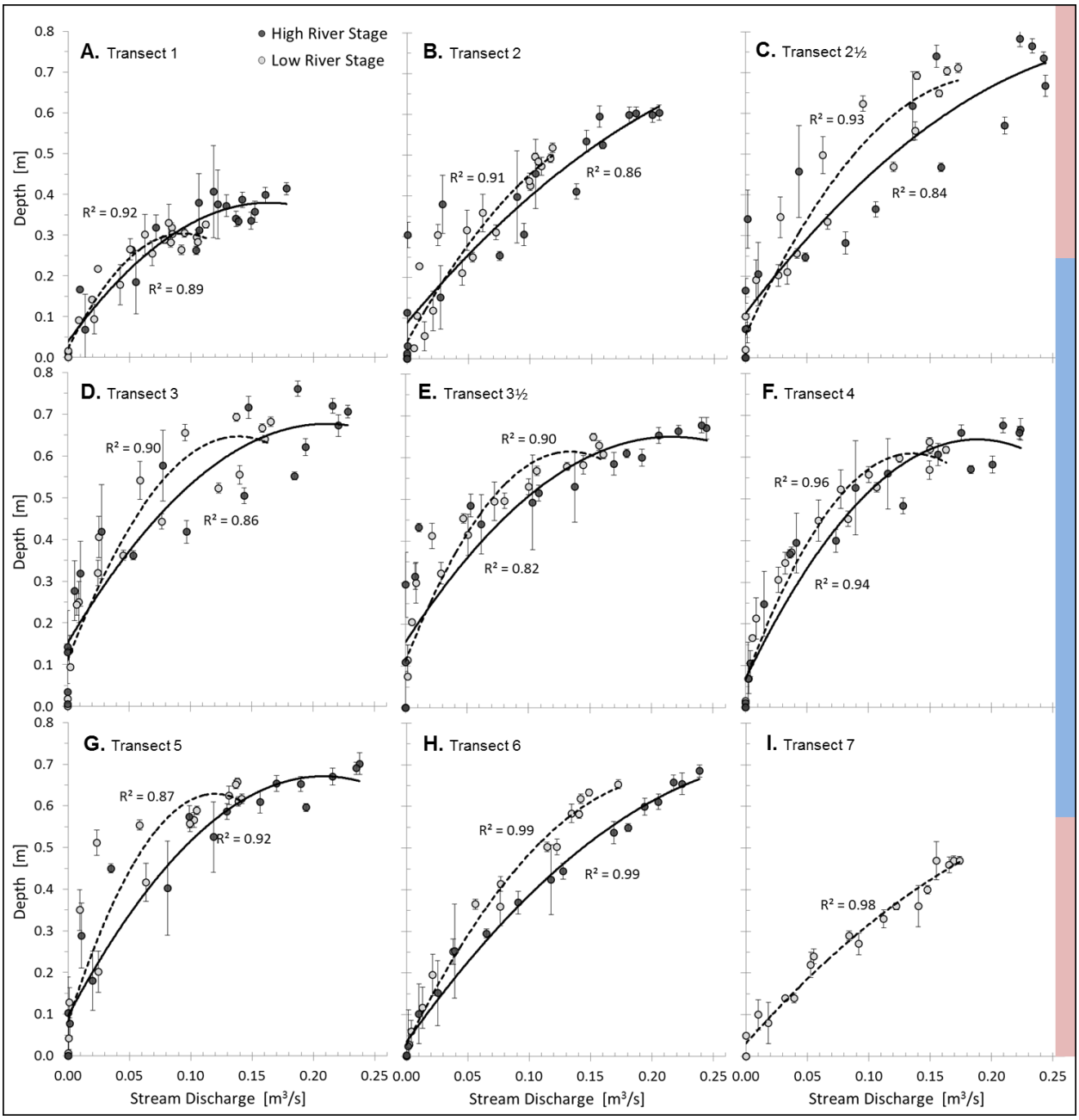

Figure 3.14. Surface water depth – discharge (Q^{sw}) rating curves, from hydrometric surveys collected at 1-m intervals along transects. Riffle [■] to pool [■] transitions occur upstream at transect 2½ and downstream at transect 5.

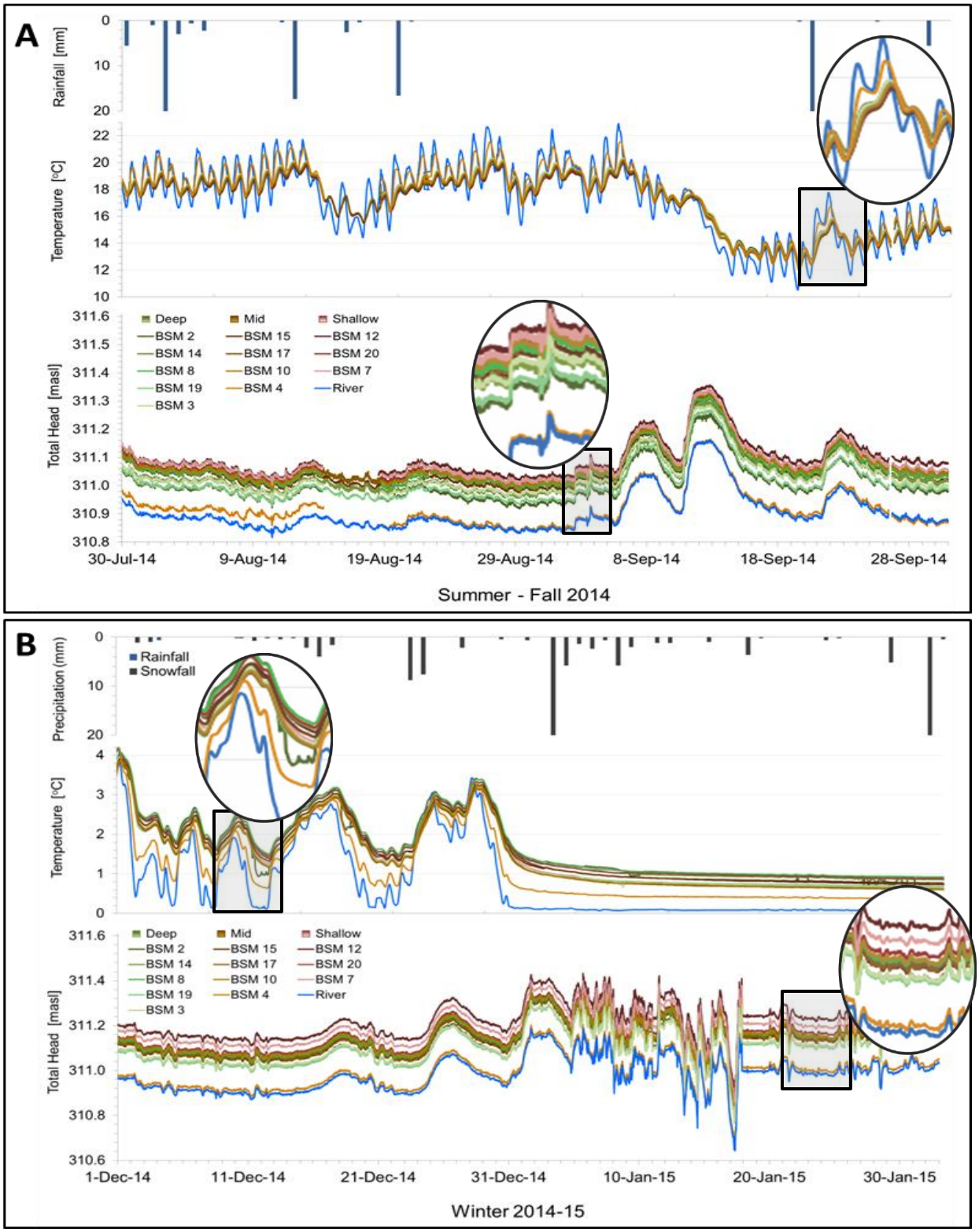

Figure 3.15. Temporal records of precipitation, temperature and hydraulic head, by elevation class of shallow [▭], mid-depth [▭] and deep [▭], for two 60-day periods during **(A)** late summer low stage conditions in 2014, when no rainfall occurred during 45 out of 60 days, and **(B)** winter freeze-up in 2014-15. River stage gauge head and temperature records are indicated by a blue line.

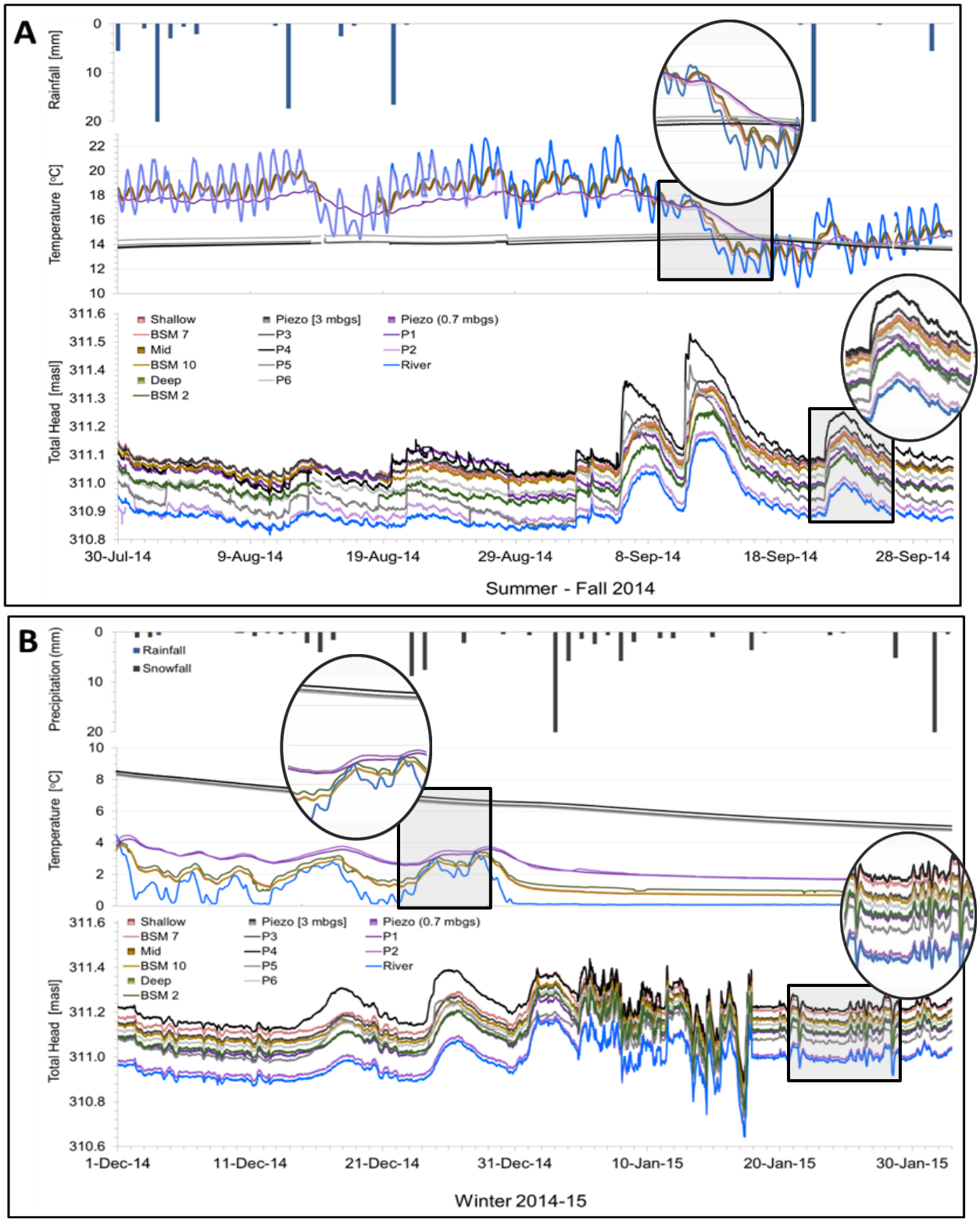

Figure 3.16. Temporal records of precipitation, temperature and hydraulic head for the shallow [▭] and deep [▭] river piezometers and representative BSMs from each of the 3 elevation classes during **(A)** summer-fall of 2014, and **(B)** the winter of 2014-15. River stage (and temperature) from the study site stage gauge is indicated by a blue line. Details of piezometer installations are detailed in Table 3.5.

Table 3.1. Field calibration test results were analyzed by difference (from a known depth) and using the straight line method. While uncertainty generally increases with transducer depth range, critical evaluation of each transducer yielded offset values that could be applied to pressure data to achieve absolute head comparisons.

Device ID	Transducer ID	Type	Range [m]	Manufacturer Accuracy [± m H_2O]	Lab Calibration Method		
					Differences Adjust. [m]	Straight Line Adjust. [m]	
						m-slope	b-intercept
BSM 1*	P1046	Micro	50	0.050	-0.10	0.997	-0.100
2	J3991	Mini	20	0.010	0.03	0.999	0.030
3	M8520	Mini	10	0.005	0.01	0.999	0.009
4	K0669	Mini	10	0.005	0.02	0.999	0.020
5	S4258	Micro	10	0.010	0.01	0.999	0.013
6*	77915	RBR	50	0.250	0.05		
7	J9798	Mini	10	0.005	0.02	1.002	0.021
8	J3415	Mini	20	0.010	0.01	1.001	0.014
9*	M6498	CTD	100	0.050	0.04	0.984	0.071
	D2746	Mini	50	0.025	0.06	1.011	0.042
10	K0687	Mini	10	0.005	0.03	1.001	0.026
11	77658	RBR	20	0.100	0.00		
12	A3698	Mini	20	0.010	0.01	1.007	0.004
13	K0713	Mini	20	0.010	0.00	0.998	0.006
14	N6481	Micro	50	0.050	-0.02	1.000	-0.022
15	R3204	Micro	10	0.010	0.01	0.996	0.019
17	K5719	Micro	50	0.050	0.02	0.999	0.026
19	R0621	CTD	10	0.005	0.01	1.001	0.005
20	N7618	Mini	10	0.005	0.02	1.001	0.013
23*	D2746	Mini	50	0.025	0.06	1.011	0.042
	N6489	Micro	50	0.050	-0.12	1.001	-0.123
P1	N5395	Micro	10	0.010	0.00	0.998	0.008
P2	N5381	Micro	10	0.010	0.00	0.998	0.000
P3	R3191	Micro	10	0.010	0.01	0.996	0.018
P4	R3193	Micro	10	0.010	0.02	0.997	0.020
P5	R3195	Micro	10	0.010	0.01	0.995	0.018
P6	R3197	Micro	10	0.010	0.01	0.997	0.017
BSG1	K8574	CTD	10	0.005	-0.02	0.996	-0.012
BSG2	M7423	CTD	10	0.005	0.00	0.995	0.009

SD of Differences Method is $\leq$ 2 cm and uncertainty of field method is $\pm$ 1 cm.

SD of Straight Line Method is $\leq$ 1 cm and uncertainty of field method is $\pm$ 1 cm.

**Pressure data discarded due to high uncertainty $\geq$ 5 cm.*

Table 3.2. Results of constant head seepage tests in **(A)** high and **(B)** low stage conditions. BSMs are organized in the direction of flow (i.e., west to east). Fluxes and fracture velocities derived from volumetric flow measurements collected during 28 tests. Uncertainties in flow measurements, expressed as a percent, comprise standard error (SE) associated with the graduated cylinders, test time and the sample size (n = 672).

A. HIGH RIVER STAGE				
BSM ID #	**Elevation** [masl]	**Flow** [n = 12] Q [m^3/s]	**Groundwater Flux** q [m/s]	**Fracture Velocity** $\bar{v}$ [m/s]
1	310.53	4.E-07 ± *17%*	5.E-06	5.E-03
13	310.43	6.E-08 ± *28%*	8.E-07	8.E-04
12	310.57	2.E-07 ± *23%*	2.E-06	2.E-03
2	310.35	4.E-07 ± *25%*	5.E-06	5.E-03
14	310.33	5.E-08 ± *32%*	6.E-07	6.E-04
15	310.46	5.E-08 ± *17%*	7.E-07	7.E-04
8	310.37	6.E-08 ± *24%*	7.E-07	7.E-04
16	310.57	7.E-08 ± *18%*	9.E-07	9.E-04
6	310.35	2.E-07 ± *29%*	2.E-06	2.E-03
11	310.59	5.E-08 ± *23%*	7.E-07	7.E-04
18	310.34	8.E-08 ± *14%*	1.E-06	1.E-03
19	310.36	1.E-07 ± *14%*	1.E-06	1.E-03
21	310.45	6.E-08 ± *15%*	7.E-07	7.E-04
22	310.30	8.E-08 ± *18%*	1.E-06	1.E-03
20	310.50	7.E-08 ± *20%*	9.E-07	9.E-04
23	310.63	1.E-07 ± *39%*	1.E-06	1.E-03
5	310.41	2.E-07 ± *29%*	2.E-06	2.E-03
7	310.50	3.E-07 ± *23%*	4.E-06	4.E-03
17	310.41	8.E-08 ± *18%*	1.E-06	1.E-03
10	310.49	3.E-07 ± *24%*	4.E-06	4.E-03
4	310.43	6.E-07 ± *21%*	7.E-06	7.E-03
24	310.48	2.E-07 ± *17%*	2.E-06	2.E-03
9	310.58	2.E-07 ± *28%*	3.E-06	3.E-03
3	310.39	3.E-07 ± *31%*	3.E-06	3.E-03
MAX		6.E-07	7.E-06	7.E-03
MIN		5.E-08	6.E-07	6.E-04

B. LOW RIVER STAGE				
BSM ID #	**Elevation** [masl]	**Flow** [n = 16] Q [m^3/s]	**Groundwater Flux** q [m/s]	**Fracture Velocity** $\bar{v}$ [m/s]
1	310.53	4.E-07 ± *25%*	5.E-06	5.E-03
13	310.43	5.E-08 ± *16%*	6.E-07	6.E-04
12	310.57	6.E-08 ± *32%*	7.E-07	7.E-04
2	310.35	9.E-07 ± *17%*	1.E-05	1.E-02
14	310.33	3.E-08 ± *16%*	4.E-07	4.E-04
15	310.46	5.E-08 ± *16%*	6.E-07	6.E-04
8	310.37	3.E-08 ± *24%*	3.E-07	3.E-04
16	310.57	7.E-08 ± *18%*	9.E-07	9.E-04
6	310.35	7.E-08 ± *13%*	9.E-07	9.E-04
11	310.59	1.E-08 ± *51%*	2.E-07	2.E-04
18	310.34	4.E-08 ± *17%*	6.E-07	6.E-04
19	310.36	1.E-07 ± *13%*	1.E-06	1.E-03
21	310.45	5.E-08 ± *14%*	7.E-07	7.E-04
22	310.30	5.E-08 ± *16%*	6.E-07	6.E-04
20	310.50	4.E-08 ± *25%*	6.E-07	6.E-04
23	310.63	-6.E-09 ± *33%*	8.E-08	8.E-05
5	310.41	6.E-08 ± *15%*	8.E-07	8.E-04
7	310.50	1.E-07 ± *23%*	2.E-06	2.E-03
17	310.41	9.E-08 ± *16%*	1.E-06	1.E-03
10	310.49	2.E-07 ± *16%*	2.E-06	2.E-03
4	310.43	6.E-07 ± *19%*	7.E-06	7.E-03
24	310.48	1.E-07 ± *18%*	1.E-06	1.E-03
9	310.58	4.E-08 ± *40%*	5.E-07	5.E-04
3	310.39	2.E-07 ± *22%*	3.E-06	3.E-03
MAX		9.E-07	1.E-05	1.E-02
MIN		-6.E-09	8.E-08	8.E-05

Table 3.3. Differential head values derived from morning groundwater head measurements from BSM transducers during a 2-hour window, collected at 1-min intervals and surface water depth measurements collected during 5 high stage and 7 low stage days. Relative head differentials were measured directly with a potentiomanometer on 2 sampling days.

A. HIGH RIVER STAGE

BSM ID #	Groundwater Head [n = 120] h_2 [masl]	Surface Water Head [n = 5] h_1 [masl]	Differential Head [n = 5] Δh [m]	Relative Head Diff. [n = 1] Δh_{rel} [m]
1		311.13 ± *0.02*		0.008 ± *0.001*
13		310.93 ± *0.02*		0.007 ± *0.001*
12	311.13 ± *0.02*	311.07 ± *0.02*	0.06 ± *0.02*	0.008 ± *0.001*
2	311.04 ± *0.02*	310.92 ± *0.02*	0.11 ± *0.03*	0.003 ± *0.001*
14	311.04 ± *0.06*	310.98 ± *0.03*	0.06 ± *0.06*	0.023 ± *0.001*
15	311.10 ± *0.02*	311.04 ± *0.02*	0.06 ± *0.02*	0.023 ± *0.001*
8	311.09 ± *0.02*	310.98 ± *0.02*	0.12 ± *0.03*	0.012 ± *0.001*
16		311.15 ± *0.02*		0.006 ± *0.001*
6		310.88 ± *0.02*		0.005 ± *0.001*
11		310.88 ± *0.02*		0.002 ± *0.001*
18		310.87 ± *0.02*		<0.001 ± *0.001*
19	311.05 ± *0.02*	311.00 ± *0.02*	0.05 ± *0.02*	0.005 ± *0.001*
21		311.10 ± *0.02*		0.010 ± *0.001*
22		310.84 ± *0.02*		0.005 ± *0.001*
20	311.12 ± *0.02*	311.05 ± *0.02*	0.07 ± *0.02*	0.010 ± *0.001*
23		311.00 ± *0.02*		0.005 ± *0.001*
5		310.95 ± *0.02*		0.003 ± *0.001*
7	311.12 ± *0.02*	311.04 ± *0.02*	0.08 ± *0.02*	0.002 ± *0.001*
17	311.12 ± *0.06*	311.04 ± *0.02*	0.08 ± *0.07*	0.005 ± *0.001*
10	311.10 ± *0.02*	311.02 ± *0.02*	0.08 ± *0.02*	0.012 ± *0.001*
4	310.96 ± *0.02*	310.95 ± *0.02*	0.01 ± *0.03*	0.004 ± *0.001*
24		310.91 ± *0.02*		0.005 ± *0.001*
9		310.91 ± *0.02*		<0.001 ± *0.001*
3	311.06 ± *0.02*	310.99 ± *0.02*	0.08 ± *0.02*	0.005 ± *0.001*
MAX	311.13	311.15	0.12	0.023
MIN	310.96	310.84	0.01	0.002

B. LOW RIVER STAGE

BSM ID #	Groundwater Head [n = 120] h_2 [masl]	Surface Water Head [n = 7] h_1 [masl]	Differential Head [n = 5] Δh [m]	Relative Head Diff. [n = 1] Δh_{rel} [m]
1		311.07 ± *0.02*		0.006 ± *0.001*
13		310.86 ± *0.02*		0.002 ± *0.001*
12	311.05 ± *0.02*	310.99 ± *0.02*	0.06 ± *0.02*	0.003 ± *0.001*
2	310.97 ± *0.02*	310.85 ± *0.01*	0.12 ± *0.02*	<0.001 ± *0.001*
14	310.99 ± *0.06*	310.95 ± *0.02*	0.04 ± *0.06*	0.006 ± *0.001*
15	311.01 ± *0.02*	310.98 ± *0.01*	0.03 ± *0.02*	0.012 ± *0.001*
8	311.02 ± *0.02*	310.89 ± *0.01*	0.12 ± *0.02*	0.002 ± *0.001*
16		311.09 ± *0.01*		0.010 ± *0.001*
6		310.85 ± *0.01*		<0.001 ± *0.001*
11		310.83 ± *0.01*		0.005 ± *0.001*
18		310.84 ± *0.01*		<0.001 ± *0.001*
19	310.97 ± *0.02*	310.88 ± *0.02*	0.09 ± *0.02*	0.002 ± *0.001*
21		310.98 ± *0.02*		0.005 ± *0.001*
22		310.76 ± *0.01*		<0.001 ± *0.001*
20	311.04 ± *0.02*	310.90 ± *0.02*	0.13 ± *0.02*	0.006 ± *0.001*
23		310.91 ± *0.02*		0.002 ± *0.001*
5		310.88 ± *0.01*		0.002 ± *0.001*
7	311.05 ± *0.02*	310.90 ± *0.02*	0.15 ± *0.02*	0.006 ± *0.001*
17	311.03 ± *0.06*	310.98 ± *0.01*	0.05 ± *0.06*	0.007 ± *0.001*
10	311.03 ± *0.02*	310.96 ± *0.01*	0.06 ± *0.02*	0.009 ± *0.001*
4	310.89 ± *0.02*	310.81 ± *0.02*	0.09 ± *0.02*	0.001 ± *0.001*
24		310.87 ± *0.01*		0.001 ± *0.001*
9		310.81 ± *0.01*		0.002 ± *0.001*
3	310.99 ± *0.02*	310.89 ± *0.02*	0.10 ± *0.02*	0.002 ± *0.001*
MAX	311.05	311.09	0.15	0.012
MIN	310.89	310.76	0.03	0.001

Table 3.4. Vertical hydraulic gradients estimated from head differentials obtained from two different methods. Specific capacity values were derived from measured flow and relative head difference, and normalized by dividing each value by the minimum specific capacity (which is therefore equal to "1").

A. HIGH RIVER STAGE

BSM ID #	Flow [n = 12] Q [m^3/s]	Vertical Hydraulic Gradient $\Delta h/\Delta L$	Vertical Hydraulic Gradient $\Delta h_{rel}/\Delta L$	Specific Capacity $Q/\Delta h_{rel}$ [m^2/s]	Specific Capacity [normalized]
1	4.E-07 ± *17%*		0.16	5.2E-05	24
13	6.E-08 ± *28%*		0.14	8.8E-06	4
12	2.E-07 ± *23%*	1.2	0.16	1.9E-05	9
2	4.E-07 ± *25%*	2.3	0.06	1.3E-04	59
14	5.E-08 ± *32%*	1.2	0.46	2.2E-06	1
15	5.E-08 ± *17%*	1.2	0.46	2.3E-06	1
8	6.E-08 ± *24%*	2.3	0.24	4.9E-06	2
16	7.E-08 ± *18%*		0.12	1.2E-05	6
6	2.E-07 ± *29%*		0.10	3.3E-05	15
11	5.E-08 ± *23%*		0.04	2.6E-05	12
18	8.E-08 ± *14%*		<0.02	7.9E-05	36
19	1.E-07 ± *14%*	0.9	0.10	2.3E-05	10
21	6.E-08 ± *15%*		0.20	5.8E-06	3
22	8.E-08 ± *18%*		0.10	1.5E-05	7
20	7.E-08 ± *20%*	1.5	0.20	6.9E-06	3
23	1.E-07 ± *39%*		0.10	2.2E-05	10
5	2.E-07 ± *29%*		0.06	6.3E-05	29
7	3.E-07 ± *23%*	1.6	0.04	1.7E-04	80
17	8.E-08 ± *18%*	1.7	0.10	1.6E-05	7
10	3.E-07 ± *24%*	1.6	0.24	2.9E-05	13
4	6.E-07 ± *21%*	0.2	0.08	1.5E-04	66
24	2.E-07 ± *17%*		0.10	3.2E-05	15
9	2.E-07 ± *28%*		<0.02	2.1E-04	98
3	3.E-07 ± *31%*	1.5	0.10	5.5E-05	25
MAX	6.E-07	2.3	0.46	2.1E-04	98
MIN	5.E-08	0.2	0.04	2.2E-06	**1**

B. LOW RIVER STAGE

BSM ID #	Flow [n = 16] Q [m^3/s]	Vertical Hydraulic Gradient $\Delta h/\Delta L$	Vertical Hydraulic Gradient $\Delta h_{rel}/\Delta L$	Specific Capacity $Q/\Delta h_{rel}$ [m^2/s]	Specific Capacity [normalized]
1	4.E-07 ± *25%*		0.12	6.3E-05	25
13	5.E-08 ± *16%*		0.04	2.3E-05	9
12	6.E-08 ± *32%*	1.2	0.06	1.9E-05	7
2	9.E-07 ± *17%*	2.4	<0.02	9.1E-04	355
14	3.E-08 ± *16%*	0.8	0.12	5.1E-06	2
15	5.E-08 ± *16%*	0.6	0.24	4.1E-06	2
8	3.E-08 ± *24%*	2.5	0.04	1.3E-05	5
16	7.E-08 ± *18%*		0.20	7.3E-06	3
6	7.E-08 ± *13%*		<0.02	7.1E-05	28
11	1.E-08 ± *51%*		0.10	2.6E-06	1
18	4.E-08 ± *17%*		<0.02	4.4E-05	17
19	1.E-07 ± *13%*	1.7	0.04	5.1E-05	20
21	5.E-08 ± *14%*		0.10	1.1E-05	4
22	5.E-08 ± *16%*		<0.02	5.1E-05	20
20	4.E-08 ± *25%*	2.7	0.12	7.5E-06	3
23	-6.E-09 ± *33%*		0.04	3.1E-06	1
5	6.E-08 ± *15%*		0.04	3.1E-05	12
7	1.E-07 ± *23%*	3.0	0.12	2.4E-05	10
17	9.E-08 ± *16%*	1.1	0.14	1.2E-05	5
10	2.E-07 ± *16%*	1.3	0.18	1.9E-05	7
4	6.E-07 ± *19%*	1.8	0.02	5.9E-04	229
24	1.E-07 ± *18%*		0.02	9.9E-05	39
9	4.E-08 ± *40%*		0.04	2.0E-05	8
3	2.E-07 ± *22%*	2.0	0.04	1.2E-04	48
MAX	9.E-07	3.0	0.24	9.1E-04	355
MIN	-6.E-09	0.6	0.02	2.6E-06	**1**

Table 3.5. Details of river piezometer installations, where all casings are sealed to the top of screen.

Piezometer ID #	Channel Elevation [masl]	Bottom of Screen [masl]	Screen Length [m]
P1	310.65	309.95	0.10
P2	310.66	309.96	0.10
P3	310.33	307.39	0.35
P4	310.82	307.82	0.40
P5	310.41	307.35	0.44
P6	310.38	307.43	0.35

Chapter 4: Conclusions

The overall objective of this research is to advance our understanding of groundwater – surface water interactions in bedrock rivers using three mechanisms:

1. Tool design and methods development for the measurement of hydraulic parameters (i.e., groundwater discharge and head differentials across the bedrock riverbed interface at the sub-meter scale.

2. Field site procurement and development for field-testing new methods in a riffle-pool sequence of an intact bedrock riverbed within the City of Guelph.

3. Study site DFN characterization and conceptual modelling of the spatio-temporal variability of groundwater discharging to surface water, together with head and temperature differentials between groundwater and surface water.

4.1 Summary of Principle Findings:

4.1.1 Profile of the Eramosa River

The Eramosa River is a 27-km channel, about half of which exhibits a bedrock boundary. It flows in a southwesterly direction from its headwaters above the Town of Everton, at an elevation of 400 m above sea level (masl), to a confluence with the Speed River at 300 masl (Figure 1.3). There are currently 8 municipal production wells within a 3-km radius of the study site. Upstream, the Arkell Spring Grounds contain 6 active production wells, supplemented by a surface water intake on the Eramosa River to recharge the overburden; and downstream, to the Southwest, the somewhat less active Carter Wellfield has 2 production wells (Figures 1.6 – 1.7). Gartner Lee Limited (2004) completed a wellhead protection study of the regional geology and recharge rates of 19 Guelph Area municipal wells and more than 4400 residential wells. Based on potentiometric surfaces identified in wells, they found that groundwater recharge along the Eramosa riverbed (i.e., bed elevation is higher than nearby potentiometric surfaces) occurred between the Everton headwaters and the Arkell Spring Grounds, and that groundwater discharge

along the channel (i.e., bed elevation is less than nearby potentiometric surfaces) occurred from Arkell Springs in a downstream direction (Figures 1.5).

Reconnaissance surveys of a 12-km reach of the Eramosa River, performed as part of this thesis and detailed in Appendix A, yielded eight segments where intact bedrock was exposed, but only five easily accessible potential field sites, being: Indian Trail, Eden Mills, County Road 29, Cooks Mill Road and Scout Camp. A short study was conducted at the Eden Mills site [Appendix A, Fig.A-5] to field-test three portable drills and conduct geophysical surveys to investigate the nature of the streambed geology (Steelman *et al.*, 2015), which was found to be karstic, sediment-rich and an inappropriate choice for BSM installations. Results from the reconnaissance infrared temperature (IRT) survey, detailed in Appendix A, provided useful insights into reaches where groundwater discharge is probable, and this has been shared with the fish biologists at the Ministry of Natural Resources and Forestry to aid in the designation of favourable spawning habitats for brown trout. Results from the ground surveys have provided a comprehensive profile of the Eramosa River to the University of Guelph G360 Institute for Groundwater Research.

4.1.2 Scout Camp Bedrock River Field Research Site

The Scout Camp field site was procured because it meets the site selection criteria outlined in Chapter 1. The 2600 m^2 field site abuts the south side of the Eramosa River, where intact dolostone is exposed along the channel bed and fluvial plain (Figure 3.4). The 1110 m^2 study reach exhibits a mean channel width of 20 m (in summer) and a riffle – pool – riffle sequence within a meander 70 m in length (Figure 3.5). Large sediment in the form of sharp angular bedrock fragments cover 80% of the study reach mostly upstream and downstream of the segment of interest [Appendix D, Fig. D-1]. The height of river stage is sufficiently low to permit fracture mapping of the vertical and bedding plane fractures terminating at surface [detailed in Appendix D], ranging from 0.1 m in summer to 0.8 m during spring freshet. The IRT survey revealed moderate thermal signatures at the water surface denoting potential groundwater discharge along the north side of the channel and along the downstream south shore (i.e.,

between transects 6 and 7) [Appendix A, Fig. A-9]. The study site is 2 km from the University of Guelph and serviced by an accessible camp road. A strong working relationship has been fostered between the University of Guelph G360 Institute for Groundwater Research, Scouts Canada, Grand River Conservation Authority and the Ministry of Natural Resources and Forestry for the continued operation of this field site renewable on a 5-year basis.

The Scout Camp field site has been conscientiously instrumented with a range of groundwater and surface water monitoring devices along the channel and floodplain to facilitate this and further bedrock river studies, specifically: 24 BSMs, 6 river piezometers, 2 river stage gauges, 2 shallow floodplain wells, 3 vertical-angled floodplain corehole pairs and 2 barometers. Accessibility to current baseline data has been preserved, (i.e., hourly streamflow data from the Water Survey of Canada Watson Road Gauging Station and precipitation data from the Environment Canada Automated Climate Station).

4.1.3 Dynamic Approach to Field Data Collection and Interpretation

The dynamic nature of groundwater – surface water exchanges in alluvial rivers has been recognized in the context of hydrological and ecological studies (Woessner 2000; Palmer 1993). Palmer (1993) presented an insightful perspective on findings from an ecological field study that identified transferable challenges and recommended a dual approach (i.e., hydrologic and geomorphic) to hyporheic studies. The hydrologic approach entails sophisticated measurements of groundwater flow under a variety of conditions, and the geomorphic approach requires knowledge of the streambed geology through core and geophysical logs. In this study, the findings presented are the result of a dual approach to data collection. Hydrologic measurements included: groundwater flow (Q), surface water flow (Q^{sw}) and the head differentials between them (of Δh and Δh_{rel}). Geomorphic quantities included: streambed geology, fracture density, length and orientation, and channel shape and contoured bathymetry.

Priority was given to quantifying groundwater fluxes and vertical hydraulic gradients using several independent measurements (i.e., flow from seepage tests and head from temporal monitoring and

manual point measurements using a potentiomanometer and a bathymetric tool) to evaluate bias and reduce uncertainty. Interpretation of hydrologic and geomorphic data sets is complex, involving numerous linkages and interdependencies. Key considerations in the evaluation of spatial and numeric variability of point measurements, were identified as: (1) a split data format of high and low river stage to detect changes in response to a declining water table, represented by river stage; (2) identification of fracture density, geometry and proximity to BSM installations; (3) elevation of the BSM relative to the channel topography and litho-stratigraphy; and (4) position of the BSM relative to channel meander geometry. Note that the threshold between the high and low stage classification of channel flow conditions observed in this study is 1.5 m^3/s measured at the Watson Road Gauging Station (refer to section 2.2.3 and Figure 3.5).

On a regional scale, a strong influence of groundwater discharging to the river in accordance with the regional flow model was expected (Gartner Lee 2004), since the glaciofluvial plain of the study site exhibits low topographic relief (Toth 1963). On a reach scale, point measurements of volumetric flow into the BSMs ranged from 3 – 35 mL/min at high stage and from -0.4 – 55 mL/min at low stage, with uncertainties that ranged from 13 – 40% (n = 672). Assuming radial flow, these measurements yielded fluxes of 0.05 – 0.63 m/day at high stage and 0.12 – 0.99 m/day at low stage. Assuming a bulk fracture porosity for the streambed dolostone of 0.1% or 10^{-3}, these measurements also yielded average linear groundwater velocities of 55 – 629 m/day at high stage and 7 – 985 m/day at low stage. Head differentials (Δh) between groundwater and surface water estimated from groundwater head transducer measurements and surface water head manual measurements, ranging from 0.01 – 0.15 m, had high uncertainties and showed poor agreement with potentiomanometer measurements. Relative head differentials (Δh_{rel}) between groundwater and surface water directly measured with a potentiomanometer reflected more consistent results and much smaller uncertainties, ranging from 0.001 – 0.023 m at high stage and from 0.001 – 0.012 m at low stage ± 0.001. Vertical hydraulic gradients across a 5-cm layer of streambed dolostone ($\Delta h_{rel}/\Delta L$) ranged from 0.02 – 0.46.

4.1.4 Spatio-Temporal Variability of Hydraulic Parameters in a Riffle-Pool Sequence

Temporal monitoring of head and temperature was collected from 12 of 24 BSMs, while seepage tests and potentiomanometer measurements were conducted in all 24 BSMs. Installing BSMs directly on fractures terminating at surface is challenging, as discussed in Chapter 1. BSMs installed on vertical fractures terminating either at surface (i.e., BSMs 2, 4 and 5) or beneath the packer (i.e., BSMs 1 and 10) yielded the highest measured fluxes, regardless of elevation or position along the channel. Vertical hydraulic gradients were small in BSMs 2, 4 and 5 (i.e., ≤ 0.08) and moderate in BSMs 1 and 10 (i.e., 0.12 – 0.24), indicating that installations on vertical fractures that do not run the full length of the seepage cavity have larger gradients, but similar fluxes. The volumetric flow (Q) measurement is a reasonable indicator of groundwater discharge or flux (q); however, the use of hydraulic head measurements within the hyporheic flow paths are needed to accurately assess results. Fluxes measured in BSMs installed directly on vertical fractures were high, which may be interpreted as indicators of high groundwater discharge. Transducers in BSMs provide quantitative insights of the groundwater pressure at each point measurement, which, as we saw in BSMs 2 and 4, can be very different. Further, the continuous temperature record provides an additional independent point measurement. In the case of BSMs 2 and 4, where there are two installations on vertical fractures terminating at surface, both exhibit high fluxes and some breakage around the rubber packer. BSM 4 yielded a small vertical gradient between its seepage cavity head and the localized river head (i.e., 0.0 – 0.06), a zero differential between its seepage cavity and the centralized river stage gauge and cavity temperatures similar to that of the river, summer and winter (Figure 3.15). Thus, the seepage measured in BSM 4 contains a component of recirculated surface water. BSM 2 yielded larger fluxes at low stage than at high stage. BSM 2 also yielded a small vertical gradient between its seepage cavity head and the localized river head (i.e., 0.02 – 0.08), a large differential between its seepage cavity and the centralized river stage gauge (i.e., 0.10 – 0.12 m) and cavity temperatures that were about 1^{o}C warmer than the river in winter, except for some short-term variability at low stage. Thus, the seepage measured at low stage likely contains surface water, since it

appears to enter the fractures intersecting BSM 2 when the water table declines (Figure 3.15). Rigorous hydro-chemical sampling in the BSMs may provide additional insights regarding the groundwater – surface water mix in these BSMs.

Topographic influences on the spatial distribution of flux and vertical gradients were observed. Groundwater discharging to surface water was greatest along the north side of the channel and in the pool downstream of transect 3. Elevation of the north side of the channel is generally lower, indicating a topographic influence is observed in the transverse direction. The reconnaissance IRT survey, detailed in Appendix A, revealed thermal signatures indicating potential groundwater discharge along the north side of the channel [Appendix A, Fig. A-9]. Elevation of the pool is lower than the riffle, indicating a topographic influence in the longitudinal direction. The summer temperature records for all BSMs (excluding BSM 4) yielded less variable temperatures, due to the moderating effect of cooler groundwater discharge, while the winter temperature records reflected a warmer groundwater influence.

Excluding BSMs 1 and 2 (installed on vertical fractures), mean fluxes in the upstream riffle – pool transition zone were small and hydrometric surveys revealed that a losing condition was occurring in this segment of the study reach. Location of the riffle coincides with the start of a river bend, where surface water flows along a small creek cutting across the neck of the meander on the north side of the channel and into the floodplain bank on the south side, contributing to streamflow losses. Short-term declines in surface water head, resulting from controlled flow system disturbances, observed in the upstream stage gauge, SG1, show evidence of a hyporheic flowpath from the riffle zone into the floodplain along the concave bend on the south side of the channel.

The continuous hydraulic record for deep piezometers, P3 – P6, (i.e., 3.0 mbgs or 307.35 – 308.22 masl) indicated upward gradients. Since groundwater in the Guelph area maintains a temperature of ~10^{o}C and temperatures in the screened intervals of the deep piezometers (i.e., 3.0 mbgs or 307.35 – 308.22 masl) reached temperatures that were about 5^{o}C colder in winter and 5^{o}C warmer in summer,

hyporheic mixing of groundwater and surface water extends to a depth of at least 307.35 masl. The shallow piezometer, P1, is installed in the upstream riffle at the entrance of the concave bend on the south side of the channel, and P2 is in the downstream riffle at the exit of the channel bend. The reconnaissance IRT survey, detailed in Appendix A, revealed a thermal signature indicating potential groundwater discharge along the south side of the channel near P2 [Appendix A, Fig. A-9]. The continuous head records reflect an upward gradient in P1 (i.e., 0.05 – 1.10) and an immeasurable gradient in P2. These shallow piezometers (i.e., between 0.30 – 0.70 mbgs or 309.95 – 310.58 masl) have similar temperature profiles, summer and winter, that are less variable than the BSMs but more variable than the deeper piezometers, P3 – P6, indicating a groundwater influence. A parallel-flow condition, therefore, likely exists near P2. The extent of hyporheic flow in discrete fracture networks interpreted from this study is based on point measurements collected on or near vertical fractures terminating at surface where intact dolostone pavement is exposed and rubble is absent. It was observed during the 2013 – 2015 field seasons that, when streamflow energies are high (i.e., during spring freshet), deposition does not occur in these regions of exposed pavement, and sediment particles as large as boulders are continually evacuated in a downstream direction beyond transect 4. Streamflow (Q^{sw}) measurements indicate variability within the study reach; however, it is difficult to conclude gaining or losing conditions in a short reach-scale study where fluxes are small, gradients are variable, and channel geometry reflects a meander bending through the fluvial plain. Consequently, further studies within the Eramosa River Basin are needed.

4.1.5 Attributes and Disadvantages of the BSM

The BSM works well in its capacity to measure groundwater discharge and hydraulic head differentials between groundwater and surface water, as well as for hydro-chemical sampling. The BSM is robust and durable. Over the 2-year prototype-testing period (June 2013 – May 2015), the BSM proved unaffected by anchor ice, high flows, boaters, fisherman and wildlife. The 0.30-m depth of the seepage cavity achieved adequate penetration of the bedding planes to measure groundwater flow from the seepage cavity, but shallow enough to be easily drilled with a concrete drill and the core extracted with a

snorkel and mask. The invasiveness of the BSM was minimized by its low profile, small diameter, shallow depth and ball valve. Application of the BSM methods at the study site between 2013 and 2015 did not appear to impact the observed populations of brown trout and turtles.

The J-plug™ (Koby Environmental, Clarence, NY, USA) and its modifications created a good seal at the streambed surface. Leaks in vertical fracture installations were a function of rock integrity, not the BSM. Attaching the polyvinyl tube empty (i.e., full of air), necessitates an equilibrium adjustment to the tube volume and to the test time which is estimated based on site response times [Chapter 2, Equation 1]. The result of starting the test with a tube full of river water would still require the deduction of the tube volume, but there would be no need to modify the test time, thereby, reducing uncertainty in the flow calculation. Calm waters at the study site and the low profile of the BSM design, with the collection bag resting at surface, negated concerns associated with bag movement or the Bernoulli Effect that might influence results.

4.2 Original Contributions:

Three key contributions came from this study in connection with the advancement of our understanding of groundwater – surface water exchanges in bedrock rivers:

1. **Tool design and methods development.** The bedrock seepage meter (BSM) has been successfully field-tested to measure groundwater discharge and head differentials between groundwater and surface water at the sub-meter scale. Its utility extends further, to measurements of fluid pressures, temperature and fluid conductivity, as well as sample collection. The BSM method, based on accepted EPM and DFN theory, was developed to characterize the spatial variability of groundwater contributions to a riffle-pool meander. Partnered with the bedrock river piezometer and stage gauge designs, it is easy to use, cost effective, minimally-invasive to install, and unaffected by anchor ice.

2. **Field site procurement and development for field-testing new methods.** The Scout Camp field site abuts the south side of the Eramosa River, where intact dolostone is exposed along the channel bed and fluvial plain. The 1110 m^2 study reach exhibits a channel meander and a longitudinally-stepped riffle – pool sequence. The height of river stage is sufficiently low to observe vertical and bedding plane fractures terminating at surface, which have been mapped. The site has been instrumented along the channel bed with robust, low-profile, minimalistic monitoring devices that have demonstrated little-to-no disruption to the flow system and riverine ecology. Floodplain and baseline data have been collected (i.e., streambed bathymetry, infrared temperature survey, geological and geophysical surveys at surface and downhole, and GPS surveys). The study site is 2 km from the University of Guelph and serviced by an accessible camp road. A strong working relationship has been fostered between the University of Guelph G360 Institute for Groundwater Research, Scouts Canada, Grand River Conservation Authority and the Ministry of Natural Resources and Forestry for the continued operation of this field site.

3. **Study site characterization and conceptual site modelling**. A general conceptual model for groundwater – surface water interaction in the discrete fracture networks of sedimentary bedrock rivers was developed from spatially-distributed and high-resolution temporal data sets. This was accomplished through evaluation of the spatio-temporal variability of groundwater fluxes and hydraulic gradients, using: (1) a split data format of high and low river stage to detect changes in response to a declining water table; (2) identification of fracture density, geometry and proximity to BSM installations; (3) elevation of the BSM relative to the channel topography and litho-stratigraphy; and (4) position of the BSM relative to channel meander geometry.

4.3 Recommendations for Future Research

Tweaking of the BSM design and method could improve the accuracy of seepage measurements, as discussed in Chapter 2 and section 4.1.7. Further tests over a range of longer test times could prove useful in assessing steady state flow in greater detail. The BSM transducer measures blended head over a 0.25-m open interval. It may be possible to log the fracture count and orientation in each BSM with an optical televiewer, although core recovery provided excellent insights on the occurrence of vertical fractures and bedding parallel partings in each of the BSMs in this study. This information could be useful in conjunction with BSM slug tests to estimate the spatial variability of transmissivities along the channel.

The pressure head data collected in BSMs, river piezometers and stage gauges is only as good as the transducers used to collect them. Since transducer accuracy declines with depth range, choice of instrumentation and independent accuracy verification is critical. In this study, 10-m range SWS Mini-, Micro-, and CTD-Divers™ (Schlumberger Water Services, Delft, The Netherlands) demonstrated accuracy of 0.5 - 3.0 cm. Working with absolute pressure (i.e., vented transducers), as opposed to relative pressure, requires a certain level of confidence in equipment accuracy that can only be achieved through stringent calibrations at regular intervals during the study period. Given the importance of groundwater - surface water research in bedrock rivers, further study of the accuracy limits that can be achieved with customized pressure transducers would be useful.

Development of the device designs was a 2-year process. Temporal data was collected during 2013-14 from prototype 1 of the BSM and other streambed installations, and during 2014-15 from the stage 2 prototypes. Thus, the temporal data evaluated in this thesis to assess flow dynamics was limited to only one 4-season cycle between 2014-15. Three angled – vertical lined floodplain corehole pairs were installed along the south side of the channel to depths of ~30 mbgs. With the infrastructure in place, a multiple-year temporal study could be conducted to monitor transient heads within and beneath the

streambed. Further, only one sampling event was conducted in this initial field study. Multiple sampling events could be linked to the temporal study to correlate transient hydraulic trends to hydro-chemistry.

The BSM has the capacity to accommodate sampling in a contaminated site and should be field-tested in this regard.

Literature Cited

Alexander, M.D., and D. Caisse. 2003. Variability and Comparison of Hyporheic Water Temperatures and Seepage Fluxes in a Small Atlantic Salmon Stream. Ground Water, 41(1): 72-82.

Allen, E., and B. Lucas. 2013. Building a Water Quality Research Platform in Urban and Urbanizing Watersheds (SOWC). Proceedings of the Water Environmental Federation, WEFTEC 2013: Session 63-69, p.4787-4798.

Anderson, M.P. 2005. Heat as a Ground Water Tracer. Ground Water, 43(6): 951-968.

AquaResource Inc. (ARI) 2010. City of Guelph Source Protection Project: Final groundwater and surface water Vulnerability Report. March 2010.

Armstrong, J.D., Kemp, P.S., Kennedy, G.J.A., Ladle, M., and N.J. Milner. 2003. Habitat requirements of Atlantic salmon and brown trout in rivers and streams. Fisheries Research, 62: 143-170.

ASTM D3858. 2014. Standard Test Method for Open-Channel Flow Measurement of Water by Velocity-Area Method.

ASTM D5541. 2014. Standard Practice for Developing a Stage-Discharge Relation for Open Channel Flow.

Banks, W. S. L., R. L. Paylor, and W. B. Hughes (1996), Using thermal- infrared imagery to delineate ground-water discharge, Ground Water, 34(3), 434–443, doi:10.1111/j.1745-6584.1996.tb02024.x.

Bear, J. 1972. Dynamics of Fluids in Porous Media. American Elsevier Publishing Company, Inc., NY., p.13-26.

Belan, K.P. 2010. Characterizing a fractured rock aquifer with hydraulic testing at a contaminated municipal well using flexible liner methods and depth discrete monitoring, MASc Thesis, University of Guelph.

Belanger, T.V., and M.T. Montgomery. 1992. Seepage Meter Errors. Limnol. Oceanogr., 37(8): 1787-1795.

Bencala, K.E., Kennedy, V.C., Zellweger, G.W., Jackman, A.P., and R.J. Avanzino. 1984. Interactions of Solutes and Streambed Sediment, 1. An Experimenta Analysis of Cation and Anion Transport in a Mountain Stream. Water Resources Research, 20(12): 1797-1803.

Bishop, P., and G. Goldrick. 2010. Lithology and the evolution of bedrock rivers in post-orogenic settings: Constraints from the high elevation passive continental margin of SE Australia. Geological Society, London, Special Publications, 346: 267-287.

Bisson, P.A., Sullivan, K., and J.L. Nielsen. 1988. Channel Hydraulics, Habitat Use and Body Form of Juvenile Coho Salmon, Steelhead and Cutthroat Trout in Streams. Transactions of the American Fisheries Society, doi: 10.1577/1548-8659(1988)117<0262:CHHUAB>2.3.CO;2.

Brunton, F.R. 2009. Update of revisions to the Early Silurian stratigraphy of the Niagara Escarpment: Integration of sequence stratigraphy, sedimentology and hydrogeology to delineate hydrogeologic units; in Summary of Field Work and Other Activities 2009, Ontario Geological Survey, Open File Report 6240, p.25-1 to 25-20

Cable, J.E., Burnett, W.C., Changon, J.P., Corbett, D.R., and P.H.Cable. 1997. Field Evaluation of Seepage Meters in the Coastal Marine Environment. Estuarine, Coastal and Shelf Science, 45: 367-375.

Carter, J.T.V., Gotkowitz, M.B., and M.P. Anderson. 2011. Field Verification of Stable Perched Groundwater in Layered Bedrock Uplands. Ground Water, 49(3): 383-392.

Cey, E.E., Rudolph, D.L., Parkin, G.W., and R. Aravena. 1998. Quantifying groundwater discharge to a small perennial stream in southern Ontario, Canada. Journal of Hydrology, 210: 21-37

Cherry, J.A., Parker, B.L., Keller, C., 2007. A new depth-discrete multilevel monitoring approach for fractured rock. Ground Water Monitoring & Remediation, 27 (2), 57-70.

Cole, J., M. Coniglio, and S. Gautrey (2009), The role of buried bedrock valleys on the development of karstic aquifers in flat-lying carbonate bedrock: insights from Guelph, Ontario, Canada, Hydrogeol. J., 17, 1411-1425, doi:10.1007/s10040-009-0441-3.

Coleman, T.I. 2012. A Novel Technique for Depth Discrete Flow Characterization: Fibre Optic Distributed Temperature Sensing within Boreholes sealed with Flexible Underground Liners. MASc Thesis, University of Guelph.

Conant, B. 2004. Delineating and Quantifying Ground Water Discharge Zones Using Streambed Temperatures. Ground Water, 42(2): 243-257.

Conant Jr., Brewster, and Neil J. Mochnacz (2009). Low Altitude and Land-Based Infrared Thermography to Identify Groundwater Discharge in NWT Rivers: Advantages and Limitations. 44th Central Canadian Symposium on Water Quality, Burlington, Ontario, Canada, February 23-24, 2009.

Constantz, J. 2008. Heat as a Tracer to Determine Streambed Water Exchanges. Water Resources Research, 44: W00D10, doi:10.1029/2008WR006996.

Cook, P.G. 2003. A Guide to Regional Groundwater Flow in Fractured Rock Aquifers. CSIRO Land and Water, Glen Osmond, SA, Australia.

Cooke, M.L., Simo, J.A., Underwood, C.A., and P. Rijken. 2006. Mechanical stratigraphic controls on fracture patterns within carbonates and implications for groundwater flow. Sedimentary Geology, 184: 225-239.

Desaulniers, D.E., Cherry, J.A., and P.Fritz. 1981. Origin, age and movement of pore water in argillaceous quaternary deposits at four sites in southwestern Ontario. Journal of Hydrology, 50: 231-257.

de Vriend, H.J., and H.J. Geldof. 1983. Main Flow Velocity in Short River Bends. J. Hydraul. Eng., 109(7): 991-1011.

Dingman, S.L. 2002. Physical Hydrology 2nd ed. Waveland Press, Inc. Long Grove, IL. p.370-375; 608-619.

Doe, T. 2014. Workflow for DFN Assessments of Groundwater Flow and Contaminant Transport. 1st International Conference on Discrete Fracture Engineering, Vancouver, BC, Canada, October 19-22, 2014.

Dumouchelle, D.H. 2001. Evaluation of ground-water/surface-water relations, Chapman Creek, West-Central Ohio, by Means of Multiple Methods. USGS Water-Resources Investigations Report 01-4202.

Elmo, D. 2014. DFN Data Collection for Underground Rock Engineering. 1st International Conference on Discrete Fracture Engineering, Vancouver, BC, Canada, October 19-22, 2014.

Environment Canada (EC). 2004. Threats to Water Availability in Canada: Climate Variability and Change – Groundwater Resources (ch.10); Rivers and Streams (ch.11). National Water Research Institute, Burlington, Ontario. NWRI Scientific Assessment Report Series No.3.

Environment Canada (EC). 2003. Winter Hydrometry: Real-time Data Issues. Canadian Geophysical Union – Hydrology Section Committee on River Ice Processes and the Environment (CGU—HS CRIPE) 12th Annual Workshop on the Hydraulics of Ice Covered Rivers, Jun.19-20 2003, Edmonton, Canada.

Fales, J., and L. Rasmussen. 2014. Bedrock Creek Fish and Fish Habitat Assessment. Nez Perce Soil and Water Conservation District, Culdesac, ID, USA.

Fomenko, A. 2015. An integrated lithostratigraphic and geomechanical conceptualization of dense fracture networks in a shallow Paleozoic dolostone. MASc Thesis, University of Guelph.

Freeze, R.A. & J.A. Cherry. 1979. Groundwater. Prentice-Hall, Inc. Englewood Cliffs, NJ.

Fritz, B.G., Mendoza, D.P., and T.J.Gilmore. 2009. Development of an Electronic Seepage Chamber for Extended Use in a River. Ground Water, 47(1): 136-140.

Fryar, A.E., Wallin, E.J., and D.L. Brown. 2000. Spatial and Temporal Variability in Seepage between a Contaminated Aquifer and Tributaries to the Ohio River. Ground Water Monitoring and Remediation, 20(3): 129-146.

Gartner Lee Limited. 2004. Guelph/Eramosa Township Regional Groundwater Character-ization and Wellhead Protection Study. GLL 22-170.

Grand River Conservation Authority (GRCA). 1998. Eramosa Watershed Study – Hydrology Report by Schroeter & Associates.

Grand River Conservation Authority (GRCA). 2005. Watershed Report, Fall 2005.

Guilbeault, M.A., Parker, B.L., and J.A. Cherry. 2005. Mass and Flux Distributions from DNAPL Zones in Sandy Aquifers. Ground Water, 43(1): 70-86.

Hakenkamp, C.C., Valett, H.M., and A.J. Boulton. 1993. Perspectives on the hyporheic zone: integrating hydrology and biology. Concluding remarks. J. N. Am. Benthol. Soc., 12(1): 94-99.

Harvey, J.W., and K.E. Bencala. 1993. The effect of streambed topography on surface-subsurface water exchange in mountain catchments. Water Res. Research, 29: 89-98.

Harvey, F.E., Lee, D.R., Rudolph, D.L., and S.K. Frape. 1997. Locating groundwater discharge in large lakes using bottom sediment electrical conductivity mapping. Water Resources Research, 33(11): 2609-2615.

Hatch, C.E., Fisher, A.T., Revenagh, J.S., Constantz, J., and C. Ruehl. 2006. Quantifying surface water - groundwater interactions using time series analysis of streambed thermal records: method development. Water Resour. Res. 42, W10410.

Hayashi, M. 2004. Temperature-electrical conductivity relation of water for environmental monitoring and geophysical data inversion. Environmental Monitoring and Assessment, 96: 119-128.

Hayashi, M., and G. van der Kamp. 2009. Progress in Scientific Studies of Groundwater in the Hydrologic Cycle in Canada, 2003-2007. Canadian Water Resources Journal, 34(2): 177-186.

Hem, J.D. 1985. Study and Interpretation of the Chemical Characteristics of Natural Water, 3rd ed., U.S. Geological Survey Water-Supply Paper 2254.

Hendricks, S.P., and D.S. White. 1991. Physiochemical patterns within a hyporheic zone of a northern Michigan river, with comments on surface water patterns. Can. J. Fish. Aquat. Sci., 48:1645-1654.

Hichin, E.J., 2004. River Hydraulics and Channel Form. John Wiley & Sons Ltd., Chichester, UK, p.2.13.

Hodge, R.A., et al., 2011. Bed load transport in bedrock rivers: The role of sediment cover in grain entrainment, translation and deposition. J. Geophys. Res., 116: F04028, doi: 10.1029/2011F002032.

Howard, K.W.F., Baba, A., and O. Gunduz. 2006. Groundwater - Surface Water Interactions. Proceedings of the NATO Advanced Research Workshop on Groundwater and Ecosystems, Canakkale, Turkey, September 5-7, 2005.

Hubbert, M.K. 1940. The theory of groundwater motion. J. Geol. 48: 785-944.

Hvorslev, J. 1951. Time lag and soil permeability in ground-water observations. Vicksburg, Mississippi: Waterways Experimental Station, U.S. Army Corps of Engineers.

Hynes, H.B.N. 1983. Groundwater and stream ecology. Hydrobiologia, 100: 93-99.

Intergovernmental Panel on Climate Change (IPCC). 2007; 2013. Climate Change 2007: The Physical Science Basis. Contribution of Working Group I to the 4th and 5th Assessment Reports of the IPCC, Cambridge University Press, Cambridge; New York.

Isiorho, S.A., and J.H. Meyer. 1999. The Effects of Bag Type and Meter Size on Seepage Meter Measurements. Ground Water, 37(3): 411-413.

Israelsen, O.W., and R.C. Reeve. 1944. Canal Lining Experiments in the Delta Area, Utah. Utah State University (previously Utah State Agricultural College), Utah Agricultural Experiment Station, UAES Bulletin No.313 (Technical).

Jacob, C.E., and S.W. Lohman. 1952. Nonsteady Flow to a Well of Constant Drawdown in an EXtensive Aquifer. Transactions, American Geophysical Union, 35(4): 559-569.

Jarrett, R.D. 1984. Hydraulics of high-gradient streams. J. Hyd. Eng., 110: 1519-1539.

Karrow, P.F. 1968. Pleistocene Geology of the Guelph Area. Open Field Report 61. Ontario Department of Mines, Toronto, ON.

Krupa, S.L., Belanger, T.V., Howell, H.H., Brock, J.T., and B.J. Jones. 1998. Krupaseep – The Next Generation Seepage Meter. Journal of Coastal Research, 26: 210-213.

Kunert, M., Coniglio, M., and E.C. Jowett. 1998. Controls and age of cavernous porosity in Middle Silurian dolomite, southern Ontario. Can. J. Earth Sci., 35: 1044-1053.

Lake Erie Region Source Protection Committee (LERSPC). 2010. Proposed Assessment Report under the Clean Water Act, 2006 (Ontario Regulation 287/07). Grand River Source Protection Area, Cambridge, ON. ch.8. http://www.sourcewater.ca/index/document.cfm?Sec=7&Sub1=8&Sub2=2. December, 2010.

Lambe, T.W., and R.V. Whitman, 1969. Soil Mechanics. John Wiley & Sons Ltd., New York, USA, p.251-253.

Lee, D.R. 1977. A device for measuring seepage flux in lakes and estuaries. Limnology and Oceanography, 22(1): 140-147.

Lee, D.R., Dal Bianco, R., and M. St.Aubin. 1993. Locating Groundwater discharge zones using electrical conductivity, paper presented at Outdoor Action Conference, Natl. Water Well Assoc., Las Vegas, NV, USA, May 25-27, 1993.

Lee, D.R. 1985. Method for locating sediment anomalies in lakebeds that can be caused by groundwater flow. Journal of Hydrology, 79: 187-193.

Lee, D.R., and H.B.N. Hynes. 1978. Identification of groundwater discharge zones in a reach of Hillman Creek in Southern Ontario. Water Pollution Research in Canada, 13: 121-133.

Lee, D.R., and J.A. Cherry. 1978. A field exercise on groundwater flow using seepage meters and mini-piezometers. Journal of Geological Education, 27: 6-20.

Legleiter, C.J., Harrison, L.R., and T. Dunne. 2011. Effect of point bar development on the local force balance governing flow in a simple, meandering gravel bed river. Journal of Geophysical Research, 116: 1-29,

Leopold, L.B, and M.G. Wolman. 1960. River Meanders. Bulletin of the Geological Society of America, vol.71: 769-794.

Libelo, E.L., and W.G.MacIntyre. 1994. Effects of surface-water movement on seepage-meter measurements of flow through the sediment-water interface. Applied Hydrogeology, 2(4): 49-54.

Lipson, D.S., Kueper, B.H., and M.J. Gefell. 2005. Matrix Diffusion-Derived Plume Attenuation in Fractured Bedrock. Ground Water, 43(1): 30-39.

MacDonald, G.D. 2015. Developing novel techniques for measuring in situ groundwater nitrate concentrations, vertical geochemical profiling and real-time remote groundwater quality monitoring, MASc Thesis, University of Guelph.

Madsen, H., and C. Skotner. 2005. Adaptive state updating in real-time river flow forecasting – a combined filtering and error forecasting procedure. Journal of Hydrology, 308: 302-312.

Malenica, A.I. 2015. Evaluation of nitrate distribution and matrix storage effects in a dual permeability fractured bedrock aquifer with heterogeneous hydrochemistry. MSc Thesis, University of Guelph.

Mathis, J. 2014. Open Pit Data Discontinuity Data Collection and Reduction. 1st International Conference on Discrete Fracture Engineering, Vancouver, BC, Canada, October 19-22, 2014.

Meier, P.M., Carrera, J., and X. Sanchez-Vila. 1998. An evaluation of Jacob's method for the inperpretation of pumping tests in heterogeneous formations. Water Resources Research, 34(5): 1011-1025.

Meyer, J.L. 1997. Stream health: incorporating the human dimension to advance stream ecology. J. N. Am Benthol. Soc., 16(2): 439-447.

Meyer, J.R. 2013. A high resolution vertical gradient approach to hydrogeologic unit delineation in fractured sedimentary rocks, PhD Thesis, University of Guelph.

Meyer, J.R., Parker, B.L., and J.A. Cherry. 2014. Characteristics of high resolution hydraulic head profiles and vertical gradients in fractured sedimentary rocks. J. Hydrol. 517: 493-507.

Meyer, J.R., Parker, B.L., and J.A. Cherry. 2008. Detailed hydraulic head profiles as essential data for defining hydrogeologic units in layered fractured sedimentary rock, Environ. Geol., 56: 27-44.

Miller, A.J., and B.L. Cluer. 1998.Modeling Considerations for Simulation of Flow in Bedrock Channels, in Rivers Over Rock: Fluvial Processes in Bedrock Channels. Geophys. Monogr. Ser., vol.107, AGU, Washington, D.C., DOI: 10.1029/GM107p0001. p.61-104.

Mossop, B., and M.J. Bradford. 2006. Using thalweg profiling to assess and monitor juvenile salmon (*Oncorhynchus* spp.) habitat in small streams. Can. J. Fish. Aquat. Sci 63: 1515-1525.

Muldoon, M., and K.R. Bradbury. 2005. Site Characterization in Densely Fractured Dolomite: Comparison Methods. Ground Water, 43(6): 863-876.

Munn, J.D. 2012. High-resolution discrete network characterization using inclined coreholes in a Silurian dolostone aquifer in Guelph, Ontario. MSc Thesis, University of Guelph.

Noorduijn, S., Cook, P.G., Wood, C., and N. White. 2015. Using Sealed Wells to Measure Water Levels Beneath Streams and Floodplains. Groundwater, 53(6): 872-876.

Northwest Hydraulic Consultants Ltd. (NHC). 2010. Peace River Water Use Plan – Peace River Mainstem Stage Discharge (GMsurface waterORKS#6). Jun.28-2010. Prepared for BC Hydro, North Vancouver, Canada.

Novakowski, K., Bickerton, G., Lapcevic, P., Voralek, J., and N. Ross. 2006. Measurements of groundwater velocity in discrete rock fractures. Journal of Contaminant Hydrology, 82: 44-60.

Novakowsky, K., Lapcevic, P., Bickerton, G., Voralek, J., Zanini, L., Talbot, C., 1999. The development of a conceptual model for contaminant transport in the dolostone underlying Smithville, Ontario. Final Report to the Smithville Phase IV Bedrock Remediation Program

Novakowski, K.S., and P.A. Lapcevic. 1988. Regional Hydrogeology of the Silurian and Ordovician Sedimentary Rock Underlying Niagara Falls, Ontario, Canada. Journal of Hydrology, 104: 211-236.

Olsen, T.C., and D. Swartzendruber. 1968. Velocity-gradient relationships for steady-state unsaturated flow of water in non-swelling artificial soils. Soil Sci. Soc. Amer. Proc. 32: 457-462.

Ong, J.B., and V.A. Zlotnik. 2011. Assessing Lakebed Hydraulic Conductivity and Seepage Flux by Potentiomanometer. Ground Water, 49(2): 270-274.

Opazo, T., Aravena, R., and B. Parker. 2016. Nitrate distribution and potential attenuation mechanisms of a municipal water supply bedrock aquifer. Applied Geochemistry, 73: 157-168.

Orghidan, T. 1955. A new habitat of subsurface waters: the hyporheic biotope. Buletin Stiintific sectia de Biologie si stiinte Agricole si sectia de Geologie si Geografie [Romania - Academy of Sciences], 7(3): 657-676.

Oxtobee, J.P.A., and K. Novakowski. 2002. A field investigation of groundwater/surface water interaction in a fractured bedrock environment. Journal of Hydrology, 269: 169-193.

Paillet, F.L., Hess, A.E., Cheng, C.H., and E. Hardin. 1987. Characterization of fracture permeability with high-resolution vertical flow measurements during borehole pumping. Groundwater, 25(1): 28-40.

Palmer, M.A. 1993. Experimentation in the hyporheic zone: challenges and prospectus. J. N. Am. Benthol. Soc., 12(1): 84-93.

Palmer, M.A. Bely, A.E., and K.E. Berg. 1992. Response of invertebrates to lotic disturbance: a test of the hyporheic refuge hypothesis. Oecologia, 89: 182-194.

Parker, B.L. 2007. Investigating contaminated sites on fractured rock and using the DFN approach. In: Proceedings of the U.S. EPA / NGWA Fractured Rock Conference: State of the Science and Measuring Success in Remediation, September 24-26, 2007, Portland, Maine.

Parker, B.L., Cherry, J.A., and S.W. Chapman. 2012. Discrete Fracture Network Approach for Studying Contamination in Fractured Rock. AQUA Mundi, Am06052: 101-116.

Paulsen, R.J., Smith, C.F., O'Rourke, D., and T.F. Wong. 2001. Development and evaluation of an ultrasonic ground water seepage meter. Ground Water, 39(6): 904-911.

Payne, B.A., and M.F. Lapointe. 1997. Channel morphology and lateral stability: Effects on distribution of spawning and rearing habitat for Atlantic salmon in a wandering cobble-bed river. Can. J. Fish. Aquat. Sci. 54: 2627-2636.

Pehme, P.E., B.L. Parker, J.A. Cherry and J.P. Greenhouse. 2010. Improved Resolution of Ambient Flow through Fractured Rock with Temperature Logs. Ground Water, 48(2): 191-205.

Perrin, J., Parker, B.L., and J.A. Cherry. 2011. Assessing the flow regime in a contaminated fractured and karstic dolostone aquifer supplying municipal water. Journal of Hydrology, 400: 396-410.

Pierce, A.A., Parker, B.L., Ingleton, R., and J.A. Cherry. 2017. Well Completions in Bedrock Coreholes created using Portable Drills. Hydrological Processes (submitted).

Portnoy, J., B. Nowicki, C. Roman, and D. Urish (1998), The discharge of nitrate-contaminated groundwater from developed shoreline to marsh-fringed estuary, Water Resour. Res., 34(11), 3095–3104, doi:10.1029/98WR02167.

Quinn, P.M., Parker, B.L., and J.A. Cherry. 2011. Using constant head step tests to determine hydraulic apertures in fractured rock. Journal of Contaminant Hydrology, 126: 85-99.

Raven, K.G. 1986. Hydraulic characterization of a small groundwater flow system in fractured monzonitic gneiss (AECL--9066). Canada.

Rawson, D.S. 2011. The Eastern Brook Trout in the Maligne River System, Jasper National Park. Transactions of the American Fisheries Society, http://dx.doi.org/10.1577/1548-8659(1940)70[221:TEBTITJ2.0.CO;2.

Razack, M., and D. Huntley. 1991. Assessing Transmissivity from Specific Capacity in a Large and Heterogeneous Alluvial Aquifer. Ground Water, 29(6): 856-861.

Rogers, J.S., and A. Klute. 1971. The Hydraulic Conductivity-Water Content Relationship During Nonsteady Flow Through a Sand Column. Soil Sci. Soc. Amer.Proc., 35: 695-700.

Rosenberry, D.O. 2008. A seepage meter designed for use in flowing water. Journal of Hydrology, 359: 118-130.

Rosenberry, D.O., and R.H. Morin. 2004. Use of an Electromagnetic Seepage Meter to Investigate Temporal Variability in Lake Seepage. Ground Water, 42(1): 68-77.

Rosenberry, D.O., LaBaugh, J.W., and R.J. Hunt. 2008. Use of monitority wells, portable piezometers, and seepage meters to quantify flow between surface water and ground water. Field Techniques for Estimating Water Fluxes between surface water and Ground Water (ch.2), US Geological Survey.

Rosenberry, D.O., Sheibley, R.W., Cox, S.e., Simonds, F.W., and D.L. Naftz. 2013. Temporal variability of exchange between groundwater and surface water based on high-frequency direct measurements of seepage at sediment – water interface. Water Resources Research, 49: 2975-2986.

Rouleau, A. & J.E. Gale. 1985. Statistical Characterization of the Fracture System in the Stripa Granite, Sweden. Int. J. Rock Mech. Min. Sci. & Geomech. Abstr., 22(6): 353-367.

Russoniello, C.J., and H.A. Michael. 2015. Investigation of Seepage Meter Measurements in Steady Flow and Wave Conditions. Groundwater, 53(6): 959-966.

Sadura, S., Martini, I.P., Endres, A.L., and K.Wolf. 2006. Morphology and GPR stratigraphy of a frontal part of an end moraine of the Laruentide Ice Sheet: Paris Moraine near Guelph, ON, Canada. Geomorphology, 75: 212-225.

Schincariol, R.A., and J.D. McNeil. 2002. Errors with Small Volume Elastic Seepage Meter Bags. Ground Water, 40(6): 649-651.

Shaw, R.D., and E.E. Prepas. 1989. Anomalous, short-term influx of water into seepage meters. Limnology and Oceanography, 34(7): 1343-1351.

Shaw, R.D., and E.E. Prepas. 1990. Groundwater – Lake Interactions: II. Nearshore Seepage Patterns and the Contribution of Ground water to Lakes in Central Alberta. Journal of Hydrology, 119: 105-120.

Shinn, E.A., Reich, C.D., and T.D. Hickey. 2002. Seepage Meters and Bernoulli's Revenge. Estuaries, 25(1): 126-132.

Smith, L., Schwartz, F.W., 1984. An analysis of the influence of fracture geometry on mass transport in fractured media. Water Resources Research, 20 (9), 1241-1252.

Sophocleous, M. 2002. Interactions between groundwater and surface water: the state of the science. Hydrogeology Journal, 10: 52-67.

Stanford, J.A., and A.R. Gaufin. 1974. Hyporheic Communities of Two Montana Rivers. Science, 185: 700-702.

Steelman, C.M., Kennedy, C.S., Capes, D.C., and B.L. Parker. 2017. Electrical resistivity dynamics beneath a fractured sedimentary bedrock riverbed in response to temperature and groundwater-surface water exchange. Hydrol. Earth Syst. Sci. doi:10.5194/hess-21-3105-2017.

Steelman, C.M., Kennedy, C.S., and B.L. Parker. 2015. Geophysical conceptualization of a fractured sedimentary bedrock riverbed using ground-penetrating radar and induced electrical conductivity. Journal of Hydrology, 521: 433-446.

Steelman, C.M., Parker, B.L., and C.S. Kennedy. 2015. Evaluating local-scale aisotropy and heterogeneity along a fractured sedimentary bedrock river using EM azimuthal resistivity and ground-penetrating radar. Journal of Applied Geophysics, 116: 156-166.

Stock, J., and D.R. Montgomery. 1999. Geologic constraints on bedrock river incision using the stream power law. Journal of Geophysical Research, 104: 4983-4993.

Storey, R.G., Howard, K.W.F., and D.D. Williams. 2003. Factors controlling riffle-scale hyporheic exchange flows and their seasonal changes in a gaining stream: A three-dimensional groundwater flow model. Water Resources Research, 39(2): doi:10..1029/2002WR001367.

Stronmer, J.L., and L.A. Smock. 1989. Vertical distribution and abundance of invertebrates within the sandy substrate of a low-gradient headwater stream. Freshwater Biology, 22: 263-274.

Sudicky, E.A., McLaren, R.G., 1992. The Laplace transform Galerkin technique for large-scale simulation of mass transport in discretely fractured porous formations. Water Resources Research, 28 (2), 499-514.

Taniguchi, M., and Y. Fukuo. 1993. Continuous Measurements of Ground-Water Seepage Using an Automatic Seepage Meter. Ground Water, 31(4): 675-679.

Taylor, R.G., Cronin, A.A., Trowsdale, S.A., Baines, O.P., Barrett, M.H., and D.N. Lerner. 2003. Vertical Groundwater flow in Permo-Triassic sediments underlying two cities in the Trent River Basin (UK). Journal of Hydrology, 284: 92-113.

Taylor, J.R. 1997. An Introduction to Error Analysis – The Study of Uncertainties in Physical Measurements, 2nd ed., University Science Books, Sausalito, CA., p.21-35.

Taylor, R., Scanlon, B., Doll, P., Rodell, M., vanBeek, R., Wada, Y., Longuevergne, L., Leblanc, M., Famiglietti, J., Edmunds, M., Konikow, L., Green, T., Chen, J., Taniguchi, M., Bierkens, M., MacDonald, A., Fan, Y., Maxwell, R., Yechieli, Y., Gurdak, J., Allen, D., Shamsudduha, M., Hiscock, K., Yeh, P. Holman, I., and H. Treidel. 2012. Ground Water and Climate Change. Nature Climate Change, doi: 10.1038/nclimate1744(2012).

Thiem, G., 1906. Hydrologische Methoden. (Hydrologic Methods). Gibhardt, Leipzig, p.56.

Theis, C.V., Brown, R.H., and R.R. Meyer. 1963. Estimating the Transmissibility of Aquifers from the Specific Capacity of Wells. Methods of determining permeability, transmissivity, and drawdown: US Geological Survey Water Supply Paper. p.331-341.

Therrien, R., Sudicky, E.A., 1996. Three-dimensional analysis of variably-saturated flow and solute transport in discretely-fractured porous media. Journal of Contaminant Hydrology, 23 (1-2), 1-44.

Thomasson, H.J., Olmsted, F.H., and E.R. LeRoux. 1960. Geology, water resources, and usable ground water storage capacity of part of Solano County, Ca. US Geological Survey Water Supply Paper 1464.693 pp.

Tinkler, J., and E. Wohl. 1998. A Primer on Bedrock Channels and Field Studies in Bedrock Channels, in Rivers Over Rock: Fluvial Processes in Bedrock Channels. Geophys. Monogr. Ser., vol.107, AGU, Washington, D.C., DOI: 10.1029/GM107p0001. p.1-18.

Toran, L. Nyquist, J., Rosenberry, D., Gagliano, M., Mitchell, N., and J. Mikochik. 2015. Geophysical and Hydrologic Studies of Lake Seepage Variability. Groundwater, 53(6):841-850.

Toth, J. 1963. A theoretical analysis of groundwater flow in small drainage basins. J. Geophys. Res. 68: 4785-4812.

Toth, J. 1970. A conceptual model of the groundwater regime and the hydrogeologic environment. J. Hydrol. 10: 164-176.

Triska, F.J., Kennedy, V.C., Avanzino, R.J., Zellweger, G.W., and K.E. Bencala. 1989. Retention and Transport of Nutrients in a Third-Order Stream in Northwestern California: Hyporheic Processes. Ecology, 70(6): 1893-1905.

U.S. Geological Survey (USGS). 2002. Standards for the Analysis and Processing of Surface-Water Data and Information Using Electronic Methods, by V.B. Sauer. Water-Resources Investigations Report 01-4044.

U.S. Geological Survey (USGS). 1998. TWRI Book 9, ch.6.3: Specific Electrical Conductance (Apr.1998). Editors: D.B. Radtke, J.V. Davis & F.D. Wilde.

Vallett, H.M., Fisher, S.G., and E.H. Stanley. 1990. Physical and chemical characteristics of the hyporheic zone of a Sonoran Desert stream. J. N. Am. Benthol. Soc., 9(3): 201-215.

Vanek, V., and D.R. Lee. 1991. Mapping of submarine groundwater discharge areas – An example from Laholm Bay, South Sweden in Groundwater Flow to Lakes and coastal Waters – Methods and Some Ecological Consequences, pp.89-103, Dep. of Ecol., Lund Univ., Lund, Sweden, 1991.

Vannote, R.L., Minshall, G.W., Cummins, K.W., Sedell, J.R., & C.E. Cushing. 1980. The River Continuum Concept. Can. J. Fish. Aquat. Sci., 37: 130-137.

Vaux, W.G. 1968. Intragravel flow and interchange of water in a streambed. United States Fish and Wildlife Service Fishery Bulletin, 66(3): 479-489.

Ward, J.V. 1989. The four-dimensional nature of lotic ecosystems. J. N. Am. Benthol. Soc., 8(1): 2-8.

Whipple, K.X. 2004. Bedrock Rivers and the Geomorphology of Active Orogens. Annu. Rev. Earth Planet. Sci. 32: 151-85.

Winter, T.C., Harvey, J.W., Franke, O.L., & W.M. Alley. 1998. Ground Water and surface water: A Single Resource. USGS Circular 1139, Denver, Colorado.

Winter, T.C., LaBaugh, J.W., and D.O. Rosenberry. 1988. The design and use of a hydraulic potentiomanometer for direct measurement of differences in hydraulic head between groundwater and surface water. Limnol. Oceanogr., 33(5): 1209-1214.

Woessner, W.W. 2000. Stream and Fluvial Plain Ground Water Interactions: Rescaling Hydrogeologic Thought. Ground Water, 38(3): 423-429.

Woessner, W.W., 1998. Changing views of stream-groundwater interaction. Eds. J.Van Brahana, U.Eckstein, L.K.Ongley, R.Schneider and J.E.Moore. Proceedings of the Joint Meeting of the XXVIII

Woessner, W.W., and K.E. Sullivan. 1984. Results of Seepage Meter and Mini-Piezometer Study, Lake Mead, Nevada. Ground Water, 22(5): 561-568.\

Wohl, E.E., and D.M. Merritts. 2001. Bedrock channel morphology. Geological Society of America Bulletin, 113: 1205-1212.

Zhang, X. 2015. Conjunctive surface water and groundwater management under climate change. Frontiers in Environmental Science, doi: 10.3389/fenvs.2015.00059.

APPENDIX A: Supplemental Summary of Stream Surveys

A-1. Low-Altitude Infrared Temperature (IRT) Survey

The use of aerial IRT as a reconnaissance tool to detect groundwater discharge in rivers and lakes is common (Conant *et al.,* 2009; Portnoy *et al.,* 1998; Banks *et al.,* 1996). Since groundwater maintains a relatively constant temperature in the subsurface of about 10^{o}C in the Guelph Area (data not shown) and surface water reflects atmospheric temperature variability, an IRT survey conducted in the cold winter season immediately prior to the formation of surface ice on the channel is optimum for detecting heat as a natural tracer in locating groundwater discharge zones.

On January 6, 2012, more than 100 hot spots (i.e., temperature differentials) were identified along a 12-km reach of the Eramosa River using an IRT helicopter survey [Fig.A-3]. The survey was completed at dawn (i.e., between 7:30 – 9:30 am) in order to avoid the effects of radiant heat transfer to the river surface. In preparation for the IRT survey, surface waterS Mini-Divers™ (Schlumberger Water Services, Delft, The Netherlands) were installed along the channel during the summer of 2011 to monitor surface water temperatures and the services of Dr. Brewster Conant Jr., were contracted to collect infrared and video data (University of Waterloo, Waterloo, ON, Canada).

Temperature contrast images between groundwater and surface water, in the form of radiation in the infrared range of the electromagnetic spectrum (i.e., 7-14 μm), were captured using a FLIR ThermaCam P25 infrared camera (FLIR Systems Ltd., Burlington, ON, Canada) with a sensitivity of <0.1°C and an accuracy of ±2.0°C. Given the accuracies of the camera and of transducers (i.e., ±0.1°C), a discernible temperature differential of not less than 5.0°C between the river and the atmosphere was verified prior to arranging the helicopter flight. Since an IR camera measures radiation at the river stage surface and calculates temperature, calibration inputs of atmospheric temperature and an emissivity value for calm water (i.e., $\varepsilon = 0.96$) were used, assuming a constant surface water condition. A PV-GS500 video camera (Panasonic Canada Inc., Toronto, ON, Canada) was used to simultaneously capture video images of the river, synchronized with the IR image capture and downloaded to a laptop in real time using

Premiere Elements Software (Adobe Systems Incorporated, San Jose, CA, USA). Continuous geo-reference records of: (1) the position of the helicopter, collected with a Thales Navigation Mobile Mapper GPS (Thales Group, Toronto, ON, Canada), and (2) the distance from the helicopter to the shoreline, measured using a TruPulse Model 200 Range Finder (Laser Technology Inc., Centennial, CO, USA), was collected in order to map all images acquired in flight. Infrared images were matched to video stills for comparison, since it was not uncommon to observe hot spots where no visual indication of groundwater discharge was observed (Fig. A-1). An equal-interval colour-scale (i.e., weak to very strong) was assigned to the data and thermal signatures captured in 165 infrared images were categorized according to RGB pixel intensity using ImageJ image-processing software (National Institutes of Health, Bethesda, MA, USA) and ranked points according to IR colour scale (weak to very strong). Some locations exhibiting a thermal signature of $< 0^{o}C$ (i.e., frozen) were included on the basis of visual indicators of potential groundwater discharge observed, such as: a tributary, man-made culvert or orthogonal pattern indicating a seep. Limitations of this method include: (1) detection of conductive heat transfer from the streambed to the river surface is limited to shallow shoreline areas, since thermal signatures of warm dense groundwater discharging in the deeper part of a stream usually attenuate before reaching the surface or remain below less-dense colder waters; and (2) over-hanging shoreline vegetation can intercept the required line-of-sight necessary to collect images with the IR camera.

All sectors identified were not more than 20 minutes' drive from the University of Guelph and a title search of the landowners along the channel, completed in 2011, is summarized in Table A-1. The Indian Trail site (Fig. A-4) was easily accessible and exhibited a reach of > 500 m with a dolostone pavement riverbed. Across a short segment of the reach, the bedrock ends abruptly, leaving a deep pool (i.e., > 1.5 m deep). In summer, the rest of the reach is quite shallow, as reflected in the discharge rating curve. The IRT results indicate few strong thermal signatures, with long stretches of shoreline where no thermal signature could be identified, due to encroaching vegetation. Eden Mills site (Fig. A-5) exhibits karstic features and broken bedding along shorelines that would make streambed installations challenging. Turbidity in the surface water is high, which has a tendency to settle out fine sediments on

the channel bed with the potential to clog fractures. Accessibility has declined over the past three years, with the removal of the dam at the millpond, causing the shoreline path, previously used to transport field equipment, to become submersed in the channel, making accessibility difficult. County Road 29 (Fig. A-6) exhibits strong thermal signatures of groundwater discharge, > 500 m of dolostone pavement, easy accessibility from the road and the height of river stage is 0.4 – 1.0 m, making it a good option for a field research site.

Arkell Springs (Fig. A-7) manifests > 500 m of dolostone pavement and a longitudinally-stepped profile below the dam, with strong thermal signatures of groundwater discharge and evidence of seeps along the south shore. The reach is quite wide (i.e., > 30 m) and the height of river stage is 1.0 m. Since Grand River Conservation Authority owns the land on the north side of the channel, where a service road connects Watson Road to the dam, an access path could be developed from the access road to the bedrock reaches of the channel and landowner authorization to install floodplain wells is likely. Because this reach abuts City of Guelph lands containing numerous municipal wells, development of a field research site here would be limited to studies investigating responses to groundwater pumping, which could be very useful. Furthermore, the reach is directly downstream of the Eramosa River intake, used to pump water from the river to recharge the overburden aquifer on the south side of the channel, so field studies would also involve responses to surface water pumping.

Watson Road (Fig. A-8) hosts a reach of exposed flat bedrock > 700 m in length, running from just east of the Watson Road bridge to just west of the Cooks Mill Road bridge. The thermal signatures, mostly on the north side of the channel, are strong to moderate, height of river stage is < 1.0 m, and easy accessibility makes this reach a good option for a field research site. The Scout Camp study site (Fig. A-9), identified as sector 7 in the IRT survey, exhibits strong thermal signatures and creeks on both sides of the channel, along with two river beds and a sparsely-vegetated floodplain on the south side. Because it is a gated youth camp, a service road runs from Stone Road right to the river for easy access. Stone Road (Fig. A-10) exhibits a high percentage of rubble across the bed, making it challenging to instrument. While the IRT survey yielded numerous thermal signatures on both sides of the river, there are several

culverts and creeks running into the river in the vicinity of an abattoir owned by Cargill Holdings on the northeast side of the river. Title documents include a requirement to address land use and contaminant concerns. Victoria Road (Fig. A-11) exhibits bedrock reaches, however, the river is deep (i.e., > 1.0 m at low stage) as evidenced by the strongly-linear discharge rating curve, making accessibility challenging. The IRT survey yielded numerous strong-to-moderate thermal signatures, however, the ground survey revealed numerous culverts draining urban holding ponds into the river. Suspended sediment content is high, making delineation of fractures difficult.

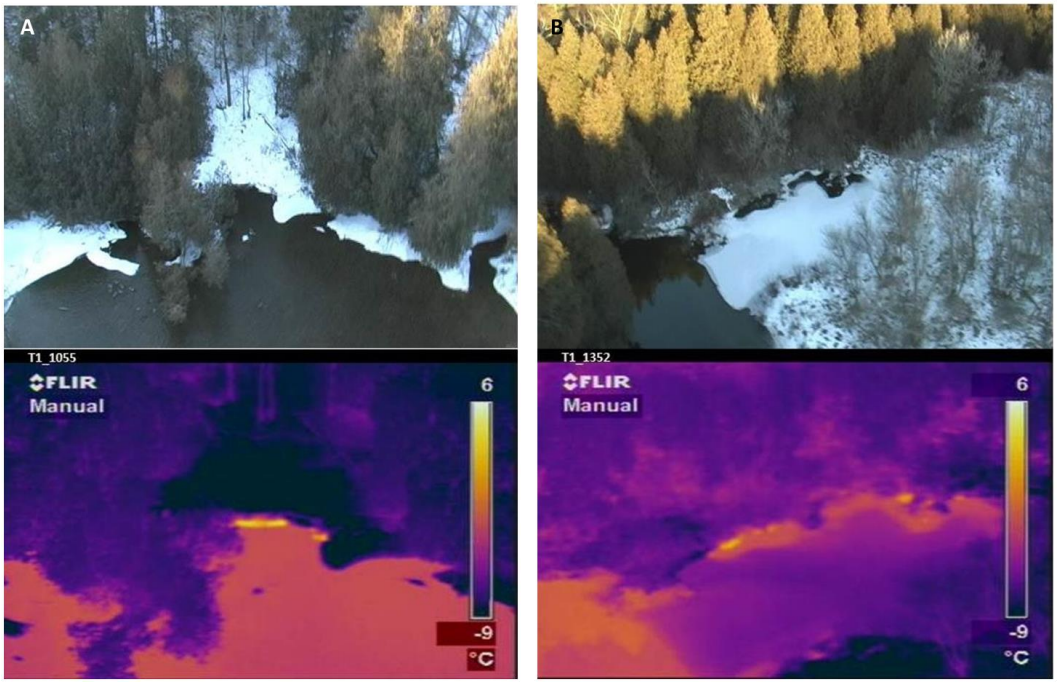

Fig. A-1. Examples of processed infrared and video images captured in IRT survey, evidencing that a thermal image may reveal a potential **(A)** shoreline seep, or **(B)** small tributary, while a visual image may not.

A-2. Bathymetric and Hydrometric Surveys

The same 12-km reach of the Eramosa River was surveyed by kayak from July 24 – August 17, 2012, with a dual objective. Attempts were made to ground-truth potential groundwater discharge zones identified by IRT survey using a drag probe instrumented with an SWS CTD Diver™ (Schlumberger Water Services, Delft, The Netherlands), constructed to detect temperature and electrical conductivity differentials at the streambed surface (Fig. A-2). Streambed surface transitions between bedrock and sediment-cover were also mapped, using photographs and bathymetric measurements of potential study sites, exhibiting intact dolostone pavement. Heat-flow theory is the basis for using temperature as a natural groundwater tracer (Constantz 2008; Anderson 2005). Since surface water in the channel water tends to reflect atmospheric temperature variability and groundwater in the Guelph Region is generally 10^{o}C (data not shown), detecting cooler temperature differences along the channel in summer is an indicator of groundwater discharge. The use of electrical conductivity (EC) as a natural tracer to detect

and map groundwater discharge in a range of alluvial environments is well documented (Cey *et al.*, 1998; Harvey *et al.*, 1997; Lee *et al.*, 1993; Vanek and Lee 1991; Lee 1985). Steelman *et al.*, (2016) used the inverse of EC (i.e., electrical resistivity) to detect groundwater flow in at the study site along the Eramosa River. EC is a function of the type and concentration of dissolved ionic species present in the water sampled (Hayashi 2004; Freeze and Cherry 1979). Since it is temperature-dependent [i.e., 2% increase in EC per 1^{o}C increase in temperature (Hem 1985)], the transducer was programmed collect specific, or temperature-compensated, EC in microsiemens per centimetre at 24^{o}C (USGS 1998).

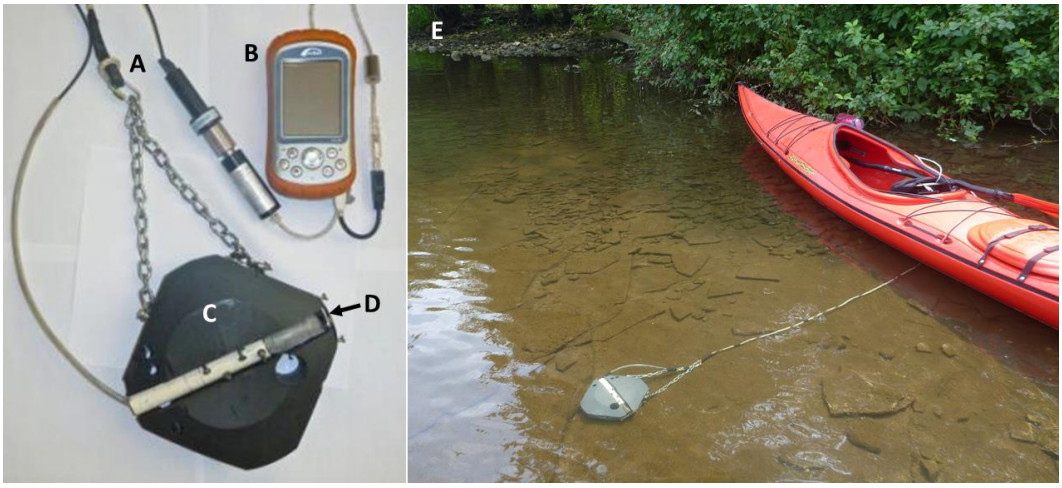

Fig. A-2. Drag probe configuration, consisting of: **(A)** Transducer – PC cable attached to length of chain for on-site real-time data display during drag; **(B)** Archer Field PC (Juniper Systems, Logan, UT, USA); **(C)** Solid pvc protective housing weighted to keep transducer close to streambed; **(D)** CTD transducer wrapped in nylon mesh to prevent sediment accumulation on sensor; and **(E)** application of tool in the field.

The 12-km segment of river was divided into 8 sectors approximately 1.5 km in length and conveniently identified by municipal roads or landmarks: (1) Indian Trail, (2) Eden Mills, (3) County Road 29, (4) Arkell Springs, (5) Watson Road, (6) Scout Camp, (7) Stone Road, (8) Victoria Road (Fig. A-3). Each sector exhibited intact bedrock along its bed, varying degrees of encroaching shoreline vegetation, various levels of accessibility and sediment cover (Fig. A-3). Results for each sector (Fig. A-4 – A-11) consist of: (a) a map of the river segment indicating the strength and location of thermal

signatures observed, along with details of any visual indicators of groundwater discharge; (b) a photograph; (c) plots summarizing bathymetric and hydrometric survey results.

Drag probe results (i.e., temperature and EC) were somewhat inconclusive for several reasons. Findings were that in a shallow bedrock channel, temperature differentials were too subtle to detect and the time required to reach equilibrium (i.e., pausing at each location to allow the probe to stabilize before collecting the measurement) was impractical for a project of this magnitude. Verification of temperature differentials was possible only at a few groundwater seeps at the Scout Camp and Arkell Springs locations. Two unavoidable challenges also biased the EC data collected. The measurement mechanism of a CTD transducer relies on the unimpeded flow of water across the electrode plate within its housing while suspended in a vertical orientation. With its horizontal, protective design, the drag probe impeded water flow and, therefore, affected the sensitivity of the transducer. Furthermore, the time required to reach was equilibrium, again, impractical for this project.

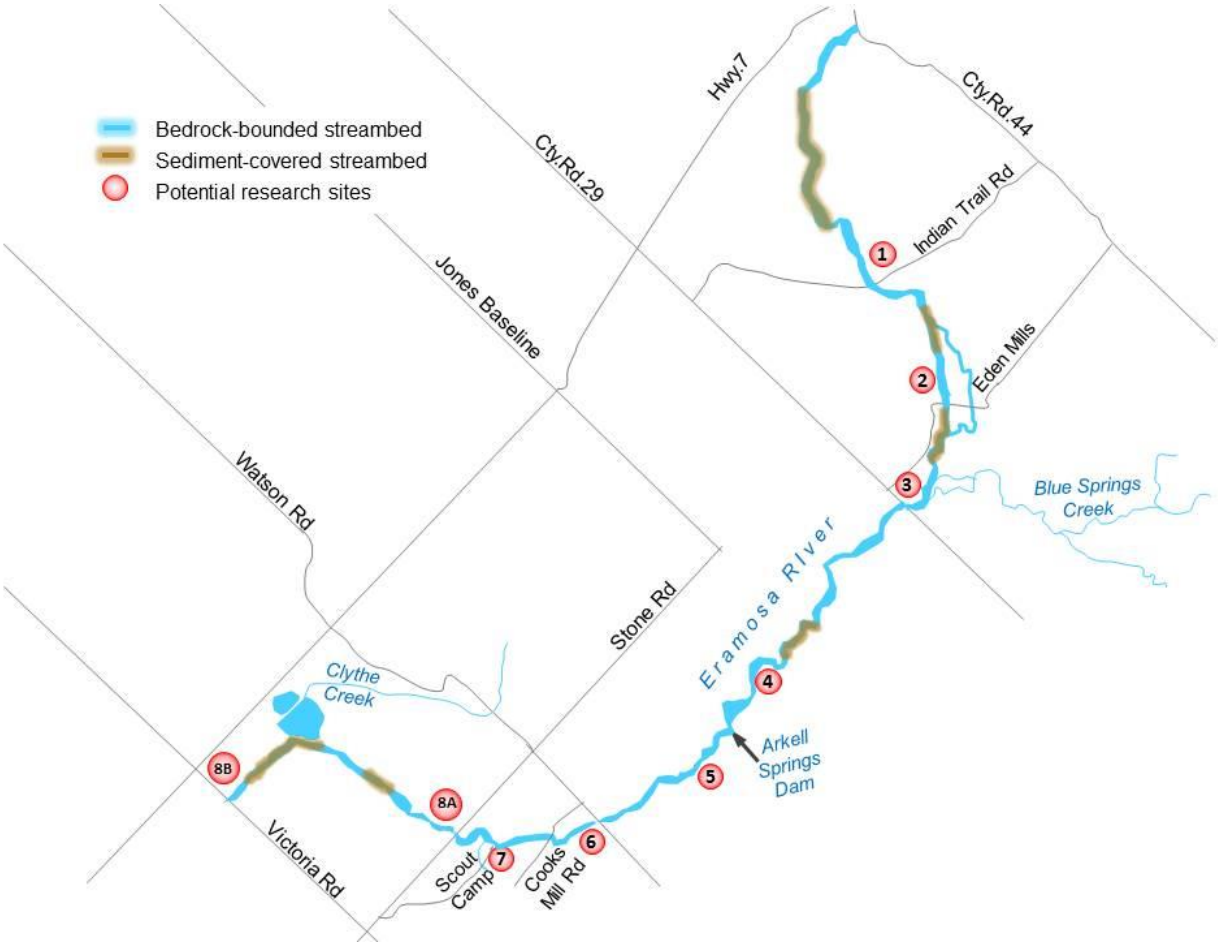

Fig. A-3. Results of 12-km ground survey of streambed conditions, completed in July – August, 2012. Possible research sites were delimited by extent of exposed bedrock and accessibility.

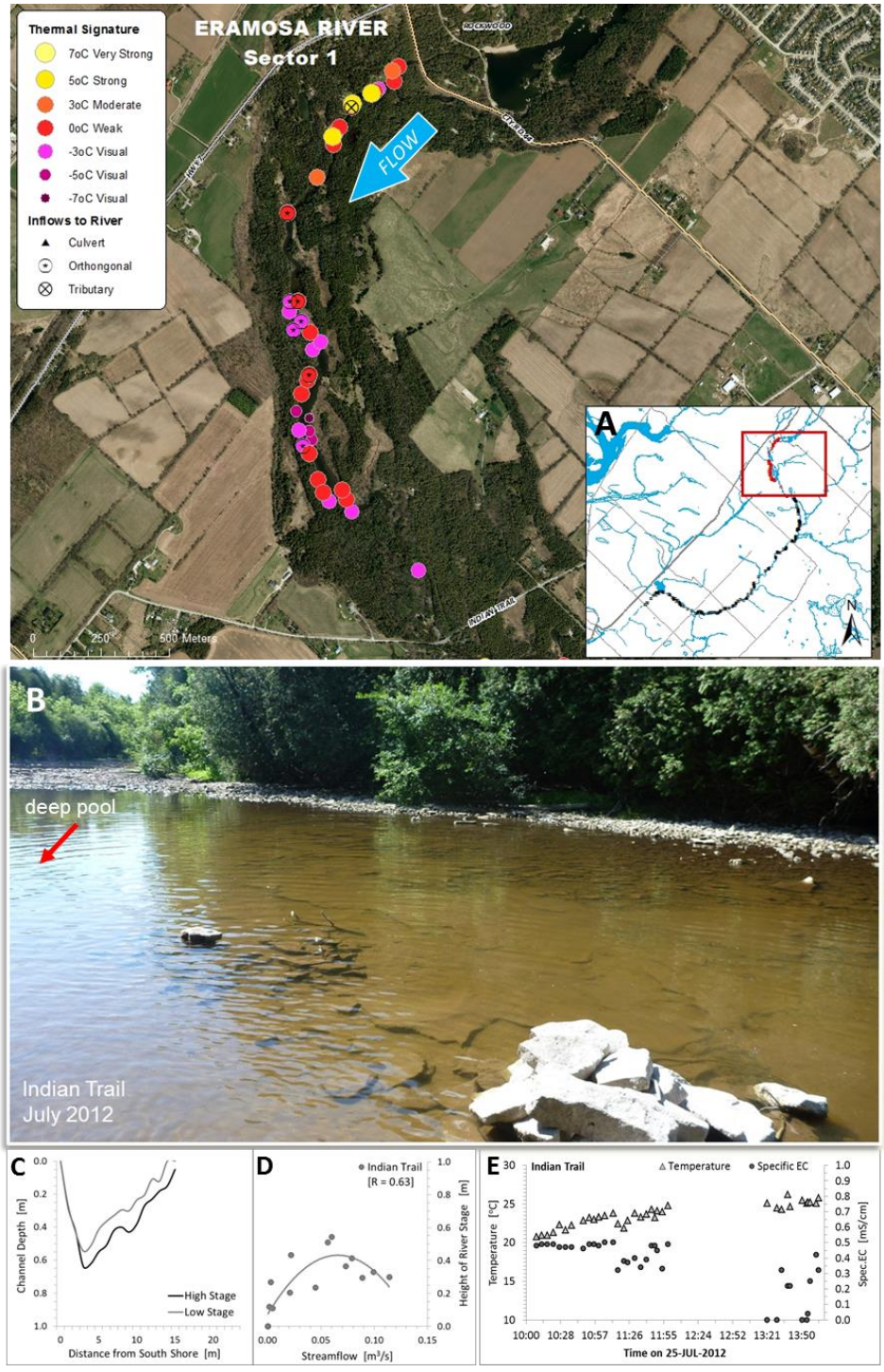

Fig. A-4. Indian Trail **(A)** Spatial distribution of hot spots, detected with IRT survey in January 2012, along the north part of the sector, where steep topography inhibits accessibility. Surface water flow is in a southwesterly direction, as indicated. Inset shows 12-km reach of the Eramosa River surveyed, while red box represents the extent of the air photo along the channel. **(B)** Photo of the south part of segment, where shallow bedding drops off at shelf. **(C)** Bathymetric profile. **(D)** Depth-discharge plot indicating a non-linear relationship (R = 0.63); and **(E)** Drag probe plot, indicating warm surface water temperatures and EC scatter. [MNR SWOOP 2010]

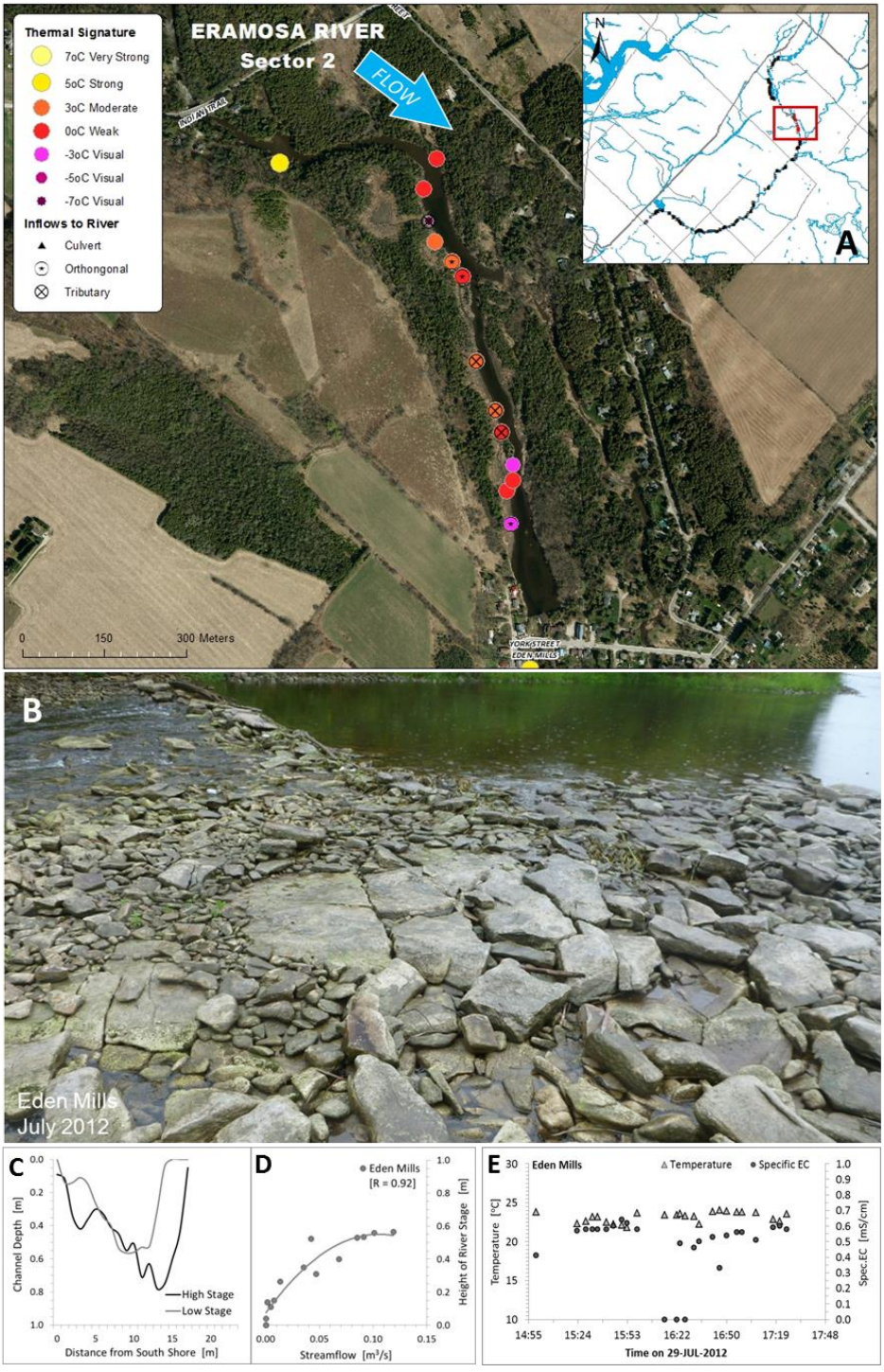

Fig. A-5. Eden Mills **(A)** Spatial distribution of hot spots, detected with IRT survey in January 2012, on the northwest side of the segment, where the fluvial plain rises 15 – 20 m above the channel and reaches are dominated by sediment. Surface water flow is in a southerly direction, as indicated. Inset shows 12-km reach of the Eramosa River surveyed, while red box represents the extent of the air photo along the channel. **(B)** Photo shows broken rock alone shorelines. **(C)** Bathymetric profile. **(D)** Depth-discharge plot indicating a linear relationship (R = 0.92); and **(E)** Drag probe plot, indicating warm surface water temperatures and EC scatter. [MNR SWOOP 2010]

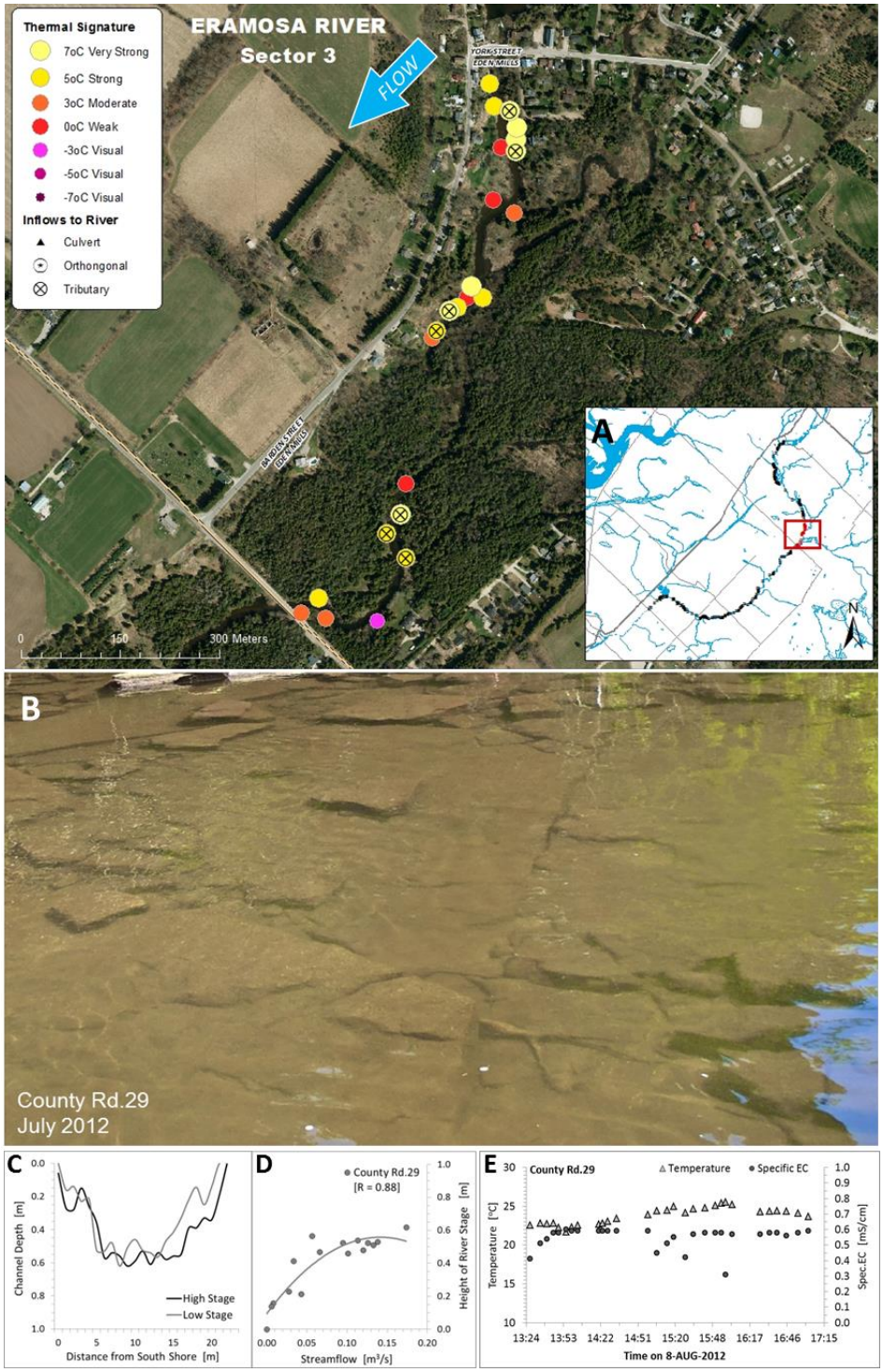

Fig. A-6. County Road 29 **(A)** Spatial distribution of numerous hot spots and creeks, detected with IRT survey in January 2012, on the west side of the channel. Surface water flow is in a southwesterly direction, as indicated. Inset shows 12-km reach of the Eramosa River surveyed, while red box represents the extent of the air photo along the channel. **(B)** Photo shows orthogonal fractures on a thick bedding plane at surface. **(C)** Bathymetric profile. **(D)** Depth-discharge plot indicating a linear relationship (R = 0.88); and **(E)** Drag probe plot, indicating warm surface water temperatures and EC scatter. [MNR SWOOP 2010]

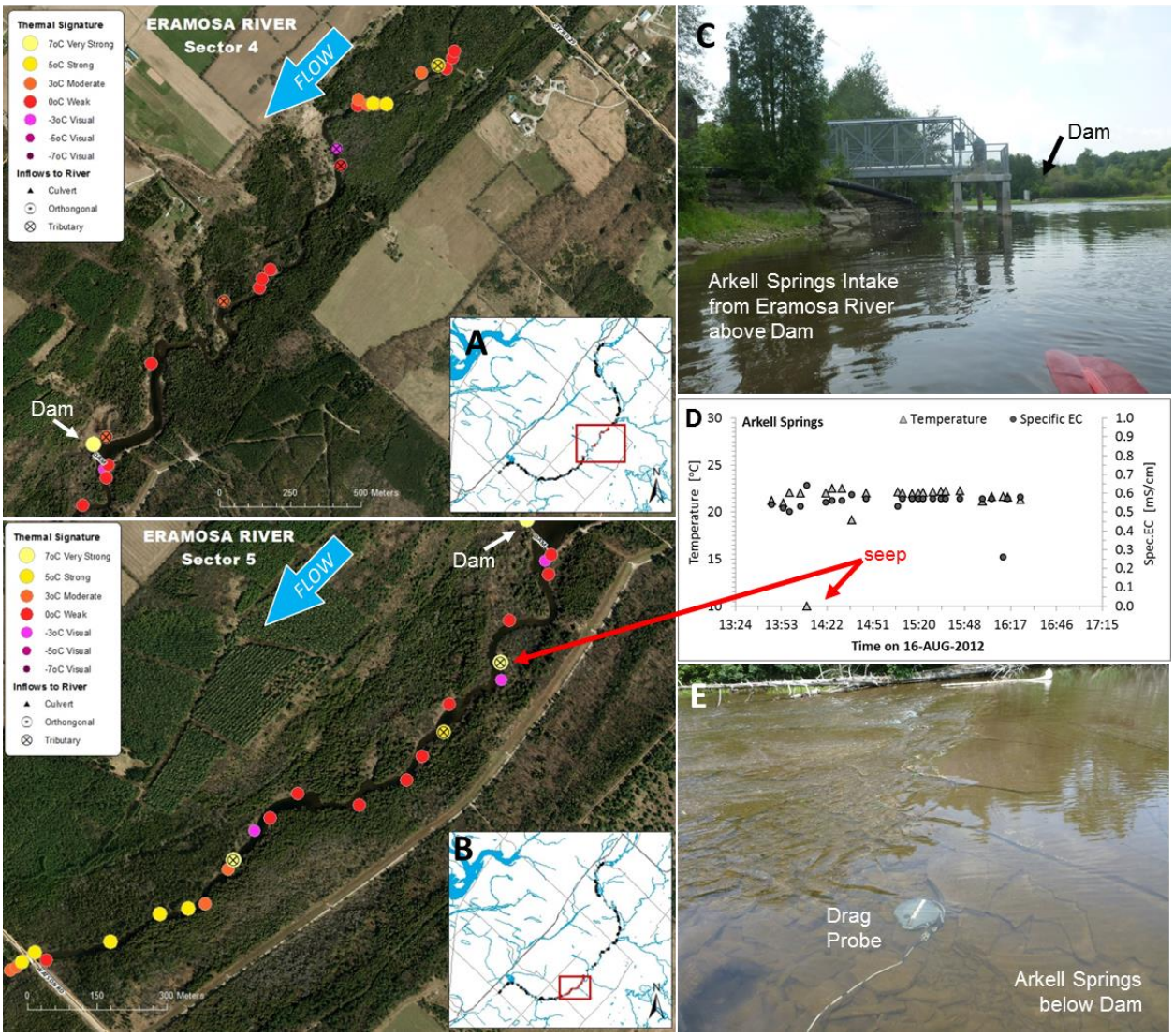

Fig. A-7. Arkell Springs. Spatial distribution of hot spots detected with IRT survey in January 2012, **(A)** above the dam, and **(B)** below the dam, where the majority of hot spots are on the east side of the channel are associated with inflows from Arkell Spring . Surface water flow is in a southwesterly direction, as indicated. Inset shows 12-km reach of the Eramosa River surveyed, while red box represents the extent of the air photo along the channel. **(C)** Photo shows the groundwater recharge intake station above the dam, where pools are deep and sediment cover is high. **(D)** Drag probe plot, where cold thermal signature of a strong seep was detected in an otherwise warm channel, and EC was consistent. **(E)** Photo of bedrock reach below dam, where several seeps were noted at riffle zones. Accessibility to bedrock reaches was only possible by boat. [MNR SWOOP 2010]

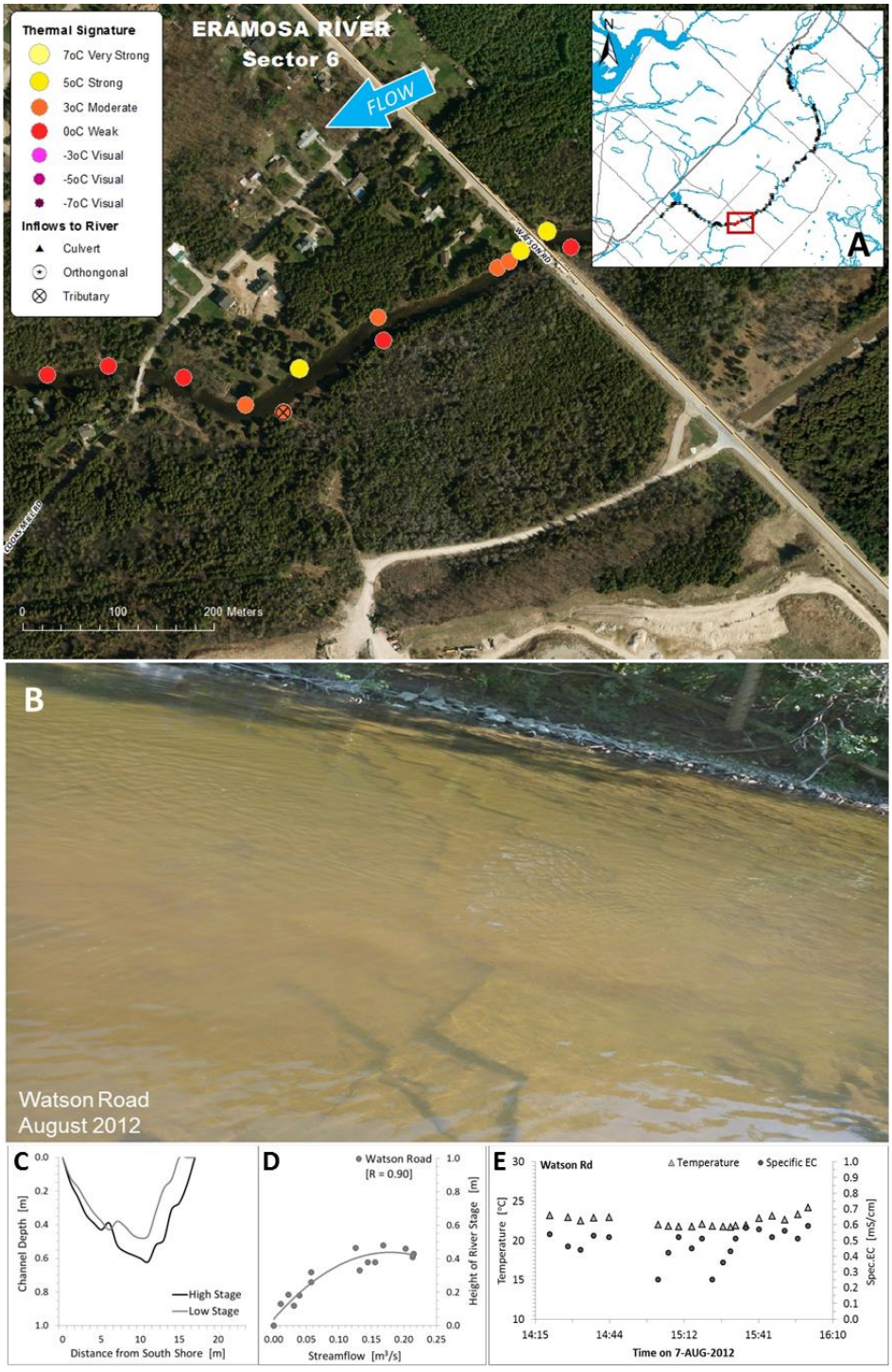

Fig. A-8. Watson Road, 900 m upstream of Scout Camp. **(A)** Spatial distribution of hot spots detected with IRT survey in January 2012, spots mainly along north shoreline. Surface water flow is in a southwesterly direction, as indicated. Inset shows 12-km reach of the Eramosa River surveyed, while red box represents the extent of the air photo along the channel. **(B)** Photo shows shore-to-shore thinly-bedded intact dolostone steps. **(C)** Bathymetric profile. **(D)** Depth-discharge plot indicating a linear relationship (R = 0.90); and **(E)** Drag probe plot, indicating warm surface water temperatures and EC scatter. [MNR SWOOP 2010]

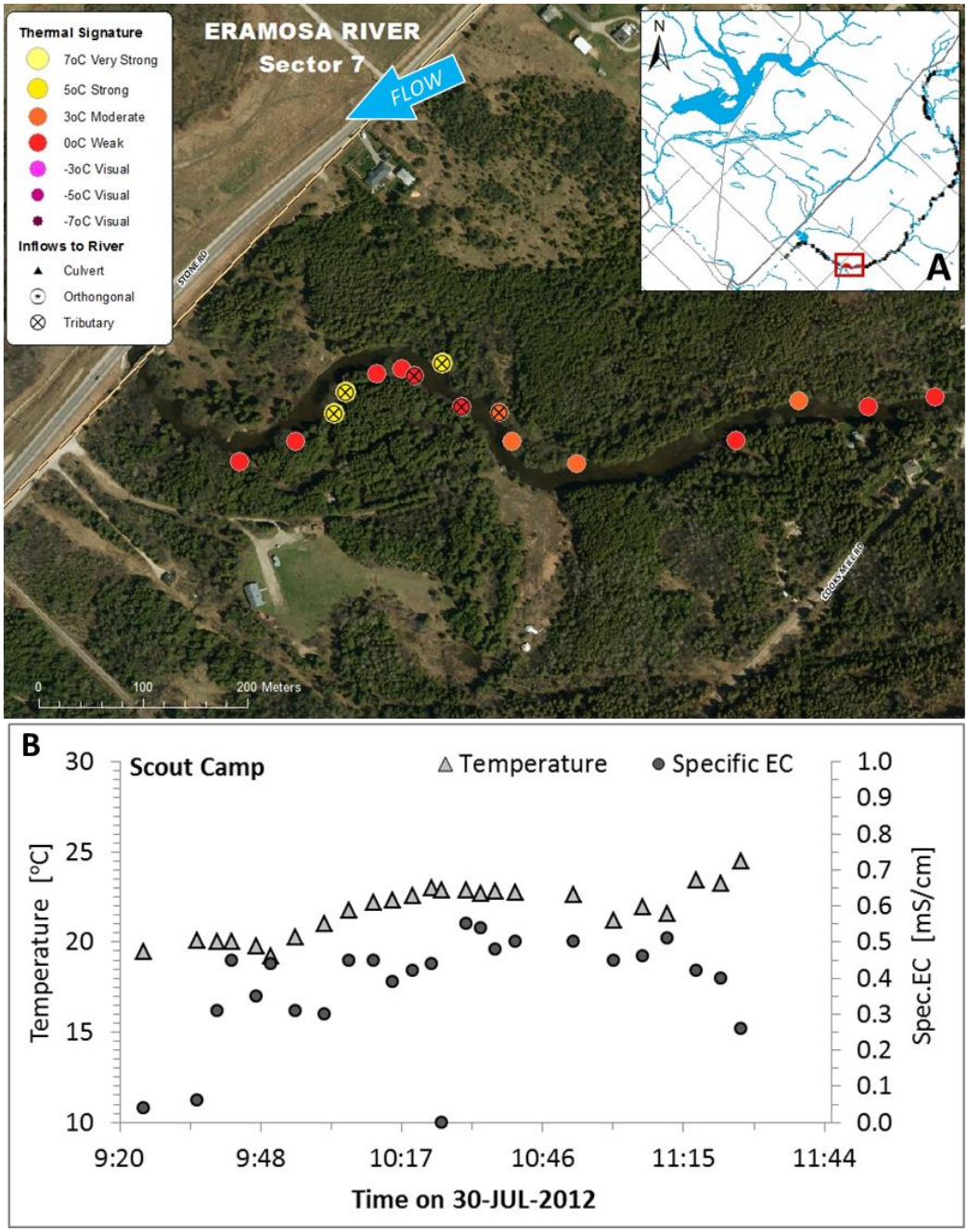

Fig. A-9. Scout Camp. **(A)** Spatial distribution of pre-meander hot spots along the north shore, followed by post-meander hot spots and seeps along the south shore, detected with IRT survey in January 2012, and indicating groundwater discharge on both sides of the channel. Surface water flow is in a southwesterly direction, as indicated. Inset shows 12-km reach of the Eramosa River surveyed, while red box represents the extent of the air photo along the channel. **(B)** Drag probe plot, indicating warm surface water temperatures and EC scatter. [MNR SWOOP 2010]

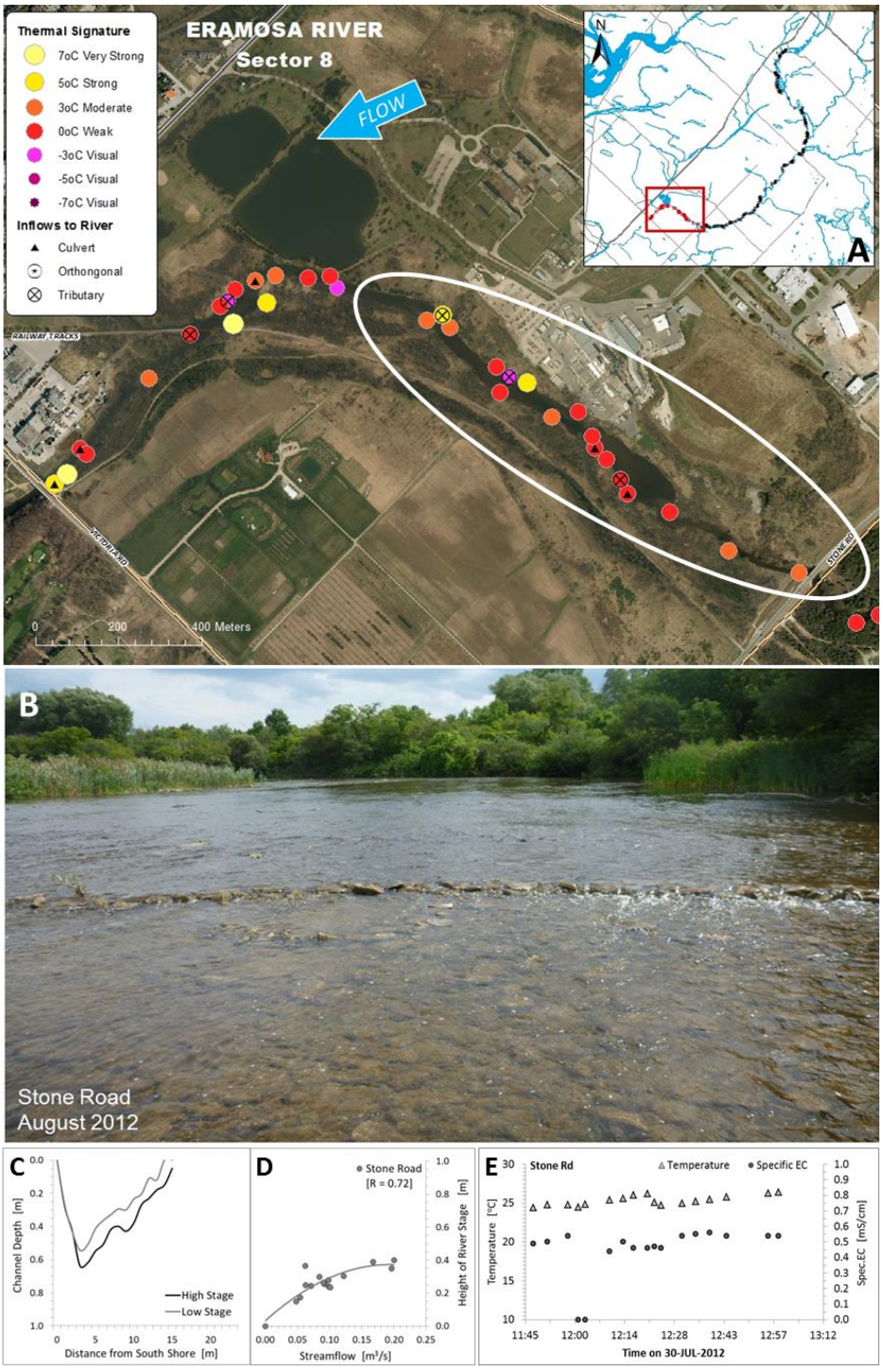

Fig. A-10. Stone Road. **(A)** Spatial distribution of hot spots detected with IRT survey in January 2012, showing weak thermal signatures and urban stormwater management inflows, where the fluvial plain rises 5-10 m along the north shore. Surface water flow is in a southwesterly direction, as indicated. Inset shows 12-km reach of the Eramosa River surveyed, while red box represents the extent of the air photo along the channel. **(B)** Photo shows shore-to-shore rubble-covered riffles near Stone Road, circled in aerial photo. **(C)** Depth-discharge plot indicating a linear relationship (R = 0.72); and **(E)** Drag probe plot, indicating warm surface water temperatures and EC scatter. [MNR SWOOP 2010]

Fig. A-11. Victoria Road. **(A)** Spatial distribution of hot spots detected with IRT survey in January 2012, spots that are likely influenced by storm water management ponds and urban inflows. Surface water flow is in a southwesterly direction, as indicated. Inset shows 12-km reach of the Eramosa River surveyed, while red box represents the extent of the air photo along the channel. **(B)** Photo shows generally deep profile and sediment-covered shorelines, circled in aerial photo. **(C)** Depth-discharge plot indicating a strongly-linear relationship (R = 0.97); and **(E)** Drag probe plot, indicating warm surface water temperatures and EC scatter. Streambed contact with probe was challenging due to debris in channel. [MNR SWOOP 2010]

Table A-1. Title search summary of lands along the Eramosa River within the 12-km segment of interest. Title abstracts held by the Halton Land Titles Office were not pulled. Survey plans and title abstracts are filed with the G360 Institute for Groundwater Research at the University of Guelph.

Reference Point	Block Plan	PIN	Owner	Deed	Address for Service
Cty.Rd.44		0272			
	71-183	0095	CLARKE, Kathryn Marie	WC332959	8128 Indian Trail
		0109	RONAN INVESTMENTS INC.	RO817646	#500 - 25 Imperial Street
		0139	(from Oelbaum Estate)	RO817647	Toronto, ON M5P 1B9
Indian Trail	71-183	0103	WORD AND WORLD ERAMOSA CENTRE OF REFLECTION AND RESPONSE	ROS588343 61R-10588	RR.5, Rockwood, ON N0B 2K0
		0104	PANGBORN, Ward Curry LAWRENCE, John & Jennet	ROS518161	48 Simcoe Blvd., Simcoe, ON N3Y 3L9, *but may now reside in Eden Mills*
		0102	BECKSTEAD, Tamara Sue Ola HOLMAN, Donald Paul	WC65342	8179 Indian Trail Eden Mills, ON
		0245	ZAWADZKI, Leszek HENDRY, Linda Gail	RO765083	8181 Indian Trail, RR.5 Rockwood, ON
		0553	COUSINS, Charles Robert Laurence COUSINS, Susan Georgina	RO734421 61R-10588	* Indian Trail Rockwood, ON N0B 2K0
		0261	RIEMER, Joan	WC352759	156 Barden Street Eden Mills, ON
		0106	ALDRICH, Robert William ALDRICH, Judith Anne	ROS548134	96 Ash Street Eden Mills, ON N0B 1P0
Eden Mills	71-183	0544			
		0171	SIMON, Charles & Anna		
Cty.Rd.29 = Tshp.Rd.1	71-182	0114			*Need to look behind PIN*
		0152	BARDEN, James Edward BARDEN, Etta BARDEN, Evelyn Kathleen	MS49018 MS51245 61R-2063	61R-2063 (1979) and 61R-10232 (2006) *Several Estate transfers - check w/Richard* *Lay re current owners*
		0112	HASTINGS, Darren SCHLETZ, Helmut	RO818794	1) 530 Governors Rd., Guelph N1K 1E3 2) 4899 Wellington Rd.29, RR.5, Guelph N1H 6J5
		0163	LUCS, Arthur Vilnis LUCS, Sandra Lilija	LT075231	44 Edgewood Dr., Eden Mills N0B 1P0
		0093	GARCIA, Jose & Maria BASABE, Louis	WC31166	4891 Wellington Rd.29, Guelph
	71-188		*Halton Registry Office No.20 @ Milton for 2 small reaches of Eramosa River shoreline*		
Arkell Springs Watson Rd = Cty.Rd.41	71-184	0010	Grand River Conservation Authority	MS111471 (1971)	Pt.Lots 1, 2, 3, Con.10, Puslinch
		0022	CITY OF GUELPH	IS7894 (1909) IS7906 (1909) IS7941 (1909) IS8872 (1915) MS26828 (1962) MS29436 (1963) MS76689 (1968)	Pt.Lots 3, 4, 5, 6, Con.10, Pt.Lots 3, 4, 5, 6, Con.11, Puslinch Tshp.
Watson Rd Cooks Mill Rd Stone Rd	71-185	0113	McKENZIE BROS. (Guelph) Limited *Sand & Gravel*	ROS233545	69 Hearn Ave., Guelph 519-822-5741 *Land: 661 Watson @Stone*
		0181	OOSTERVELD, Rance OOSTERVELD, Shirley Margaret	ROS526189 61R-3458	6 Cabot Cres., Guelph N1G 3E4 *Land: RR.2, Guelph, ON N1H 6H8*
		0200	BILTMORE HOMES LTD.	WC350072 61R-9472 (Pt.2)	160 Southgate Dr., Guelph N1G 4P5
		0201	KRITZ, James David	WC171461 61R-9472 (Pt.1)	88 Cooks Mill Rd., RR.2, Guelph N1H 6H8
		0018	DROLC, John & Helen	MS115824	745 Stone Rd.E., Guelph N1L 1B8
		0017	MURDOCH, Robert William *(Trust)* *Sketch @ road allowance between Guelph and Puslinch Tshp.*	ROS608650	17 Fernbank Place, Guelph N1H 6J3
		0016	SCOUTS CANADA *Charles Wesley Barber Camp Grounds* *"...should lands be no longer used by Boy Scouts for >1yr, reconvey lands back to Grantor"*	RO684990 (1992)	Scouts Canada Head Ofc (613-224-5131) 1345 Baseline Rd., Ottawa, ON K2C 0A7 *Ronald Sansom (Local Lawyer on land transfer)* *285 Woolwich St., Guelph N1H 3V8*
Stone Rd Victoria Rd = Cty.Rd.38	71-236	0103	CITY OF GUELPH from CROWN w/easement	61R-9688 *checked Plan*	along and under bridge up to RR tracks
		0108			
		0116	CITY OF GUELPH from MNR	WC162123	easement over river 61R-9849
		0093	CARGILL CANADA HOLDINGS (2005-7) LIMITED *from BETTER BEEF LIMITED and Dev.Agmt w/CITY OF GUELPH*	ROS619560, WC112369, WC170417	300- 240 Graham Ave., Winnipeg, MB R3C 0J7
		0096	CROWN Lands	BS6216, BS6224, BS6264	w/ easements to City of Guelph, Bell Canada, Better Beef
		0104	CROWN Lands *w/easements to City of Guelph and Hydro*	BS6220, BS6245	
		0125	AGRICULTURAL RESEARCH INSTITUTE OF ONTARIO *from CROWN*	WC166384	2nd Flr- 1 Stone Rd.W., Guelph N1G 4Y2 OMAFRA: 519-826-4199

APPENDIX B: Supplemental Strategy for Drilling Along Rivers

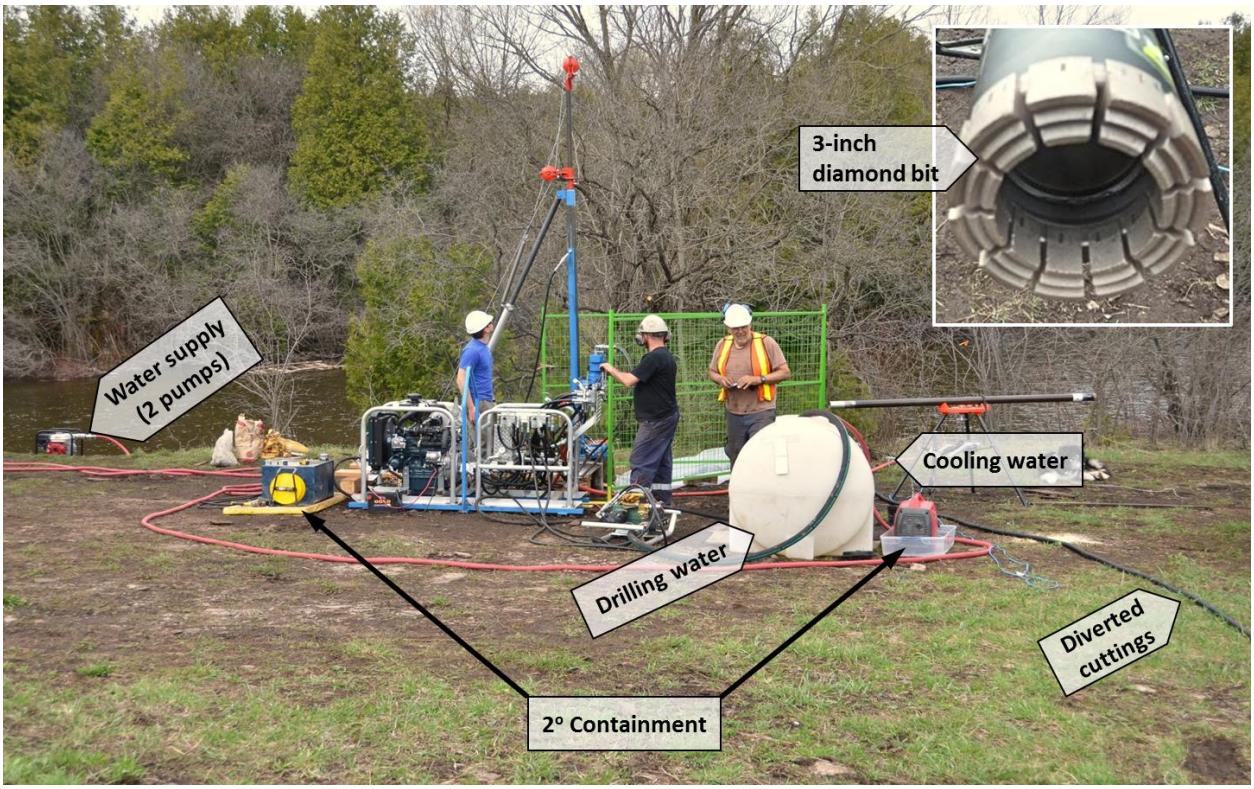

Fig. B-1. Drilling method developed at the Scout Camp for working on a fractured rock floodplain next to a river. The Prospector (Hydracore Drills, Delta, BC, Canada) used for installing floodplain wells, used only river water as drilling fluid, with a double-pump system to cool the water before returning it to the river. Cuttings were captured during drilling and diverted to a natural depression away from the channel using a sump pump, so as not to disrupt fish habitats. Secondary containment was used with all fuel tanks.

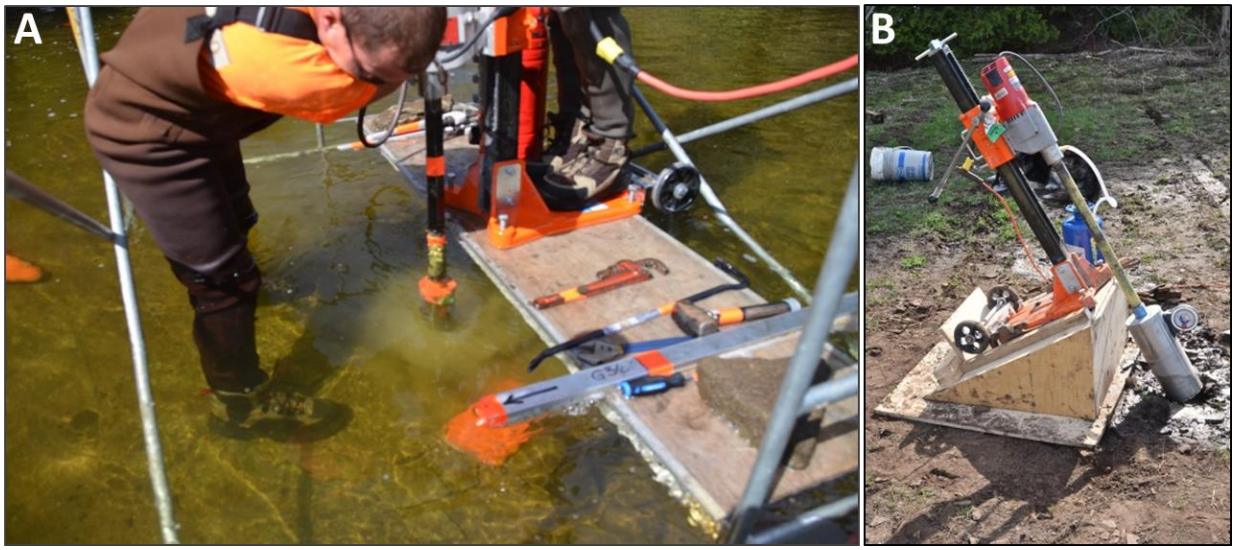

Fig. B-2. The DR520 Concrete Drill (Norton Construction Products, Stephenville, TX, USA) was used **(A)** supported by scaffolding to drill 30-cm seepage cavities in the bedrock streambed, and **(B)** supported by a platform constructed at a 30^{o} angle to set the casings for the floodplain wells plunging beneath the streambed.

Fig. B-3. The Shaw Backpack Drill (Shaw Tool Ltd., Yamhill, OR, USA) was used to install riverbed piezometers. Scaffolding was used to support the water pump and battery used to cool the diamond bit during drilling.

APPENDIX C: Supplemental Fracture Logs from Core and Geophysics (Downhole)

A series of three floodplain well pairs were drilled to a depth of ~30 m along the South side of the channel between April 30 - May 22, 2013. Each pair consists of an inclined well plunging at 60° to maximize the number of vertical fractures intercepted (Munn 2012), and a nearby vertical well, ~3 m away, for comparative analysis of hydrogeologic findings. Based on a geophysical reconnaissance survey, using ground penetrating radar (GPR) to verify the dominant fracture orientations, azimuths of 340° and 50° were selected for angled holes SCA1 and SCA2 plunging beneath the streambed. Since floodplain access to the North side of the channel could not be secured, evaluation of the site geometry using a stereonet revealed a *blind spot* in the southwest quadrant. SCA3 was, therefore, drilled at an azimuth of 195° *away* from the channel to inform the 3-D fracture network geometry (Fig. C-1). Wells were installed with a small-diameter portable Prospector Drill (Hydracore Drills, Delta, BC, Canada) and a 75-mm or NQ diamond coring bit. Steel casings were set 0.60 mbgs with a portable DR520 Concrete Drill (Norton Construction Products, Stephenville, TX, USA) and a 122-mm or PQ diamond coring bit. Core logs were collected on-site on a run-by-run basis during drilling while core was still wet to: (1) minimize the inclusion of mechanically-induced fractures due to handling, transportation or expansion, and (2) observe staining due to oxidation that occurred prior to core extraction (as opposed to being confused with post-extraction oxidation). Logging methods for recording features and lithology used the site-specific, quantifiable DFN-style developed by the G360 Institute for Groundwater Research at the University of Guelph (Meyer 2013; Munn s 2012).

Geophysical logs collected in each well were used in conjunction with core logs to construct fracture logs in 3-D geometry beneath and adjacent to the channel. OTV logs were collected with a QL40OBI optical televiewer [Advanced Logic Technologies (ALT), Redange, Luxembourg, and Mount Sopris Instruments, Denver, CO, USA], which is a camera that captures a forward fish eye view of the corehole wall and digitally converts it to a side view image in true colour. ATV logs were collected with a

QL40ABI acoustic televiewer (also from ALT and Mount Sopris Instruments). These tools use gyros, inclinometers and magnetometers to remain oriented relative to magnetic north during data collection, producing images oriented to north. This allows measurements of fracture strike and dip to be deduced, which is particularly helpful when working in angled holes. Gamma logs were also collected to assess the amount of clay mineral in the formation using a QL40-GR probe (also from ALT and Mount Sopris Instruments). WellCAD Software (v.5.0, ALT – Luxemborg) was used to process, edit and display field data collected in core, ATV and OTV logs in a cross-sectional view. The resultant fracture log was then input into FracMan (v.7.5, Golder Associates Inc. – FracMan Technology Group, Redmond, WA, USA) to generate a 3-D conceptual model of the fracture network beneath the streambed. For this study, results reported are limited to the upper 3 m, to coincide with streambed installations.

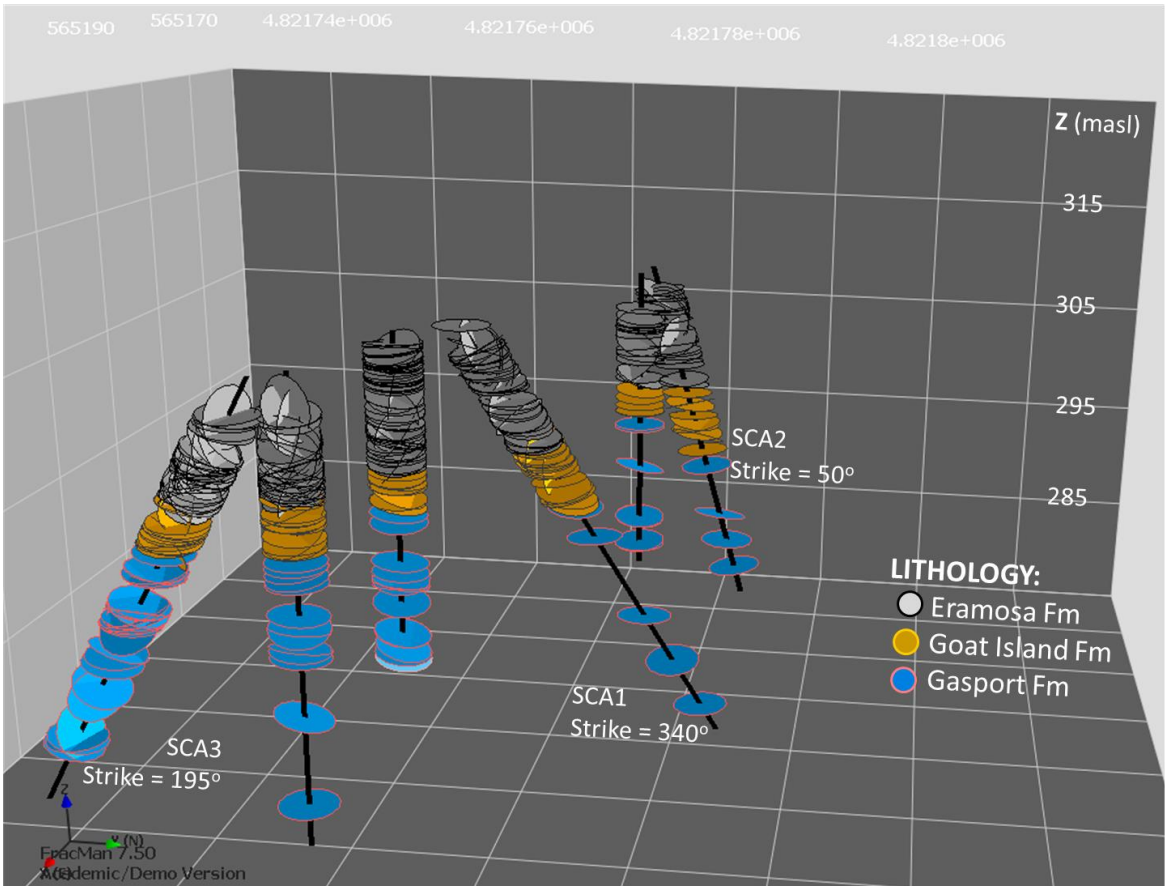

Fig. C-1. Post-drilling conceptual model of corehole pairs installed to inform the 3-D static fracture model, constructed with FracMan (v.7.5, Golder Associates Inc. – FracMan Technology Group, Redmond, WA, USA).

APPENDIX D: Supplemental Fracture-Mapping Method (Surface)

The study reach was divided into 10 transects orthogonal to flow, at 10-m intervals, identified by 0.10-m galvanized carriage bolts drilled into the streambed along the channel centre and both shorelines. All markers were surveyed by Van Harten Surveying Inc., (Guelph, ON, Canada), using a Leica Diva GPS, where 15 readings per measurement were taken and averaged to produce 1-cm accuracy, using permanent reference stations corrected to orthometric elevations with Geoid Model HTv2.0 supplied by Natural Resources Canada. The highest concentration of dolostone pavement, stripped of any large sediments in the form of sharp angular bedrock fragments, was observed in the centre of the pool, where Transects 2½ and 3½ were installed at 5-m intervals. Ropes, marked at 1-m intervals, were installed across the river at each transect and along the centre line during data-collection events. Transects 0-3½ were extended 24 m up on to the floodplain on the South side of the channel. Fracture mapping of the streambed and floodplain outcrops was completed in low river stage conditions from August 7-11, 2014, using linear and window methods, geo-referenced to transects, for objective sampling with reduced bias (Doe 2014; Elmo 2014; Mathis 2014). Additional scanlines were set relative to the transects. Measurements were truncated at 0.1 m and results were constrained by what is visible (i.e., rubble zones were deemed unmappable). A tape measure screwed to 6-ft length of steel rectangular tubing was used to measure streambed fractures under water. Field data containing fracture strike, length and position along a given transect or scanline were input into FracMan (v.7.5, Golder Associates Inc. – FracMan Technology Group, Redmond, WA, USA) to generate a 2-D conceptual model of the fracture network that was merged with a base map of the study site constructed in ArcMAP (v.10.2.1, ArcMAP by ESRI Canada, Edmonton, AB) using data obtained from the Ministry of Natural Resources Southwestern Ontario Orthoimagery Project (surface waterOOP) 2010 (Fig. D-1). Point measurements along transects were collected to map rubble zones in the same fashion and converted to polygons in ArcMAP. Statistical analysis of fracture length, frequency and orientation were completed in FracMan.

Total observed vertical fractures on the streambed was 197, located in the rubble-free zone between transects 1 and 4. Dominant fracture orientations were NNE – Ssurface water and ESE – WNW (Fig. E-1). Trace length statistics, by degree censoring, revealed the dominant trace length to be 2-3 m, with most fractures extending at one end, often under the bedding of an upstream or shoreline step. (Rouleau and Gale 1985) (Fig. D-2A). Fracture density at the riffle-pool transition at transect 2, where P_{20} = 1.09, was almost twice that of the downstream pool (i.e., transect 3), where P_{20} = 0.66. Total fracture length was 20% higher at transect 2, where P_{21} = 2.45, compared to that of the pool. An additional 102 vertical fractures were observed on floodplain outcrops, where 75% of the fractures were 1 m in length and all terminations were visible (Fig. D-2B).

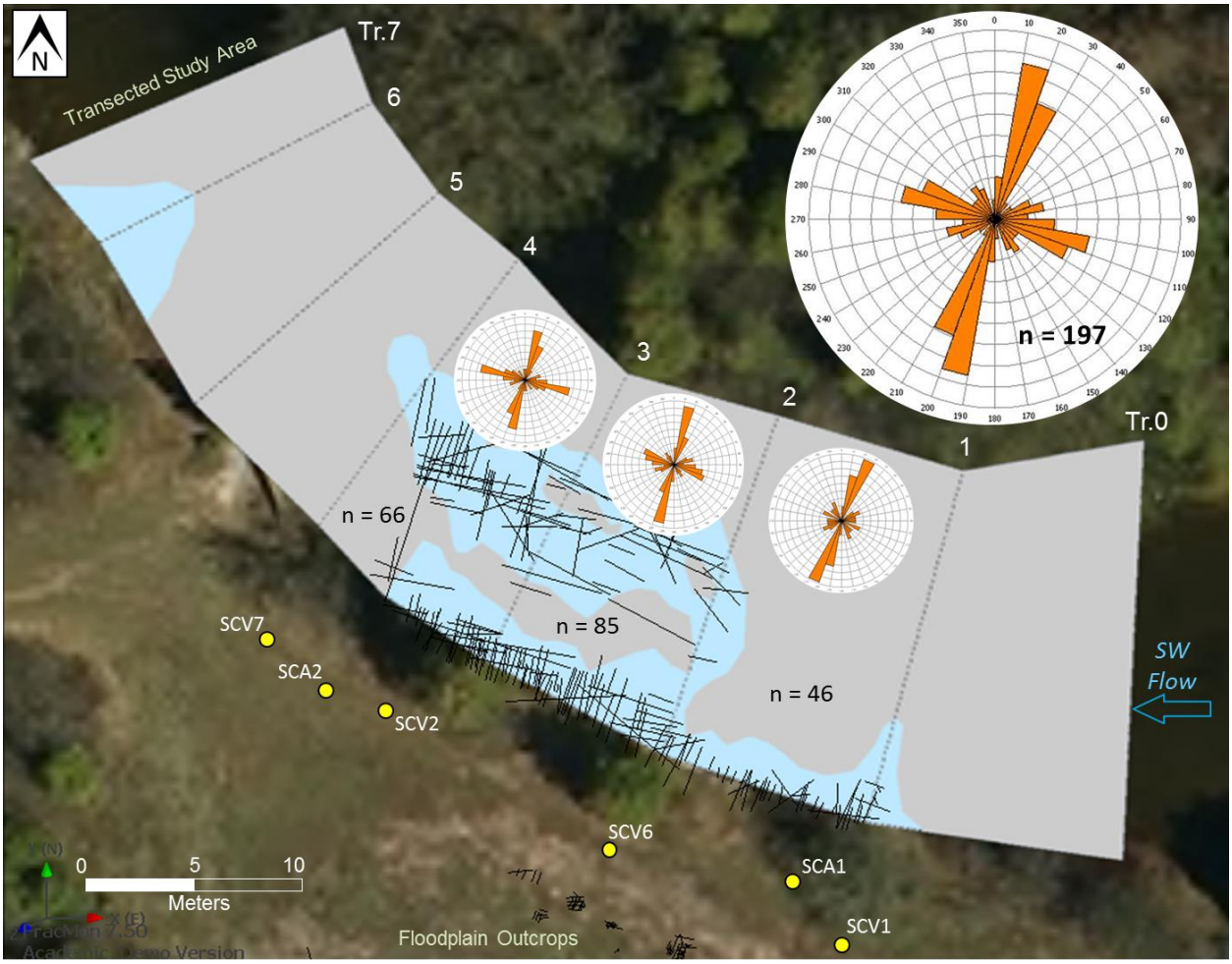

Fig. D-1. Transected study reach, where vertical fractures were measured in rubble-free zones between transects 1 -4. Rose diagrams show fracture distribution and orientation on streambed.

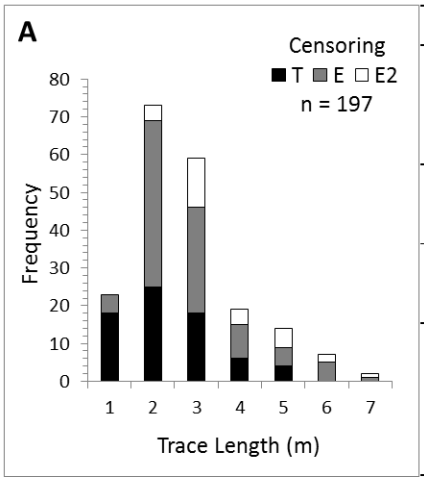

B Transect Number:	1	2	3	Floodplain
Rubble-free area [m^2]	168	78	100	62
Number of fractures observed	46	85	66	102
Total length [m]	74.09	191.37	202.81	93.08
P_{20} (number of fractures per unit area) [m^{-2}]	0.27	1.09	0.66	1.65
P_{21} (length of fractures per unit area) [m^{-1}]	0.44	2.45	2.03	1.50
Max [m]	6.75	6.11	9.56	5.90
Min [m]	0.41	0.40	0.56	0.11
Mean [m]	1.61	2.25	3.07	0.91
SD [m]	1.08	1.10	1.94	1.12

Fig. D-2. (A) Trace length histogram of streambed fractures, by degree censoring of terminating ends visible (T), extending at one end (E) or extending at both ends (E2); and **(B)** table of statistics, including additional floodplain outcrops (n = 102).